STUDIES ON NONLINEAR DYNAMICAL SYSTEMS IN NEUROPHYSICS AND ASTROPHYSICS

LALAJA VARGHESE

THESIS SUBMITTED IN
PARTIAL FULFILMENT OF THE REQUIREMENTS
FOR THE DEGREE OF
DOCTOR OF PHILOSOPHY

DEPARTMENT OF PHYSICS
COCHIN UNIVERSITY OF SCIENCE AND TECHNOLOGY
COCHIN - 682 022
INDIA

1990

CERTIFICATE

Certified that the work reported in the present thesis is based on the bonafide work done by Ms. Lalaja Varghese under my guidance in the department of Physics, Cochin University of Science and Technology and has not been included in any other thesis submitted previously for award of any degree.

Cochin 682 022

24.09.1990

Prof. V.P.N. Nampoori

(Supervising Teacher)

CONTENTS

LIST OF FIGURES

LIST OF TABLES

PREFACE

The dynamics of a complex system can be modelled from a single measurable quantity of the system using the recently developed methods in deterministic chaos (Schuster, 'Deterministic chaos', Physik Verlag, Heidelberg 1984). In the case of experimental signals, the existing techniques using qualitative measures like Fourier transform, autocorrelation function, etc., do not enable one to classify between low-dimensional deterministic chaos and broad band stochastic noise. But recent studies have shown that time series analysis can reveal the underlying characteristics of nonlinear dynamical systems. Moreover, such analyses give quantitative measures which are the invariants of the system (Grassberger P and Procaccia I, Phys. Rev. Lett. 50A 1983, GP algorithm). One of the interesting properties of the GP technique is that, it can give significant insight into the nature of the given system, whose basic equations are unknown.

In the analysis based on GP algorithm, equally spaced, digitized temporal or spatial variation of any measurable quantity of the system can be used as time series and finite data set is enough to give valuable information about the long-term behaviour of the system. GP algorithm is mainly used for the characterization of nonlinear dissipative systems, the basic assumption being that, time series contains *all* the information about the system (Packard N.H, Crutchfield J.P, Farmer J.D and Shaw R.S, Phys. Rev. Lett. 45 1980).

Time series analysis is successful in many complex systems like, for example, biological systems, climatic systems, Astronomical systems, Laser - matter interactions, chemical reactions etc. The complexity of the system is mainly due to the existence of nonlinear interactions and this leads to unpredictability in the frame work of conventional methods of dynamics.

In the case of nonlinear dissipative systems, which can be represented by n ordinary differential equations, evolution of state function constitutes a flow in phase space, and in time. The flow converges towards a finite dimensional subset of the phase space known as the attractor, which is invariant under the action of flow. The geometric structure and dimension of the attractor varies with systems. In the case of a periodic system, the behaviour of the system is predictable and the attractor is independent of the set of initial conditions and such attractors are called regular attractors. But, for chaotic systems, two initially close trajectories will diverge exponentially, resulting in loss of resemblance. The attractor is said to be sensitive to initial conditions and this subset has a complicated structure and is known as strange attractor. We can model the dynamics of a nonlinear system by estimating different characteristic properties of attractors, like generalized entropies (K_q), generalized dimensions (D_q), Lyapunov exponents (λ), $f(\alpha)$ spectrum etc.

In the present thesis, we give prime importance for the Second order dimension D_2, and Second order Kolmogorov entropy K_2. D_2 and K_2 are significant among D_q's and K_q's (Caputo J.G and Atten P Phys. Rev. 35A, No.3, 1987). D_2 and K_2 are reported to be sensitive parameters to characterize dynamical systems.

D_2 and K_2 are helpful in understanding whether a system exhibits regular (D_2=integer, K_2=0), chaotic (D_2=noninteger, K_2>0) or completely stochastic (D_2=undefined, K_2=∞) behaviour. More than that, these parameters quantify the degree of chaos in a nonlinear system.

The present thesis deals with the following studies we have carried out on neural system and certain astronomical systems in terms of D_2 and K_2.

i) Human brain under clinically normal condition and under various pathological conditions like Epilepsy, Migraine, Tumour, Head ache and Psychotic, based on the analysis of Electroencephalogram (EEG), which is the electrical activity of brain.

ii) Particle distribution in Asteroidal system.

iii) Matter distribution in Saturn ring structure.

The thesis contains eight chapters. The first chapter gives a general idea about different types of dynamical systems and their phase space behaviour.

The different signal processing techniques like, fast fourier transform (FFT), autocorrelation function (ACF), Poincare method and their limitations are described in chapter II. The chapter also includes certain new concepts in nonlinear analysis, like generalized dimensions, generalized entropies, correlation dimension and Kolmogorov entropy. Detailed discussion on GP algorithm and its advantages are also given.

Usually experimental signals include noise. Hence such signals should be filtered to eliminate noise before any nonlinear analysis are done. Chapter III describes a mathematical technique to filter out noise from a time series.

A major portion of the thesis is devoted to the classification of Neural system under various pathological conditions. Studies on the relation between mental and neural activities are also attempted. Hence a general idea about the Neural system is unavoidable, and this is the subject matter of

the fourth chapter.

The evaluation of D_2 and K_2 from EEG pattern is explained in chapter V. D_2 is a static parameter and K_2 is a dynamic parameter, so that K_2 is more sensitive than D_2. Kolmogorov entropy K_2, which is a measure of information content, is used to characterize the dynamics of brain during mental activity and the results obtained are described in this chapter. The generalized dimensions as well as $f(\alpha)$ spectrum of a clinically normal person during rest and mental activity are compared.

Sixth chapter introduces the idea that K_2 can be used to classify different pathological conditions of the brain. The variation of K_2 at different points of the brain during an epileptic seizure is studied. The capacity of the brain to regain its original state is investigated through the analysis of EEG of a person having headache. The variation of K_2, in the case of psychotic, tumour and epilepsy (with demylination) are also studied.

In the case of Astronomical system, the spatial variation of particle density is used as "time series" to characterize the system. We study in chapter VII the dynamics of two astronomical systems - the matter distribution in asteroidal belt and Saturn ring structure.

In the last chapter, we discuss the results and general conclusions obtained from the present studies. Future scope of this work is also included.

In the Appendix, we discuss the algorithm (modified from GP algorithm to develop Fortran code) used in the evaluation of D_2 and K_2. This appears to be an efficient computer program which therefore enabled us to carrying out the work successfully.

Part of the investigations described in the thesis has provided materials for the following publications.

List of Research papers published

a) Standard refereed journals

1. Lalaja V, Nampoori V.P.N and Pratap R, "Nonlinear analysis of an EEG during epileptic seizure", Current Science, 56, No.20, pp.1039-1041, (1987).

2. Pratap R, Nampoori V.P.N, and Lalaja V, "Invariant characterization of Neural systems", Int. Jl. Neurosci. 39, pp.245-251, (1988).

3. V. Lalaja, V.P.N. Nampoori and R.Pratap, "Strange attractors in the Saturn ring system", Jl. of Earth, Moon and Planets, 44, pp.105-119 (1989).

4. Lalaja V, "Brain functioning during an epileptic seizure", Physics News, 20, N0.1, pp.4-8, (1989).

b) Symposia

1. Lalaja V, Nampoori V.P.N and Pratap R, "A new methods of Signal processing - Application to EEG analysis", Proceedings of symposium on Signals, Systems, Sonars (NPOL, Cochin), B2.4/1-B2.4/5, (1988).

2. Lalaja V, Nampoori V.P.N and Pratap R, "Invariants in Neural Dynamics - A plausible diagnostic tool in Neurology", Proceedings of Symposium on current trends in Pure and Applied physics (Oct 24-25,1988).

3. Tessy Joseph, Lalaja V, and Nampoori V.P.N, "Nonlinear interactions in Stimulated Raman scattering", Proceedings of Symposium on current trends in Pure and Applied physics (Oct 24-25,1988).

c) **Papers communicated / under preparation**

1. Lalaja V, Nampoori V.P.N and Pratap R, "Information flow as inferred from EEG", Communicated to Jl. of Neuropsycobiology, (1988).

2. Lalaja V, Nampoori V.P.N and Pratap R, "An algorithm to extract signal from noise embedded data", Communicated to Electronics Letters, (1990).

3. Sreekumar J, Lalaja V, Nampoori V.P.N and Pratap R, "Neural activity as inferred from f(α) spectrum of EEG", Communicated to Phys. Lett. **A**, (1990)

4. Lalaja V, Sreekumar J, Nampoori V.P.N and Pratap R, "Signature of mental activity in the f(α) spectrum", Communicated to Int. Jl. Neurosci., (1990).

5. Lalaja V, Nampoori V.P.N and Pratap R, "Imaging of Brain using Kolmogorov entropy" (under preparation).

6. Lalaja V, Nampoori V.P.N and Pratap R, "Nonlinear analysis of EEG under various pathological conditions" (under preparation).

CHAPTER 1

INTRODUCTION

Various aspects of nonlinear dynamics in the context of chaotic phenomena are introduced. Important parameters which describe nonlinear phenomena are included in this chapter.

INTRODUCTION

The rapid developments that have taken place in the study of nonlinear dynamics provide a better understanding of many physical systems. They have totally changed the way of analysing the dynamics of a number of interesting systems like laser-matter interactions, hydrodynamical systems, climatic system, the neural system, and many astronomical systems. In this thesis we shall be doing the nonlinear analysis of Neural system and certain Astrophysical systems. Instead of going straight into such analysis, we shall describe the recent trends and methods of nonlinear analysis in this and the next chapter.

The rudiments of nonlinear dynamics can be understood on the basis of the phase space dynamics. To make this chapter self contained, we shall introduce the concept of phase space and study the nature of the phase space dynamics of conservative and dissipative systems. After a brief discussion on the attractors encountered in the phase space dynamics of dissipative systems, we shall discuss the dimension of such attractors. Chaos, one of the most interesting properties exhibited by nonlinear systems, shall be explained during the end of this chapter.

1.1 PHASE SPACE

As has already been stated, it is easy to describe the dynamics of nonlinear systems in the phase space. In this section we shall discuss briefly what a phase space is.

One can define phase space as an n-dimensional Euclidean space, where a point can describe the state of the system under

consideration at any given time. The dimension of the phase space, n, is chosen to be the lowest possible integer satisfying the above condition. This could be formulated mathematically as follows.

Let the given physical system, whose state is described by n variables $X_1, X_2 \ldots\ldots X_n$, be described by the set of equations

$$\frac{dX_i}{dt} = F_i(X_1 \ldots\ldots\ldots X_n) , \qquad i=1, \ldots\ldots n , \qquad (1.1)$$

where the functions F_i possess continuous partial derivatives and time t is the single independent variable. The phase space of such a system would be n-dimensional, whose coordinates are $X_1, X_2, \ldots\ldots\ldots X_n$. Each point in phase space represents a possible instantaneous state of the system.

Different points in the phase space could therefore represent the state of a given system at different times. Hence as the system evolves in time, the point representing the state of the system can trace out a trajectory - called the phase space trajectory.

Another important term, which needs explanation in this context is the 'degrees of freedom'. The degrees of freedom of a given dynamical system can be defined as the number of initial conditions that can be chosen independently to define the state of the system.

The concept of phase space has been used successfully in the development of statistical mechanics and in the treatment of differential equations. The dynamics of nonlinear systems in phase space has many interesting and peculiar characteristics. Nonlinear systems can, in general, be classified into conservative and dissipative systems. In the next two sections

we shall discuss the general nature of the phase space dynamics of these two classes of systems.

1.2 CONSERVATIVE SYSTEMS

In simple words, a conservative system can be described as one with an invariant total energy. It is possible to get a clear idea of a conservative system with the example of a free oscillator like the simple pendulum. The equation governing such a system is

$$\frac{d^2\theta}{dt^2} + \frac{g}{l} \operatorname{Sin} \theta = 0 \qquad (1.2)$$

where g is the acceleration due to gravity and l is the length of the pendulum. In the present example, the phase space is two dimensional and when the amplitude of oscillation is small, the phase space trajectory is a circle with its center at the origin. A family of circles centered at $\theta=0$ and $\theta=\pm 2\pi n$ $(n=0,1,2,\ldots)$ gives the complete phase portrait of the system when executing small oscillations.

Any conservative system can be described by the Hamiltonian function H such that

$$\frac{dH}{dt} = 0$$

or $$H(q_1,q_2,\ldots\ldots q_n\ ,p_1,p_2,\ldots\ldots p_n) = E = \text{Constant} \qquad (1.3)$$

i.e. conservative systems are characterized by the invariance of energy. Another important property of conservative systems is that the volumes (area in the example of harmonic oscillator) are

conserved in phase space. Initially close trajectories remains so, even at large times.

1.3 DISSIPATIVE SYSTEMS

Damped oscillator is a typical example of a dissipative system, represented by the equation (1.4)

$$\frac{d^2\theta}{dt^2} + \gamma \frac{d\theta}{dt} + \omega^2 \theta = 0 \qquad (1.4)$$

where γ is the damping coefficient and $\omega^2 = g/l$.

In the equation (1.4), if we try a solution $e^{\alpha t}$, we get an algebraic equation as

$$\alpha^2 + \alpha\gamma + \omega^2 = 0$$

which results in

$$\alpha = \frac{-\gamma \pm \sqrt{\gamma^2 - 4\omega^2}}{2} \qquad (1.5)$$

The quantity under the radical sign is always less than γ. It can also be negative, giving a phase factor. Three possibilities can arise (Minorsky 1969).

1) $\gamma > 0$. In this case, α will have a negative real part and a phase factor. Hence asymptotically, the solution goes over to zero and the system is said to have a limiting point in the asymptotic limit.

2) If $\gamma \equiv 0$, then equation (1.4) characterizes an oscillatory system and a first integral exdsts *viz.*,

$$\frac{\dot{\theta}^2}{2} + \theta^2 = E \qquad (1.6)$$

In the phase space characterized by θ-$\dot{\theta}$, this is an equation for a circle and we obtain a limiting circle.

3) If $\gamma < 0$, α will have a positive definite real part besides a phase factor and the solution goes to infinity as $t \to \infty$. Thus two trajectories starting from two neighbouring initial states, will diverge out and separate from each other as $t \to \infty$. The system is said to be unstable.

The energy change of the system is governed by (1.7)

$$\frac{dE}{dt} = -\gamma \dot{\theta}^2 \qquad (1.7)$$

Energy is conserved if $\gamma = 0$, while it decreases if $\gamma > 0$, and the trajectory converges towards the origin. The trajectory diverges away from the origin if $\gamma < 0$.

If $\gamma > 0$ ($\gamma < 0$) all trajectories are attracted towards (repelled away from) a fixed point known as attractor. In the present example the attractor is the origin. The dynamical properties of a dissipative system differ from those of a conservative system. Dissipative systems can not preserve volume in phase space. As $t \to \infty$, the phase space volume decreases and the motion is confined to a certain attractor. In other words, all trajectories passing through a certain domain of phase space are attracted towards a geometric hypersurface of an object in the subspace called the attractor.

Another interesting example of a dissipative system is the Van der Pol oscillator. In this case, the attractor is not a point, but a circle, called as the limit cycle. The equation for

the Van der Pol oscillator could be obtained by substituting

$$\gamma = -\gamma_o \left[1 - \frac{\theta^2}{\theta_o^2} \right] \qquad (1.8)$$

in equation (1.4)

i.e $$\frac{d^2\theta}{dt^2} - \gamma_o \left[1 - \frac{\theta^2}{\theta_o^2} \right] \frac{d\theta}{dt} + \omega^2\theta = 0 \qquad (1.9)$$

Here, if the oscillation amplitude θ is greater than θ_o then $\gamma>0$. Hence the oscillation amplitude decreases continuously till $\theta=\theta_o$, at which point $\gamma=0$ and the oscillation is asymptotically stable. On the other hand if $\theta<\theta_o$, then $\gamma<0$ and the oscillation amplitude increases with time till $\theta=\theta_o$, which is a stable orbit. Thus, for the Van der Pol oscillator, any given initial amplitude of oscillation would give an asymptotic oscillation amplitude θ_o. That is, the system has an attractor - the limit cycle - which is a circle with radius θ_o (measured along the θ-axis in the phase space).

We can develop an idea of the attractor by generalizing what we have said about the limit cycle. For this, consider a set of n ordinary differential equations (continuous autonomous flow)

$$\frac{d\vec{X}(t)}{dt} = F(\vec{X}(t)) , \qquad \vec{X} \in R^n \qquad (1.10)$$

As time evolves, for a given initial condition, equation (1.10) will create an orbit or time series or a flow, which will converge towards a region of the phase space called attractor, which has the following properties (Froehling et al 1981).

i) The attractor is invariant under the action of flow.

ii) The dimension of the attractor is less than the dimension

of the phase space.

iii) Attractor is contained in a domain, of nonzero volume known as the basin of attraction. The basin of attraction is defined to be the set of points from which trajectories are originated and converge towards the attractor.

The geometry of the attractor is characteristic of the given system. The attractor has a dimension D, which will obviously be less than the phase space dimension. A brief description of the dimension of attractor is given in the next section.

1.4 DIMENSION

The dimension of an attractor is a quantitative parameter which characterizes the property of the system. It can be interpreted as the number of independent frequencies present in the system or minimum number of variables needed to model the dynamics of the system. It can also be defined as the amount of information necessary to specify the position of a point on the attractor. For example, fixed point has a dimension zero, limit cycle has a dimension one, while an oscillator having two fundamental frequencies (whose attractor is a torus) has dimension two. In all these cases, the dimension is an integer. But there can exist systems having attractor, of noninteger dimensions. We shall discuss about such systems later. It is worth pointing out that integer dimension of the attractor indicates regular system (Farmer 1982 & 1983, Schuster 1984), while fractal (non integer) dimension depicts a chaotic system.

1.5 CHAOTIC SYSTEMS

The phase space trajectories of certain dissipative systems behave in a strange manner. Two nearby trajectories may separate exponentially with time. That is, the system has sensitive dependence on initial conditions (S.I.C). Such systems are said to be chaotic. There is, in fact, no generally accepted definition for chaos. It is a bounded steady-state behaviour

(Eckmann and Ruelle 1985, Parker and Chua 1987) which is not an equilibrium point, and neither periodic, nor quasiperiodic. (Quasiperiodic system is one having large number of independent frequencies, as explained in section 2.1). The frequency spectrum of a chaotic system is not composed of discrete frequencies but is a continuous one (Gollub et al 1975, Kürten et al 1986, Brandstater et al 1983).

Now, the question arises about the nature of the attractor in a chaotic system. It is not a simple geometric object like a circle or a torus. It was Landau who, in 1944, first tried to answer this question. He studied the behaviour of fluid flow, which makes a transition from laminar to turbulent when the Reynolds number (the control parameter) is increased. He concluded that the existence of a continuous Fourier spectrum is due to the presence of a large number of incommensurate frequencies, and its attractor is a torus T^r (T^r represents a torus of dimension r) with r very large . Landau's idea was that only those systems which have a large number of independent frequencies can display chaotic behaviour, since the dimension of the phase space must be greater than that of the attractor. However, these ideas had to be changed later, with the discovery of chaos in certain low dimensional systems.

Ruelle and Takens in 1971 (Berge et al 1984) introduced certain attractors which are topologically different from a torus. They are named as strange attractors due to their strange behaviour viz., the sensitive dependence of trajectories on initial conditions. Two initially close trajectories diverge exponentially on the attractor (Figure 1.1).

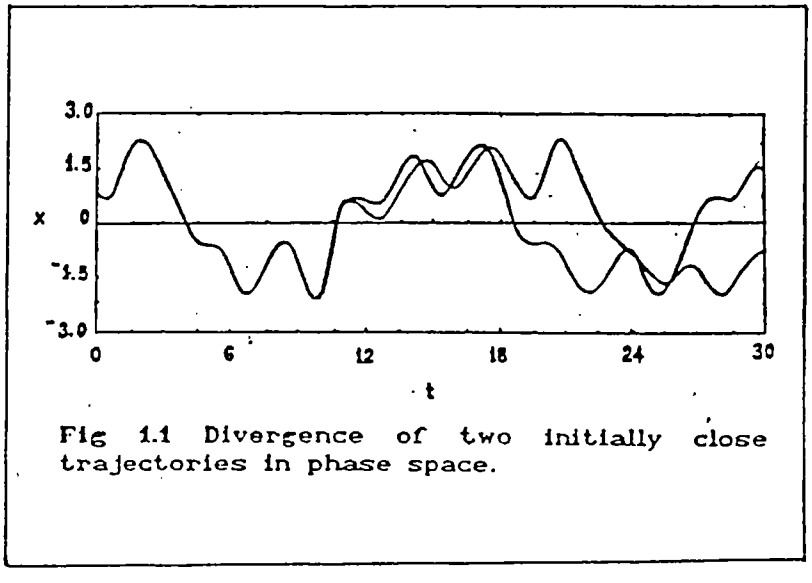

Fig 1.1 Divergence of two initially close trajectories in phase space.

A periodic (or quasiperiodic) signal resembles itself at later times. However a chaotic system does not display this behaviour. Also, the predictive power is lost as time increases. These properties of loosing self resemblance or predictability can be thought of as the quality which defines chaos. In the case of periodic system the dynamics become insensitive to initial conditions when the trajectory is on the attractor. But in the case of chaotic system, the loss of memory as the system evolves is due to the sensitivity of the initial conditions. In other words, different initial states of a chaotic system evolve in an unpredictable way to many final states.

Parker and Chua [1987] explained information gain in the following way. Consider an autonomous system with a contracting flow ϕ_t (Young 1983). Suppose that the system can be measured to within a resolution of ε, that is, if the state is observed to be x, the actual state lies somewhere in $B_\varepsilon(x)$, the ε-ball centered at x. Assume that there are two observers who measure the state of the system at two different times. Observer 1 observes the state of the system at time t_1 to be x_1. Observer 2 measures the state at time $t_2 > t_1$, to be x_2. Now the question is, which observer knows more about the state of the system.

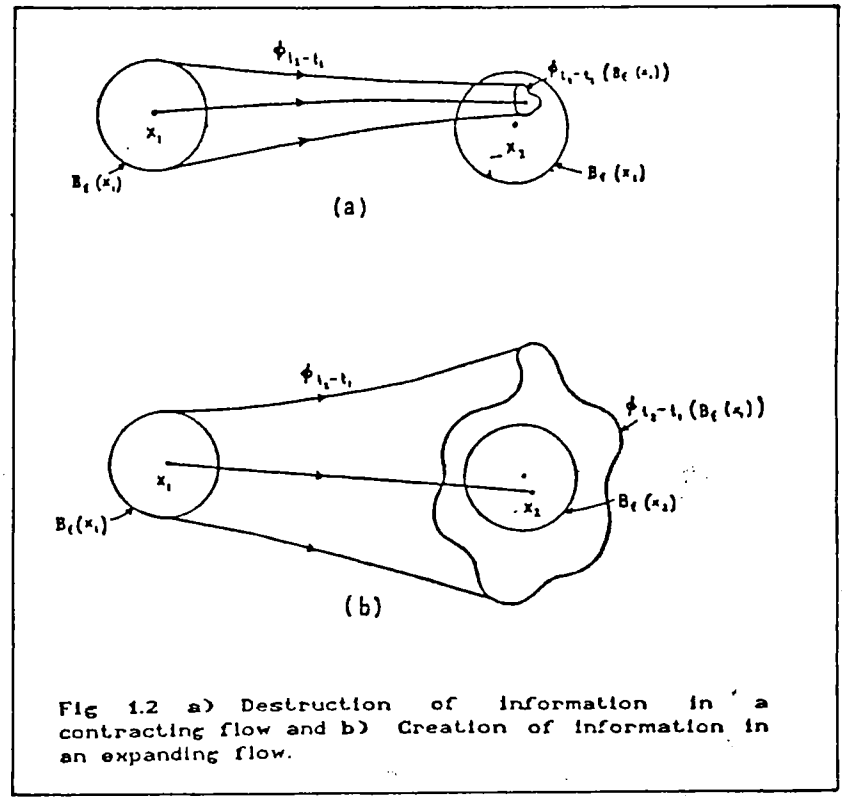

Fig 1.2 a) Destruction of information in a contracting flow and b) Creation of information in an expanding flow.

Observer 1 knows that the state at t_1 lies somewhere inside $B_\varepsilon(x_1)$ and, therefore, that the state at t_2 must lie inside $\phi_{t_2-t_1}(B_\varepsilon(x_1))$ (Figure 1.2a). Observer 2 knows that the state at t_2 lies somewhere inside $B_\varepsilon(x_2)$ and,

therefore, observer 1 knows the state of the system more accurately. Since the earlier observer possess more information about the state of the system, a contracting system may be thought of as destroying information.

Now consider the opposite case of an expanding flow (Figure 1.2b). The later observer, number 2, knows more about the state of the system because $B_\varepsilon(x_2)$ is contained in $\phi_{t_2-t_1}(B_\varepsilon(x_1))$. The longer one waits to observe the state, the more one learns. In other words, an expanding flow may be viewed as creating information.

For a contracting system, it is more accurate to use x_1 to predict the state at time t_2 than to observe the state at time t_2. Larger the value of t_2-t_1, greater is the accuracy of prediction. Thus for a contracting (information destroying) system, the predictive value of initial conditions increases with time. On the other hand, for an expanding (information creating) system, the predictive value of initial condition deteriorates with time.

This argument shows that expanding systems exhibit sensitive dependence on initial conditions, but a purely expanding flow also implies unbounded behaviour. By definition, a chaotic trajectory is bounded. It follows that a chaotic system must contract in certain directions and expand in others, with the contraction outweighing the expansion. The rate of divergence or convergence of trajectories in each direction of phase space can be measured. Such rates characterize the dynamics of the system. Lyapunov exponent is one such quantity, much helpful in identifying chaotic and regular systems.

1.6 LYAPUNOV EXPONENT

Lyapunov exponents (LE) are used to quantify the expansion and contraction occurring in the phase space of a dynamical system. LE is the average exponential rate of divergence or

convergence of nearby trajectories in phase space. Negative LE indicates exponential convergence of trajectories. On the contrary, a positive LE expresses the exponential divergence, indicating a chaotic system.

Consider a dynamical system with n dimensional phase space and let the system be governed by n initial conditions. We can represent the behaviour of the system by the long term evolution of an infinitesimal n-sphere of initial conditions. The sphere will become an ellipsoid due to SIC nature of the flow. The i^{th} one dimensional LE (λ_i) is then defined in terms of the length of the principal axis $p_i(t)$ of the ellipsoid as

$$\lambda_i = \lim_{t \to \infty} \frac{1}{t} \ln \frac{p_i(t)}{p_i(o)} \qquad (1.11)$$

If λ_j is the largest positive LE, then two initially close points on the attractors grow as $e^{\lambda_j t}$ (Wolf et al 1985, Eckmann et al 1986 , Stoop et al 1988)

1.7 CHAOTIC ATTRACTORS

We have seen that the rate of loss of predictive power is equal to the rate of information gain. Then the important point is that, if a dynamical regime is represented by an attractor on which neighbouring trajectories diverge, then the regime is chaotic.

There was an earlier belief that only those systems, with large number of degrees of freedom show chaotic behaviour. But recently it has been established that certain low-dimensional systems also exhibit SIC (Lorenz 1963). SIC is not possible on a two dimensional attractor, due to the topological reason that the trajectories of a dynamical system in phase space cannot intersect. Therefore only systems with at least three phase

space dimensions can exhibit chaos. In a three dimensional phase space, the existence of strange attractor requires two operations - stretching due to SIC, followed by folding. The stretching and folding are necessary to ensure that the trajectories will remain in a bounded space.

Smale horseshoe attractor is a theoretical model of the strange attractor. As mentioned above, the basic operations necessary for creating a strange attractor are stretching, followed by folding. ABCD is a rectangle (Fig.1.3a) and stretch it by a factor of two in the x-direction, while contracting it by a factor 2η in the y-direction. If $\eta > 1$ we will get $A_1B_1C_1D_1$ with less area than ABCD. Then fold $A_1B_1C_1D_1$ back on itself as shown in Figure (1.3a) and fit the image back in the rectangle ABCD. Then we will get a hairpin shaped curve, and is named as horseshoe. Repeat this (Fig 1.3b) - stretching in x-direction and folding in the y-direction. After a number of iterations we obtain a complex layered structure, which has all the properties of a strange attractor.

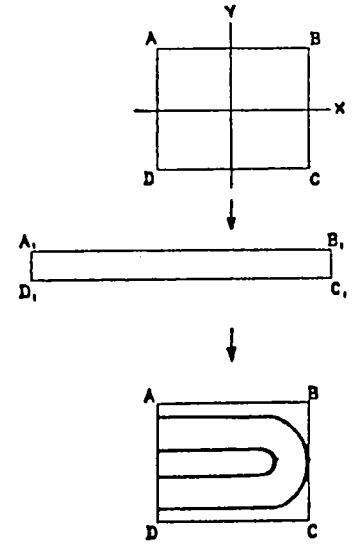

Fig 1.3 a) First stretching and folding of the rectangle ABCD.

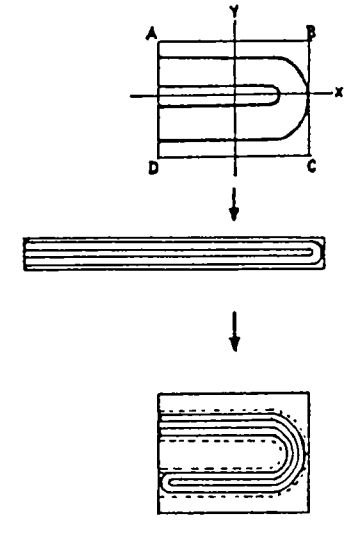

Fig 1.3 b) Second iteration of the Smale horseshoe attractor.

Certain physical systems exhibit irregular or chaotic

motion whose time dependence is deterministic. Thus the chaotic behaviour exhibited by systems whose time evolution can be described from its previous behaviour is called deterministic chaos. Another definition of deterministic chaos is connected with degrees of freedom. Landau's idea was that only systems with large number of degrees of freedom can exhibit chaos. But it has been shown that even systems with three degrees of freedom exhibit chaotic behaviour. The chaos exhibited by systems with small number of degrees of freedom is also called deterministic chaos. The motive behind deterministic chaos is the SIC.

Consider a system with three-dimensional flow. The requirements for SIC is that, the dimension of the attractor D is greater than two, and the dimension of the attractor is less than the dimension of the phase space. Then the dimension of the attractor representing a chaotic regime must be greater than 2, but less than 3, i.e; the attractor has a fractal dimension (2<D<3). In general, for a system with n-dimensional flow, the strange attractor is characterized by noninteger dimension or fractal dimension.

Thus a dissipative dynamical system can become chaotic if the phase space dimension is greater than or equal to three. Chaos with small number of degrees of freedom is due to the SIC of trajectories on strange attractors.

The behaviour of a strange attractor can be explained in terms of Lorenz model.

1.8 LORENZ ATTRACTOR

One of the first systematic studies on a chaotic system is due to Lorenz in the context of climatic dynamics (Lorenz , 1963). His study was connected with equations governing convective phenomena in fluids. Temperature differences in a thermally expansive fluid placed between two plates, where the upper plate is at a constant temperature T_o and the lower plate at temperature $T_o+\delta T$ ($\delta T > 0$), create convection if $\delta T > \delta T_c$,

where δT_c is the critical temperature below which the system is at the state of rest. These convections set up tubes with a hexagonal cross section along the height of the tube and these are called Benard cells. This was first observed by Benard in 1900 and was satisfactorily interpreted by Lord Rayleigh in 1916, so that this convection is called Rayleigh - Benard convection.

The convective phenomena can be explained in terms of three nondimensionalized equations. The coupled transport of momentum of the fluid can be described by a set of equations. The momentum equation is given by

$$Pr^{-1}\left[\frac{\partial \vec{v}}{\partial t} + \vec{v} \cdot \nabla \vec{v}\right] = -\nabla p + \theta\,\vec{\lambda} + \nabla^2 \vec{v} \qquad (1.12a)$$

We define the Prandtl number $Pr=\nu/D_T$, where ν is the kinetic viscosity of the fluid and D_T is the thermal diffusivity, p is the hydrostatic pressure, $\vec{\lambda}$ is the unit vector along the vertical axis in the direction of gravity and $\theta(\vec{r},t)$ is the temperature deviation.

Incompressibility of the fluid is represented by

$$\nabla.\vec{v} = 0 \qquad (1.12b)$$

and the heat propagation through the temperature deviation $\theta(\vec{r},t)$

$$\frac{\partial \theta}{\partial t} + \vec{v} \cdot \nabla\theta = Ra\,\vec{\lambda} \cdot \vec{v} + \nabla^2\theta \qquad (1.12c)$$

where Ra is the Rayleigh number

$$Ra = \left[\rho_o g \alpha d^3 / \eta D_T \right] \delta T \qquad (1.13)$$

g is acceleration due to gravity

ρ_o is the mean density ,α is expansion coefficient, η is dynamic viscosity and d is the thickness of the fluid

When $Ra < Ra_c$ (critical Rayleigh number) the fluid remains at rest while, if $Ra > Ra_c$, the convection begins. Convective rolls are created between the two plates, with adjacent rolls rotating in the opposite directions with velocity $\vec{v}$.

Lorenz reduced the dynamical behaviour of the convecting fluid into the following form

$$\frac{dX}{dt} = Pr\ Y - Pr\ X$$

$$\frac{dY}{dt} = -\ X\ Z + r\ X - Y \qquad (1.14)$$

$$\frac{dZ}{dt} = X\ Y - b\ Z$$

The values of the parameters Pr and b are fixed. Usually Pr=10 and b=8/3 and r is taken as the control parameter. The nature of the phase space trajectory varies with r. For r > 24.74, trajectories become irregular (Ruelle 1980).

The contraction of volume in phase space can be described by Lie derivative. It gives the relative rate of change of a volume V in phase space under the action of the flow.

$$\frac{1}{V}\frac{dV}{dt} = \sum_{i=1}^{n} \frac{\partial \dot{X}_i}{\partial X_i} \qquad (1.15)$$

where X_i is the i^{th} component of $\vec{X}$ and $\vec{X} \in R^n$. Lie derivative is negative for dissipative system, which measures the rate of contraction. For Lorenz attractor, the Lie derivative is

$$\frac{\partial \dot{X}}{\partial X} + \frac{\partial \dot{Y}}{\partial Y} + \frac{\partial \dot{Z}}{\partial Z} = -(Pr + b + 1) = \frac{-41}{3} \qquad (1.16)$$

i.e; the volume is reduced by a factor of $e^{-41/3}$ or $10^{-\delta}$ in each unit of time.

The complex nature of the system can be confirmed to be chaotic if the dimension of the attractor is fractal. But if the system exhibits strong volume contraction in phase space, then the fractal value can be very close to an integer. In such cases we have to resort to other methods like, for example, studying the evolution of separation distance in phase space.

Chaotic nature of the system can be understood by studying the temporal evolution of initially close trajectories in phase space by measuring separation between the two trajectories. Figure (1.4) gives the separation distance δ versus time for Lorenz model. First consider two points separated by a distance $\delta_o = 10^{-8}$. The distance δ between the two trajectories increases

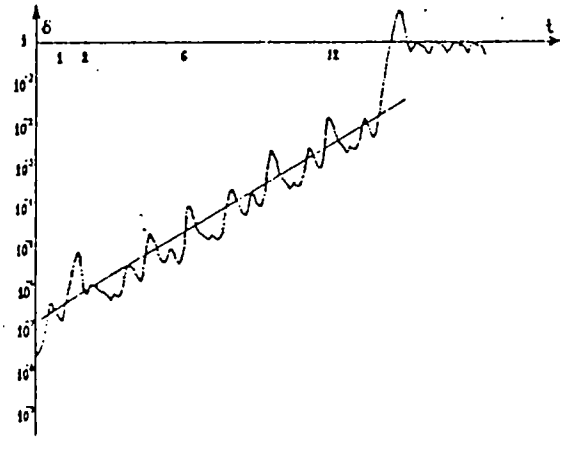

Fig 1.4 Evolution of separation distance.

exponentially as $\delta=\delta_o \exp(\lambda t)$ where λ is the largest LE. λ is the average slope of the curve of the Figure (1.4). If λ is positive, the system is chaotic.

Usually, in experiments, one records the time variation of a measurable quantity which characterizes the dynamics of the system. From such time series, it is difficult to calculate LE. However, evaluation of dimension which is an important parameter to quantify chaos is comparatively easier. There are different classes of dimensions, such as phase space dimension, fractal dimension, information dimension and correlation dimension. General description of these classes of dimensions are given below.

1.9 FRACTAL DIMENSION

The fractal dimension is referred in different terms such as Capacity, Hausdorff-Besicovitch dimension, etc. Consider an attractor A, and cover this set by hypercubes of linear dimension ε. Let $N(\varepsilon)$ be the number of cubes necessary to cover this attractor and if D is the dimension of this attractor, then for small ε,

$$N(\varepsilon) = k\varepsilon^{-D} \qquad (1.17)$$

where k is a constant. Then the Fractal dimension D_f is

$$D_f = \lim_{\varepsilon \to 0} \frac{\ln N(\varepsilon)}{\ln(1/\varepsilon)} \qquad (1.18)$$

If the set is a single point then $N(\varepsilon)$=constant=1 and D_f=0. If the set is a line $N(\varepsilon) = L\varepsilon^{-1}$, and hence $D_f = 1$; for a surface $N(\varepsilon) = S\varepsilon^{-2}$ and leading to $D_f = 2$.

Noninteger values of D_f are exhibited by certain physical systems. A complicated structure called Cantor Set displays this behaviour. The Cantor set is constructed as follows. Take a line segment between (0,1). Remove the central third as shown in Figure (1.5b). Then we will get two pieces in the interval $[0,1/3]$ and $[2/3,1]$. Remove the middle third of each of these intervals, then we will get four units. Repeat this process ad infinitum. The resulting set is called middle third Cantor set.

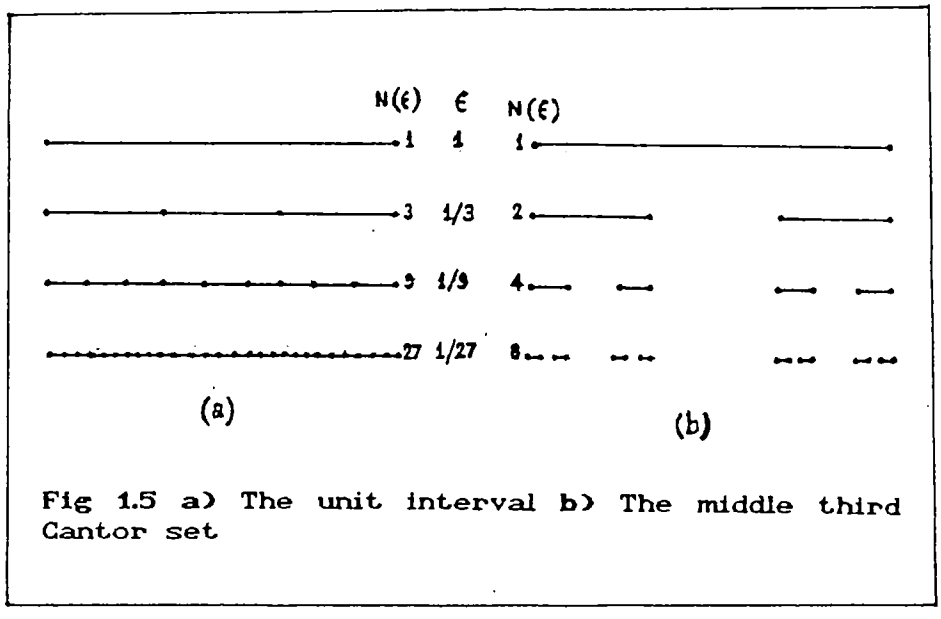

Fig 1.5 a) The unit interval b) The middle third Cantor set

The fractal dimension of the line can be obtained by covering it with volume element of length $\varepsilon = (1/3)^n$ (Fig 1.5a). Then

$$D_f = \lim_{n\to\infty} \frac{\ln 3^n}{\ln 3^n} = 1$$

because $N(\varepsilon) = 3^n$

The fractal dimension for the middle third Cantor set (fig 1.5b) is

$$D_f = \lim_{n\to\infty} \frac{\ln 2^n}{\ln 3^n} = 0.6309$$

That is, the fractal dimension of the Cantor set is greater than that of a point but less than that of a line. Hence, it is

interesting to note that the dimension of the line is integer but its convoluted nature is characterized by noninteger dimension (Lichtenberg and Lieberman 1983).

1.10. INFORMATION DIMENSION

Fractal dimension is only a metric dimension, and it does not consider the information about the temporal behaviour of the dynamical system. The attractor volume is partitioned into cubes of equal size, so that all cubes are equally important even though the trajectories are visiting the cubes at different frequencies. The information dimension on the other hand, is probabilistic in nature, and is related to the information necessary to specify the position of a point on the attractor. In most cases the partition do not have equal probability, then the information needed to specify a point with accuracy ε is

$$I(\varepsilon) = - \sum_{i=1}^{N(\varepsilon)} p_i \ln (p_i) \qquad (1.19)$$

where p_i is the probability associated with the i^{th} box. The information dimension D_I is defined as

$$D_I = \lim_{\varepsilon \to 0} I(\varepsilon) / \ln(1/\varepsilon) \qquad (1.20)$$

If all boxes are of equal probability p_i, i.e., $p = p_i = 1/N(\varepsilon)$, then

$$I(\varepsilon) = -\sum_{i=1}^{N(\varepsilon)} 1/N(\varepsilon)\ \ln 1/N(\varepsilon) = N(\varepsilon)(1/N(\varepsilon)\ \ln\ N(\varepsilon))$$

$$I(\varepsilon) = \ln N(\varepsilon) = D_f \ln (1/\varepsilon)$$

$$\therefore \qquad D_f = D_I \qquad (1.21)$$

1.11 CHARACTERISATION OF A SYSTEM FROM ITS TIME SERIES

Fractal dimension and Information dimension are very handy in describing the dynamics of nonlinear systems. But these quantities are difficult to extract from an experimental data. However a third type of dimension, the correlation dimension is easy to compute from such experimental data. Hentschel et al [1983] and Pawelzik et al [1987] have introduced the concept of generalized dimension so as to bring the fractal, information and correlation dimensions under one roof. A detailed explanation of generalized dimension and correlation dimension shall be given in the second chapter. The method of calculation of these quantities from experimental data shall also be discussed there.

We have mentioned that it is difficult to compute the LE's from experimental data. However it is comparatively easy to calculate a quantity, Kolmogorov entropy, which is related to LE's (Benettin et al 1976). The next section gives a description of this.

1.12 KOLMOGOROV ENTROPY

The exponential rate of divergence of trajectories on a strange attractor leads to the creation of information. This rate of divergence can be identified in terms of Lyapunov exponents. The Kolmogorov Sinai or Kolmogorov entropy is another

parameter which quantifies the divergence of trajectories and is the mean rate of creation of information.

For the calculation of this entropy, the phase space is partitioned into n elements, each of which is assigned with a symbol s_i. Let us consider a sequence $S_i(m)$ of m successive measurements made at a time interval Δt. $S_i(m)=s_{i1}, s_{i2}, \ldots\ldots, s_{im}$. The probability of the sequence of $S_i(m)$ is $P(S_i(m))$. Hence,

$$\sum_i P(S_i(m)) = 1 \qquad (1.22)$$

The amount of information contained in the sequence of length m is

$$I_m = - \sum_i P(S_i(m)) \ln P(S_i(m)) \qquad (1.23)$$

The Kolmogorov entropy is the information per unit time in a sequence of measurements

$$K = \frac{I_m}{\Delta t} \qquad (1.24)$$

For regular or predictable systems, the evolution of trajectories do not give any new information. For example, in the case of a stable fixed point and limit cycle, new measurements would not give any further information, so that $K=0$. But, for chaotic system $K > 0$. (Eckmann and Ruelle 1985). K is also expressed as

$$K = \sum_i \sigma_i \qquad (1.25)$$

where σ_i is the LE. The generalized entropy and Second order Kolmogorov entropy are described in detail in the next chapter.

CHAPTER 2

QUANTIFICATION OF CHAOS IN NONLINEAR DYNAMICS

Detailed description of the method of nonlinear analysis used in the present work is given. Parameters which can quantify the degree of chaos are dealt with in detail.

QUANTIFICATION OF CHAOS IN NONLINEAR DYNAMICS

Simple linear systems are easy to handle and one can develop the basic equations of dynamics without much difficulty. In case of complex systems, it may be difficult to obtain equations of motion, especially when the interactions are nonlinear. However, the dynamics will reflect up on the time dependence of certain easily measurable quantities. The temporal development of such quantities is known as the time series. Time series analysis, which is currently attracting much interest, can give immense insight into the dynamics of the system. In this chapter we describe various methods used in time series analysis. We shall describe in detail the methods suitable for nonlinear systems, after giving a brief description of conventional techniques usually employed in time series analysis.

2.1 FOURIER SPECTRA

Discrete fourier transform is one of the usual methods used to determine the kind of evolution produced by a dynamical system by studying a time dependent signal $x(t)$, the time series. This will help us to find out various frequencies present in the system under consideration. This method is used to identify the general nature of the system and has recently been successfully applied to the studies of asteroidal belt (Pratap 1977) and Neural system (Hinrichs 1987, Dumermuth and Molinari 1987). In this section we study the method of fourier analysis of a time series. We shall explain the spectra to be observed for different classes of signals like sinusoidal, non-sinusoidal, quasi periodic etc. The limitations of the method in the analysis of chaotic system shall be discussed.

We assume that the signal x(t) is a continuous function of time. This signal is then sampled such that the experimental results provide a discrete sequence of real numbers x_j which are regularly spaced in time with an interval of Δt. The number of data is finite, containing n values for a total length of time $t_{max} = (n-1)\Delta t$. The smallest frequency obtainable from such a time series, $\Delta f = 1/t_{max}$. We can define Fourier transform of a discrete time series x_j as discrete fourier series $\hat{x}_k$,

$$\hat{x}_k = \frac{1}{\sqrt{n}} \sum_{j=1}^{n} x_j \exp\left(-i \frac{2\pi jk}{n}\right) \qquad (2.1)$$

$k = 1, \ldots\ldots\ldots n$, $i = \sqrt{-1}$

The graph representing $|\hat{x}_k|^2$ as a function of the frequency f ($f = k.\Delta f$) is called the power spectrum. The nature of the power spectrum is characteristic of the system.

Let us consider a periodic signal x(t) of period T, so that

$$x(t) = x(t+T) \qquad (2.2)$$

If the signal is sinusoidal its power spectrum contains only a single frequency at 1/T Hz (Figure 2.1). A nonsinusoidal signal (Figure 2.2a), gives rise to the spectrum containing the frequencies located at 2/T Hz, 3/T Hz ... etc,.

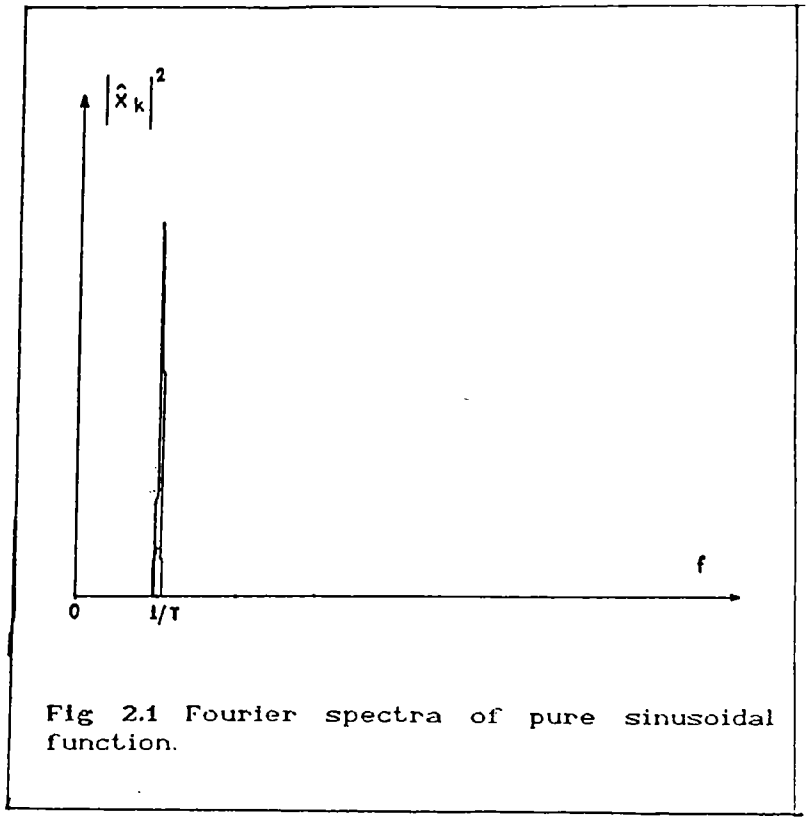

Fig 2.1 Fourier spectra of pure sinusoidal function.

(Figure 2.2b) which are the harmonics of the fundamental frequency 1/T Hz. That is, the presence of harmonics in the spectrum shows that the system is nonsinusoidal. The Figure (2.2b) represents a system in which the duration of measurement is an integer multiple of signal period T i.e; $t_{max} = pT$, $p > 1$ (a positive integer).

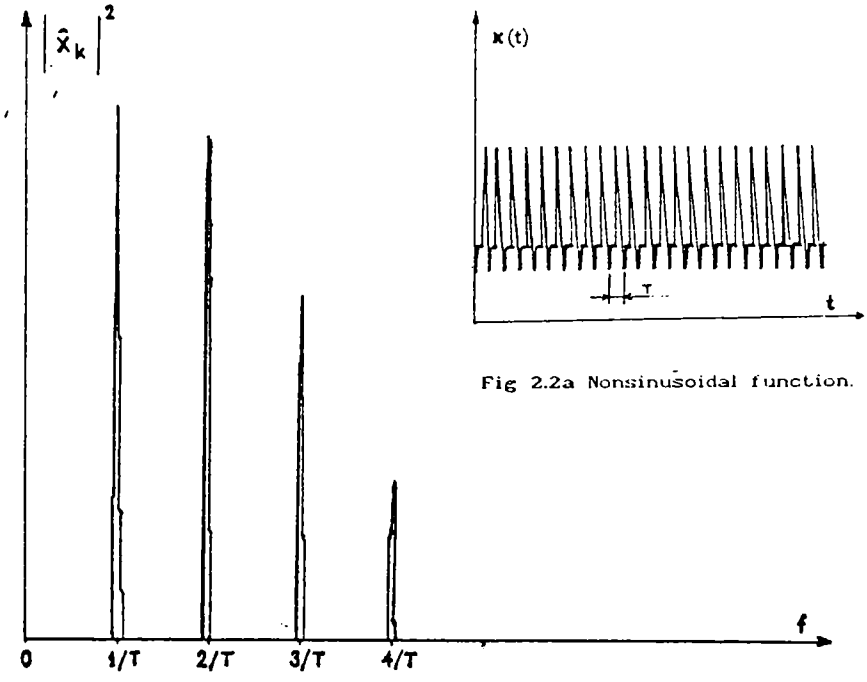

Fig 2.2a Nonsinusoidal function.

Fig 2.2b Fourier spectra of a periodic function (nonsinusoidal).

If we have a situation, where t_{max}/T is noninteger, then

$$|\hat{x}_k|^2 \simeq n \frac{\mathrm{Sin}^2(n\pi\phi_k)}{(n\pi\phi_k)^2} \qquad (2.3)$$

In this case the behaviour of the function is like that of $\mathrm{Sin}^2 z/z^2$ as shown in Figure 2.3. The function has a maximum amplitude at z=0, with a series of secondary maxima at $\pm(l+1/2)\pi$, whose amplitude decreases as $1/z^2$ where l is a positive integer.

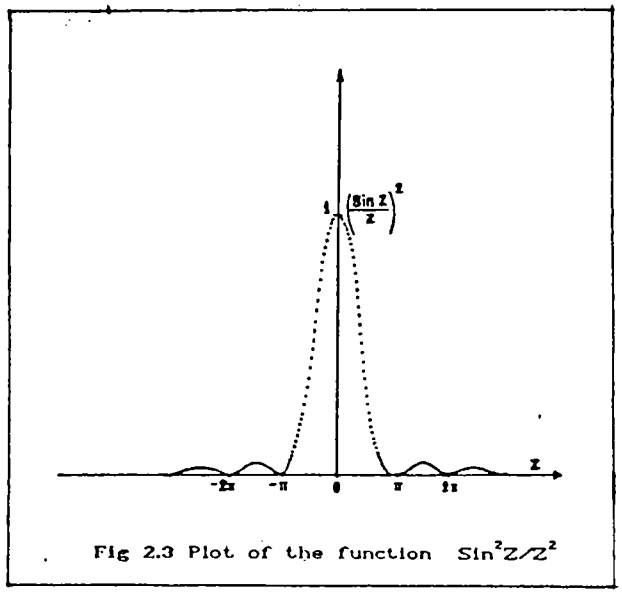

Fig 2.3 Plot of the function $\mathrm{Sin}^2 z/z^2$

A dynamical system, whose behaviour is due to the superposition of oscillations which differ in amplitude, period and ratio of harmonics, will show a totally different frequency spectrum. This type of system can be represented by a function y of r independent variables t_1, t_2, ... t_r, which is said to be periodic with period 2π and has the property

$$y(t_1,t_2\ldots\ldots t_j,\ldots,t_r) = y(t_1,t_2\ldots\ldots t_j+2\pi\ldots\ldots t_r)$$

$$j = 1,\ldots\ldots r \qquad (2.4)$$

The function y is said to have r-periods and it represents a quasiperiodic system with multiple periodicity. An example of a quasiperiodic system can be given in terms of the astronomical position of a point on the surface of the earth. In this system, rotation of the earth about its axis takes 24 hours (T_1=24 hours), the rotation of the earth around the sun takes 365.242 days (T_2 = 365.242 days) and the precession of the earth's axis of rotation takes 25,800 years (T_3 = 25, 800 years). This system contains three frequencies. Hence it is not possible to describe the trajectory of this in a phase space in terms of limit cycle or fixed point, used for periodic systems. An alternate description can be made for such systems in terms of the new mode of phase space trajectory, *viz.*, 'torus' of dimension r (i.e. T^r).

There are two types of quasiperiodic systems. If the quasiperiodic function $x(\omega_1 t, \ldots\ldots\ldots\omega_r t)$ is the sum of periodic functions

$$x(\omega_1 t, \ldots\ldots\ldots\omega_r t) = \sum_{i=1}^{r} x_i(\omega_i t) \qquad (2.5)$$

then its power spectrum is the sum of r spectra of each of

functions $x_i(\omega_i t)$. Then the spectrum contains a set of peaks located at the fundamental frequencies f_1, f_2 . . . f_r and of their harmonics,

$$m_1 f_1,\ m_2 f_2 \ \ldots\ldots\ldots\ldots\ m_r f_r$$

where m_1, m_2, ... m_r are positive integers. But if the quasiperiodic function includes term like the product of circular function ($\mathrm{Sin}(\omega_i t)\ \mathrm{Sin}(\omega_j t)$), then Fourier spectrum has a complex appearance and contain frequencies $|f_i - f_j|$ and $|f_i + f_j|$ and their harmonics

$$\mathrm{Sin}\,(\omega_i t)\ \mathrm{Sin}\,(\omega_j t) = \frac{1}{2}\,\mathrm{Cos}\,(|f_i - f_j|2\pi t) - \frac{1}{2}\,\mathrm{Cos}\,(|f_i + f_j|2\pi t) \qquad (2.6)$$

Inorder to study a quasiperiodic system in detail, consider a biperiodic case in which each of the nonzero component of the spectrum of the signal $x(\omega_1 t, \omega_2 t)$ is a peak with abscissa $|m_1 f_1 + m_2 f_2|$. We can classify the systems in terms of the ratio of f_1/f_2, *viz.*, whether it is rational or irrational. If f_1/f_2 is rational, then the Fourier spectrum is not dense (Fig.2.4).

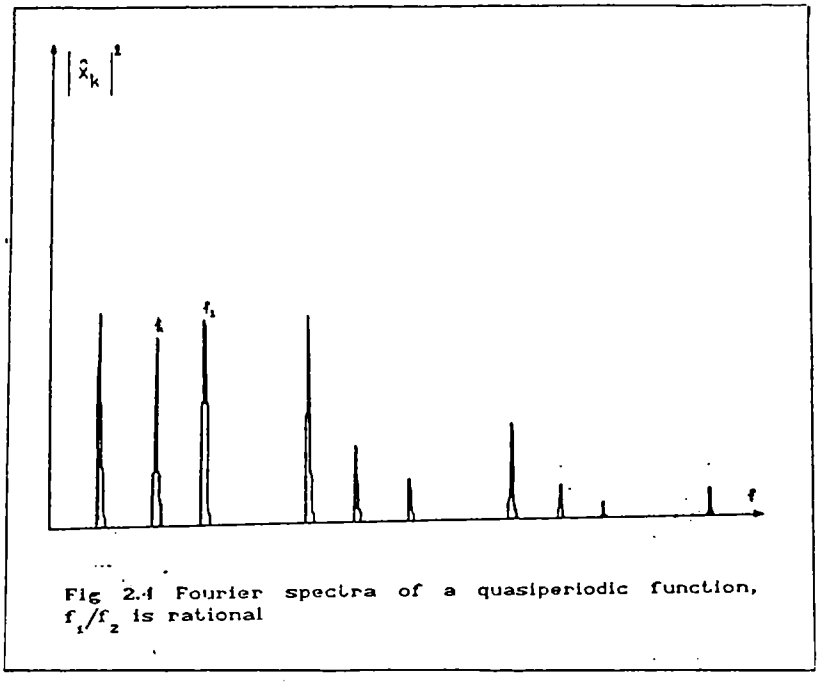

Fig 2.4 Fourier spectra of a quasiperiodic function, f_1/f_2 is rational

$$\frac{f_1}{f_2} = \frac{n_1}{n_2} \qquad (n_1,\ n_2 \text{ integers}) \qquad (2.7)$$

i.e; quasiperiodic signal is periodic with period

$$T = n_1 T_1 = n_2 T_2$$

So, we can write

$$x(\omega_1 t,\ \omega_2 t) = x(\omega_1 t + 2\pi n_1,\ \omega_2 t + 2\pi n_2)$$

$$\text{i.e,} \quad x(\omega t_1,\ \omega t_2) = x(\omega (t_1 + n/f_1)_1,\ \omega (t_2 + n/f_2))_2 \qquad (2.8)$$

In this type of system, there is a 'frequency locking' of f_1 with f_2. This means that all the lines of spectrum are always separated by same amount of $1/T$.

But if f_1/f_2 is irrational (the system contains incommensurate frequencies), then the power spectrum has a complex appearance. Two peaks are so close together with the appearance of a continuous function. However, usually only for very limited number of frequencies have significant amplitudes. Higher order frequencies have amplitudes too low to be detected. In this case, the higher amplitude lines are presented

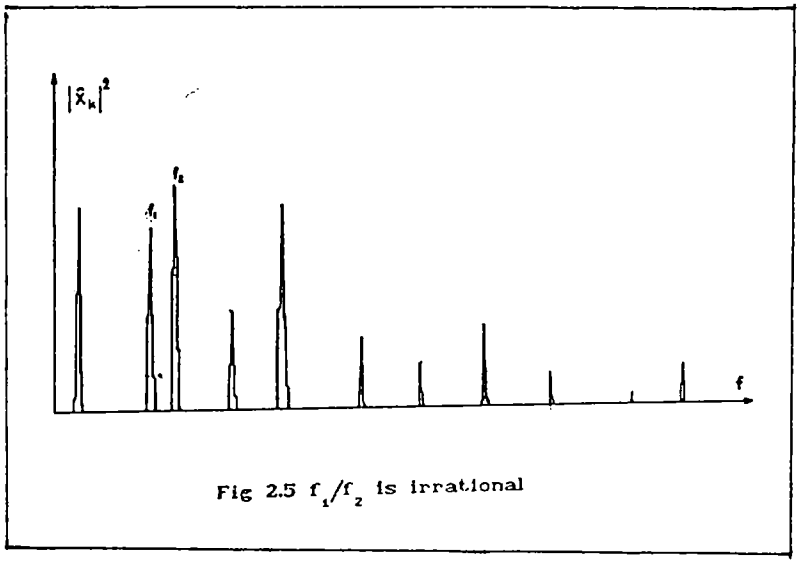

Fig 2.5 f_1/f_2 is irrational

by the combinations $|m_1 f_1 + m_2 f_2|$ with m_1 and m_2 having small values; 0,±1,±2 (Figure 2.5).

The Fourier spectrum of an aperiodic signal is continuous as shown in Figure (2.6) (Gollub et al 1975, Kûrten et al 1986, Brandstater et al 1983). However, we will not be able to

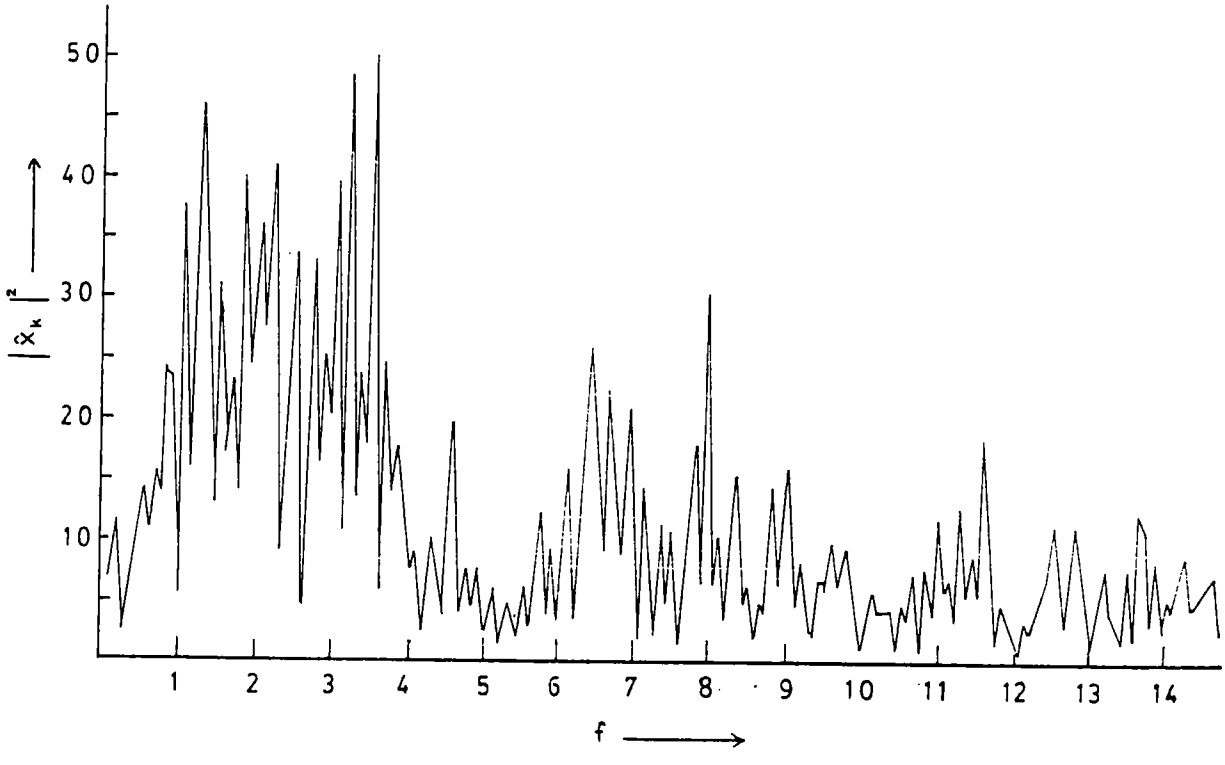

Fig 2.6 Fourier spectra of an aperiodic function

conclude that a signal is aperiodic from the appearance of Fourier spectrum alone, since quasiperiodic signals also give a similar looking Fourier spectrum, when the number of frequencies are very high. Moreover, random signals also exhibit similar spectra. It is also known that signals arising from a system exhibiting deterministic chaos have quasi continuous spectra.

2.2 FAST FOURIER TRANSFORM (FFT)

FFT is an algorithm to compute discrete fourier transform from time series (developed by Cooley and Turkey in

1965), and is one of the first techniques usually employed in the identification of deterministic chaos. Deterministic chaos has a fourier spectrum where a few dominant frequencies are superimposed on a broad band noise floor. FFT technique is useful when the number of data (n) is very large with small Δt. For example, to calculate discrete fourier transform with $n=10^3$, we have to calculate 1000 sums, each of which contains 1000 terms. This means that the number of operation needed is of the order of n^2. It will take a large time for the computation of the frequencies using conventional method. However, when n is a power of two, the FFT algorithm speeds up the calculation of spectrum. For $n=2^{10} = 1024$, the gain of computational time is by a factor of 100, while it attains 7000 for $n=2^{18}$. Hence, the importance of FFT techniques increases as the number of data increases (Berge et al 1984).

2.3 AUTOCORRELATION FUNCTION (ACF)

Like the FFT, Autocorrelation function can also be used to characterize a given system. ACF gives an idea about how predictable the system is. It is useful to estimate the disorder by measuring the resemblance of x at time t with itself at a later time $t+\tau$ or it is the degree of resemblance of signal with itself as time passes. It represents the average of the product of the signal values at a given time and at a time $m.\Delta t$ later.

The ACF of a signal x_j can be described in the following manner

$$\psi_m = \frac{1}{n} \sum_{j=1}^{n} x_j \, x_{j+m} \qquad \psi_m = \psi\,(m.\Delta t) \qquad (2.9)$$

where ψ is the ACF of the signal x_j.
If we consider the time series (V_1, V_2, V_n) (Babloyantz et al 1986), then,

$$\psi(\tau) = \left(\frac{1}{n}\right) \frac{\sum_{i=1}^{n} \left[V(t_i) - \bar{V} \right] \left[V(t_i+\tau) - \bar{V} \right]}{\frac{1}{n} \sum_{i=1}^{N} \left[V(t_i) - \bar{V} \right]^2} \qquad (2.10)$$

where $\bar{V} = \frac{1}{n} \sum_{i=1}^{n} V(t_i)$

According to Wiener-Khintchine theorem,

$$\psi_m = \frac{1}{n} \sum_{k=1}^{n} |\hat{x}_k|^2 \cos\left(\frac{2\pi mk}{n}\right) \qquad (2.11)$$

where $\hat{x}_k$ is a fourier component.
Thus the ACF is, up to a factor of proportionality, the fourier transform of $|\hat{x}_k|^2$. This means that the periodic or quasiperiodic signal resembles itself at later times. That is the behaviour of such systems are predictable.

In the chaotic regime, the power spectrum has a continuous floor, so that $\psi(\tau)$ necessarily tends to zero as τ increases (Figure. 2.7) (Gollub et al 1975, Babloyantz et al 1986). The resemblance of the signal disappears as time increases. In other words the predictability of the signal looses within finite time. Here also it is difficult to distinguish between aperiodic and random signal.

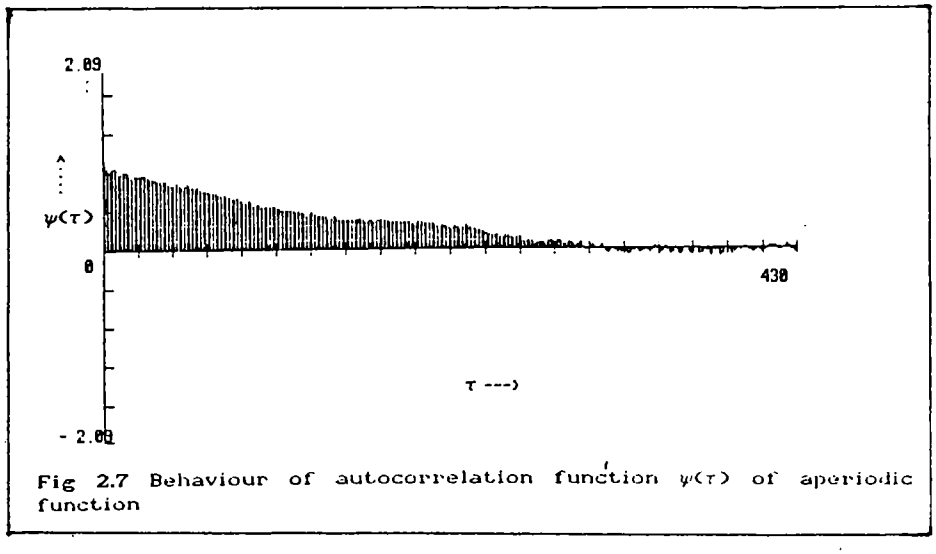

Fig 2.7 Behaviour of autocorrelation function $\psi(\tau)$ of aperiodic function

2.4 POINCARE METHOD

We found in earlier sections that with both FFT and ACF, it is difficult to distinguish between quasiperiodic, aperiodic and random signals. Hence other methods should be searched for. One such method which gives more information about the behaviour of the system in the phase space was developed by Henri Poincare, and is popularly known as the method of 'Poincare section'.

In the case of a three dimensional system (x_1, x_2, x_3) Poincare plane S defined by x_3=constant and trajectory Γ intersect the plane S at $p_0, p_1, \ldots$, where the dynamics are assumed such that x_3 continually crosses from one side of S to the other. Thus starting from an initial condition, we eventually get a number of points on S, which is called the Poincare section.

The transformation leading from one point on S to the next is a continuous mapping T of S into itself called the Poincare map.

$$P_{k+1} = T(P_k) = T(T(P_{k-1})) = T^2(P_{k-1}) = \ldots\ldots = T^l(P_{(K-l+1)})$$

$$= \ldots\ldots = T^{K+1}(P_0) \qquad (2.12)$$

Thus, it is clear that P_0 completely determines P_1, which in turn determines P_2 and so on.

Poincare section and map reflects the property of flow of the system. For example, if the flow is dissipative, its volume in phase space contracts.

In the Poincare method, there is no restriction on the dimension n of the phase space. It converts an n-dimensional

flow into (n-1) dimensional difference map. If the flow is three dimensional, then this method maps the flow on to a plane, reducing the number of coordinates by one. Secondly, the time is discretized and time interval between two successive points is not constant. The differential equations are replaced by difference equations, by Poincare map P→T(P), so that it is easy to manipulate the equations to get a sequence of points x_1, x_2, ... , x_n by successive iterates of a difference map

$$x_{n+1} = f (x_n) \qquad (2.13)$$

The Poincare sections usually have the following appearance, a point or a number of points are located along a single curve, or distributed on a surface. In the case of a periodic system the Poincare section is a single point in a plane and this point is called fixed point of Poincare map T. This can be represented by

$$P_o = T (P_o) = T^2 (P_o) = ... \qquad (2.14)$$

In the case of a truly quasiperiodic system, the Poincare section has a number of points which looks like a simple curve (Fig. 2.8a). If the frequencies are commensurate the curve will have only a limited number of points while with incommensurate frequencies it will be densely filled. For aperiodic or chaotic system the points are distributed on a

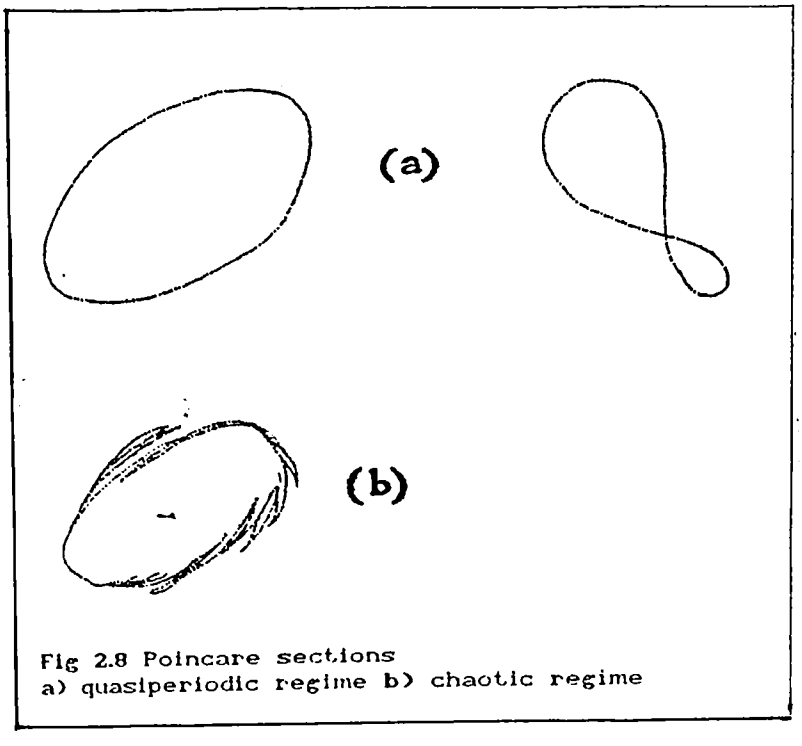

Fig 2.8 Poincare sections
a) quasiperiodic regime b) chaotic regime

surface as shown in Figure (2.8b). But even with this method, it may not always be helpful to distinguish between an aperiodic system which is strongly contracting and a quasiperiodic system. This is because the contraction of area for a strongly contracting aperiodic system may be too rapid so that Poincare section will look like a simple curve as in the case of quasiperiodic systems.

For example in the Lorenz model, the Poincare section in the X,Y plane with Z=r-1 consists of only two line segments as in Figure (2.9). This implies that the trajectories can be inscribed almost on a surface and the attractor has dimension two. But Lorenz attractor has a complex structure consisting of a large number of closely packed sheets. Its Hausdorff-Besicovitch dimension is 2.06. These results prove that the Lorenz attractor is not a simple surface. The reason for the fractal dimension to be very close to two is due to the strong volume contraction.

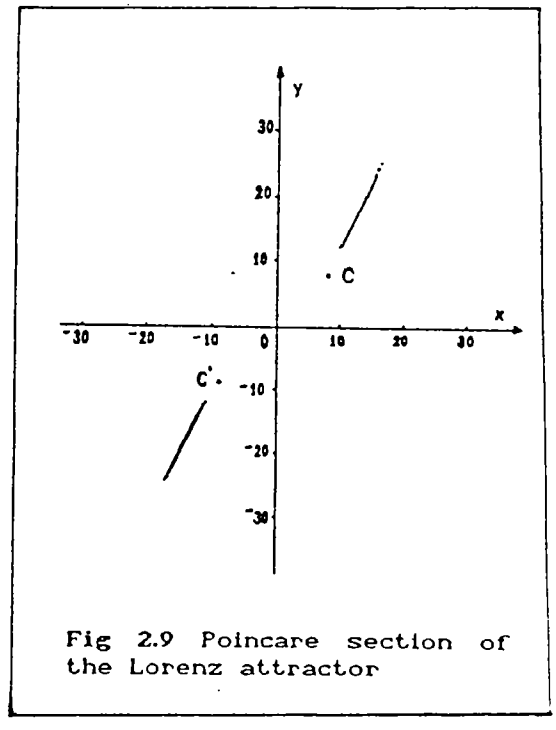

Fig 2.9 Poincare section of the Lorenz attractor

2.5 LIMITATIONS OF CONVENTIONAL TECHNIQUES

FFT, ACF and the method of Poincare section are three signal processing techniques which are useful for classifying the systems in a general way. However, these give only qualitative ideas about the dynamics of the system. They do not quantify any of the characteristic properties of the system. Even though we are able to say that whether or not the system is chaotic, these methods do not tell us how much chaotic, the system is. A study, therefore, using these techniques will have its own limitations

(Froehling et al 1981).

FFT and ACF are usually valid only for linear systems which obey Dirichlet's condition regarding the continuity and finite number of finite discontinuities. Any Fourier decomposition of a given dynamical process would imply the existence of a fundamental frequency and other frequencies could be commensurate to this fundamental frequency. However, a nonlinear process can arise from the existence of two or more incommensurate fundamental frequencies in the system, and this will not be revealed by a Fourier decomposition or ACF. Thus for thermodynamically open nonlinear systems like, for example, the neural network, principles like superposition and ergodicity are not valid and hence FFT or ACF methods are inadequate for this analysis. Furthermore, such systems can also exhibit non Markovian characteristics giving, thereby, memory effects. Mathematically speaking, superposability of harmonic functions which is the basic property used in Fourier analysis, would break down if the system is nonlinear.

It is in the above context that recently developed theories of nonlinear dynamical systems exhibiting deterministic chaos (Atmanspacher and Scheingraber 1986, Grassberger and Procaccia 1983a,b,c & 1984, Schuster 1984, Holden 1986, Hao Bai-Lin 1985, Cvitanovic 1984) gets more attention in the field of nonlinear physics.

2.6 NONLINEAR ANALYSIS

Dissipative dynamical systems are characterized by the attraction of all trajectories passing through certain domain of phase space towards a geometrical object called attractor. The attractor is a compact set in phase space which is invariant under the action of the flow or mapping. The set of initial conditions giving rise to trajectories converging towards the attractor is called the basin of attraction.

There are four types of attractors. Let us briefly describe them. The simplest among these is the point attractor. It describes a solution which is independent of time - that is a steady state. This is essentially a fixed point in the phase space. The limit cycle is the second type of attractor, and is basically characterized by its amplitude and period. Its fourier spectrum contains only a single fundamental frequency and possibly a certain number of harmonics. The solution to the flow can always be expressed as a Fourier series and if the state of the system is known at a given time, one can predict its state at all later times.

A third type of attractor is the torus T^r $(r \geq 2)$ which corresponds to a quasiperiodic regime with r independent fundamental frequencies. Here also the Fourier spectrum is composed of a set of lines, whose frequencies are linear combinations of fundamental frequencies. While the solution to the flow cannot generally be put into the form of an ordinary Fourier series, it is still possible to calculate the state of the system starting from a given initial condition.

The attractor of systems exhibiting chaos are quite different. They are called strange attractors (Ruelle and Takens 1976). To understand the strange behaviour of such attractors, it is necessary to discuss some of the general features exhibited by almost all chaotic systems (Roux et al 1983, Babloyantz et al 1986, Reghunath et al 1987, Nicolis and Nicolis 1986, Albano et al 1985), (i) its power spectrum is continuous or broad band and (ii) the autocorrelation function of the time signal has only finite support, that is, it goes to zero in finite time. The strange attractors have the following properties (Schuster 1984, Atmanspacher et al 1986)

1) phase trajectories are attracted towards it
2) Pairs of neighbouring trajectories diverge on it
3) trajectories are sensitive to initial conditions
4) its dimension D is fractal

We have seen that there are two types of systems *viz.*, Regular systems characterized by simple attractors (equilibrium

point, limit cycle or torus) with integer dimension and chaotic systems characterized by strange attractors which have noninteger dimension. How can we classify these systems ? Even though they can be characterized by Fourier analysis, the method does not distinguish between chaos involving small number of degrees of freedom and white noise. Such a distinction can be made with the help of Poincare section. But this method offers only qualitative information and also it is not quite practicable for systems with higher dimensions.

A quantitative characterization can be done using certain characteristics of attractors in phase space. Two of such significant properties of chaotic systems are the Hausdorff dimension of the attractor and Kolmogorov entropy.

Kolmogorov entropy, as we have already seen (section 1.12), is connected with the divergence of trajectories in phase space (Benettin et al 1976) or creation of information. In this connection we can define a whole set of dimension D_q (Hentschel et al 1983) and entropies K_q (Grassberger and Procaccia 1983 b & c), which generalize the concept of Hausdorff dimension and Kolmogorov entropy (Pawelzik and Schuster 1987). We shall discuss about these in the latter part of this chapter.

2.7 GENERALIZED DIMENSIONS

Trajectories of certain dissipative dynamical systems exhibiting chaotic behaviour shrinks towards an attractor whose dimension is less than the dimension of phase space, and is strange in character (Lorenz 1963, 1984, Ruelle et al 1971, Ott 1981). As indicated earlier, strange attractors can be characterized by their characteristic dimensions. Some of the important dimensions among generalized dimensions which are commonly used to describe nonlinear systems are fractal dimension, information dimension and correlation dimension.

We try to understand the generalized dimension in detail in this section. Let us describe the given dynamical system by a differential equation $\frac{dX}{dt} = F(X)$, where X is a d-dimensional vector obtained from a single time series by using a delay time τ,

$$X(t) = \left\{ x(t),\ x(t+\tau) \ \ldots\ldots\ldots\ldots\ x(t+(d-1)\tau) \right\} \qquad (2.15)$$

Now consider a d-dimensional phase space which is uniformly partitioned into boxes of size ε, and N points $\{X_i\}_{i=1}^{N}$ in a time sequence which are given by sampling the signal X(t). One can estimate the invariant probability measure p_i associated with box i by N_i/N, where N_i is the number of points falling within the box i, provided N is large enough. In general, it has been shown that generalized dimension D_q , of order q (Hentschel and Procaccia 1983, Sato et al 1987) can be defined as

$$D_q = \frac{1}{(q-1)} \underset{\varepsilon \to 0}{Lt} \frac{\ln \left(\sum_i p_i^{\,q} \right)}{\ln (\varepsilon)} \qquad (2.16)$$

The order of parameter q can take all real values between $-\infty$ and $+\infty$. For $q=-\infty$, it characterizes the rarer regions, while for $q=\infty$, describes the denser regions of the set. Thus in (2.16) an infinite hierarchy of dimensions are implied.

In (2.16) $p_i(\varepsilon)$ is the probability that the trajectory X_1, X_2, ...X_N on the strange attractor visits the box i. Since $\sum_i p_i^q$ can be written in terms of the natural probability measure $\mu(x)$ on the attractor as

$$\sum_i p_i^{\,q} = \int d\mu(x) \left[\mu \left(B_\varepsilon(x) \right) \right]^{q-1} \qquad (2.17)$$

where $B_\varepsilon(x)$ denotes a ball of radius ε around x and

$$\sum_i p_i^q = \frac{1}{N} \sum_{j=1}^{N} \tilde{p}_j^{q-1}(\varepsilon) \qquad (2.18)$$

where $\tilde{p}_j(\varepsilon)$ is the probability to find a point of the trajectory within the ball of radius ε around a point X_j of the trajectory. The change q to (q-1) in the exponents in equation (2.18) is due to the fact that we switch from $p_i(\varepsilon)$ to $\tilde{p}_j(\varepsilon)$ (Pawelzik and Schuster 1987). That is, we are switching from the probability to find the trajectory in one of the homogeneously distributed boxes introduced above, to the probability to find the trajectory within a ball around one of the inhomogeneously distributed points of the trajectory.

$$\tilde{p}_j(\varepsilon) = \frac{1}{N} \sum_i \Theta (\varepsilon - |X_i - X_j|) \qquad (2.19)$$

By combining equation (2.16)-(2.19)

$$D_q = \lim_{\varepsilon \to 0} \frac{1}{\ln(\varepsilon)} \ln C^q(\varepsilon) \qquad (2.20)$$

where

$$C_d^q(\varepsilon) = \left[\frac{1}{N} \sum_i \left[\frac{1}{N} \sum_j \Theta (\varepsilon - |X_i - X_j| \right]^{q-1} \right]^{1/(q-1)} \qquad (2.21)$$

and

$$C_d^q(\varepsilon) = \left[\frac{1}{N} \sum_i \left[\frac{1}{N} \sum_j \Theta\left(\varepsilon - \left[\sum_{m=0}^{d-1} (x_{i+m} - x_{j+m})^2 \right]^{1/2} \right) \right]^{q-1} \right]^{1/(q-1)} \qquad (2.22)$$

Among D_q, the important ones are D_o, D_1 and D_2 with $D_o \geq D_1 \geq D_2$. It has been shown that D_o corresponds to D_f, the fractal dimension and D_1 is identical to D_I, the information dimension (Hentschel and Procaccia 1983) and D_2 is known as the correlation dimension. For a homogeneous system, all these dimensions are equal to fractal dimension, i.e., $D_o = D_1 = D_2 = \ldots\ldots D_\infty$. The inhomogeneity of the system is reflected in the inequalities of D_q for different q's (Schuster 1984).

2.8 BOX-COUNTING ALGORITHM

Fractal dimension D_o (D_f) is usually used to describe the dynamics of the system quantitatively. Consider a set of points in a d-dimensional space, and if $N(\varepsilon)$ is the smallest number of cubes necessary to cover this set, then D_o is defined as

$$D_o = \lim_{\varepsilon \to 0} \frac{\ln N(\varepsilon)}{\ln(1/\varepsilon)} \qquad (2.23)$$

Box-counting by Taken's algorithm (Takens 1981) is used to evaluate this fractal dimension, which does not take into account of the probabilities. This algorithm counts the number of boxes necessary to cover the set. The time dependence of the system with finite capacity can be described by finite-dimensional deterministic mathematical model. Nonintegral capacity represent

a chaotic system. Infinite capacity implies that an infinite number of degrees of freedom are needed to describe the dynamical system, which is not possible in terms of both Landau's theory and theory of strange attractors.

If the set has volume V, the number of boxes of side ε needed to cover the set is

$$N(\varepsilon) \cong V\ \varepsilon^{-D_o}$$

for small ε.

Then,

$$\ln N(\varepsilon) = D_o \ln (1/\varepsilon) + \ln V \qquad (2.24)$$

Equation (2.24) is more suitable than equation (2.23) especially for processing experimental data because it has a slowly vanishing correction to the capacity $V/\ln(1/\varepsilon)$. D_o can be calculated as the asymptotic slope of the plot $\ln(N(\varepsilon))$ against $\ln(1/\varepsilon)$ for small ε.

Takens (Takens 1981) showed that it is possible to compute D_o from a single time series, represented by the infinite sequence of real numbers $\{a_i\}_{i=1}^{\infty}$. For this purpose, he constructed a phase space with infinite set of D=n+1 dimensional vectors,

$$S_D = \left\{ < a_i, \ldots\ldots\ldots a_{i+n} > \right\}_{i=1}^{\infty} \qquad (2.25)$$

$$n \geq 0$$

Capacity calculated using Taken's method in the case of 2/3 Cantor set, Quadratic return map and Henon map are in good

agreement with other methods (Greenside et al 1982).

2.9 IMPRACTICABILITY OF BOX-COUNTING ALGORITHM

Box counting algorithm is very slowly converging even for low dimensional attractors ($D_o < 2$). Also, it has severe computational difficulties in calculation for any set whose capacity is greater than two (Mizrachi et al 1984).

Greenside et al [1982] tested Taken's box counting algorithm on several dynamical systems, the capacity of which has been known by other methods. For low dimensional systems, $D_o \leq 2$, the method works and the number of points necessary to determine the capacity is within the limits.

They have also applied Taken's algorithm in hydrodynamical models, three variable model by Lorenz (Lorenz 1963) and 14 variable model by Curry (Curry 1978). Taken's algorithm converges for large ε. However, for smaller ε, the algorithm failed to converge for both models even when about a million points were used.

One of the fundamental reasons why enormously long time series may be needed to calculate the capacity by box-counting method is the exponential dependence of $N(\varepsilon)$ on D_o. Two other reasons are, (i) the set S_D often fills out the attractor in a highly nonuniform way and (ii) dynamical system may rapidly contract the volumes in phase space, making it difficult to obtain the nonintegral part of the capacity, which arises from the fractal structure.

Hence the box-counting algorithm is not useful for high dimensional and rapidly contracting attractors, like those encountered in the Lorenz model. But this method gives successful results in the case of low dimensional systems like 2/3 Cantor set and Henon map which have slow rate of phase space contraction.

2.10 CORRELATION DIMENSION

We have seen that fractal dimension D_o is difficult to evaluate for higher dimensional systems. To override this difficulty a new dimension called correlation dimension D_2 is introduced. It has been suggested that strange attractors can be characterized by D_2 (Grassberger and Procaccia 1983a,b,c, Mizrachi et al 1984). The Grassberger-Procaccia algorithm (GP algorithm) to evaluate D_2 are efficiently converging even with small number of experimental points and even at higher dimensions (Atmanspacher et al 1986). For example, this algorithm yields accurate value of D_2 for higher dimensional system, with as small as 500 data points (Abraham et al 1986).

Correlation dimension D_2 is a probabilistic type of dimension. It can be calculated in terms of correlation integral

$$C_d(\varepsilon) = \lim_{N\to\infty} \sum_{i,j=1}^{N} N^{-2} \; \Theta \; (\varepsilon - |\vec{X}_i - \vec{X}_j|) \qquad (2.26)$$

$$= \int_o^{\varepsilon} d^d \varepsilon' \; c \; (\vec{\varepsilon}')$$

where $\theta(x)$ is the Heaviside function and $C_d(\varepsilon)$ is the standard correlation function in d dimensional space. $\theta(x)=0$ for $x\leq 0$ and unity for $x>0$. N^{-2} is a normalization factor and $|X_i-X_j|$ represents the Euclidean norm of (X_i-X_j). Equation (2.26) gives the number of vector difference which are less than ε. This can also be considered as the number of vector tips which lie in a hyperbox whose volume is ε^d in the phase space and in this sense, one can interpret equation (2.26) as a probability measure. The $C_d(\varepsilon)$ behaves as a power of ε for small ε,

(Grassberger and Procaccia 1983a)

$$C_d(\varepsilon) \sim \varepsilon^{D_2} \qquad (2.27)$$

In most of the cases D_2 is very close to D_o, but is never greater than D_o. Now let us find, how D_2, D_1 and D_o are related.

Let us suppose that the attractor has dimension D_o and cover this by hypercube of side length ε. Each cube will have a volume ε^{D_o} and the number of cubes required to cover the attractor is

$$M(\varepsilon) \sim \varepsilon^{-D_o} \qquad (2.28)$$

We have to get a measure of $M(\varepsilon)$ from the correlation function (2.26). Since the equation (2.26) gives the number of points on the attractor, we have to connect $M(\varepsilon)$ with the number of points. Following Grassberger and Procaccia [1983a], let μ_i be the number of points from the set $\{X_i\}$ which are in the i^{th} nonempty cube. We ,then, have

$$C_d(\varepsilon) \simeq \frac{1}{N^2} \sum_{i=1}^{M(\varepsilon)} \mu_i^2 = \frac{M(\varepsilon)}{N^2} \langle \mu^2 \rangle \qquad (2.29)$$

where we have used the box counting. Using Schwartz inequality, in the asymptotic state

$$\lim_{\substack{\varepsilon \to 0 \\ d \to \infty}} C_d(\varepsilon) \geq \frac{M(\varepsilon)}{N^2} \langle \mu^2 \rangle = \frac{1}{N^2 M(\varepsilon)} \left[\sum \mu_i \right]^2 = \frac{1}{M(\varepsilon)} \sim \varepsilon^{D_o} \qquad (2.30)$$

as we take the limit of $d \to \infty$, and used the fact that $\sum_i \mu_i = N$

$$D_2 \leq D_o \tag{2.31}$$

Now, to show that $D_1 \leq D_o$, we consider the following equations

$$D_1 = \lim_{\varepsilon \to o} \frac{S(\varepsilon)}{\ln(1/\varepsilon)} \tag{2.32}$$

where

$$S(\varepsilon) = - \sum_{i=1}^{M(\varepsilon)} p_i \ln p_i$$

where p_i is the probability for a point to fall in the i^{th} cube, as $N \to \infty$. We write,

$$p_i = \mu_i / N \tag{2.33}$$

and for uniform coverage

$$p_i = \frac{1}{M(\varepsilon)} \tag{2.34}$$

The entropy is defined as

$$S^{o}(\varepsilon) = \ln M(\varepsilon) = \text{constant} - D_o \ln \varepsilon \tag{2.35}$$

$S^{o}(\varepsilon)$ is the maximum information needed .

In general,

$$S(\varepsilon) < S^{o}(\varepsilon) \tag{2.36}$$

therefore

$$S(\varepsilon) = S_o - D_1 \ln\varepsilon$$

This means that

$$D_1 \leq D_o \qquad (2.37)$$

By combining equations (2.31) & (2.37), and following the arguments presented by Grassberger and Procaccia (1983a), we get

$$D_2 \leq D_1 \leq D_o \qquad (2.38)$$

Thus D_2 is a significant quantity to characterize the strangeness of the attractor, it is a lower bound on the Hausdorff dimension and it is easy to calculate D_2 from time series. It has also been shown that D_2 is a very prominent one among the set of D_q's (Caputo and Atten 1987). It has also been established that D_2 is integer for regular system, noninteger for chaotic system and $D_2 \sim d$ for completely stochastic system (see table 2.1) (Atmanspacher and Scheingraber 1986).

Table 2.1 Dimensions and entropies of different systems

	Dimension	Entropy
Regular	$D_2 = D_o$ integer	$K_2 = K_1 = 0$
Chaotic	$D_2 \simeq D_o$ fractal	$K_2 > 0$
Stochastic	$D_2 \to d$	$K_2 \to \infty$

Correlation integral becomes independent of d as $d \to \infty$ and for small values of ε,

$$C_d(\varepsilon) \sim \varepsilon^{D_2}$$

therefore

$$D_2 = \lim_{\substack{d\to\infty \\ \varepsilon\to 0}} \frac{\ln C_d(\varepsilon)}{\ln \varepsilon} \qquad (2.39)$$

$C_d(\varepsilon)$ can be calculated using the equation (2.26).

2.11 GENERALIZED ENTROPY

Unpredictability of chaotic systems due to the exponential rate of divergence of trajectories on strange attractors lead to the creation of information. But in predictable systems trajectories do not create new information. This is an essential difference between chaotic and regular systems. Kolmogorov entropy provides a quantitative measure to classify regular and chaotic system, and is defined to be the mean rate of creation of information (Farmer 1982)

Estimation of Kolmogorov entropy K directly from time signal enable us to quantify, how chaotic the system is, or it will help us to study the information flow in the system using isentropy curves.

To evaluate Kolmogorov entropy, consider a dynamical system with F degrees of freedom. Suppose that the F dimensional space is partitioned into boxes of size ε^F and that there is an attractor in the phase space. The trajectory $\vec{X}(t)$ is assumed to be in the basin of attraction. The state of the system is now measured at intervals of time τ. Let $p(i_1,i_2,i_3,\ldots\ldots i_d)$ be the joint probability that $\vec{x}(t=\tau)$ is in box i_1, $\vec{x}(t=2\tau)$ is in box i_2, and $\vec{x}(t=d\tau)$ is in i_d. The Kolmogorov entropy K is then

$$K = -\lim_{\varepsilon\to 0}\lim_{\tau\to 0}\lim_{d\to\infty} \frac{1}{\tau d} \sum_{i_1\ldots i_d} p(i_1\ldots\ldots i_d) \ln p(i_1\ldots i_d) \qquad (2.40)$$

As is well known (Schuster 1984, Grassberger and Procaccia 1983c, Cohen et al 1985) K=0 for an ordered system, and K=∞ for stochastic system and K is a nonzero constant for a chaotic system.

Calculation of Kolmogorov entropy K is not difficult for analytically defined models in terms of evolution of the distance between two initially close points, but it is very difficult to determine K directly from a measured time signal (Grassberger and Procaccia 1983c).

2.12 KOLMOGOROV SECOND ENTROPY (K_2)

Grassberger and Procaccia (1983c) defined a new quantity, *viz.*, Kolmogorov Second entropy K_2, which can be extracted easily from an experimental signal. K_2 is an invariant measure of the system, and has the following properties (see table 2.1).

i) $K_2 \geq 0$

ii) $K_2 \leq K$

iii) K_2 is infinite for random system (Completely stochastic system).

iv) $K_2 \neq 0$ for chaotic system

v) $K_2 = 0$ for ordered system

For typical cases, K_2 is close to K. K_2 is a member of the set of generalized entropies (order-q Renyi entropies) which is defined as

$$K_q = - \lim_{\varepsilon \to 0} \lim_{\tau \to 0} \lim_{d \to \infty} \frac{1}{\tau d} \frac{1}{q-1} \ln \sum_{i_1 \ldots i_d} p^q (i_1 \ldots i_d) \qquad (2.41)$$

q can take any real values between $-\infty$ and $+\infty$ and $p(i_1, i_2, \ldots i_d)$ is the joint probability that the trajectory visit the boxes

$i_1, i_2 \ldots i_d$.

First order entropy,

$$K_1 = \lim_{q \to 1} K_q ,$$

is the metric entropy which is a measure of the internal information production of the system during its temporal evolution. On putting

$$p^q = p \exp(q-1) \ln p$$

in equation (2.41), we obtain

$$K_1 = - \lim_{\varepsilon \to 0} \lim_{\tau \to 0} \lim_{d \to \infty} \frac{1}{\tau d} \sum_{i_1 \ldots i_d} p(i_1 \ldots i_d) \ln p(i_1 \ldots i_d) \qquad (2.42)$$

Thus $K_1 = K$, the Kolmogorov entropy. Here K_1 is approximately identical with the sum of positive LE's of the system. From equation (2.20) & (2.21), K_q can be defined in terms of correlation integral (Pawelzik and Schuster 1987) as

$$K_q = \lim_{\varepsilon \to 0} \lim_{d \to \infty} \left[- \frac{1}{d\tau} \ln C_d^q(\varepsilon) \right] \qquad (2.43)$$

K_2 gives the lower bound for the Kolmogorov entropy. It can be defined in terms of correlation integral as in the case of D_2. K_2 is singled out from K_q due to its ease of calculation from a time series. We shall establish this as follows, consider the equation (2.41) for q=2 and for any value of d, and let ε be

fixed. The equation for $C_d^2(\varepsilon)$ (Grassberger et al 1983c) is

$$C_d^2(\varepsilon) = \sum p_i^2 \qquad (2.44)$$

where p_i is the probability to visit the i^{th} box and sum i runs over all the boxes in phase space which contain a piece of attractor. This quantity $C_d^2(\varepsilon)$ can be easily calculated from a given time series.

We have already shown (Equation 2.27) that $C_d(\varepsilon)$ scales like

$$C(\varepsilon) \sim \varepsilon^{D_2}$$

Hence this equation and (2.41) would yield

$$C_d(\varepsilon) \underset{\substack{d\to\infty \\ \varepsilon\to 0}}{\sim} \varepsilon^{D_2} \exp(-d\tau K_2) \qquad (2.45)$$

Then

$$C_{d+1}(\varepsilon) \sim \varepsilon^{D_2} \exp\left(-(d+1)\tau K_2\right)$$

and $K_{2,d}(\varepsilon)$ is

$$K_{2,d}(\varepsilon) = \frac{1}{\tau} \ln \left\{ \frac{C_d(\varepsilon)}{C_{d+1}(\varepsilon)} \right\} \qquad (2.46)$$

If we plot log $C_d(\varepsilon)$ vs log(ε) we will get a series of lines with a linear part of slope $D_{2,d}$, and which are separated from each other by a factor $\exp(-d\tau K_{2,d})$. The second Kolmogorov entropy K_2 is

$$K_2 \sim \lim_{\substack{d\to\infty \\ \varepsilon\to 0}} K_{2,d}(\varepsilon) \qquad (2.47)$$

2.13 EVALUATION OF D_2 AND K_2 FROM TIME SERIES - GP ALGORITHM

GP algorithm is an efficient method to evaluate D_2 and K_2 from an experimental data obtained as a time series.

Consider the time series

$$\vec{X} = \left\{X(t_1), X(t_2) \ldots\ldots\ldots\ldots X(t_N)\right\} \qquad (2.48)$$

where $X(t_i)$ is the voltage or temperature or density distribution or any fluctuations measured at the instant t_i. We usually take the time interval between two consecutive readings at constant τ, and this series is rearranged in the following matrix form

$$\begin{array}{llll}
x(t) & x(t+\tau) & \ldots\ldots\ldots & x(t+\overline{m-1}\tau) \\
x(t+\tau) & x(t+2\tau) & \ldots\ldots & x(t+m\tau) \\
\vdots & \vdots & & \vdots \\
x(t+\overline{d-1}\tau) & x(t+d\tau) & \ldots\ldots\ldots & x(t+\overline{m+d-2}\tau)
\end{array} \qquad (2.49)$$

This forms a matrix of m columns and d rows and is called a delayed matrix (Broomhead & King 1986). The matrix (2.49) can be considered as m vectors (columns) defined in a d-dimensional phase space and $m \geq d$. The matrix (2.49) can be represented by the following,

$$\vec{X}_i(t_i) = \left\{ X_i(t_i),\ X_i(t_i+\tau) \ldots\ldots X_i(t_i+\overline{d-1}\tau)\right\} \qquad (2.50)$$

where $t_i = t + (i-1)\tau$, i running from 1 to m. Equation (2.50) represents the various vectors (column) and using these vectors, one can evaluate the correlation integral (equation 2.26),

$$C_d(\varepsilon) = \sum_{i,j=1}^{N} N^{-2} \Theta (\varepsilon - |\vec{X}_i - \vec{X}_j|) ,$$

by counting the number of points whose distance is less than a pre assigned value ε, where ε varies from small value ($\sim$ 0, say 0.0012), to large value ($\sim$ 1). $C_d(\varepsilon)$ is calculated using (2.26) for various ε and for each particular dimension d of the constructed phase space. The plot of log $C_d(\varepsilon)$ vs log (ε) for each d (Figure 2.10) will have a linear region with a slope ν.

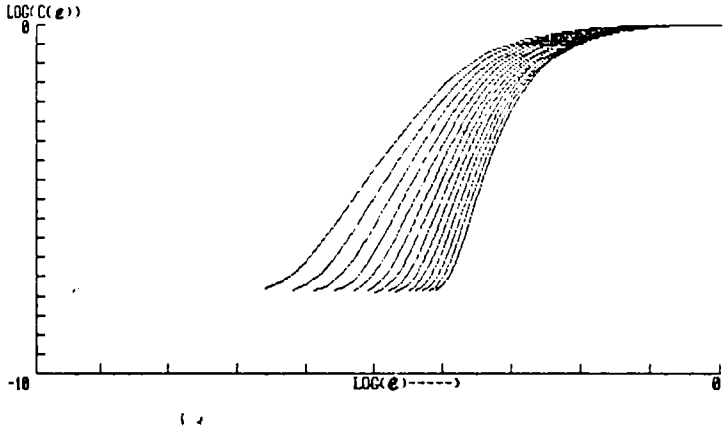

Fig 2.10 A typical Log-Log plot of $C_d(\varepsilon)$

$$\nu = \frac{\ln C_d(\varepsilon)}{\ln (\varepsilon)}$$

2.14 CALCULATION OF D_2

The slope ν of the linear part of log $C_d(\varepsilon)$-log(ε) plot for each dimension d is evaluated. The plot of ν vs dimension d (Figure 2.11), saturates to a finite value as d increases, and the saturated value of ν is the second order dimension or correlation dimension D_2. If the data set consists of completely random noise, then the points would lie on the

straight line with 45° to the d-axis (Babloyantz et al 1986). On the other hand, if there exists a deterministic component in the system, the curve would saturate to D_2 and would become independent of d. The dimension d at which the ν curve starts to saturate or the region at which the deterministic and random parts completely separate is the embedding dimension (In figure 2.11 saturation starts at d=12).

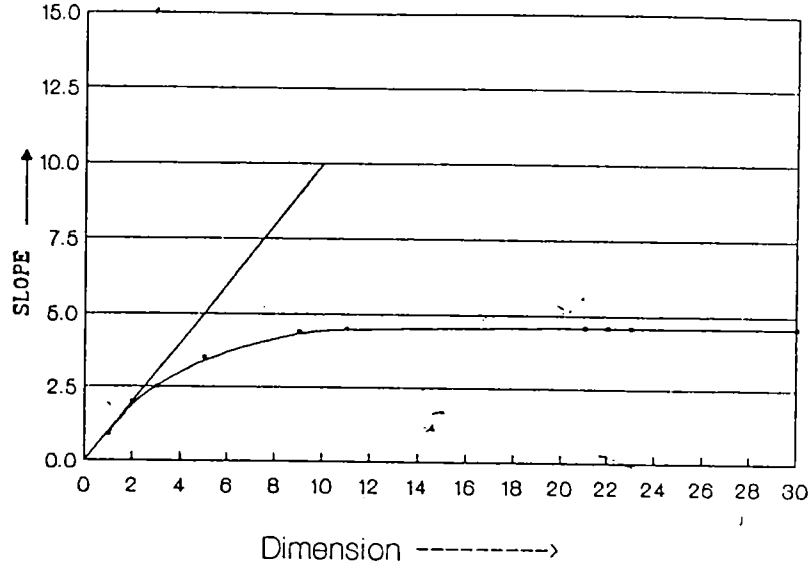

Fig 2.11 Slopes of the linear part of the curves in figure 2.10, plotted against dimension d.

2.15 CALCULATION OF K_2

The second quantity of great interest is the Kolmogorov Second entropy K_2. This can be measured using the correlation integral by evaluating the ratio of spatial separation between the curves in Figure (2.10) for dimension d and d+1. The mean value of $C_d(\varepsilon)/C_{d+1}(\varepsilon)$ over the linear range of ε is calculated for each dimension and we write

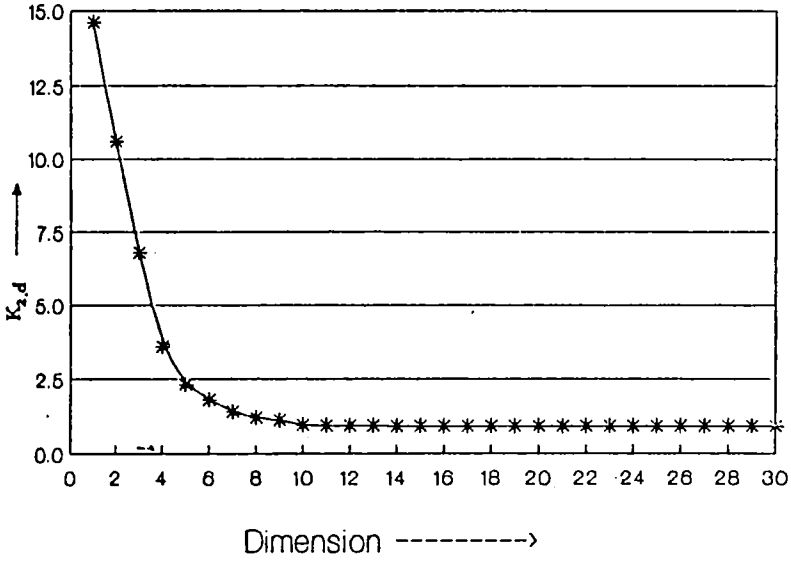

Fig 2.12 K_2 is the asymptote of the curve (d → ∞).

$$K_{2,d} = \lim_{\substack{\varepsilon \to 0 \\ \tau \to 0}} \frac{1}{\tau} \ln \left[C_d(\varepsilon) / C_{d+1}(\varepsilon) \right]$$

$K_{2,d}$ is plotted against dimension d, and the curve will saturate as shown in Figure (2.12). The saturated value of $K_{2,d}$ as $d \to \infty$ is the Second Kolmogorov entropy (Equation 2.46).

$$\lim_{d \to \infty} K_{2,d} \longrightarrow K_2$$

We can classify the systems by comparing the values of D_2 and K_2 with values in the table (2.1).

The algorithm we shall be using in the thesis is the one developed by Atmanspacher and Scheingraber [1986] which has been modified for smaller data sets by Abraham et al [1986]. But, before any numerical scheme is used for the purpose of analysis of any unknown system, it should be subjected to certain known system, so that an evaluation of the efficiency and accuracy of the numerical code could be done.

2.16 PERIODIC SYSTEM

To test our algorithm, we used the sine series. The correlation integral was calculated for d varying from 1 to 30 from 512 data extracted from the digitized values of ten successive periods of the sine function (Sin X). Then log $C_d(\varepsilon)$ is plotted against log ε. All the curves are parallel to each other with equal slopes. Slopes of the curves (ν) were plotted against dimension d and it is seen that the ν curve is parallel to d-axis (Figure 2.13), and D_2=1. The behaviour of entropy also shows that the system is ordered ($K_2 \approx 0$) (Figure 2.14). Sine

function represents a periodic system with a single frequency, so

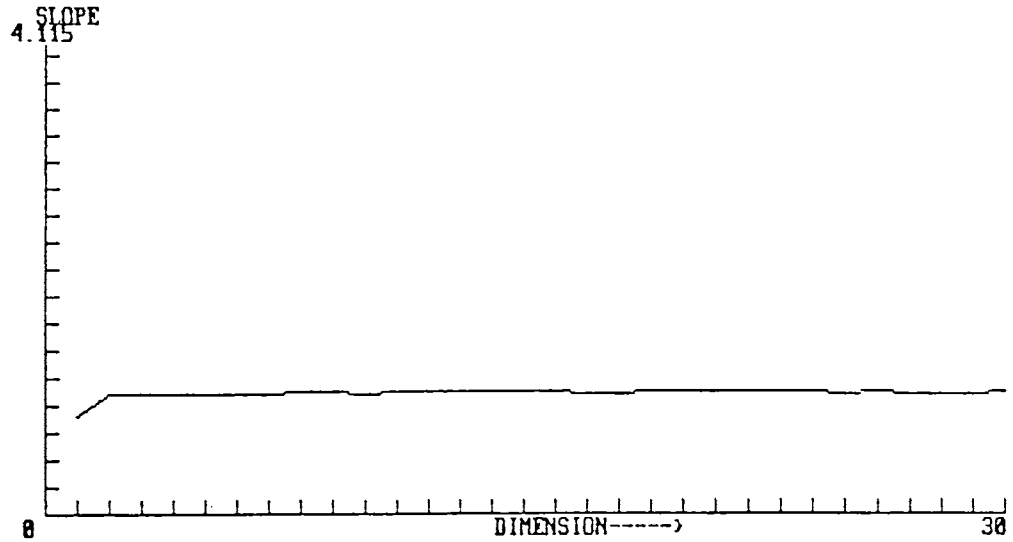

Fig 2.13 Slope of the linear part of log-log curves $C_d(\varepsilon)$ of sine series, plotted against dimension.

that $D_2=1$ is an expected result. Thus the Second order dimension represent the number of frequencies present in the system, or it measures the number of independent parameters required to define the system. Therefore our algorithm is in good agreement with what we are expecting.

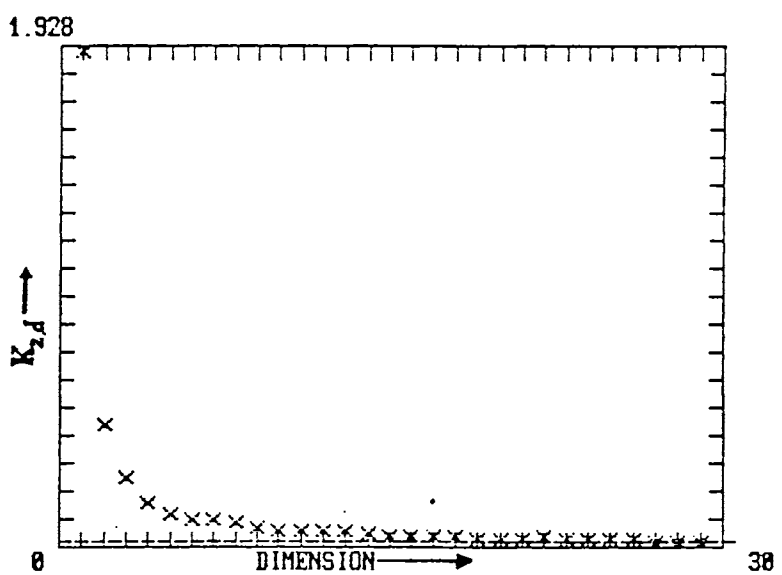

Fig 2.14 $K_{2,d}$ vs d of sine series

2.17 CALCULATION OF D_2 AND K_2 FROM SMALL DATA SETS

Box-counting algorithm is not practical for dimension calculation since it needs large computer memory and time and also requires large amount of data to obtain satisfactory results.

The GP algorithm is suitable for D_2 and K_2 evaluation, but there is a usual assumption that a large number of data is required for accurate results. This has been first investigated by Abraham and his colleagues [1986]. They evaluated the dimension of logistic equation using 500, 1200, 5000 data, and in all these cases D_2 was found to be more or less same (D_2 is 0.92 for N=500, D_2=0.94 for N=1200, D_2=0.93 for N=5000). In the case of Henon attractor they got D_2=1.28 for N=500, D_2=1.20 for N=1200, D_2=1.24 for N=4000 and D_2=1.24 for N=10,000. These results show that the GP algorithm leads to successful results in the case of small data sets. Abraham et al [1986] calculated the slope in a slightly different way. They calculated slope of the curve log $C_d(\varepsilon)$ vs log(ε) for each ε and plotted it against log $C_d(\varepsilon)$. For small values of ε, slope fluctuates due to noise, and for larger values of ε it displays an increase in the slopes as the largest interpoint distances on the attractor are reached, and then saturate to a constant value of log C_d.

We investigated the data dependence of GP algorithm in Neural system also. For this, we used a digitized Electroencephalogram data. We calculate D_2 for 1357 and 227 data points and obtained the values of D_2 as 3.56 and 3.50 respectively.

2.18 ADVANTAGES OF GP ALGORITHM

The correlation dimension D_2 as mentioned earlier, is one of an infinite set of dimensions that characterize the strange attractor. It is singled out by the ease of the actual calculation from time series (Caputo and Atten 1987). D_2 is defined in terms of correlation integral (equation 2.26) using the power law given in equation (2.27).

Now the question arises about the role of noise present in the time series. The basic idea is that when we have a deterministic motion on a strange attractor, the existence of noise will not ruin the structure of the attractor, but will cause fuzziness on the length scales that are much smaller or equal to the noise strength (Shaw 1981, Zardecki 1982). But the quantification of strangeness using GP algorithm gives a clear demarcation between deterministic and random part of the signal.

According to Mizrachi et al [1984] if we embed the attractor in a d-dimensional space, we expect that the noisy trajectory will be space filling on length scales smaller than the noise strength and scales like

$$C(\varepsilon) \sim \varepsilon^d \qquad (2.51)$$

The plot of log $C(\varepsilon)$ as a function log(ε) will have a slope of D_2 down to length scales characterized by the noise strength and then a slope of d.

To find D_2 according to GP algorithm, we construct a phase space with dimension d and plot log $C(\varepsilon)$ vs log(ε). For each value of d we get a curve with a linear part with slope equal to $D_{2,d}$ above the length scales characterizing the noise strength. All curves will break at that value of ε, below which the slope is equal to d. Mizrachi et al [1984] explained it in terms of Mackey-Glass equation, and showed that for a given parameter the

strange attractor is characterized by D_2=1.95. The noise strength is 10^{-3}.

Thus GP algorithm has the following advantages

1) Suitable for small data sets
2) It characterizes attractors
3) It gives information on the noise level of the system, i.e; the position of break in $\log_2 C(\varepsilon)$ vs $\log_2(\varepsilon)$ plot
4) It separates deterministic and random component present in the system.

2.19 SPECTRA OF SCALING INDICES (f(α) SPECTRA) FOR FRACTAL GEOMETRIES

The subset of phase space to which a typical orbit of a chaotic noncommensurate system asymptotes with time is called strange attractor and can have fractal geometry. Fractal measures can provide a phenomenological description of strange attractors. In order to obtain a more complete characterization we should consider the structure of scaling indices or singularities on a fractal measure (Halsey et al 1986b). We consider a function f(α) where α is the scaling index of the measure about a point on the fractal and f(α) is the dimension of the set of points on the fractal with same value of α.

Suppose that we have a time series of N points on a strange attractor in the phase space of a dynamical system. Typically, trajectories in chaotic dynamics does not fill the d-dimensional phase space even when N→∞, because the trajectory lies on a strange attractor of dimension D , D < d. Defining

$$p_i = \lim_{N\to\infty} N_i / N$$

where N_i is the number of times the time series visits the

i^{th}box, we generate the measure on the attractor. If the system is divided into pieces of size l, and defining a scaling exponent α, we can write

$$P_i \sim l_i^{\alpha} \qquad (2.52)$$

α can take on a range of values, corresponding to different regions of the measure (Halsey et al 1986a). The number of times α takes on a value between α' and $\alpha'+d\alpha'$ will be of the form

$$d\alpha' \; \rho(\alpha') \; l^{-f(\alpha')} \qquad (2.53)$$

where $f(\alpha')$ is a continuous function (Halsey et al 1986c). The exponent $f(\alpha')$ reflects the differing dimensions of the sets with singularities of strength α'. Thus we model fractal measures by interwoven sets of singularities of strength α, each characterized by its own dimension $f(\alpha)$.

We can relate $f(\alpha)$ to a set of dimensions which have been introduced by Hentschel and Procaccia [1983], the set of D_q defined by (see section 2.7)

$$D_q = \lim_{l \to 0} \left\{ \frac{1}{q-1} \frac{\ln \chi(q)}{\ln l} \right\} \qquad (2.54)$$

where $\chi(q) = \sum_i p_i^q$

D_o is the fractal dimension, D_i is the information dimension and D_2 is the correlation dimension (Grassberger and Procaccia 1984, Grebogi et al 1988). Substituting for p_i

$$\chi(q) = \int d\,\alpha'\ \rho(\alpha')\ \iota^{-f(\alpha')}\ \iota^{q\alpha'} \qquad (2.55)$$

since ι is small, the integral will be dominated by value of α' which makes $q\alpha'-f(\alpha')$ smallest (Sato et al 1987)
Thus,

$$\frac{d}{d\alpha'}\left[q\alpha' - f(\alpha')\right]_{\alpha'=\alpha(q)} = 0 \qquad (2.56)$$

also $$\frac{d^2}{d(\alpha')^2}\left[q\alpha' - f(\alpha')\right]_{\alpha'=\alpha(q)} > 0$$

so that $$f'\left[\alpha(q)\right] = q \qquad (2.57a)$$

$$f''\left[\alpha(q)\right] < 0 \qquad (2.57b)$$

It follows that (Halsey et al 1986b)

$$D_q = \frac{1}{(q-1)}\left[q\alpha(q) - f[\alpha(q)]\right] \qquad (2.58)$$

Thus if we know the $f(\alpha)$ spectrum, we can find D_q. Alternatively, knowing D_q we can find $\alpha(q)$ since

$$\alpha(q) = \frac{d}{dq}\left[(q-1)D_q\right] \qquad (2.59)$$

and hence $f(\alpha)$ can be evaluated from equation (2.58).

If a continuous scaling spectrum $f(\alpha)$ exists, then the above relationships implies that it must be convex. Furthermore, $f_{max}(\alpha)$ will be equal to the dimension D_o of the attractor. The minimum scaling exponent α_{min} will correspond to the most concentrated region of measure on the attractor and α_{max} will correspond to the most rarefied region of the measure (Halsey et al 1986c).

$f(\alpha)$ spectrum can be measured experimentally and will result in new tests of scaling theories of nonlinear systems. We have evaluated $f(\alpha)$ spectra from EEG recording, results of which are included in later chapters.

CHAPTER 3

NOISE FILTERING IN TIME SERIES ANALYSIS

A mathematical technique for filtering noise from time series data is described.

NOISE FILTERING IN TIME SERIES ANALYSIS

In most of the experiments, the output signal is mixed with noise. It may not be possible to filter out the noise completely from signal using electronic circuits due to various reasons such as very small signal to noise ratio (SNR), large frequency band width of noise, etc.

As already discussed in chapter 2, GP algorithm (Grassberger and Procaccia 1983a, b, c) discriminates between the deterministic and random part of a system using time series. The noise makes the correlation curve (Fig.2.10) to deviate from linearity. The slope vs dimension curve (Fig.2.11) also show the noise effect at low values of d, where the curve coincides with 45° line. However, this method does not have any means for separating noise from raw data (Passamante et al 1989). The phase space representation of the system shows that the presence of noise will not ruin fractal structure, but it may change the view of the attractor (Mizrachi et al 1984).

This chapter describes a mathematical technique for filtering noise embedded data. The method is suitable to enhance SNR when signal is immersed in random noise. This is an extension of the method described by Broomhead and King (BK method) (Broomhead and King 1986). We applied a modified version of the BK method to a sine series and a sine series mixed with random noise. The technique was also applied to EEG data.

3.1 DYNAMICAL SYSTEM THEORY

A dynamical system can be represented by a deterministic equation

$$\frac{dy}{dt} = F(y) \qquad (3.1)$$

where each $y=(y_1, y_2, y_3.....)$ represents a state of the system and specifies a point in the phase space S. The dimensionality of S is associated with the degrees of freedom of the system. F(y) represents the vector field, which is a nonlinear operator acting on a point in S. For initial value of y_o, and at time t, the solution of (3.1) is $y_t = \phi_t\ y_o$; where it represents one-parameter family of maps of the phase space into itself.

For a dissipative system, the trajectories evolve towards the attractor M whose dimension is less than that of S (Schuster 1984). The search for complete solution of (3.1) is sometimes not possible. Hence the study of the system in terms of phase space trajectory is favourable, and an equivalence relation is suitable for classifying the system. Members of same equivalence class are said to have same qualitative dynamics.

Consider a compact manifold M of dimension m. For pairs (F,v), F a smooth vectorfield and v a smooth function on M, it is a generic property that $\Phi_{F,v}(y) : M \to R^{2m+1}$ defined by

$$\Phi_{F,v}(y) = (v(y), v(\phi_1(y)), \ldots\ldots\ v(\phi_{2m}(y)))^T \qquad (3.2)$$

is an embedding space, where ϕ_t is the flow of F and v(y) corresponds to the value of measurement made on the system in a state given by $y \in M$.

3.2 METHOD OF DELAYS

It is possible to construct a phase space from time series using above theorems by the technique known as 'Method of delays' (Broomhead and King 1986, Abarbanel et al 1989). For convenience, we introduce certain terms. The space which contain the image of $\Phi_{F,v}$ is called the embedding space and its dimension is called embedding dimension. Let us denote the embedding dimension as d, which is greater than or equal to 2m+1, by Whitney embedding theorem (Whitney 1936). The time series is represented as

$$(v) = (v_1, v_2 , ... v_M) \qquad (3.3)$$

By method of delays, from time series in single variable, say $v_o(t)$, we can construct d variables, which are taken to be the time delay co-ordinates (Packard et al 1980, Takens 1981). So that,

$$v_1 = v_o(t), \quad v_2 = v_o(t+\tau_L), \ldots\ldots v_d = v_o(t+(d-1)\tau_L) \qquad (3.4)$$

where τ_L is the time lag. We introduce the concept of (d,J) window, which makes visible elements of the time series. If J=1, then the elements are consecutive, and if J>1, there is an interval of J sample times between each visible elements. (d,1) window is referred as d-window. If the sampling time is τ_s, then lag time $\tau_L = J\tau_s$ and window length is $\tau_w = d\tau_L$. (d,J) window constitute the components of a vector in the embedding space R^d. The vector can be represented as

$$x_i = \Phi_{F,v}(\phi_i(y))$$

$$= (v_i, v_{i+j}, \ldots\ldots\ldots\ldots v_{i+(d-1)\tau})^T \qquad (3.5)$$

Thus we can construct N vectors in d-dimensional space as

$$x_1 = \begin{bmatrix} v_1 \\ v_2 \\ \vdots \\ v_d \end{bmatrix}, \quad x_2 = \begin{bmatrix} v_2 \\ v_3 \\ \vdots \\ v_{d+1} \end{bmatrix}, \quad \ldots\ldots x_N = \begin{bmatrix} v_N \\ v_{N+1} \\ \vdots \\ v_{N+d-1} \end{bmatrix}$$

$\ldots\ldots$ (3.6)

If d-window is introduced in a time series with M data, then it will provide N=M-d+1 vectors and $\{x_i \in R^d \mid i=1,2,\ldots.N\}$ in the embedding space. The trajectory matrix with d-window is defined as

$$X = N^{-1/2} \begin{bmatrix} x_1^T \\ x_2^T \\ \vdots \\ x_N^T \end{bmatrix} = N^{-1/2} \begin{bmatrix} v_1 & v_2 & \ldots\ldots v_d \\ v_2 & v_3 & \ldots\ldots v_{d+1} \\ \vdots & \vdots & \\ v_N & v_{N+1} & \ldots\ldots v_{d+N-1} \end{bmatrix}$$

$\ldots\ldots$ (3.7)

where $N^{-1/2}$ is the normalization factor. The trajectory matrix and its transpose may be thought of as linear maps between the spaces R^d and R^N (Broomhead and King 1986).

We can extract the i^{th} vector x_i, from the trajectory matrix X in R^N by using the property that the standard basis vectors can be used as an indexing system for points on the

trajectory in R^d. e_i is the i^{th} column of the N×N unit matrix. Multiplying equation (3.7) with $N^{1/2}e_i^T$ from the left, we get,

$$x_i^T = \sqrt{N}\ e_i^T X \qquad (3.8)$$

For calculating the dimensionality of the subspace which contains the embedded manifold, one needs to know the number of linearly independent vectors that can be constructed from the trajectory in the embedding space by forming linear combination of the x_i. Consider a set of vectors $\{s_i \in R^N\}$, which will give a set of linearly independent vectors c_i in R^d by their action on X, i.e., $\{c_i \mid i=1,2,.....d\}$. Then the following relationship holds

$$s_i^T X = \sigma_i c_i^T \qquad (3.9)$$

where σ_i are a set of constants. The orthogonality of the $\{c_i\}$ imposes the following condition

$$s_i^T XX^T s_j = \sigma_i\sigma_j \delta_{ij} \qquad (3.10)$$

where δ_{ij} is the Kronecker delta. The N×N matrix $H=XX^T$ is a real symmetric matrix and its eigen vectors form a complete orthogonal basis for R^N and, equation (3.10) becomes

$$H s_i = \sigma_i^2 s_i \qquad (3.11)$$

$$\text{where} \quad H = N^{-1} \begin{bmatrix} x_1^T x_1 & x_1^T x_2 & \cdots & x_1^T x_N \\ x_2^T x_1 & x_2^T x_2 & \cdots & x_2^T x_N \\ \vdots & \vdots & & \vdots \\ x_N^T x_1 & x_N^T x_2 & \cdots & x_N^T x_N \end{bmatrix} \tag{3.12}$$

This H is called the trajectory matrix, $\{\sigma_i^2\}$ are the eigen vales and c_i are eigen vectors. But equation (3.9) shows that only d of the $\{\sigma_i\}$ are nonzero, and also the diagonalization of N×N matrix is tedious. So we can look for an inverse relation of (3.9).

i.e., $$X c_i = \sigma_i s_i \tag{3.13}$$

Then by taking the transpose of (3.9) and operating from the left with X and using equation (3.11), we will get,

$$Z c_i = \sigma_i^2 c_i \tag{3.14}$$

where $Z=X^TX$ is a real, symmetric d×d matrix

$$Z = \frac{1}{N} \sum_{i=1}^{N} x_i x_i^T \tag{3.15}$$

or Z is the covariance matrix of the components of $\{x_i\}$, averaged over entire trajectory.

$$Z = \frac{1}{N} \begin{bmatrix} \Sigma v_i v_i & \cdots & \Sigma v_i v_{i+1} & \cdots & \Sigma v_i v_{i+d-1} \\ \vdots & & \vdots & & \vdots \\ \Sigma v_{i+d-1} v_i & \cdots & \Sigma v_{i+d-1} v_{i+1} & \cdots & \Sigma v_{i+d-1} v_{i+d-1} \end{bmatrix}$$

$$\cdots\cdots\cdots \qquad (3.16)$$

The nonzero eigen value of structured matrix is equal to nonzero eigen values of co-variance matrix. This means that rank H = rank Z = d' $\leq$ d. Thus R^N space can be decomposed into a subspace of dimension d' and its orthogonal complements. The d' dimensional subspace is spanned by a set $\{s_i \mid i=1,2,\ldots\ldots d'\}$ which is such that each corresponding average over the x_i gives rise uniquely to a basis vector $c_i \in R^d$ according to equation (3.9). $\{c_i \mid i=d'+1,\ldots\ldots N\}$ constitute the complementary subspace, which is the Kernel of X mapping onto the origin of the embedding space through equation (3.9). The maximum number of linearly independent vectors is d', which is the rank of Z, and it is the dimensionality of the subspace containing the embedded manifold.

Now our attempt is to remove the noise from the signal than calculation of dimension. So consider the orthogonal d×d matrix C which has columns consisting of vectors $\{c_i\}$, $C=(c_1,c_2,\ldots\ldots c_d)$, and the diagonal matrix G = diag$(\sigma_1,\sigma_2\ldots\ldots\sigma_d)$ and we can write the eigen value equation as

$$Z\,C = C\,G^2 \qquad (3.17)$$

and by definition of Z

$$(XC)^T\,(XC) = G^2 \qquad (3.18)$$

XC is a trajectory matrix projected on to basis $\{c_i\}$. To separate the noise part we follow singular value decomposition of the trajectory matrix

$$X = S\ G\ C^T \tag{3.19}$$

where S is Nxd matrix of eigen vectors of H, d' of which have nonzero eigen values. The vectors of C and S will henceforth be referred to as the singular vectors of X, and elements of G will be called associated singular values.

Time series with a noise component ξ_j can be written as

$$v_j = \bar{v}_j + \xi_j \tag{3.20}$$

Over bar indicates a quantity associated with the deterministic component, and

$$Z = \bar{Z} + \langle \xi^2 \rangle I_d$$

$$\sigma_i^2 = \bar{\sigma}_i^2 + \langle \xi^2 \rangle I_d \tag{3.21}$$

where $\bar{\sigma}_i^2$ is the eigen value of $\bar{Z}$.

Inorder to partition the embedding space, consider the matrices $P^{(i)}: P^{(i)}_{jk} = \delta_{ij}\ \delta_{jk}$, which are the representation of projection operators onto the basis function $\{c_i\}$. These can be used to construct projection operators onto the corresponding subspaces of the embedding space.

$$\mathbf{Q} = \sum_{\sigma_i = \text{noise}} \mathbf{P}^{(i)} \tag{3.22}$$

$$\mathbf{P} = \sum_{\sigma_i > \text{noise}} \mathbf{P}^{(i)} \tag{3.23}$$

and $\mathbf{P} + \mathbf{Q} = \mathbf{I}_d$.

Inserting the identity in equation (3.19), we get

$$\mathbf{X} = \bar{\mathbf{X}} + \Delta\mathbf{X} \tag{3.24}$$

where

$$\bar{\mathbf{X}} = \mathbf{S}\ \mathbf{P}\ \mathbf{G}\ \mathbf{C}^{\mathbf{T}} \tag{3.25}$$

is the deterministic part of the trajectory matrix and

$$\Delta\mathbf{X} = \mathbf{S}\ \mathbf{Q}\ \mathbf{G}\ \mathbf{C}^{\mathbf{T}} \tag{3.26}$$

is the noise-dominated part. In terms of above relation we can define $\bar{\mathbf{X}}$

$$(\bar{\mathbf{X}})_{ij} = \mathbf{S}_{ik}\ \mathbf{P}^{(i)}_{kl}\ \mathbf{G}_{lm}\ (\mathbf{C}^{\mathbf{T}})_{mj}$$

where $\mathbf{G}_{lm} = \sigma_l\ \delta_{lm}$

$$(\bar{X})_{ij} = S_{ik} \sum_{\sigma_i > noise} P_{kl}^{(i)} \sigma_l \delta_{lm} (C^T)_{mj}$$

since $P_{kl}^{(i)} = \delta_{ik} \delta_{kl}$, we can write

$$\bar{X} = \sum_{\sigma_i > noise} s_i \sigma_i c_i^T$$

and using equation (3.13), we get,

$$\bar{X} = \sum_{\sigma_i > noise} (Xc_i) c_i^T \qquad (3.27)$$

where (Xc_i) is a column vector and c_i^T is a row vector. $\bar{x}_i^T = \sqrt{N} e_i^T \bar{X}$ gives the noise free data. $\bar{X}$ represents trajectory matrix, which contains all the information about the deterministic trajectory and we can extract it from the experimental signal.

We developed a Fortran code for the extraction of signal from the noise dominated data. We diagonalize the trajectory matrix X and get eigen values σ_i, and eigen vectors c_i, usually taking d as 30. Then C is a 30×30 matrix, and c_i is a column vector and c_i^T represents a co-ordinate axis of the embedding space. σ_i's have d' non-zero values.

Inorder to find σ_i's above noise floor, plot $\log[\sigma_i / \Sigma \sigma_i]$ against i, and identify the σ_i's above the floor level (Fig.3.1) and allow the corresponding eigen vectors to operate on the trajectory matrix (Xc_i), which is a column vector containing a time series of the i^{th} component, in the basis $\{c_i\}$, of the vectors in the trajectory, and sum over $(Xc_i)c_i^T$ for σ_i's above the floor level according to equation (3.27). (Xc_i) is a N×1 matrix, which on operation with (c_i^T) changes to N×d matrix.

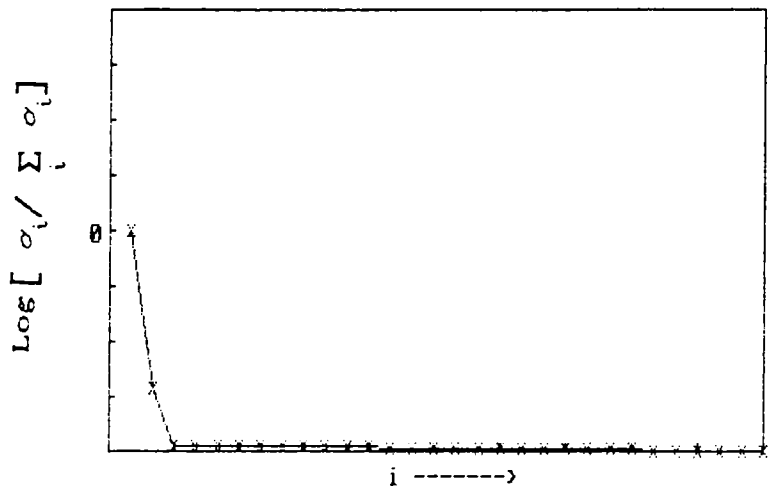

That is, $\bar{X}$ is a N×d matrix. However, by construction, it consists of a trajectory confined to the deterministic subspace of R^d having dimension $d^* \leq d$ (where d^* is the number of the $\{\sigma_i\}$ above the noise floor). Then the noise eliminated time series is

$$x_i^T = \sqrt{N}\ e_i^T \bar{X} \qquad (3.28)$$

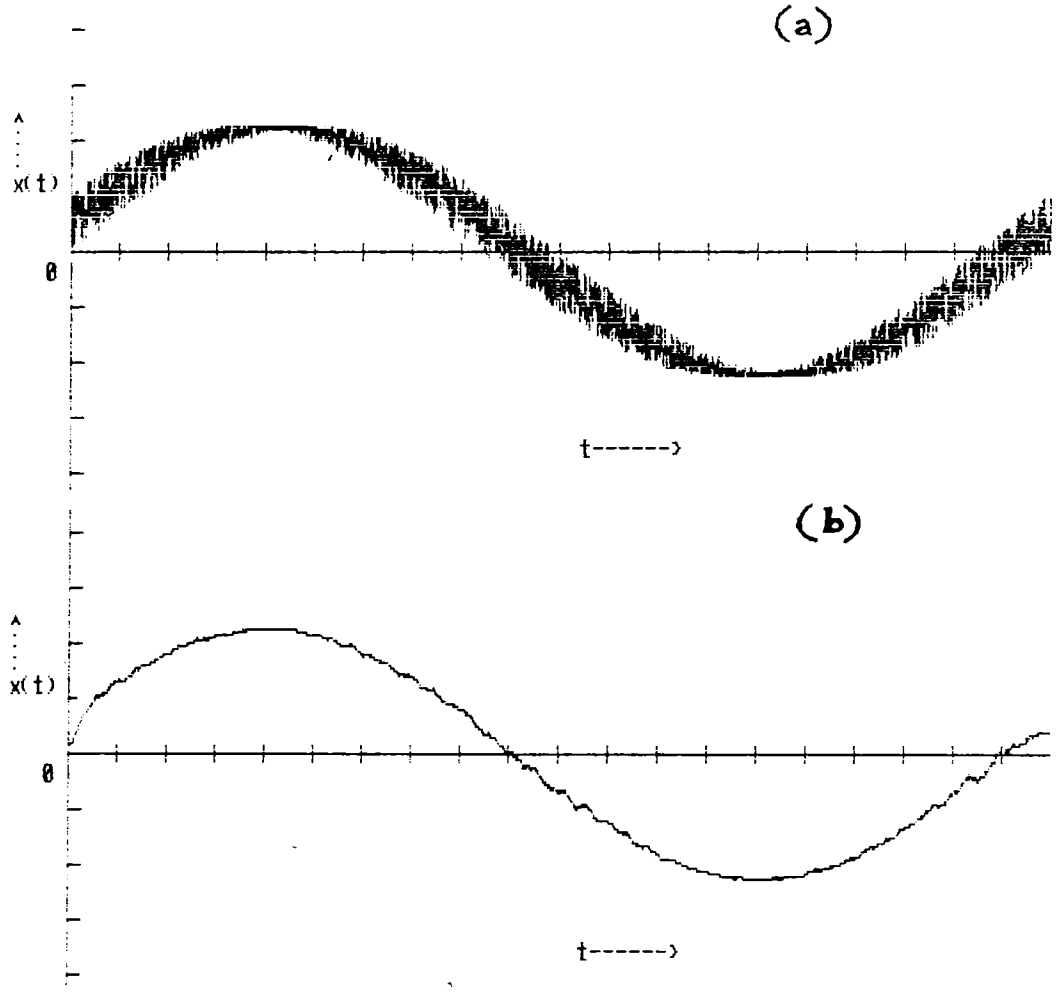

Fig 3.2 a) The noise embedded sine function, Sin(x+ηr) with η=0.1. b) The filtered output.

Inorder to study the effectiveness of this method, we applied it first to the sin(x) series. Noise embedded sine function was obtained by adding random numbers to the argument i.e; $\sin(x+\eta \times \bar{r})$ (see fig.3.2a & 3.3a), where $\bar{r}$ is a random function. η controls the strength of noise.

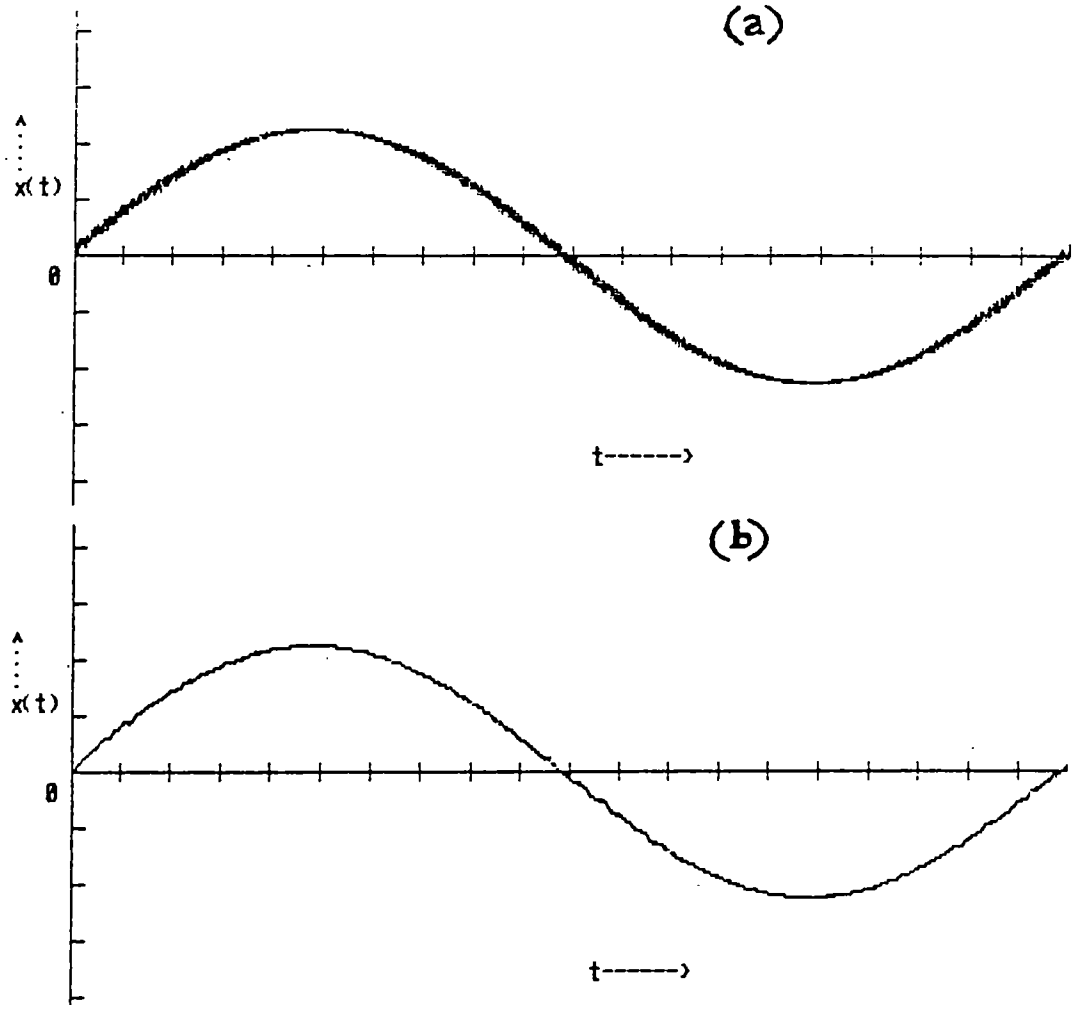

Fig 3.3 Plot of
a) $\sin(x+\eta r)$, η=0.5 and b) the filtered output.

Enhancement of SNR after filtering is obvious from Figure (3.2b) and (3.3b) for two different noise levels.

This analysis shows that the present mathematical technique can be used to filter noise embedded digitized data and SNR can be enhanced. We tried this method on all EEG signals

analysed in the present thesis, and it was observed that these

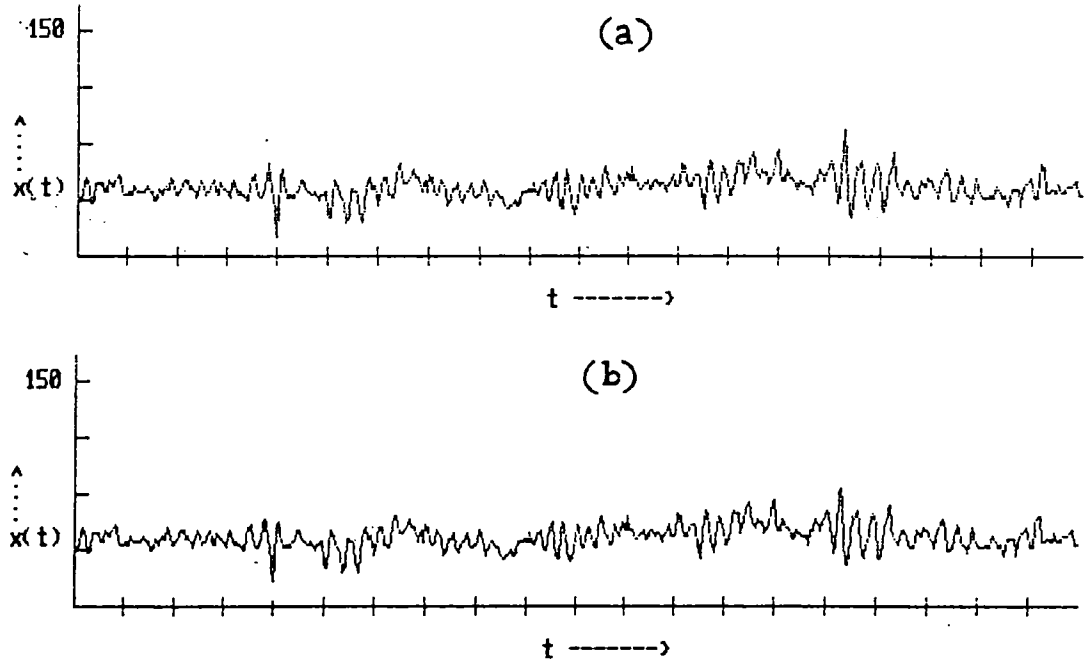

Fig 3.4 a) The time series of raw data of EEG
b) The noise filtered EEG

signals were almost noise free (Fig 3.4), so that the original signal can be used without any filtering. This agrees with the results obtained by Dvorak and Siska [1986].

CHAPTER 4

NEURAL SYSTEM

A description of neural system is the subject matter of this chapter. Stress is given to physical and dynamical aspects of human nervous system, relevant pathological conditions of brain are also included.

NEURAL SYSTEM

A description of human nervous system is given in the present chapter to enable a better understanding of the contents of this thesis.

Nervous system is the prime fundamental unit in a living organism which correlates all the various functions of life. Nervous system can, in general, be divided into two parts - the central nervous system (CNS) and autonomic nervous system (ANS). The CNS consists of the brain, the spinal cord and the peripheral nerves - nerve fibres or neurons that transmit sensory information. Afferent (or sensory) neurons carry signals from receptors (the sense organs) to the CNS and efferent (or motor) neurons transmit signals from CNS to the effectors (muscles). The ANS controls various internal organs such as the heart, intestine, glands etc.

Brain which is the most important part of the CNS is highly complicated in structure and consists of about 10^{10} nerve cells, 10^{10}-10^{15} synapses through which interconnections take place and about 10Km of the fibrous axonic cables along which electric impulses travel. The brain consists of mainly Cerebrum, Cerebellum and Medulla and also Thalamus, epithalamus and pituitary. The most elaborate cognitive processing of the brain takes place in cerebral cortex, a densely packed assembly of neural elements. Because of the highly sophisticated nature of the brain, it needs a special protection . Brain is surrounded by three membranes within the protective skull and it "floats" in the shock-absorbing cerebrospinal fluid. The brain is connected to the spinal cord, which is also surrounded by cerebrospinal fluid and is protected by the vertebrae of the spinal column. (Cameron and Skofronick 1978, Domany 1988).

4.1 NEURON

The basic structural unit of the nervous system is the neuron (Fig. 4.1), a nerve cell specialized for the reception, interpretation and transmission of electrical messages. There are many type of neurons, varying greatly in size and structure. The most complex structure is found in those of the cerebral cortex and cerebellum apparently because of the complexity of the functions performed by these parts of the brain.

Each neuron consists of a soma, or cell body and processes, consisting of a single axon and a large number of dendrites. Axons are long slender extensions or processes whose function is to convey impulses from the cell body to other cells or to peripheral organs. Axon hillock is the place on the cell body from where axon starts. The axon is wrapped by what is called the medullary sheath. But the axon does not have these covering fo. a length of approxd-mately 50 to 100 microns, near the axon hillock. This portion is called the initial segment. This part has high excitability, and its stimulus threshold is about one--third of that of other

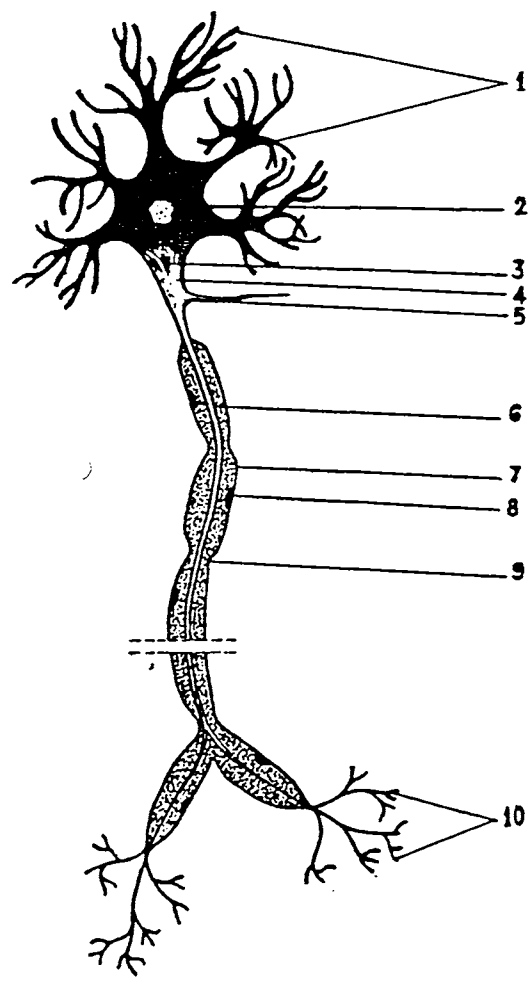

Fig 4.1 Schematic diagram of neuron
1. dendrites; 2 cell body; 3 axon hillock; 4 axon; 5 axon collateral; 6 medullary sheath; 7 Schvann sheath; 8 Schwann nucleus; 9 node of Ranvier; 10 nonmyelinated terminal of axon.

parts of neuron. The neuron surface is also covered with glial or Schwann cells. The membrane of Schwann cells form a myelin sheath which is a multilayer membrane. It protects the axon membrane from the environment. The sheath is interrupted at regular intervals, say at every 1-2 mm of the length of the axon. These constrictions are called the nodes of Ranvier. Axon membrane comes into contact with environment at the nodes. There exists unmyelinated axons also (Volkenshtein 1983).

Dendrites are the processes, whose functions are the reception of impulses arriving from other neurons and their conduction to the body of the nerve cell.

In view of the presence of the concentration of various parts of neurons, the C.N.S is said to have grey matter and white matter. Grey matter is that portion of C.N.S that contains mainly cell bodies and complex synaptic connections involving axons and dendrites. White matter refers to regions of C.N.S that are composed mainly of the myelin covered processes. It is composed of long axons and dendrites and contains few or no synapses. It is white in colour because of the fat-like myelin sheath surrounding the axons and dendrites.

Both the cerebrum and cerebellum are composed of an outer covering of grey matter with a core of white matter. In other areas of the brain the grey matter occurs primarily in clumps within the main matter of white matter (Stephenson, 1980).

4.2 CELL MEMBRANE

The body and processes of a nerve cell are covered with cell membrane. The three layered structure of the cell membrane is shown in Fig.4.2. A biological membrane consists mainly of protein and lipids. The membrane consists of a double layer of phospholipids, the circles shown in the figure are the polar heads of the lipids. The phospholipids are lined on the inside with a layer of protein molecules and on the outer side

with a layer of molecules of compound carbohydrates-mucopolysaccharides.

The molecules of water, ions and other substances pass in and out of the cell through the minute channels or pores (a few angstrom in diameter) of the cell membrane.

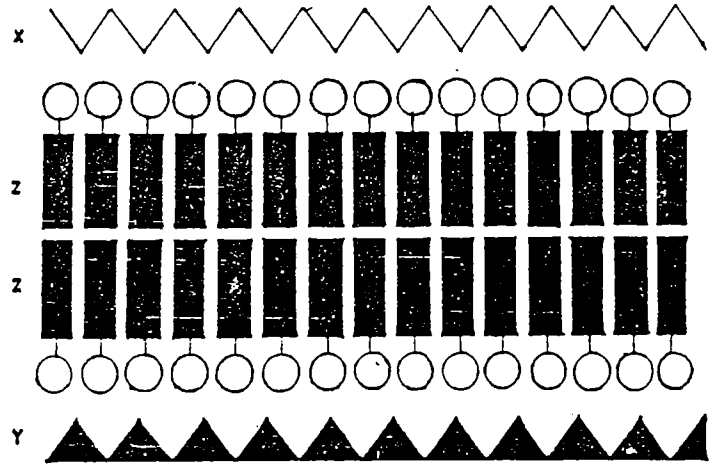

Fig 4.2 The model of the cell membrane
X - mucopolysaccharide Y - Protein
Z - Bimolecular lipid layer
Circles are the polar heads of lipids.

There are various types of ions existing in the membrane. These ions give particular electric charge to the walls of the pores, thereby impeding or facilitating the passage of other ions. Because of the presence of carboxyl groups and dissociated phosphate, the membrane of the nerve fibre is much less permeable to anions than to cations. Permeability to different cations also varies, according to the functional conditions of the tissue. For example, at rest, the permeability of the nerve fibre membrane to potassium ions is between 10 and 20 times that to sodium ions, whereas in an excited state the ratio is reversed (Babsky et al 1989, Volkenshtein, 1983, Cameron and Skofronick 1978).

4.3 RESTING POTENTIAL

The production of nerve impulses and their propagation is based on electrochemical process. There exists a potential difference of the order of 60-90 mv between the outer surface of the cell and its protoplasm, the cell surface being electrically positive with respect to the protoplasm. This

potential difference is commonly called the resting membrane potential. According to Hodgkin and Huxley (1952) potentials are caused by unequal concentration of Potassium, Sodium, Chlorine and Protein ions within the cell and outside, and by the variable permeability of the membrane with respect to different types of ions.

Table 4.1 Concentration of ions (in mmole per Kg H_2O) inside and outside of neurons.

Ion	inside	outside
Na^+	50	440
K^+	400	20
Cl^-	40-150	560

The concentration of ions inside and outside the cell membrane is given in Table (4.1) and diagrammatically represented in Figure 4.3.

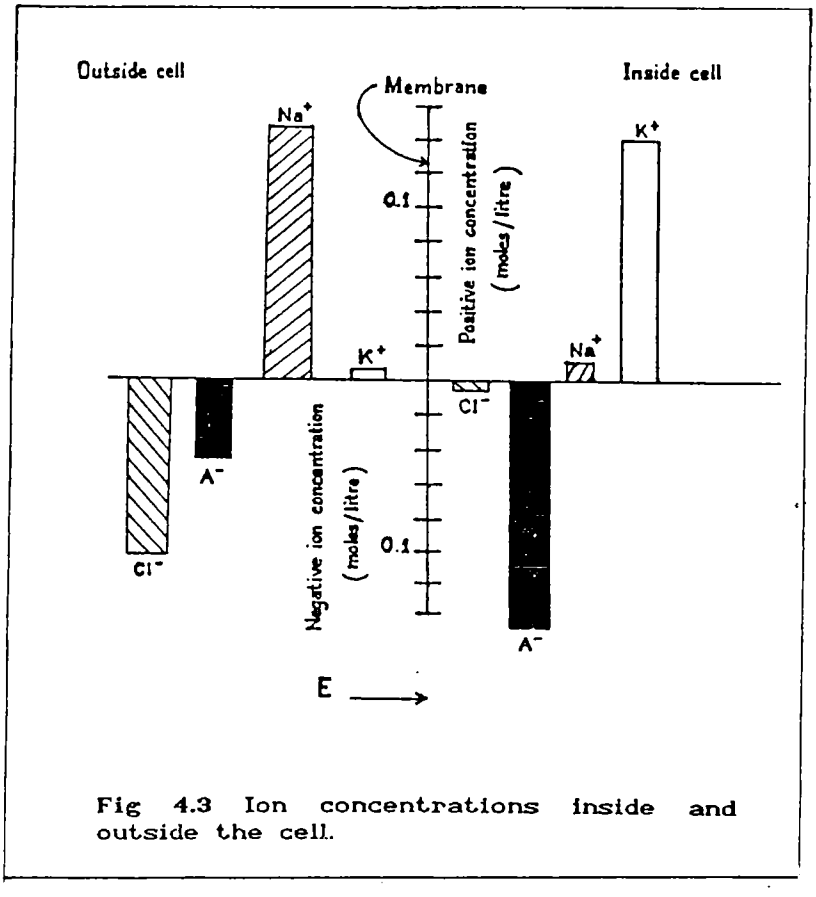

Fig 4.3 Ion concentrations inside and outside the cell.

The protoplasm inside the cell contains potassium ions 10-20 times higher than the outside of cell, and the concentration of Na^+ ions is in the reverse order. The resting state is characterized by the ratio of ion permeabilities;

$$P_k : P_{Na} : P_{Cl} = 1 : 0.04 : 0.45 \qquad (4.1)$$

The resting potential can be explained by a model, in

which a cell membrane separates a high concentrated solution (H) of KCl from one that is less concentrated (L). In the solution, KCl forms K^+ ions and Cl^- ions. As in the case of cell membrane, we assume that the membrane permits K^+ ions to pass through but does not permit the passage of the Cl^- ions. Then the K^+ ions diffuse from the high concentrated region H to low concentrated region L. This results in an excess of positive charges in L and excess of -ve charges in H. These charges form layers on the membrane, and retards the flow of K^+ ions, and a condition of equilibrium exists. If electrodes are now put into the right and left half of the vessel (Fig. 4.4), the measuring instrument will show the potential difference such that L is electrically positive with respect to the solution with the greater concentration H. Then the potential can be calculated by the Nernst's formula,

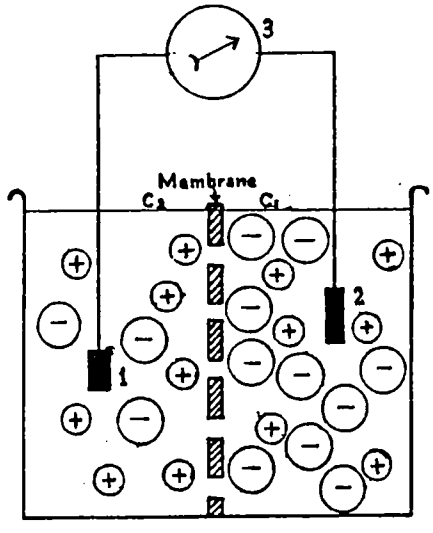

Fig 4.4 Membrane transport is illustrated by an artificial membrane separating KCl solution of different concentrations.

$$\Delta\psi = \frac{RT}{\mathcal{F}} \ln \frac{c_1}{c_2} \qquad (4.2)$$

where R is the gas constant, T is the absolute temperature, $\mathcal{F}$ is the Faraday's constant and c_1 and c_2 are ion concentrations (see fig.4.4).

In the case of cell membrane, the resting potential exists because the membrane is impermeable to the large A^- (Protein) ions as shown in Figure 4.3. While, due to the diffusion of

positively charged potassium ions from the protoplasm to the external fluids lends a positive charge to the outer surface of the membrane and a negative charge to the inner one.

The resting membrane-potential is developed due to variable permeability of the cell membrane to different types of ions. Hodgkin and Katz in 1949 (Hodgkin 1964) derived a formula for resting membrane-potential assuming the uniform electric field throughout the entire thickness of the membrane as

$$\Delta\psi = \frac{RT}{\mathcal{F}} \ln \frac{P_K c_K^i + P_{Na} c_{Na}^i + P_{Cl} c_{Cl}^e}{P_K c_K^e + P_{Na} c_{Na}^e + P_{Cl} c_{Cl}^i} \qquad (4.3)$$

where P is the permeability coefficient and c^i and c^e are the concentrations of ions inside and outside the membrane respectively. Thus one can conclude that the existence of resting potential can be attributed to the following facts:

1. At rest, the concentration of K^+ in protoplasm is about 10-20 times greater than the outside of the cell membrane, and the membrane is more permeable to K^+ ions.

2. The principal anions inside the cell such as protein and nucleic acids are not free to leave and Cl^-, which is abundant inside, (Fig.4.3), crosses only slowly.

3. Permeability of Na^+ is only one-twentieth that of K^+.

Thus the distribution of K^+ determines the transmembrane electromotive potential and hence the resting potential is called K^+ potential (Das 1987).

4.4 ACTION POTENTIAL

If a stimulus is applied to a nerve, or muscle fibre, the mode of permeability of the membrane gets changed, and a

variation of membrane potential takes place, as a result of which an electrical signal is generated, which is known as action potential.

Action potential can be measured using extracellular leads or intracellular leads. With an extracellular lead, it can be observed that the surface of the excited portion of the fibre becomes electrically negative in relation to the adjacent areas at rest, for a brief interval of a millisecond duration. Intracellular leads show that action potential exceeds the value of resting potential by 30 to 50 mv.

From the curve showing the temporal evolution of the action potential (Fig.4.5), we can see that there are two phases for this process - the ascending phase and descending phase. During the ascending phase, the initial polarization of the membrane disappears and is called depolarization phase represented by 'a' in Figure 4.5. The membrane potential reverts to the resting membrane potential during descending phase which is called repolarization phase (represented by 'b' in Figure 4.5). This swing occurs over a time of about 1 msec, and usually repolarization phase is longer than depolarization phase. During this time the nerve fibre is in refractory state, and it cannot be excited again.

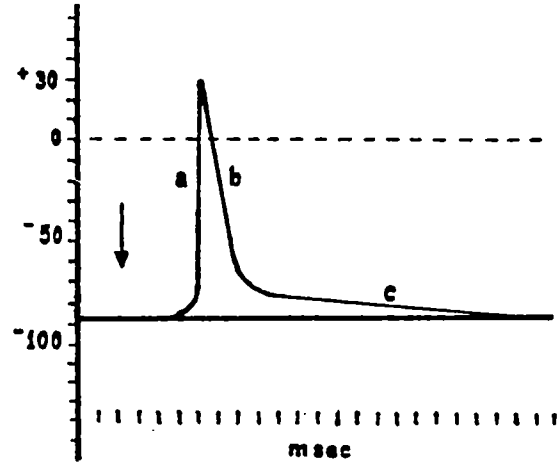

Fig 4.5 Appearance of an action potential.

4.5 ION THEORY OF ACTION POTENTIAL

Difference in concentration of sodium and potassium ions inside and outside the fibre is the source of the

electromotive force giving rise to the resting and action potentials. The action potential is caused by change in the ion permeability of cell membrane due to passive membrane transport. In a state of rest, the membrane permeability to potassium exceeds to that of sodium, and flow of positively charged potassium ions from the protoplasm to the surrounding fluids exceeds the contrary flow of sodium cation from the outside into the cells, which will make the membrane electrically positive than the inner one.

When an exciting potential is applied to the membrane, it becomes more permeable to Na^+ ions. The Na^+ ions enter the axon as a result of which inner surface of the membrane changes the sign of its charge from negative to positive and will create action potential. The internal fluid will become more concentrated in Na^+ ions. The action potential is mainly Na^+ potential which is opposite to K^+ potential. During the depolarization phase the membrane potential swings from -70 mv to +50mv . This will remain only for a few milliseconds and is followed by the appearance of restorative processes, that is, the permeability to Na^+ ions decreases and that to K^+ ions increases. The process leading to a fall in the sodium permeability of the membrane is called 'Inactivation' by Hodgkin. During the inactivation process, the K^+ ions will flow to the outside of the cell, and again outside becomes more positive than the protoplasm, and will become ready to receive new impulses. During these stages the membrane is not actively taking part, and hence, the transport of ions is termed as 'passive membrane transport'.

4.6 STIMULATION AND TRANSMISSION OF NERVE IMPULSE

Stimulation of nerve impulse depends on two important parameters - the stimulus threshold and utilization time.

The action potential does not arise if a certain threshold

value is not reached by the electrical stimulus. The lowest strength of stimulation required to give rise to an action potential in an excitable tissue is called the 'threshold of stimulation'. The nerve fibre acts according to the all-or-none law generating an action potential. When once the firing takes place, it attains a constant value irrespective of the intensity of stimulus. However a stronger stimulus increases the frequency of firing, and not an increase in the amplitude of the action potential.

The strength of the stimulus and duration of its application are inversely proportional. When an electric current is used as a stimulus, certain minimum quantity of electricity is required. As the duration Δt of the transmitted impulse is reduced, the current I must be increased. Figure 4.6 shows such strength-duration curve. The minimum strength of the current required to produce the excitation is called rheobase represented by OA in Figure 4.6, and the minimum time that a current equal to the rheobase must act to induce an action potential is called the utilization time. Utilization time implies that further prolongation of the effect of current has no value or is useless in generating action potential. A weak current is inefficient at any duration. The strength-duration curve takes the form of an equilateral hyperbola. The threshold current required to generate impulse can be described by the empirical formula,

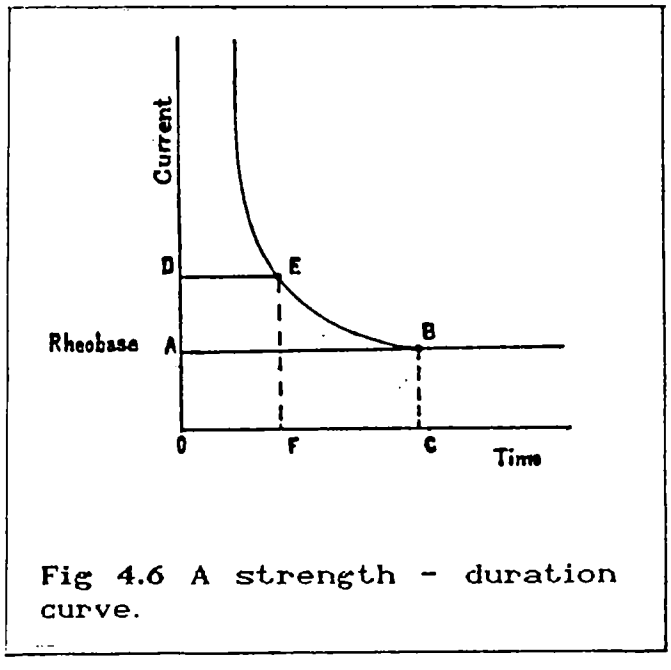

Fig 4.6 A strength - duration curve.

$$I_{th} = \frac{a}{\Delta t} + b \qquad (4.4)$$

The quantity b is the rheobase, Δt is the utilization time, a is a constant that characterizes the threshold level of the amount of electricity.

Lapicque in 1909 proposed the measurement of another parameter, known as Chronaxie, which is the least time required for a current equal to double the rheobase (OD in figure 4.6) to produce the excitation in a tissue. Utilization time and Chronaxie characterize the rate at which a stimulus causes excitation, 'OF' in Figure 4.6 corresponds to the chronaxie (Babsky et al 1989).

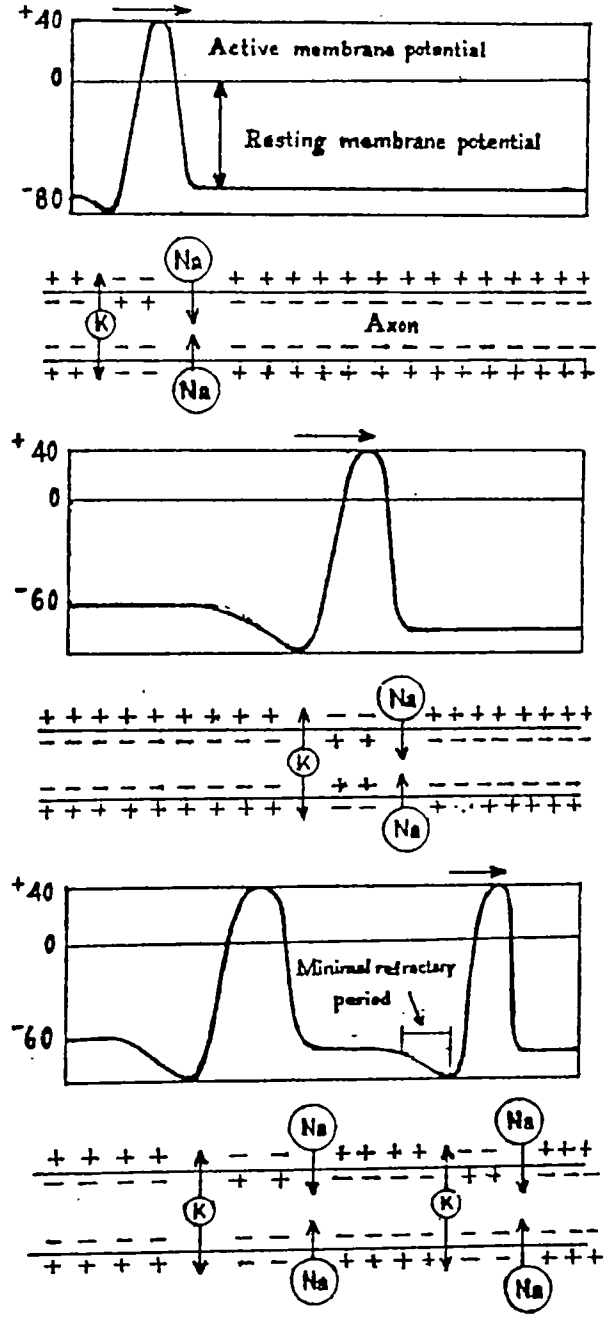

Fig 4.7 The propagation of nerve impulse and corresponding change of axon membrane permeability to ions.

The propagation of impulse is a self sustained process. The nerve impulse resembles a burning spark travelling along the length of the fuse. The depolarization of the membrane gives rise to current, and becomes a stimulus for adjacent resting part of the fibre. The mechanism by which excitation is conducted from one portion of the fibre to another does not

differ in principle from that by which an impulse is produced at the point of stimulation. In both cases an action potential arises when depolarization reaches the critical value. The propagation of nerve impulse is portrayed in Figure 4.7. It is necessary to consider the electrical equivalent circuit of a nerve cell to describe the permeability changes. The axon membrane has a resistance of 1000 ohm cm^2 and a capacitance of 1 $\mu F/cm^2$. During the generation of impulse the conductance of the membrane increases by about 10^3 times. Figure (4.8) gives the equivalent circuit for one element of the membrane, the sodium emf (E_{Na}) is directed opposite to the potassium emf (E_K) and leakage emf (E_L). The resistance of axoplasm is represented by R. E_{Na} and E_K determine the generation of an impulse and E_L depicts the movement of other ions, whose permeabilities do not change upon excitation. If E_r is the resting potential, then the potential change V is

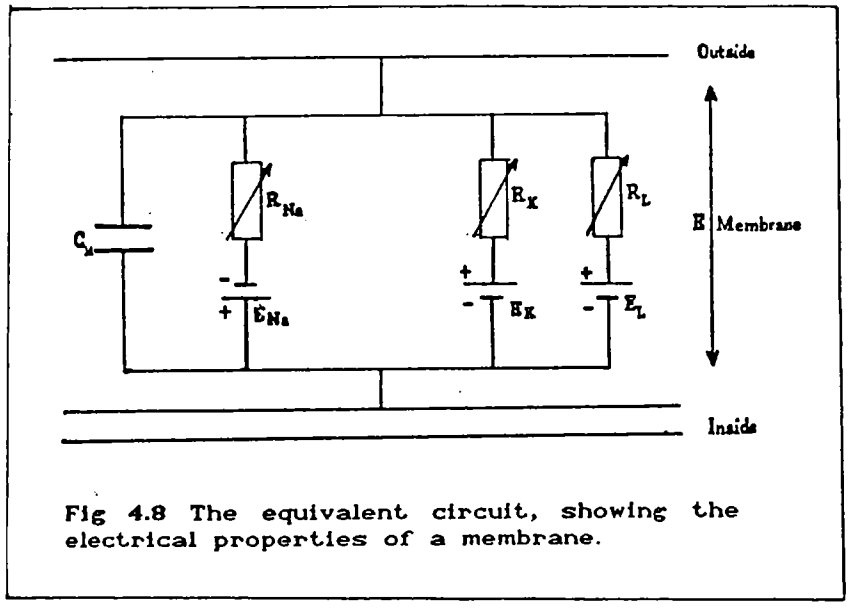

Fig 4.8 The equivalent circuit, showing the electrical properties of a membrane.

$$V = E - E_r \qquad (4.5)$$

where E stands for E_{Na} , E_K or E_L .

Therefore the relative potential for sodium, potassium and leakage can be defined as

$$V_{Na} = E_{Na} - E_r$$

$$V_K = E_K - E_r \qquad (4.6)$$

and

$$V_L = E_L - E_r$$

If I represents the density of the current flowing through the membrane, then

$$I = C_M \frac{dE}{dt} + I_i \qquad (4.7)$$

where $I_i = I_{Na} + I_K + I_L$

with

$$I_{Na} = \mathcal{G}_{Na} (V - V_{Na})$$

$$I_K = \mathcal{G}_K (V - V_K)$$

$$I_L = \mathcal{G}_L (V - V_L)$$

where C_M is the membrane capacitance and $\mathcal{G}_K$, $\mathcal{G}_{Na}$ and $\mathcal{G}_L$ stands for the conductance of potassium, sodium and leakages respectively.

Rate of travel of nerve impulse varies with the nature of axons. The nerve impulse travels in a myelinated fibre faster than in an unmyelinated fibre. In the myelinated axon, the nerve impulse jumps from one node of Ranvier to another. Potassium and sodium channels open and close only at the nodes of Ranvier. The myelin sheath has a low capacitance, which accounts for the high rate of transmission of the nerve impulse. The travel speed of the signal, v is 1-100 m/sec. The resistance per unit length of

the fibre with a diameter of 1μm is 10^{9}-10^{10} ohm cm which exceeds the resistance of a copper wire of the same diameter by 10^{8} times. In such a conductor, losses and leakages are high, but the nerve impulse is transmitted by the axon to distances of up to several meters without being damped and distorted (Volkenshtein 1983).

During the repolarization process, the sodium-potassium status is destroyed. For example single nerve impulse in the giant axon of a squid allows about 20,000 sodium ions to enter the protoplasm through each square micron of the membrane, and as many potassium ions pass out of the fibres. An axon of 0.5 millimeter in diameter losses about one millionth part of its total potassium content during each impulse. The mechanism by which the membrane actively removes sodium ions from the protoplasm and supplies it with potassium ions is called the sodium-potassium pump, which is represented in Figure 4.9. The membrane actively takes part in this process, hence it is called active membrane transport.

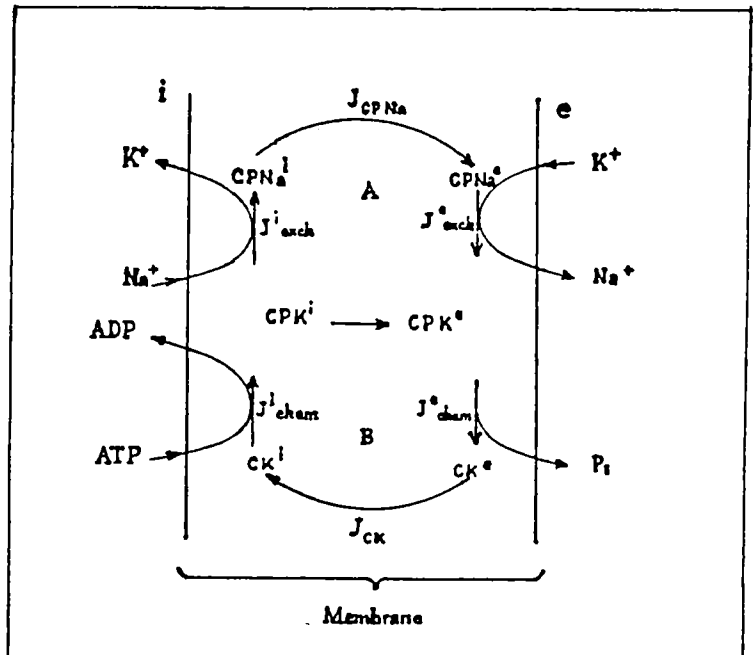

Fig 4.9 Sodium pump i - internal side
e - external side of the membrane

The transfer of Na^+ and K^+ take place in the direction of their increased concentration, so that a large amount of energy is required for this process and is taking part at the expense of energy of hydrolysis of ATP (Adenosine triphosphate). In this pump, the transport is accelerated due to the presence of carriers - substances which interact with the transported ions or molecules in the membrane. This complex is broken down on the innerside. The carrier (C) and the complex (CS) always remain inside the

membrane. The following reaction is taking place inside the membrane.

$$S + C \rightleftharpoons CS \qquad (4.8)$$

where S is the transported substance.
The key role in the operation of the sodium pump is the enzyme - the K^+,Na^+- activated ATPase. The phosphorylation and dephosphorylation take place in the various parts of the membrane. The ATP to ADP conversion takes place only on the innerside of the membrane.

$$C + ATP \longrightarrow CP + ADP \qquad (4.9)$$

The dephosphorylation is taking place on the outerside of the membrane (see Figure 4.9).

$$CP \xrightarrow{H_2O} C + P \qquad (4.10)$$

C and CP are proteins but there affinities are different. C has high affinity to K^+ ions, so that it collects K^+ ions from the environment and releases it to axoplasm using the energy released in ATP-ADP hydrolysis, and the protein CP has high affinity to Na^+. Thus the sodium pump operates as a system of two cycles. The first cycle is of the ion-exchange type

$$CPK + Na^+ \rightleftharpoons CPNa + K^+ \qquad (4.11)$$

The second cycle is chemical and involves phosphorylation and dephosphorylation reactions. Thus excess Na^+ is removed from axoplasm and transferred to outside of the cell or environment. Similarly K^+ ions is transferred from outside to axoplasm and

thus it regains the resting state.

4.7 ELECTRICAL ACTIVITY OF BRAIN

The electrical activity of Brain was first observed by Hans Berger in 1929. If two electrodes were placed on the scalp and the electrical activity is measured, one will obtain a very weak complex electrical signal. Traces of these oscillations are called Electroencephalogram (EEG). The technique which deals with the recording of the electrical activity of the brain and their interpretation is called Electroencephalography. Electrodes for recording the signals are often small discs of chlorided silver. They are attached to the head at locations that depend upon the part of the brain to be studied. Usually, the international standard 10-20-20-20-20-10 system of electrode location, as shown in Figure (4.10), is used for recording. There are two methods of recording electroencephalograms, bipolar and monopolar.

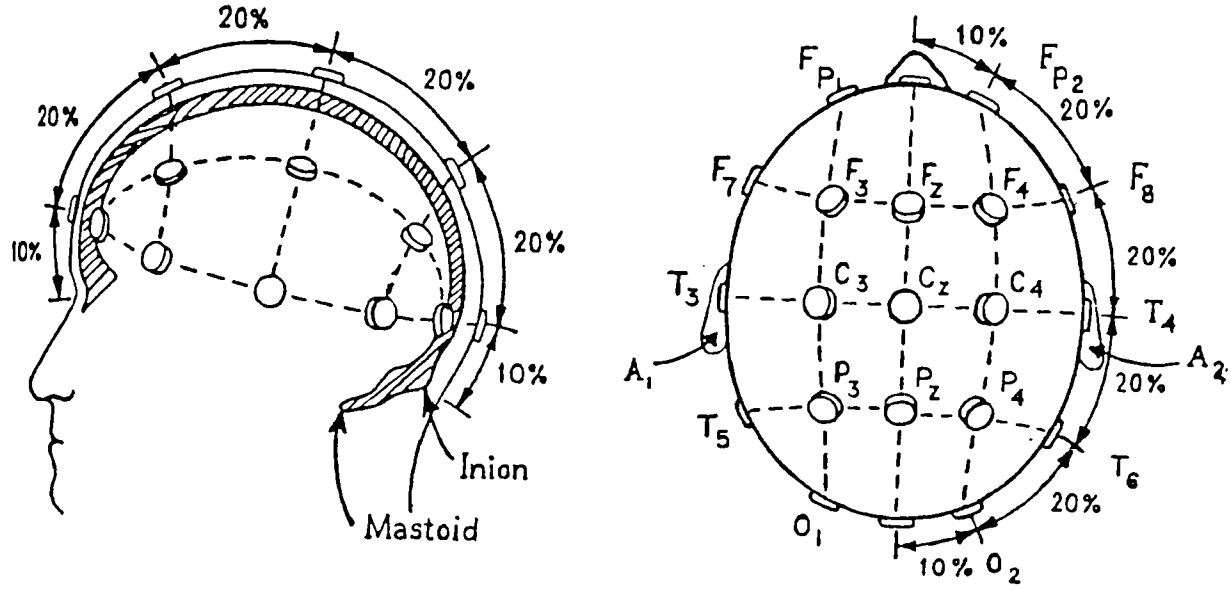

Fig 4.10 International standard 10-20-20-20-20-10 system of electrode location for EEGs.

In the bipolar method, two recording electrodes are applied to the cortex or to the corresponding areas of the scalp and both electrodes are active. The electroencephalograph then records the potential difference of the cortical areas beneath the electrodes.

In monopolar technique only one electrode is active, *viz.*, the electrode that is applied to the cortical regions and an indifferent (grounded) electrode is applied to the ear lobe in the case of man or to the nasal bone in the case of animals. Then the waves under active electrode are recorded. In the case of man, amplitude of EEG varies from 5 or 10 to 200 or 300 microvolts and frequency lying between 0.5 and 70 Hz. Usually multichannel electroencephalographs are used, to record the activity at four to more than thirty two points in the brain simultaneously, and thus to study the relationship and variations of electrical activity at different areas of the cerebral cortex (Kooi et al, 1978).

EEG signals are produced mainly due to the electrical activity of the cerebral cortex of the brain. One hypothesis about EEG is that the potentials are produced through an intermittent synchronization process involving the neurons in the cortex, with different groups of neurons becoming synchronized at different instants of time. According to this hypothesis the signals consists of consecutive short segments of electrical activity from groups of neurons located at various places of cortex (Cameron and Skofronick 1978). The frequencies of EEG signals seem to be dependent on the mental state of the subject. EEG signals of a relaxed person have frequencies ranging from 8 to 13 Hz, but an alert person can have EEG with frequencies well above 13 Hz.

4.8 EEG RHYTHMS

The Electroencephalograms are classified according to the frequency, amplitude and physiological characteristics of

their electrical waves (see Figure 4.11). The EEGs are represented as the "Hand writing" of the brain, which are the records of the different disorders and activities of the brain (Anninos et al 1977). The EEG is mainly classified into four types, as discussed below (Table 4.2).

Table 4.2 Frequency and amplitudes of EEG rhythms.

rhythms	frequency in cycles/sec	amplitude in microvolts
α	8 to 13	up to 50
β	above 13	20 to 25
θ	between 4 and 8	100 to 150
δ	between 0.5 to 3.5	250 to 300

Alpha Rhythm has a frequency lying between 8 to 13 Hz and has an amplitude of up to 50 microvolts. This type of wave is usually found in the EEG pattern of a relaxed person. The amplitude of alpha waves is greatest and most stable in the two cortical regions, one in the occipital lobe, and the other in the parietal. The occipital alpha rhythm arises in the visual area of the cortex and is, as a rule, absent or faint in the blind.

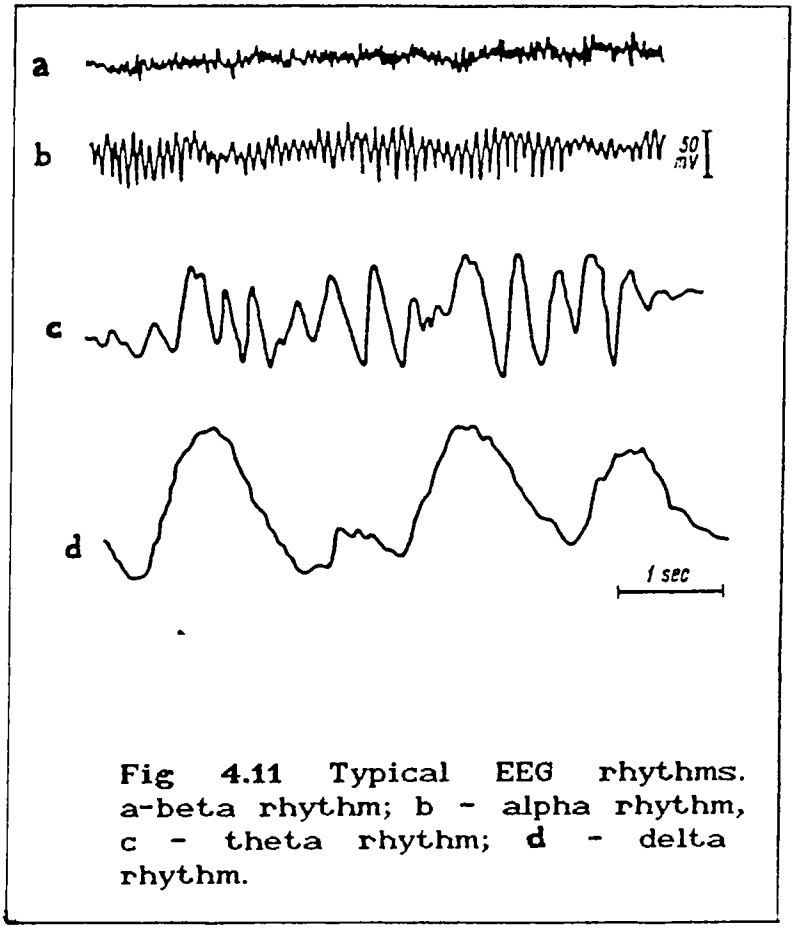

Fig 4.11 Typical EEG rhythms. a-beta rhythm; b - alpha rhythm, c - theta rhythm; d - delta rhythm.

Beta Rhythm is characterized by wave frequencies above 13 Hz with an amplitude of 20 or 25 microvolts. It is most distinct in the frontal region and is less in parietal region. Emotional excitement, mental work and light stimulation changes the alpha rhythm of occipital region into beta rhythms.

Theta Rhythm consist of waves with a frequency lying between

4 and 8 cycles per second and has an amplitude of 100 to 150 microvolts. This type of wave is found during sleep and in various pathological conditions.

Delta Rhythm is characterized by slow waves with a frequency between 0.5 to 3.5 Hz having an amplitude of 250 or 300 microvolts. They are registered during deep sleep, general anesthesia, hypoxia and various pathological processes in the cortex.

Clinitians use EEG patterns for diagnostic purpose. EEG pattern is sensitive to different drugs especially anesthesia, so that EEG is used as a monitor during surgery. EEG is being used for the study of the different stages of sleep (Babloyantz et al 1985). When a person becomes drowsy, particularly with eye closed, the frequencies from 8 to 13 Hz (alpha waves) dominate in the EEG. As the person moves from the light sleep to deep sleep the amplitude of EEG increases while the frequency decreases. If a stimulus is applied to a person continuously, the EEGs show response to the first few pulses and the last few pulses. The lack of response in between is called habituation. EEG can be mainly used for the diagnosis of pathological conditions like epilepsy, tumor, head ache and Migraine and are discussed in the subsequent sections.

4.9 SIGNAL ANALYSIS OF EEG

The usual signal analysis employed for EEG are spectral, frequency, cross-correlation, coherence, pattern recognition and distribution analysis. Electroencephalographer does these analysis and give clinical interpretation of the electroencephalograms. The accuracy of the interpretation depends upon the ability of the electroencephalographer to see, analyze, and interrelate the information contained in the graphic write-out of the scalp-derived signal. These analysis could also be done by computational machinery, but a high speed computer is necessary.

Spectral method is one of the usual techniques which gives certain useful information. Usually, Clinicians are doing frequency analysis visually by describing various waves of EEG belonging to different frequency bands.

Inorder to do spectral analysis, one must first sample the signal properly, extract the frequency information, analyze this information and then make some decision about the outcome of the analysis. The spectral analysis can be done in a very limited time using FFT. The development of algorithms for high speed calculation of the parameters of the neural system, as well as the evaluation of suitable sensitive parameters for diagnosis do still have room in medical physics.

4.10 DISORDERS OF BRAIN

EPILEPSY

Epilepsy is considered as the uncontrollable episodes of abnormal neurological or mental function or both. In the definition of epilepsy the term disease has been avoided on purpose, because in the large majority of cases an epileptic seizure is essentially a symptom of any one of a number of diseases.

In the normal brain, neuronal interaction proceeds in a highly integrated and orderly manner with a background random firing. The factors regulating the level of membrane polarization and the rate and temporal patterning of cell discharges are delicately balanced. In contrast, the epileptic process is evidenced by sudden, rapid and excessive depolarization of the membrane potential and prolonged high frequency discharge of individual neurons. An additional property of the epileptic process is its capacity to recruit neural elements that are in functional relationship to those initially involved, providing a mechanism whereby it can

replicate itself as it spreads from one area to another.

The epilepsy can generally be divided into two groups. The existence of seizures without known demonstrable organic causes is classified as idiopathic or cryptogeneic or essential epilepsy. The symptomatic or secondary epilepsy is the much frequently encountered group of seizures resulting from various types of underlying disorders.

In addition to these two main types, seizures are classified in different groups according to other criteria to achieve some uniformity in the use of diagnostic terms to permit comparison of cases and better evaluation of therapy. They are generally classified according to criteria such as symptomatology, anatomical origin, electroencephalographic patterns, etiology, chronological patterns and so on. Usual type of seizures, *viz.*, Grand mal and Petit mal belong to the group symptomatology. The experiences of patients during different types of epilepsy are entirely different. For example, circumscribed sensory seizures called somato-sensory seizures are characterized by numbness or tingling sensations, visual seizures characterized by moving flashes of light, dark spots, colours and auditory seizures are characterized by buzzing and roaring sounds.

The electroencephalogram is an essential aid in the evaluation of the patient with suspected or known epilepsy. It provides assistance in determining the correct diagnosis, the etiology of the disorder, the location of epileptogenic foci, the presence and absence of associated brain damage, the effectiveness of therapy, and the suitability of the patient for surgical management (Kooi et al 1978).

The more common type of seizures are grand mal and petit mal. In our analysis in later chapters, we have applied our method of analysis mainly in grand mal and petit mal. We shall describe below these two types very briefly.

GRAND MAL

Grand mal is the most prevalent and spectacular form of epileptic seizure, and occurs in 60% of the cases. The seizure is immediately preceded by an aura or warning, such as an unpleasant odour, and during an attack the individual losses consciousness and breathing is suspended. His muscles become rigid, jaws clenched, arms extended, and legs outstretched and he pitches forward or slumps to the ground. With the return of air to the lungs, his movements instead of being rigid, become jerking. Muscular spasms begin, the head strikes the ground, the arms repeatedly thrust outward, the legs jerk up and down, the jaws open and close, and the mouth foams. Usually in about a minute the convulsive movements decrease, the muscle relax, and the individual gradually returns to normality - in some cases after a deep sleep lasting few minutes to several hours (Anninos et al 1977).

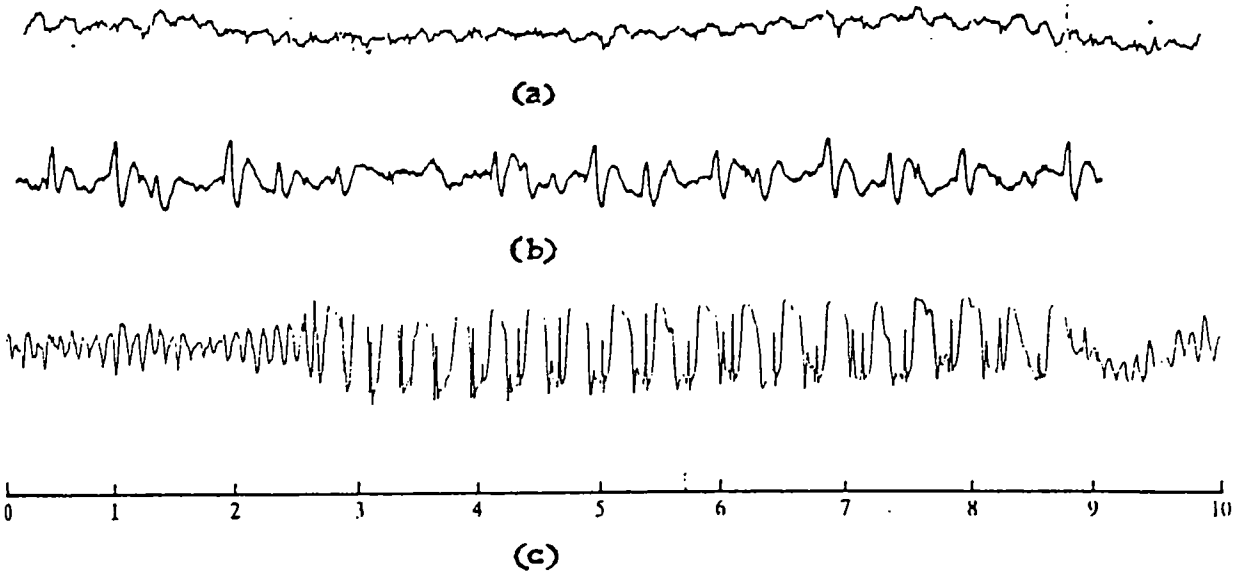

Fig 4.12 EEG of a) 'clinically' normal brain
b) Grand mal and c) Petit mal

The EEG pattern shows fast and comparatively higher voltage spikes in all leads from the skull (represented by the curve 'b' in Fig.4.12), the most common sites are temporal and frontal areas (these areas are identifiable from Fig.4.10).

PETIT MAL

In petit mal seizures there is usually a diminution, rather than a complete loss, of consciousness. The individual stops whatever he is doing, stares vacantly ahead or toward the floor and then in a few second resumes his previous activity. In certain cases, the seizure may occur several times a day.

The EEG of petit mal seizure shows up to 3 rounded waves per second followed or preceded by fast spikes (curve 'c' Fig.4.12). In some patients, the discharges may be most prominent over frontocentral regions or, less frequently, over parietoccipital regions (Kooi et al 1978).

BRAIN TUMOR

Electrical activity is reduced in the region of tumor, and this will show up in EEG. Focal slow activity is the most frequent electrographic sign of a hemispheric brain tumor, occurring in about 90% cases. Slow activity is usually in the form of intermittent single or brief rhythmic theta or delta discharges. In more pronounced cases, delta activity (0.5 to 3.5Hz) becomes prominent relative to theta activity (4 to 7Hz) and wave form less regular in the primary focal zone. A secondary zone showing theta activity may develop.

HEADACHE AND MIGRAINE

Headache is a deep form of pain, as opposed to superficial or cutaneous forms partaking of the aching quality of other deep pains and distinguished from them chiefly on the basis of locus of origin.

Causes of most headaches are the distending forces applied to intracranial blood vessels. One of the other assumptions is that the massive patterns of sensation involved in headache are the free nerve endings embedded in the walls of vascular structure inside the head. Stretching of these fibres by agents

producing traction displacement, distension or inflammation constitutes the stimulus, even as such forces, when exerted on visceral organs and muscle tendons, evolve deep aching pain and, when acting on superficial cutaneous tissues, arouse prickling or burning pain.

One of the other causes for headache is reduction of intracranial pressure. Removal of 1% of the total cerebrospinal fluid (about 20 ml) from the spinal canal create headache, due to variation in pressure.

Among the most intense headaches are those associated with migraine, severe throbbing pains localized chiefly in the frontal, occipital and parietal regions of head, and often accompanied by visual patterns - streaked, striped, or scintillating "saw tooth" images of central origin.

Headache is also produced by other malfunctioning of brain, the brain tumors, and also from eye strain and hypertension.

4.11 DYNAMICAL ASPECTS OF NEURAL SYSTEM

Some of the usual techniques, which are employed for the diagnosis of brain-disorders using EEG have already been explained in previous sections. The Clinitians usually compare the EEG patterns of the patients with standard EEG recording by frequency analysis. But in some cases, the EEG pattern of diseased person looks normal (Schmidt and Wilder 1965), and in such cases the usual EEG pattern analysis fails to give correct directions.

The Fourier analysis is a linear analysis and hence it does not give any information about the nonlinear interactions present in the system. Moreover, pattern analysis and fourier

analysis give only qualitative information. We approached the problem with a new mode of analysis which would give quantitative information, suitable for a highly nonlinear system like the neural system. The details of this work which takes into account the collective behaviour of the system form the subject matter of chapters 5 & 6.

The new method of analysis is based on the existence of more than one incommensurate frequencies in the system which could generate nonlinear pattern as also it can be as a result of the existence of various nonlinear mechanics in the system. Our aim is primarily to examine this aspect and get a deeper insight into the nonlinear dynamics of the system. This is all the more expected from the system when one realizes the fact that the phenomenon is a consequence of a co-operative mechanism. Hence the final point is to determine the class of plausible time scales that could exist in the system. This could be determined as one does in nonequilibrium statistical mechanics.

Certain relevant parameters which are usually employed in the theoretical framework of neurophysics are described below.

BIOPOTENTIALS

In the neural firings, as explained earlier, a potential change is generated due to changes in Na and K ion conductances across the membrane of an axon. This is highly nonlinear, which is however a single neuron process. It is known that there exist a resting potential of -80mv and a threshold potential -50mv. If the potential difference across a membrane is less than 50 mv, there is no firing. But if this is grater than the threshold value, a firing takes place, and the peak potential of this is about 40mv. Thus each firing has an amplitude of about 120 mv, and one of the most significant features of this is that the amplitude of this firing is independent of the strength of the simulation. Furthermore, the

firing as it proceeds along the length of the axon, does not get attenuated. Again the transmission is not like a current in a conductor. The firing takes place at the various nodes of Ranvier in a sequential manner. The electric potential (e/r) has dimension $(MLT^{-2})^{1/2}$.

REFRACTORY TIME (τ)

Each neuron, at a given time, has a potential firing frequency which could be anything up to 1000 firings per second, for a given stimulus. The time lapses between two successive firings, called the refractory time, is therefore of the order of a millisecond. Hence at a given instant, one can classify neurons on the basis of this refractory time. The same neuron can however have different refractory times at different instants, but they all have a least upper bound. Hence the number of neurons firing with a specified refractory time is time dependent. Again the refractory time depends on the strength of the stimulus.

SIGNAL PROPAGATION SPEED (v)

The electrical signals propagated along the length of the axon has a finite measurable speed and is about 100 m/sec. It is worth mentioning that this is much less than the speed of light, which is taken as the interaction speed in electrodynamics.

AXON CURRENT (I)

This is the current that flows between two consecutive nodes of Ranvier. This consists of two parts : a displacement current component through the membrane capacity and an ion current through the membrane. Thus the current that flows

from the medium (1) to (2) (I_{12}) depends on the voltage across the membrane V nonlinearly, and I_i, the ion current. These currents are normally defined as current density per unit area and is about 1 mA/sq. cm and has dimension $(MLT^{-4})^{1/2}$. For a volume current this would be $(ML^{-1}T^{-4})^{1/2}$.

NEURAL DENSITY

A signal received by one nerve or a group of nerves, will be communicated to a large number of nerves by a cascading process, through axonal tree, the branches of which end in synapses connecting them with other cell bodies and dendrites. This cascade process however will not connect all neurons in the system but will end up with the distribution of regular tubes and stripes (Law and Constantine 1981). Hence all neurons are not involved, and therefore one can define neural density as the number of involved neurons per unit volume. One can also define this as a fraction of affected neurons to total neurons n/N in unit volume (Pratap R, 1988, Parikh and Pratap 1989, 1984).

CHAPTER 5

CHARACTERISATION OF NEURAL SYSTEM DURING MENTAL ACTIVITY

An attempt is made to understand the neural system during mental activity using the technique in nonlinear dynamics and the results obtained from the studies are given. Various time scales which may present in neural dynamics are also described.

CHARACTERISATION OF NEURAL SYSTEM DURING MENTAL ACTIVITY

Even though the basic physiological properties of the nerve cells in the brain are understood to a certain extent, little is known about the dynamics of mental activities or higher functions of the brain such as pattern analysis, learning, memory, association and abstraction (Clark et al 1985). An understanding of these requires the knowledge of the general dynamics of human brain, which has about 10^{10} neurons interconnected in a complex manner. A large amount of research (Cooper 1973, Rapp et al 1985, 1987 Kürten et al 1986) has gone towards this end and scientists are trying to explain the complex dynamical behaviour of the brain in terms of the electrical activity of individual neurons. However, to explain the higher functions of the brain, one has to realize the necessity of a new approach, taking into account, the collective behaviour of a set of "connections" which is very highly dynamical in nature (Babcock et al 1987). It is in this context that we examine the dynamics of such networks which can exhibit collective or cooperative electrical behaviour (Choi & Huberman 1983, Parikh and Pratap 1984). It should be realized that even if the various evolution centres are localized, it can still be a consequence of collective action of a large number of neurons. The process that we envisage is one in which a small stimulus at a certain point in the system generates electrical signal which "cascades" in and affect a large number of neurons resulting into collective response.

We undertake the study of collective modes by studying the EEG. EEG is a manifestation of electrical activity of the brain due to the collective behaviour of a large number of neurons (Laidlaw and Stanton 1966). Collective activity of a large number of cells may yield coherence in the neural dynamics (Parikh and Pratap 1984).

As explained in the previous chapter, a qualitative study of the EEG traces by counting the average number of peaks per second is usually undertaken to classify various rhythms in the so called "brain waves" such as δ (0.5 to 3.5 Hz), θ (3.5 to 7.5Hz), α (8 to 13 Hz) and β (13.5 to 30 Hz) (Laidlaw and Stanton 1966). The characteristic time scale τ_c for these waves are of the order of 0.1 sec, while the refractory time scale τ_r associated with the electrical activity of a single neuron is 1-2 ms. Thus, there is a factor of 100 between the two time scales τ_c and τ_r and this implies that an EEG reflects the cooperative behaviour of neurons (Parikh and Pratap 1989). Thus the neural networks are very much dynamical in nature and therefore only an analysis from the point of view of nonlinear dynamics can explain the collective behaviour of the system (Babcock et al 1987, Dvorak et al 1986, Babloyantz et al 1986).

To study the collective behaviour of any dynamical system (Nicolis and Nicolis 1986), it is necessary to know the number of independent variables that are required to characterize the system and also the information flow in the system (Parikh and Pratap 1989 & 1984). Basically there exists two different approaches in the study of dynamics of a neural system. In the first approach, general equation of evolution incorporating the collective nature was formulated for the first time by Parikh and Pratap [1984] as an integral equation in which the present state of a given system is connected to an earlier state by a "mapping" or a "connection" or a "transition probability". This equation has been written by drawing inspiration from nonequilibrium statistical mechanics of the Brussel School initiated by Prigogine. The formulation given by Anderson and Cooper in 1973 has been shown as a special case of the above equation. It has

further been shown that this is capable of explaining the higher functions of the brain such as learning, recollection and association.

The second approach is the one initiated by Hopfield [1982,1984], wherein, the fact that there exists a threshold for neural firing is associated with the dynamics of spin glasses in which the starting point is a many spin Hamiltonian with a random distribution of flipping spins. Both methods described above are based on certain model-equations. However, for a complex nonlinear system like brain, it is difficult to obtain the equations of motion which will describe the exact dynamics. Hence, it will be of much help if one can have a method of analysis where equations of motion are not needed. Work in this direction has resulted in novel methods of time series analysis. A new approach in time series analysis (Grassberger et al 1983) using actual EEG records (Babloyantz et al 1986, Dvorak et al 1986), is very useful for analysing such systems whose exact equations of motion are not known. Being highly nonlinear, fourier and autocorrelation techniques have only a restricted use in such systems. The basic assumption is that a time series contains *all* the information about the system (Packard et al 1980, Atmanspacher et al 1986) even though it describes the variation of a single quantity. Hence time series analysis should provide valuable information (Nicolis & Nicolis 1986) about collective neural dynamics. We should also be able to obtain a quantitative estimate of the number of independent variables necessary to characterize the system. A detailed description of the method has already been given in chapter 2.

It has now been realized that the neural system is highly nonlinear, dissipative, and non Markovian since it is capable of retaining a memory. This implies that there should exist in the system, more than one incommensurate frequencies which manifest itself in the increased dimensions as seen in a time series analysis. This fact has already been incorporated in the evolution equation by Parikh and Pratap [1984]. However to get a clear understanding it is useful to know various time scales

involved in the neural dynamics.

5.1 TIME SCALES IN NEURAL DYNAMICS

An electrical signal corresponding to an individual impulse conducted along an axon is called the action potential or spike potential, represented by ϕ, and it is of the order of 100 mv and has dimension of $(MLT^{-2})^{1/2}$. Action potential is the basic unit of information transmitted along the nerve fibre. The signal propagation speed is the rate of travel of the nerve impulse, v and is 1-100 m/sec. If two successive stimuli separated by a certain time interval are applied to the nerve fibre, the behaviour of the fibre will depend on this time interval. Immediately after a nerve impulse has been initiated, the given part of the fibre is in the absolute refractory state, i.e., it cannot be excited again. This is followed by a relative refractory state in which the threshold potential is somewhat increased. The duration of the entire refractory time, varies from one to a few milliseconds.

Axon current is defined as the current that flows between two consecutive nodes of Ranvier (Volkenshtein 1983 & Das 1987). This is also defined as current density per unit area and is about 1 mA/sq. cm and has dimension $(MLT^{-4})^{1/2}$. For a volume current this would be $(ML^{-1}T^{-4})^{1/2}$. All neurons are not involved in the transmission of a signal, and therefore one can define neural density as the involved neurons per unit volume. This can also be defined as the fraction of affected neurons to total neurons n/N in a unit volume.

The parameters, *viz.*, the action potential ϕ($\sim$ 100mv), the time duration τ_ε ($\sim$ 1-2 ms), the axon current I ($\sim$ 1 mA/cm^2) and neuron density n are necessary to find the plausible time and length scales in neural dynamics.

5.2 DIMENSIONAL ANALYSIS

Following Parikh and Pratap [1984] each of the parameters described above has a dimension defined in terms of mass, length and time. By doing a dimensional analysis of the various quantities we can construct a dimensionless parameter Γ . First we define

$$\Gamma = \phi^x \, v^y \, I^z \, \tau^u \, n^w \qquad (5.1)$$

where x,y,z,u,w are parameters. Substituting dimension of ϕ as $(MLT^{-2})^{1/2}$, v as LT^{-1}, I as $(ML^{-1}T^{-4})^{1/2}$, τ as T and n as L^{-3}, we have

$$\Gamma = (MLT^{-2})^{x/2} (LT^{-1})^{y} (ML^{-1}T^{-4})^{(1/2)z} T^{u} L^{-3w} \qquad (5.2)$$

Sine Γ is dimensionless, we set powers of M,L and T in (5.2) to zero. We then get three equations

$$\frac{x}{2} + \frac{z}{2} = 0 \qquad (5.3)$$

$$\frac{x}{2} + y - \frac{1}{2} z - 3w = 0 \qquad (5.4)$$

$$-x - y - 2z + u = 0 \qquad (5.5)$$

There are only three equations for the five unknowns, so that we can solve only for three of them, in terms of the other two. By keeping x and v independent, we will get three equations as

$$z = -x$$
$$y = 3w - x$$
$$u = 3w - 2x$$

Substituting for z,y,u in equation (5.1), we get

$$\Gamma = \phi^{x}\ v^{3v-x}\ I^{-x}\ \tau^{3v-2x}\ n^{v}$$

$$= (\phi^{x}\ I^{-x}\ v^{-x}\ \tau^{-2x})\qquad (v^{3v}\tau^{3v}\ n^{v})$$

$$= (\phi\ /vI\tau^{2})^{x}\ (v^{3}\tau^{3}n)^{v}$$

put w=y/3

$$\Gamma = (\phi\ /\ vI\tau^{2})^{x}\ (v\tau\ n^{1/3})^{y} \qquad (5.6)$$

where x and y are two parameters. The dimensionless quantity consists of two parts, the first one depends on the electrodynamic variables ϕ and I, besides the dynamic variables such as propagation velocity v and the refractory time τ. This is the resistance per unit length per unit time. The second term however consists of only mechanical variables and is the ratio of the distance travelled by the signal during a refractory period to a characteristic length defined by $n^{-1/3}$. This clearly shows that the mechanical and electrical processes can be independent, but they can also get coupled by the choice of x and y.

A general time scale can be written as

$$T = (\phi\ /\ vI\tau^{2})^{x}\ (v\tau n^{1/3})^{y}\tau\ = \Gamma\tau \qquad (5.7)$$

The infinite possibilities are evident from (5.7) by giving

various values of x and y. Since time scales are real, x and y can take only real values, but can be rational or irrational. If x=0, y=0, equation (5.7) reduces to the refractory time. If x=y=1, then time scale reduces to $T=(\phi n^{1/3}/I)$, the ratio of the potential gradient to the axonal current and is independent of the refractory time, as well as the velocity of signal propagation. On the other hand, if x=1/2, y=0, we get a different time scale as $(\phi/vI)^{1/2}$. The various time scales are given in Table (5.1).

Table 5.1 Time scales

	x	y	z	Symbol	Order of Magnitude
1.	0	-1	$(vn^{1/3})^{-1}$	t_M Mechanical	10^{-6}
2.	0	0	τ	t_r Refractory	10^{-3}
3.	1/2	0	$(\phi/vI)^{1/2}$	t_{em} Electro-Mechanical	10^{-1}
4.	1	1	$(\phi n^{1/3}/I)$	t_{EM} Electro-Magnetic	10^{4}

It may be seen that the scales (1), (3), and (4) (see table) are all independent of refractory time. The numerical values given in the table show a wide range of magnitude. In this we have taken the density of neurons as 10^6 per c.c. The longest time scale is 10^4 sec while the shortest is 10^{-6} sec. Thus with the known parameters of the system, the longest and the shortest time scale differ by 10 orders of magnitude (Pratap 1988).

In the absence of an understanding of mutual neuronal activities, we cannot stipulate the domain of x and y. To get a feel for this, we invert this problem and determine the value of

x from the equation (Parikh and Pratap 1989),

$$T = (r\phi \,/\, \tau_\varepsilon^2 \, vI)^x \, \tau_\varepsilon \qquad (5.8)$$

where r is the fraction of neurons that are on an average electrically active. From the observed value of T_{obs} (average $\sim$ 0.1 sec) and assuming that r=1, we find that x=1/2, so that the collective time scale $\tau_c = \sqrt{r\phi/vI}$ is independent of τ_ε. Hence we can identify two distinct values τ_ε and τ_c. Clearly different values of n would lead to different values of x. It is worth repeating that the time scale for a single neuron $\tau_\varepsilon \sim (1\text{-}2)\times10^{-3}$, whereas the time scale τ_c from the EEG records is 0.1 sec ie., latter is about 100 times larger and hence the EEG patterns can justifiably be considered as being cooperative electrical activity of neuron (Parikh and Pratap 1989 & 1984). Considering these time scales present in the system we can develop the Statistical Mechanics of the systems. Also we can find the number of independent variables to characterize the state of the neural system from the EEG analysis and can use it for the model development of the system (Babloyantz et al 1986, Babcock et al 1987).

5.3 ANALYSIS OF EEG - TIME SERIES APPROACH

Time series analysis of EEG revealed that there does exist a deterministic component, which could be used to classify the neural system taking into account of nonlinear, non Markovian and nonstationary nature. The analysis of EEG records from single neuron (Rapp et al 1985) and multiple neurons (Kûrten et al 1986) have revealed the existence of deterministic component. Rapp et al [1985] recorded the extracellular action potentials of single neuron from different regions of squirrel monkey cortex by glass micro pipette electrodes with a tip diameter of 1 micrometer filled with 3M KCl, and dimensions of corresponding

attractors are calculated. They also calculated dimensions of a group of neurons. In all these cases they found that D_2 is fractal. Kûrten et al also have done the analysis using single neuron, a network of 26 neurons and also after giving stimulus, and found that chaos do exist in the system.

The quantitative analysis of EEG gives more information than the qualitative analysis where the number of peaks per second in the EEG is counted. This is further enhanced by the dichotomy in the statement "it is usually believed that a patient may have a completely normal EEG and yet have a well documented epilepsy and also an abnormal EEG may be obtained from patients with no history of seizures" (Schmidt and Wilder 1965).

We have seen in earlier chapters that any nonlinear dissipative system will shrink in phase space to a small dimensional space (Packard et al 1980, Swinney 1983, Nicolis and Nicolis 1986) called attractor (Rosseler 1976, Lorenz 1963) asymptotically in time, and it requires a lesser number of free parameters to characterize the state. The dimension of this state is called attractor dimension and the space to which the system evolve is called embedding space. The information flow in the system can be measured in terms of Kolmogorov entropy (Bennettin 1976).

The present method of analysis gives three significant quantities viz.,

1. Attractor dimension D_2, which indicates the smallest number of variables that are required to characterize the asymptotic state of the system.

2. Embedding dimension d_ε , indicating the dimension of the subspace of the total phase space to which the system shrinks due to nonlinear dissipation.

3. Kolmogorov entropy K_2, which indicates the information capacity of the system.

This method answers the questions: (i) Does all neural system evolve to an attractor state and if so, do they have an integer dimension (regular attractor) or a fractional or fractal dimension (strange attractor), (ii) whether this is an invariant characteristic of all the systems and can this be used to classify neural system in a quantitative manner ? (iii) Does information flow occur in such a system ?

To answer these questions we analysed the EEG (eight channels) of a 'clinically' normal (without any known malfunctioning of the brain) person (age 39). We have undertaken the analysis at two stages : first in the resting state and second when the subject is given simple numerical problems of multiplication and division. These EEG records were taken under the same conditions.

5.4 IMPORTANCE OF D_2 AND K_2

A system which is nonstationary, nonlinear and chaotic is not amenable to the usually known analytical techniques and hence one has to resort to methods to find out as to whether there are any invariant parameters in the system which could characterize the system and can be used as an index for classification. The two parameters D_2 and K_2 falls in this category. It may be realized that D_2 - the dimension of the attractor as well as the dimension of the subspace of the phase space in which the attractor is embedded can be obtained by evaluating $C_d(\varepsilon)$ in the limit $\varepsilon \to 0$ and $d \to \infty$. D_2 gives the minimum number of parameters that one requires to characterize a dissipative nonequilibrium system in its asymptotic state. As no limiting process is involved in time, these are known as static parameters. However in obtaining K_2, one takes the limit of $\tau \to 0$ or the time interval between the consecutive readings is also subjected to a limiting process. K_2 is hence considered as a

dynamic parameter. The Kolmogorov entropy can be considered as the rate at which information about the system is lost in course of time (Schuster 1984). There is however a basic difference between the Kolmogorov entropy and thermodynamic entropy, since while the former is infinite for a completely chaotic system, the latter attains a maximum stationary value when the system attains an equilibrium. Thus while thermodynamic entropy defines the degree of disorder in the system, Kolmogorov entropy determine how chaotic a dynamical system is. One would appreciate the difference if one realises the difference between disorder and chaos. The former is characterized by a completely stochastic process, while there is determinism in the latter and are characterized by deterministic equations.

5.5 DATA ACQUISITION

Figure 5.1 represents the diagram of the electrode positions as seen from the top.

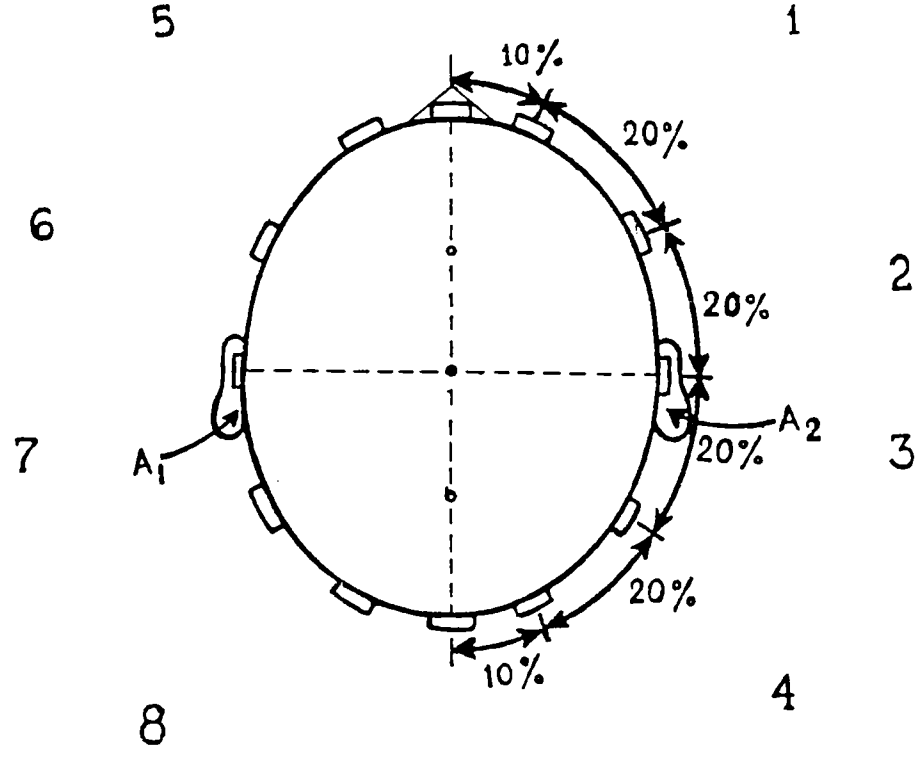

Fig 5.1 10-20-20-20-20-10 system of electrode positions used for rest and mental activity.

Eight channels of EEG are taken simultaneously according to the 10-20-20-20-20-10 international scheme (i.e; EEG records from electrodes located at the left and right sides of the skull - Frontal, Temporal, Parietal and Occipital). Each ear is grounded and this is connected to the front posterior at either side. The electrical fluctuation with respect to this is amplified and recorded on a chart recorder. We have taken, in all cases, data of duration 10 seconds each and digitized at 20 millisecond interval. We thus get a set of 500 data points for each channel. The record was made when the subject is at rest as well as when he was given simple arithmetic problems such as multiplication and division of small numbers. The process was repeated for three consecutive days at 8 am everyday. The purpose was basically to find out (a) whether there is any difference in the characteristic parameters if the person is subjected to mental activity and (b) having known about the kind of exercise the person is subjected to, is there any change in the mental activity on subsequent days ?. This would imply a direct connection between neural activities and the psychological conditions of the subject.

5.6 AUTOCORRELATION IN EEG RECORDING

As mentioned in previous chapters, Autocorrelation analysis is a qualitative analysis, which tells us how system resembles itself as time increases. In the case of periodic system it shows a repetitive nature, whereas in the case of chaotic system, autocorrelation function $\psi(\tau)$ tends to zero as τ increases.

In order to study the possible variation of autocorrelation in EEG patterns during mental activity, autocorrelograms were constructed from recordings of all the

eight channels during rest and mental activity period on all the three days. Fig.(5.2) give typical autocorrelograms for rest and mental activity, for three consecutive days.

It has been observed that the nature of the autocorrelograms varies from channel to channel (Fig.5.3 a &b) due to differences in the neural activity at respective locations. However, the structure of autocorrelograms does not show much variation during mental activity as compared to, when the person is at rest. In almost all cases $\psi(\tau) \to 0$ as $\tau \to \infty$.

The fact that autocorrelation is not much sensitive to the state of the neural system demands alternate techniques to analyse EEG recordings. As described earlier, analyses involving the evaluation of K_2 and D_2 thus assume importance in the field of neurophysics.

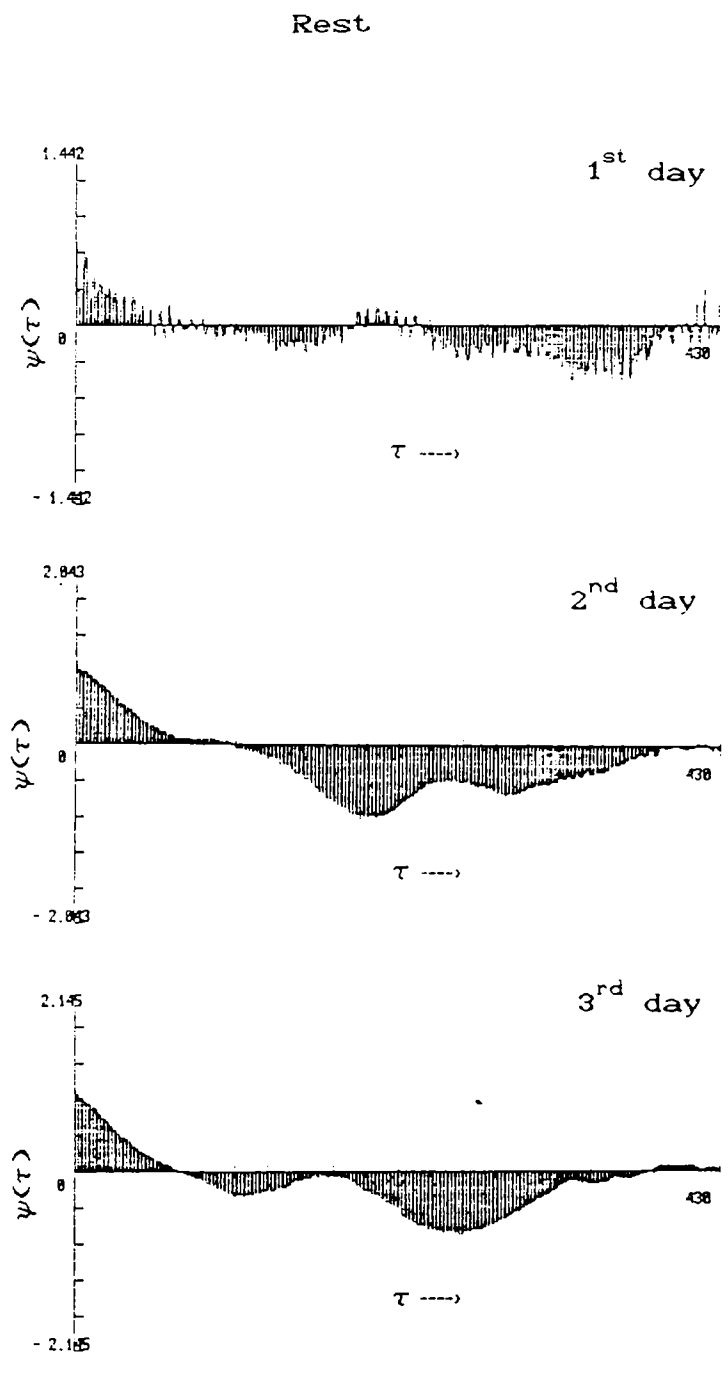

continued....

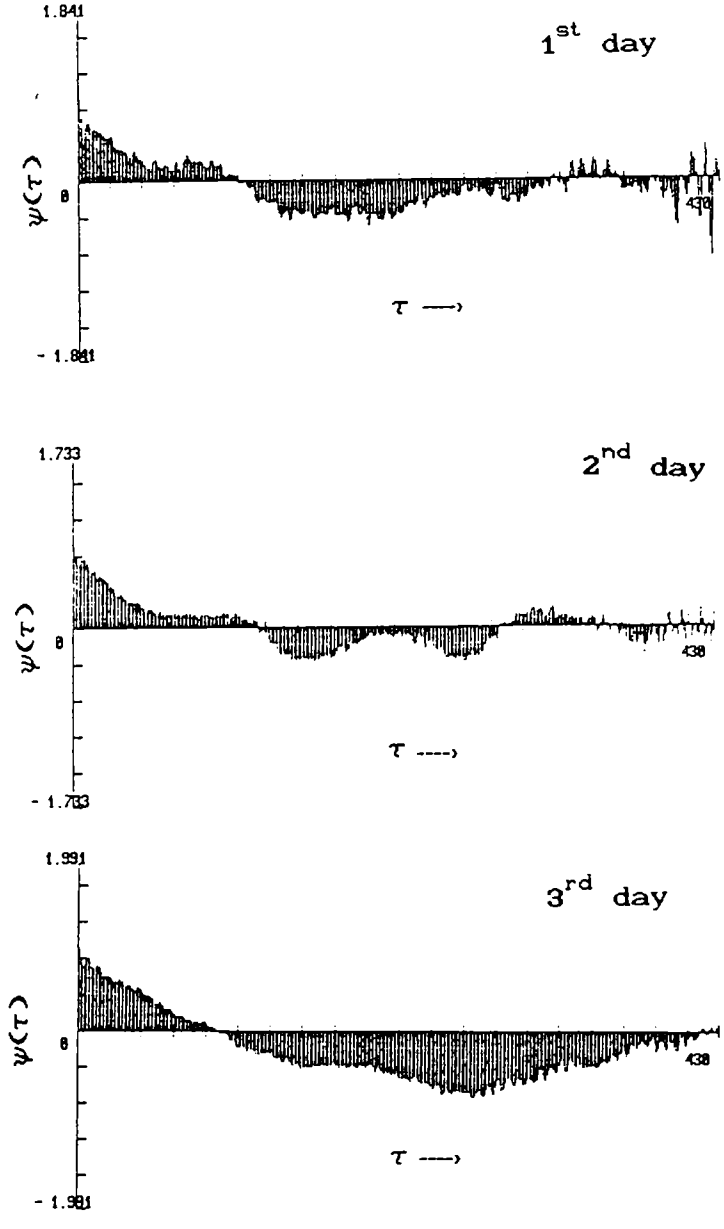

5.2 Comparison of $\psi(\tau)$ (2^{nd} channel) between rest and mental activity for three consecutive days.

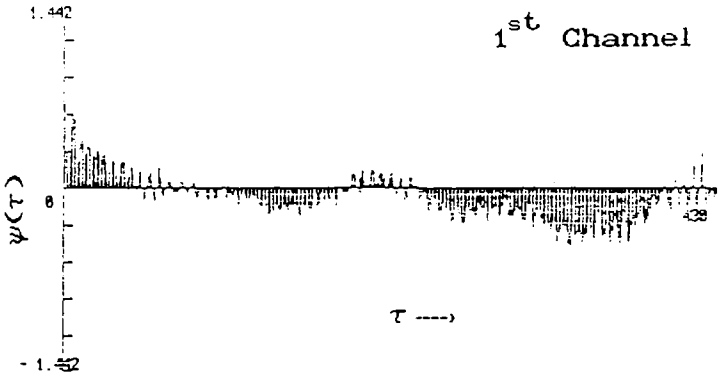
1.442
1st Channel
ψ(τ)
0
τ ---->
- 1.452

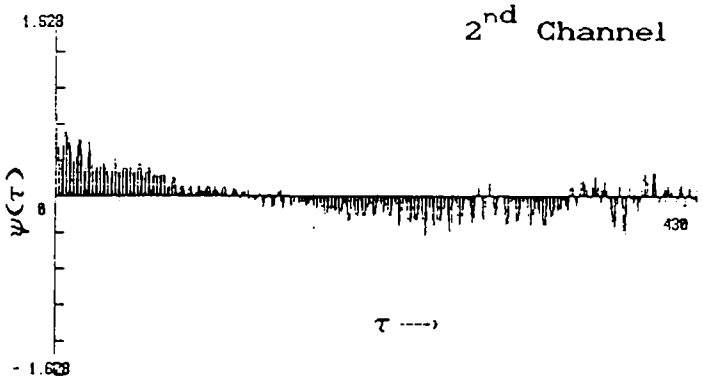
1.628
2nd Channel
ψ(τ)
0
τ ---->
- 1.628

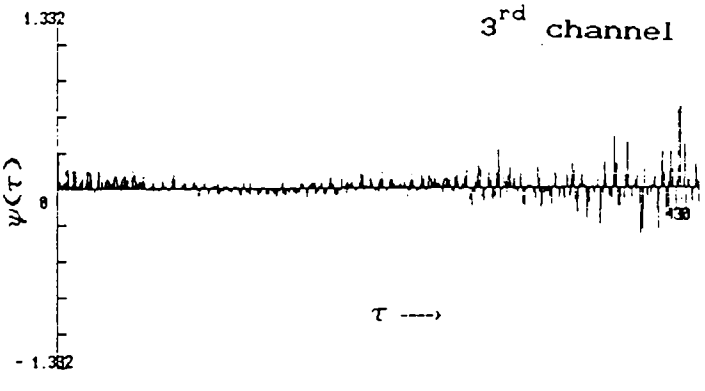
1.332
3rd channel
ψ(τ)
0
τ ---->
- 1.382

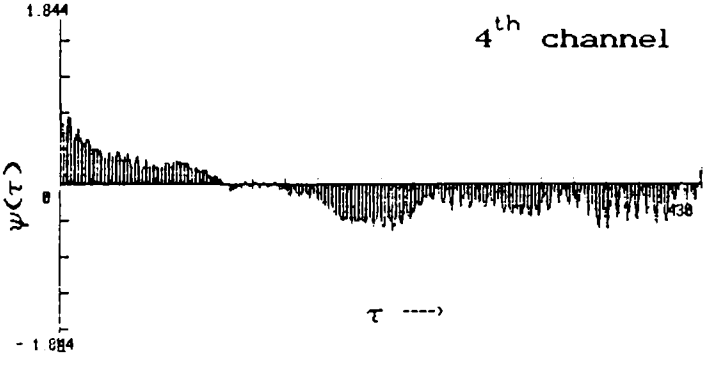
1.844
4th channel
ψ(τ)
0
τ ---->
- 1.884

continued.....

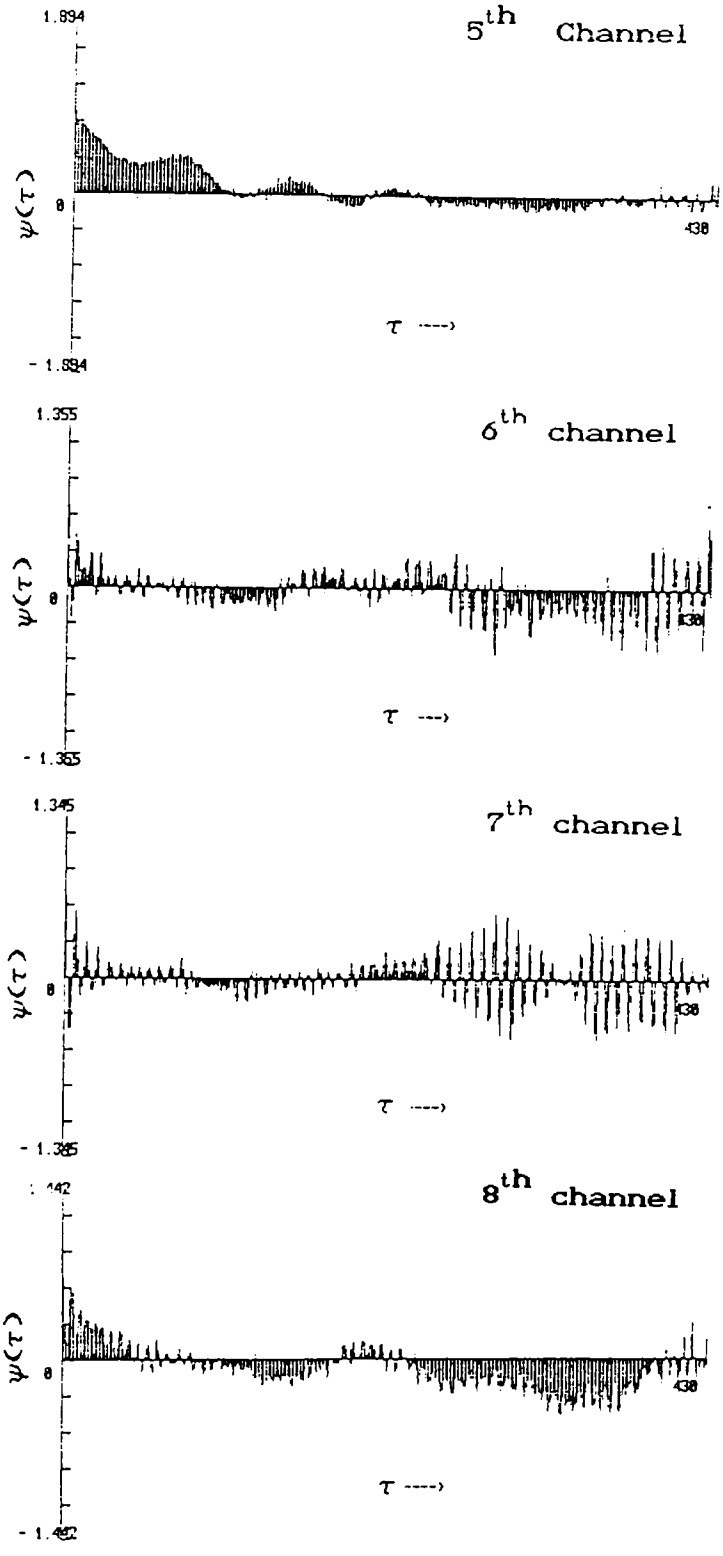

5.3a Autocorrelation function $\psi(\tau)$ in all the eight channels of a 'clinically' normal person (1st day) during rest.

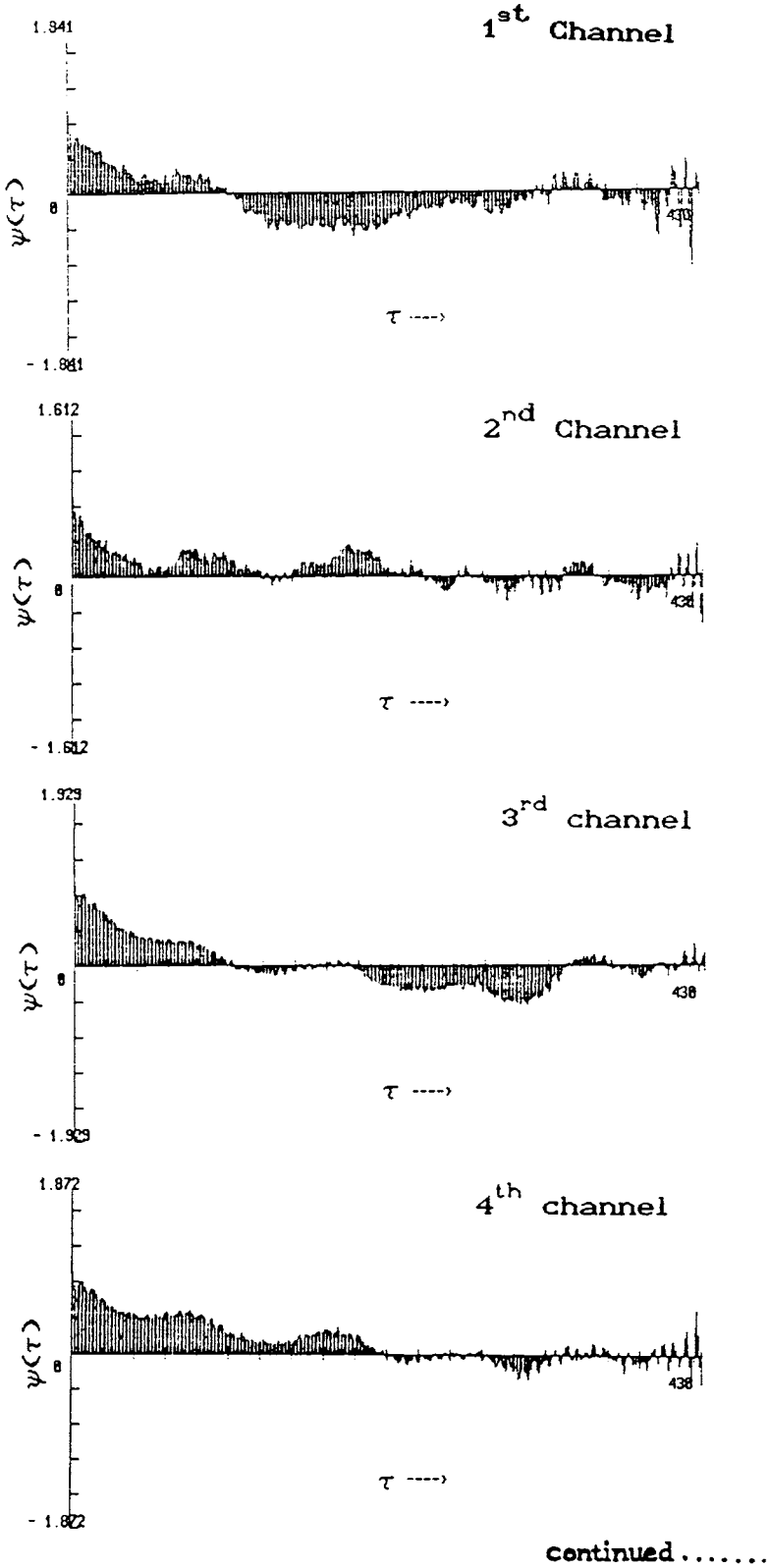
1st Channel
1.341
ψ(τ)
0
- 1.861
τ ---->
2nd Channel
1.612
- 1.612
3rd channel
1.929
- 1.929
438
4th channel
1.872
- 1.872

continued.....

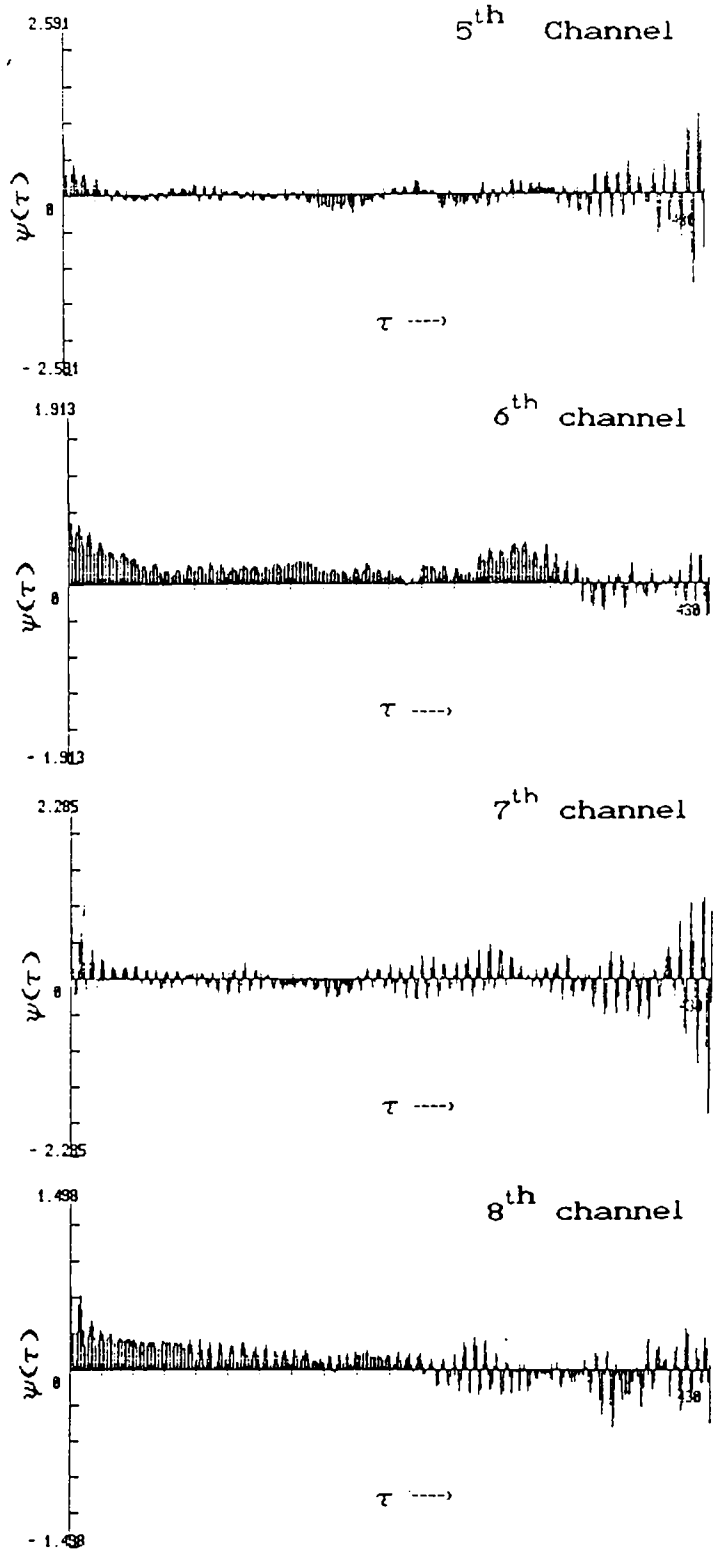

5.3b Autocorrelation function $\psi(\tau)$ in all the eight channels of a 'clinically' normal person (1^{st} day) during mental activity.

5.7 ANALYSIS (Evaluation of D_2 and K_2)

Each data set for eight channels, during the resting as well as during the mental activity for three consecutive days (in all 48 sets) were analysed separately. Each data set was

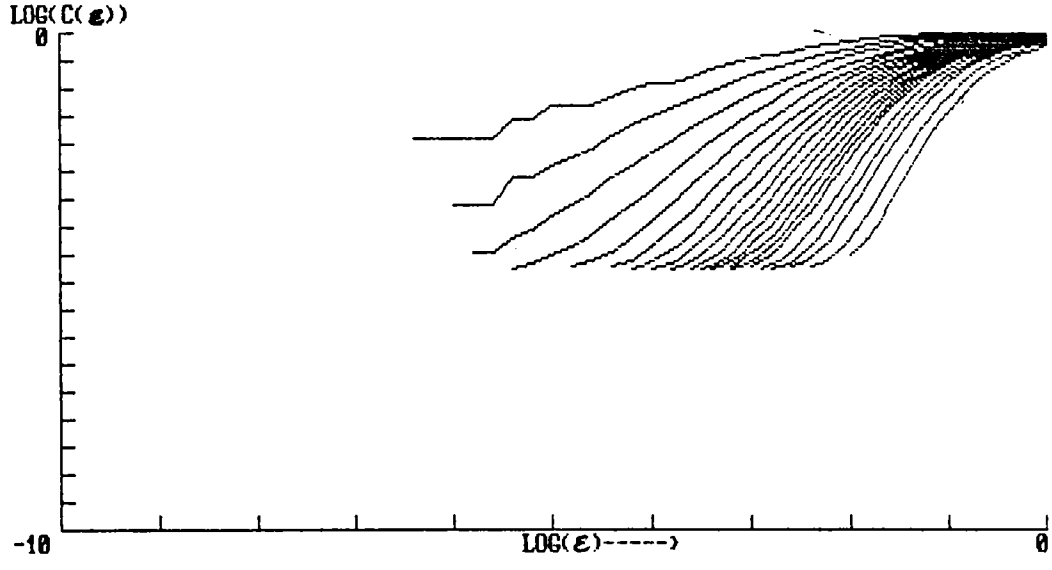

Fig 5.4 A plot of log $C_d(\varepsilon)$ for the 6th channel of a clinically normal person during rest.

used to calculate the correlation integral $C_d(\varepsilon)$ as given in equation (2.26) and a plot of log $C_d(\varepsilon)$ against log(ε) was made for d=1 to 30, as shown in figure (5.4). This plot was then used to calculate the mean slope of each curve and Figure (5.5) gives a plot of this slope against dimension. If the system were completely stochastic, this plot would be a straight line inclined at 45° to the d-axis or the relation would be $C_d(\varepsilon) \approx \varepsilon^d$. In the present case, the curves for all 48 EEG data sets deviate from this straight line and saturate for large d. This saturation value, when it becomes independent of d, gives the characteristic correlation dimension D_2. The separation from the asymptote takes place as d attains the embedding dimension. The results are presented in Table 5.2a, b and c for three consecutive days. The results are arranged for each channel as

seen in Figure (5.1). The values in parenthesis give the correlation dimension during mental activity.

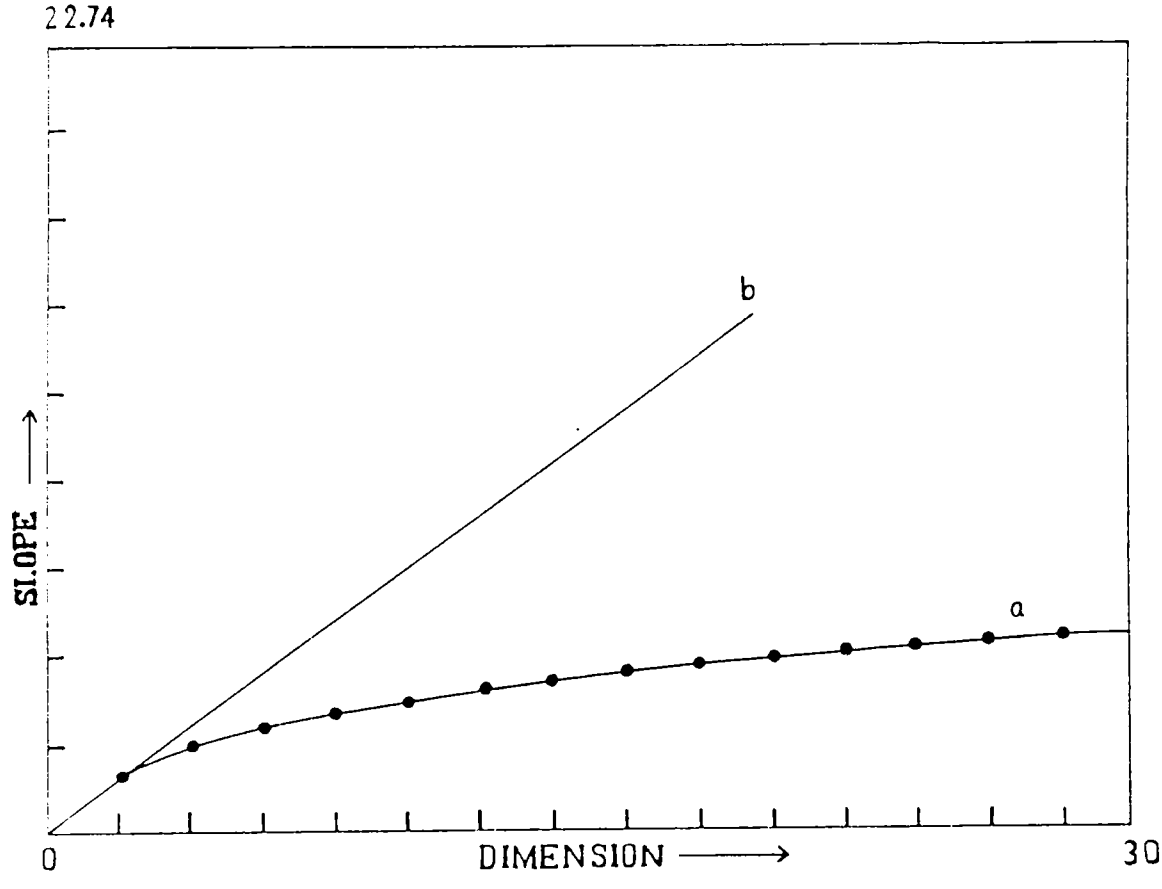

Fig 5.5 The average slope $d(\log C_d(\varepsilon))/d \log(\varepsilon)$ of the linear part of the curves of Figure 5.4 plotted as a function of d.

It may be noted that the dimensions are all fractal, thereby, representing strange attractors. Again the eighth channel shows a steady decrease from the first day to the third day during the resting stage. This feature however is not seen in the other channels. By and large, for other channels, there is a slight increase for the second day, but get reduced on the third day. However in the case of during the mental activity the eighth channel registers an increase and then seems to get stabilized.

In Figure 5.6 we have plotted $K_{2,d}$ for a particular

channel as a function of d.

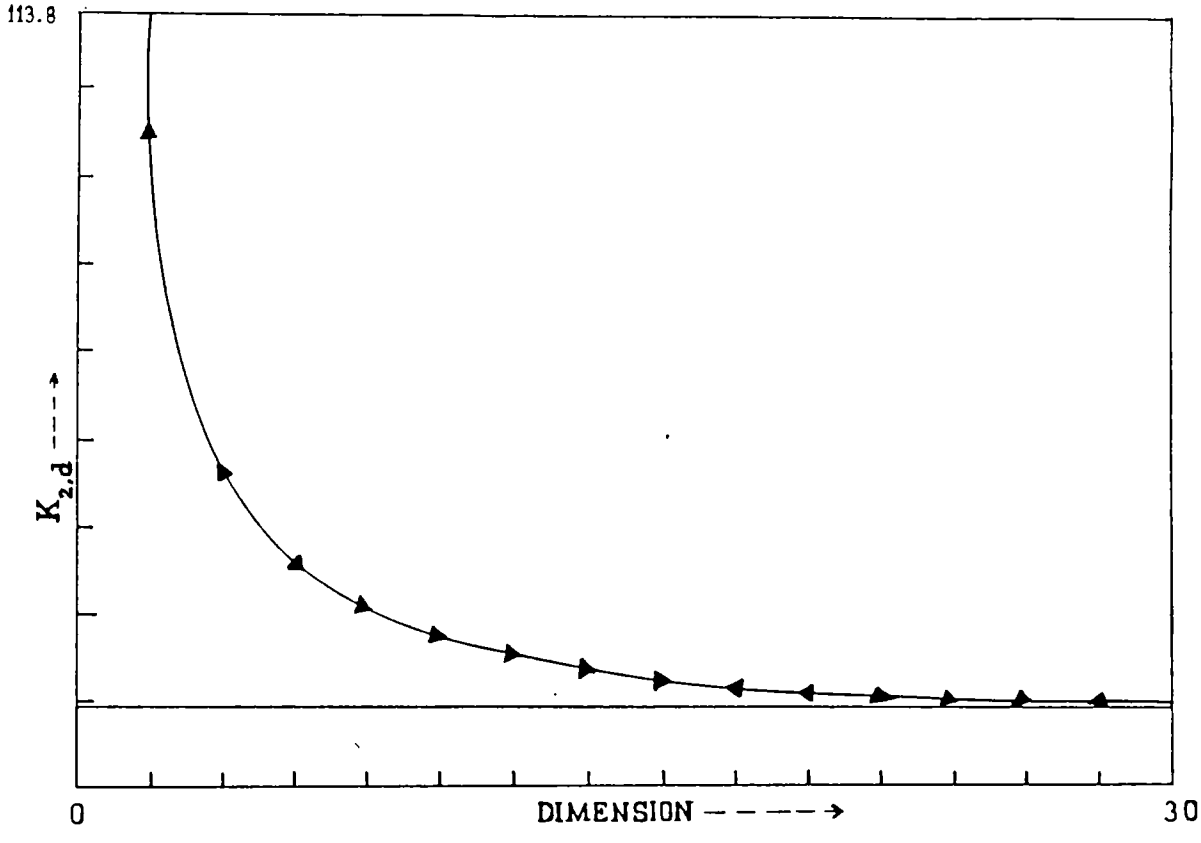

Fig 5.6 The spatial separation $\tau^{-1}\log(C_d/C_{d+1})$ of the correlation curves as a function of d.

One remarkable feature to be observed is that for lower dimension the data is noise dominated and hence a larger K_2 and the deterministic component becomes dominant only when d attains larger values resulting in the saturation value of K_2. Thus to obtain tangible results, one has to go for higher dimensions. A nonzero second entropy indicates the existence of deterministic chaos.

5.8 GENERALIZED DIMENSIONS AND f(α) SPECTRUM

As described in chapter 2, strange attractors have fractal geometry and can be characterized by a set of generalized dimensions D_q. Knowing D_q, we can evaluate sets of singularities of strength α (scaling index), and corresponding dimension f(α).

As indicated earlier, $f_{max}(\alpha)$ corresponds to D_o.

We have evaluated D_q and $f(\alpha)$ spectrum from the 7^{th} channel of EEG recording of a normal person at rest. Fig.(5.7) shows the variation of D_q with q and is of standard form reported by earlier workers (Halsey et al 1986a & c, Grebogi et al 1988, Broggi et al 1989).

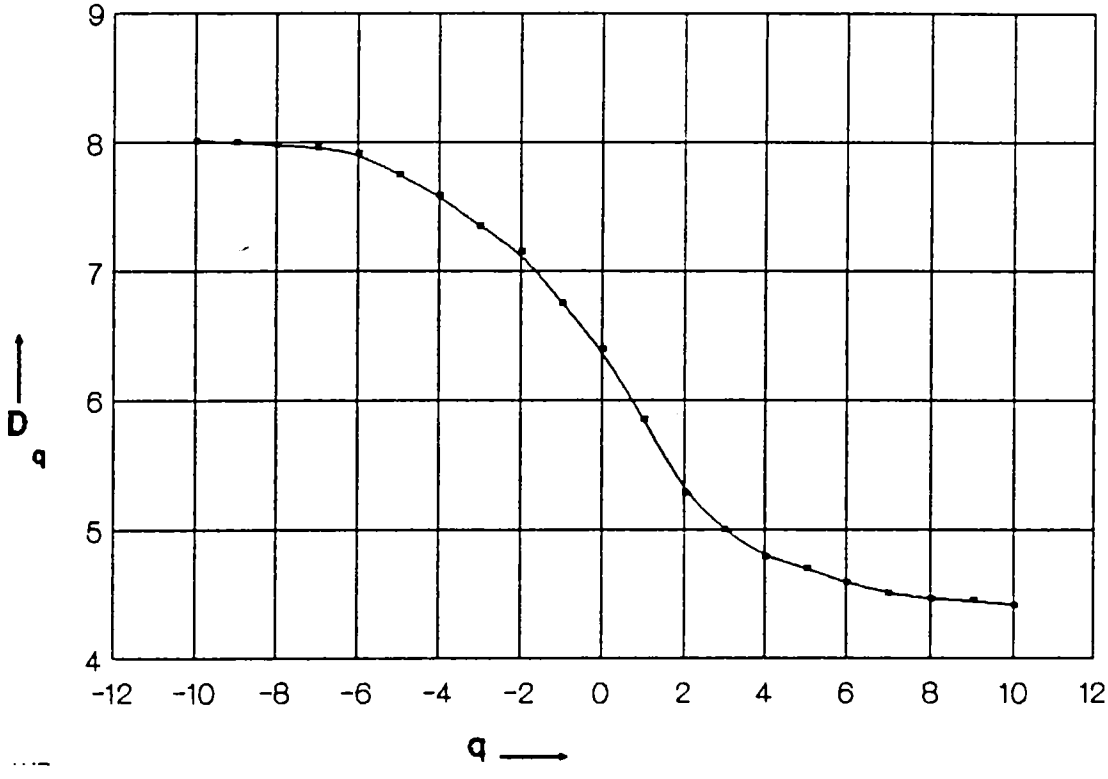

Fig 5.7 D_q as a function of q for the EEG (7^{th} channel) of a 'clinically' normal person during rest.

Scaling spectrum $f(\alpha)$ has been evaluated using the equation 2.59 *viz.*,

$$\alpha(q) = \frac{d}{dq}\left[(q-1)\, D_q \right]$$

Fig.5.8 shows $f(\alpha)$ spectrum for the EEG recording of the 7^{th} channel of a normal person at rest. The $f_{max}(\alpha) \equiv D_o = 6.39$,

$D_{\infty}^{(\alpha_{min}\sim 4.09)}$ and $D_{-\infty}^{(\alpha_{max}\sim 8.74)}$ points correspond to the most concentrated and the most rarefied region of the measure (see section 2.7). There exists two peaks in the spectrum - one broad (peak height 6.39)and the other sharp (peak height 6.65).

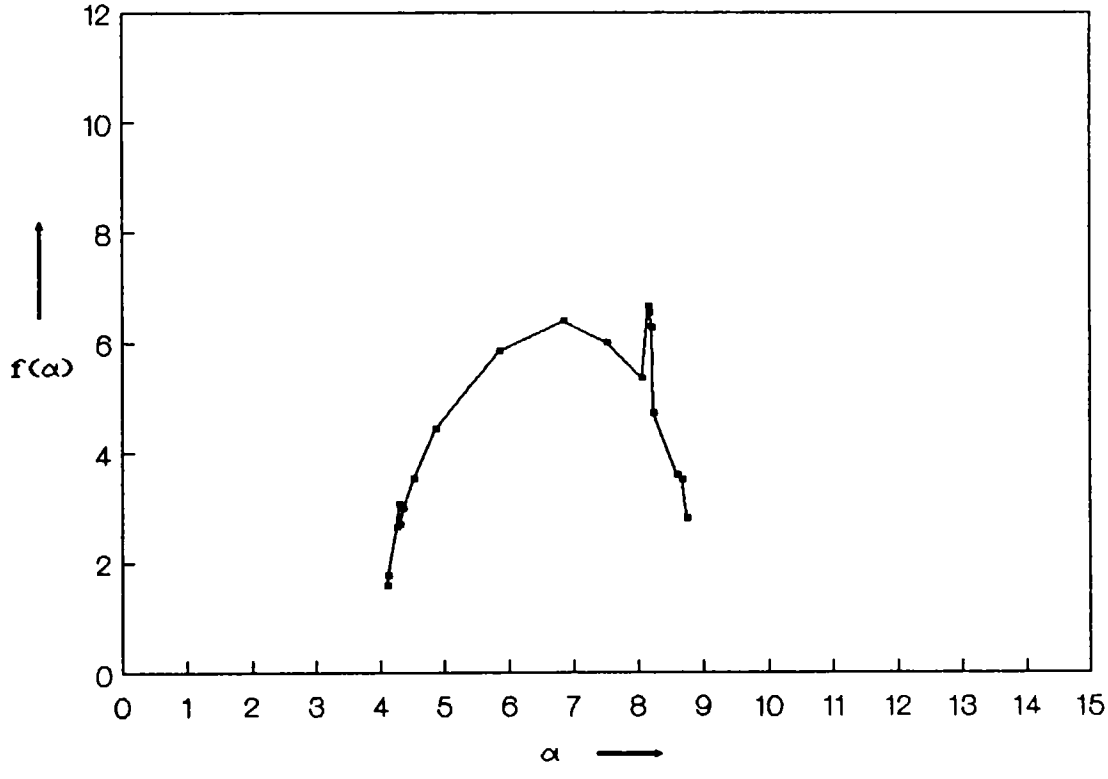

Fig 5.8 f(α) vs α for the EEG (7^{th} channel) of a 'clinically' normal person during rest.

It should be noted that the f(α) spectrum evaluated in the present case is not symmetrical unlike in the case of other systems like two-scale cantor set and period-doubling attractor (Halsey 1986a). Non symmetric f(α) spectra have been observed earlier also in the cases of circle map (Halsey 1986a) and NMR laser (Broggi et al 1989). Broggi et al observed that structure of f(α) spectrum will depend on the state of the nonlinear system. For example, in NMR laser, f(α) spectrum shows double humps when the laser is modulated with certain critical strength. The double peak of f(α) spectrum characterises the co-existence of two attractors (Broggi et al 1989).

We have also evaluated D_q values (Fig 5.9) and f(α) spectrum of the same person under mental activity.

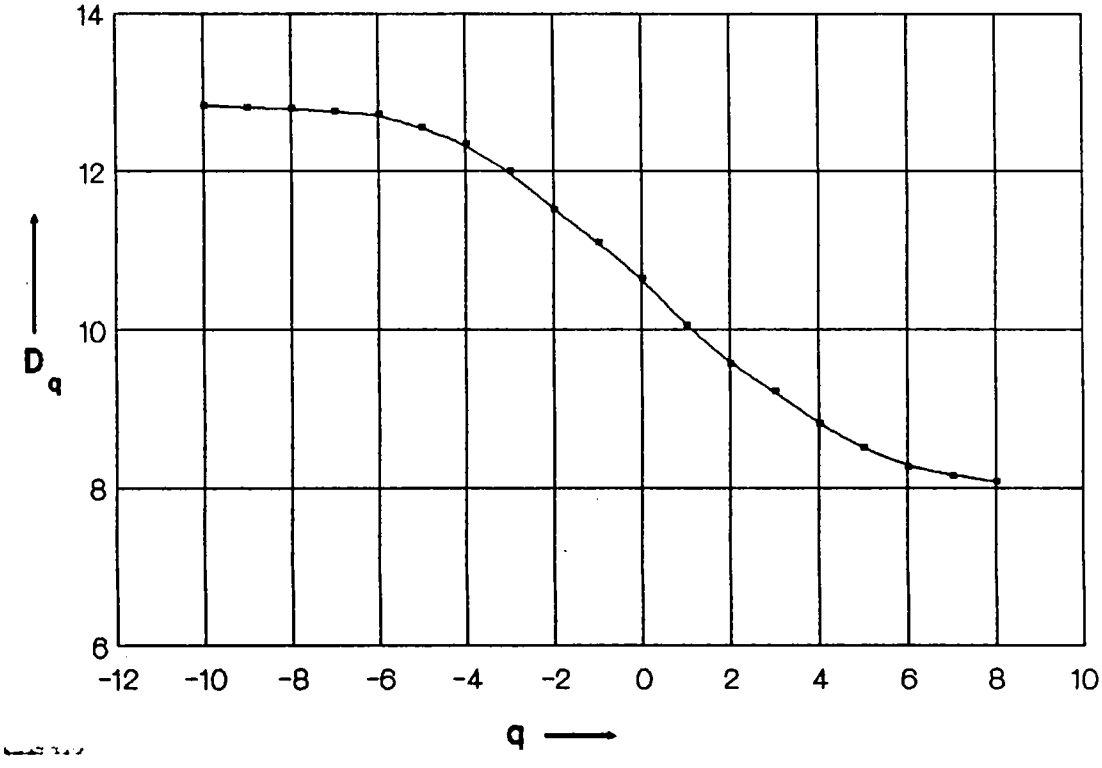

Fig 5.9 D_q as a function of q for the EEG (7^{th} channel) of a 'clinically' normal person during mental activity.

Results show the variation in f(α) spectrum in comparison with that evaluated during the rest (Fig 5.10). The f(α) spectrum in this case also shows two peaks. The height of both the peaks increase by a considerable amount (10.6 for main peak and 11.01 for the sharp peak). Also, the width of f(α) spectrum during mental activity almost doubles ($\Delta\alpha$ = 6.3) in comparison with that during rest ($\Delta\alpha$ = 3.6). This means that the attractor takes up a more complex structure during the mental activity. It is to be noted that during mental activity the f(α) spectrum as a whole shifts to higher α-values. Thus the present observations suggest that f(α) spectrum depends on the mental state of the person.

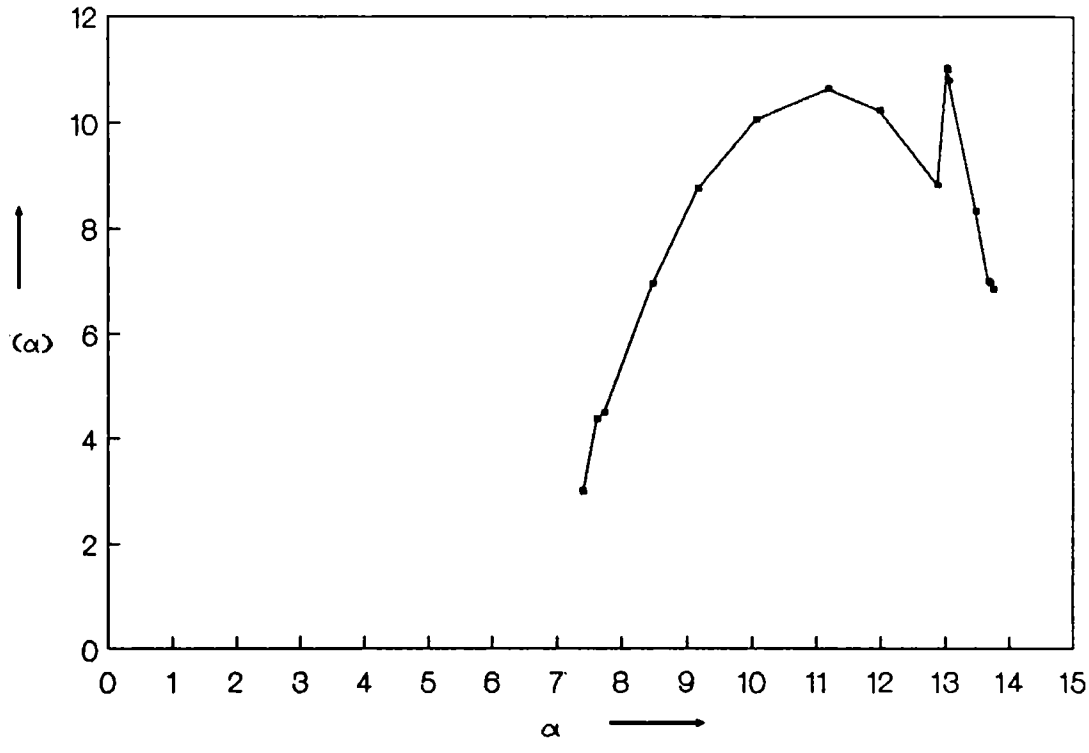

Fig 5.10 f(α) vs α for the EEG (7th channel) of a 'clinically' normal person during mental activity.

5.9 INFORMATION FLOW IN BRAIN

If P(A) is the probability of the occurrence of a certain event A, then P(A)=0.99 would indicate the almost certainty that the event would occur while P(A)=0.001 indicate the almost certainty that the event will not take place. Hence in either case, there is very little uncertainty. However, maximum uncertainty would be when P(A)=0.5. Again the uncertainty that exists before an experiment is performed is removed when once the quantity A_i becomes known after the experiment has been performed and we get information of the system. This information that one obtains in a series of experiments is known as entropy, defined as

$$K_q = - \lim_{\varepsilon \to 0} \lim_{\tau \to 0} \lim_{d \to \infty} \frac{1}{\tau d} \frac{1}{q-1} \ln \sum_{i_1 \ldots i_d} p^q (i_1 \ldots i_d)$$

and this can also be a measure of unpredictability of the system. Thus the entropy can be considered as a measure of information as well as uncertainty. This quantity however is not a static parameter, for, if the uncertainty before the input X_n is $K(X_n)$, then if the channel is noise free, then the output Y_n would reduce the uncertainty and as such $K \to 0$. Thus one can have a single valued mapping between X_n and Y_n. However, if the process is noisy, the uncertainty may be reduced but it will not be completely removed so much so X_n cannot uniquely defined by knowing Y_n. Thus, if $K(X_n/Y_n)$ is the conditional probability then the quantity

$$I(X,Y) = K(X) - K(X/Y) \qquad (5.9)$$

is called information flow (Parker and Chua 1987). In the present analysis, the entropy that is measured after the person has been subjected to mental activity could be identified as the conditional probability, since this has happened because of the input. Thus isentropy curves and their difference would give a means of the information flow. The numerical values are given in the Table 5.2, while the numbers in the parenthesis are the values corresponding to mental activity.

Figures (5.11), (5.12) and (5.13) give the isentropy curves for three consecutive days. Indeed to draw the isentropy curves, one requires a much closed grid of numbers. Nevertheless the curves here, indicate the trends. The solid curve represent the isentropy curves during the resting state while the broken ones are for the state when the mental activity is on. The space is the same as indicated in Figure (5.1); the right hand side indicate the channel 1 to 4 and the left 5 to 8. The arrows

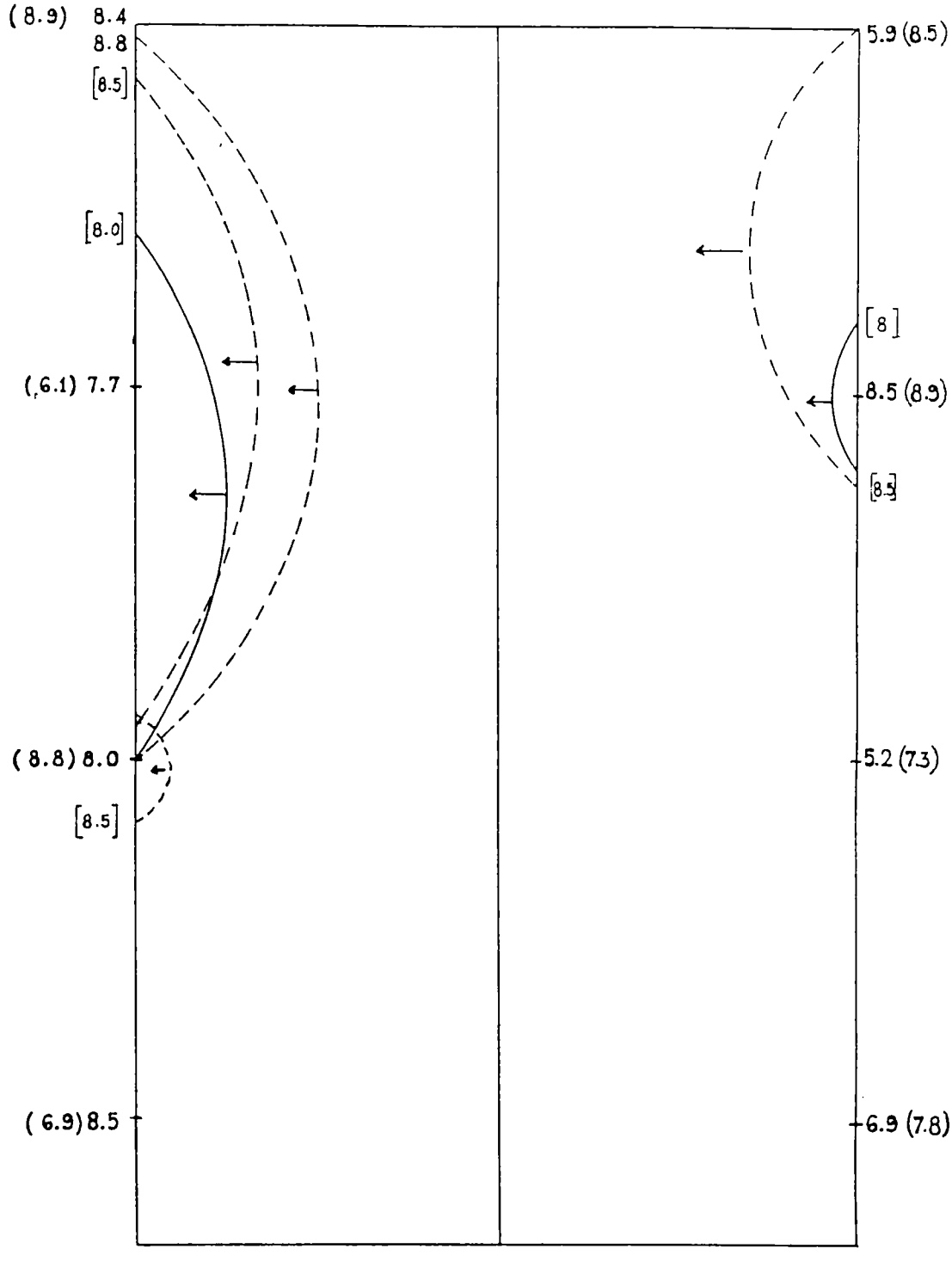

Fig 5.11 The figure indicates the Kolmogorov entropy for the first day. Numbers on the right hand side indicate the channels 1-4 and on the left hand side the channels 5-8 as indicated in Figure 5.3. The numbers in the simple bracket indicate the K_2 values during mental activity. The numbers in square bracket is the constant value of K_2 for the curve. The solid curve represents the resting state, the dotted ones for the period of mental activity. The arrow indicates the downward gradient direction.

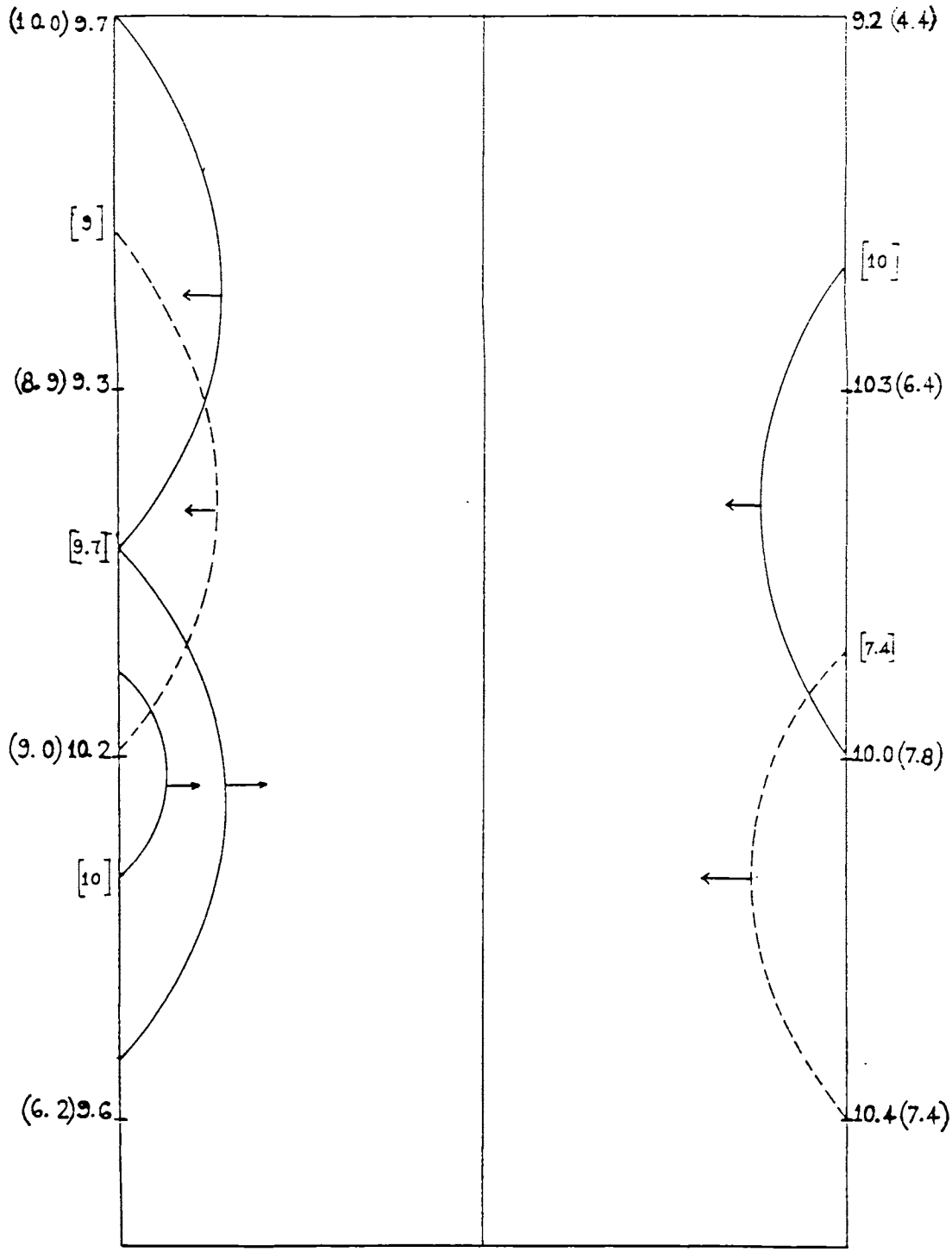

Fig 5.12 The same kind of curve as in Figure 5.7 for the second day. It may be noted that the gradient direction during the mental activity is the same for all the three consecutive days.

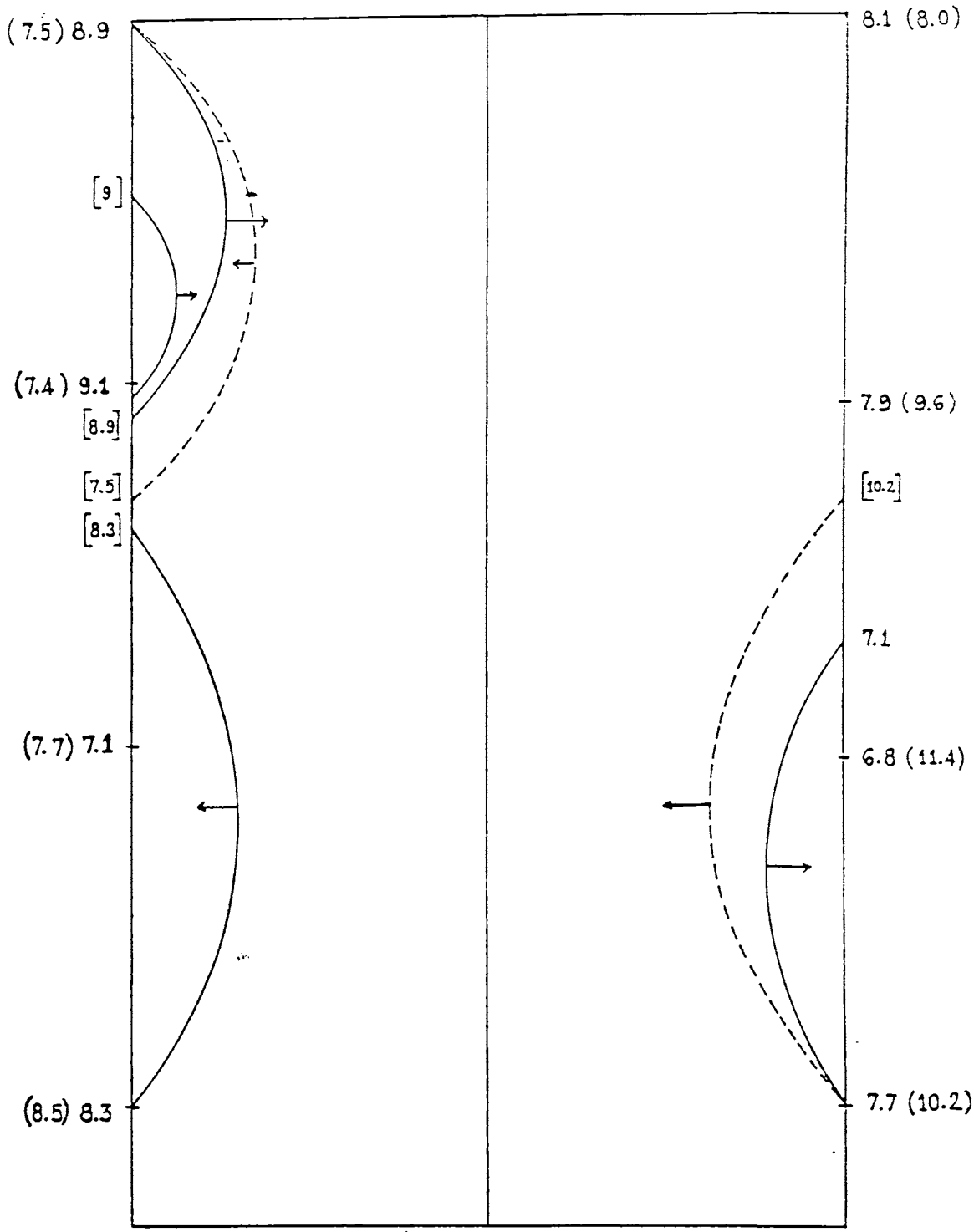

Fig 5.13 The Kolmogorov entropy plot for the third consecutive day. Here again the gradient direction during the resting position differs from the earlier days, while the mental activity component maintains the same direction as on the previous two days.

Table 5.2 D_2 and K_2 of a 'clinically' normal person during rest and mental activity, for three consecutive days.

FIRST DAY (a)

channel		D_2		K_2	
5	1	5.22(4.63)	3.50(5.94)	8.41(8.85)	5.85(8.54)
6	2	5.72(4.53)	4.17(5.21)	7.72(6.14)	8.53(8.87)
7	3	4.97(5.56)	3.18(6.04)	7.96(8.77)	5.15(7.28)
8	4	6.17(3.50)	4.50(5.56)	8.52(6.90)	8.91(7.84)

SECOND DAY (b)

channel		D_2		K_2	
5	1	5.96(5.46)	5.07(5.38)	9.73(10.04)	9.21(4.35)
6	2	5.14(4.74)	5.95(3.37)	9.33(8.31)	10.31(6.38)
7	3	5.58(5.46)	4.70(5.18)	10.22(9.02)	9.97(7.79)
8	4	5.52(4.77)	6.46(5.43)	9.55(6.31)	10.38(7.36)

THIRD DAY (c)

channel		D_2		K_2	
5	1	4.20(5.32)	3.39(5.06)	8.90(7.50)	8.09(8.01)
6	2	5.13(4.31)	3.59(5.32)	9.11(7.41)	7.88(9.62)
7	3	4.46(5.06)	4.54(6.53)	7.13(7.67)	6.77(11.41)
8	4	4.49(4.45)	4.77(6.17)	8.29(8.54)	7.07(10.15)

indicate flow from maximum to minimum - i.e, an outward arrow indicate the fact that the values inside are higher than the entropy value of the curve, while an inward arrow indicate a lower value inside the curve. This is equivalent to an information gradient. On the first day both the resting as well as active curves have a flow from the right to left. Thus the information flow has a structure in which the entire brain takes part. Here also the person was not let known about the type of exercise he is going to be subjected to. Again the flow pattern show a reverse in the parietal and occipital as compared to the frontal part. This is more obvious on the second day. On this day, the subject knows the kind of exercise, he has to undertake.

Nevertheless, the pattern during the mental activity is from right to left. On the third day again the mental activity curve preserves the same structure, while the resting one have a different structure as compared to the previous days. The random firings taking place in the neural system during the resting time could probably account for the apparent inconsistency in the pattern which completely vanishes when the mental activity is on. Thus flow patterns in the system would indicate the state of mental activity in a subject. It may also be noticed in Figure (5.6) that the curves do not go asymptotically parallel to the d-axis. While the present method is indeed one which separates the stochastic part from the deterministic one, some element of weak stochasticity may still persist in the data system. Any major instrumental artifacts may also be filtered out, as we take $|X_i - X_j|$ in the evaluation of correlation integral.

CHAPTER 6

PATHOLOGICAL CONDITIONS OF THE BRAIN

This chapter describes how D_2 and K_2 values varies with respect to various pathological conditions of the brain. Analysis shows a trend in which K_2 values depend on the state of neural system and hence can be used as a diagnostic tool. Spatial mapping of K_2 values at high spatial resolution can be used for imaging purpose.

PATHOLOGICAL CONDITIONS OF THE BRAIN

In the literature there are a large number of references, describing the existence of chaos in biological systems especially in neural system (Holden 1982, Chay 1984). Recent progress in the theory of nonlinear dynamical systems has provided new methods for the analysis of EEG as a time series which will reveal the underlying dynamics of the neural system. Details are given in Chapter 2. By using this technique Babloyantz and Destexhe [1985, 1986] have shown the existence of deterministic chaos in the neural system, by evaluating the attractor dimension. Rapp et al [1987] have shown the existence of chaotic behaviour by analysing the spontaneous activity of cortical neurons of squirrel monkey and EEG of human brain.

The basic assumption of the present analysis is that the time series contains all the informations regarding the physical process (Packard et al 1980). The usual method of using the EEG by neurologists is to count the average number of peaks per second and to attribute various rhythms such as δ, θ,α or β as described in earlier chapter. The amount of sophistication that has undergone into the design of an EEG apparatus has therefore not been adequately exploited.

There is a great deal of information in EEG which has not been extracted. The present method extracts the deterministic component from an apparently random signal, and it is hoped that this method would result in a more quantitative diagnostic tool

for understanding the state of the neural system under various pathological conditions.

In all the previous studies (Babloyantz et al 1985, 1986,Rapp et al 1985, 1987) only one of the eight channels of an EEG were considered and the underlying assumption was that the system is self similar with all the channels having similar characteristics. But in order to test this assumption we analysed all the eight channels of an EEG of a "clinically" normal person known to be free from any malfunctioning of the brain. It was found that at each point in the Head - space, there is a different strange attractor with different embedding dimension as well as different dimension and different Kolmogorov entropy. It is therefore inferred that a normal system should include a collection of interacting strange attractors.

Previous workers (Babloyantz et al 1985, 1986 Dvorak et al 1986, Destexhe et al 1988) have used second order dimension to characterize the neural system. But analyses show that (Caputo and Atten 1987, Pratap et al 1988, Reghunath et al 1987), Second Kolmogorov entropy (K_2) is more sensitive than the second order dimension (D_2) to characterize the state of the brain. (In our later discussions we use K_2 and D_2 instead of second Kolmogorov entropy and second order dimension). In the case of neural system, the K_2 is higher implying that system is more complex. We extended our studies in order to understand the different pathological conditions of the brain such as epileptic case during seizure, tumor affected brain, mild cases of Migraine and persistent headache, in terms of K_2. We tried to identify the regions of the brain which are actively taking part under various pathological conditions. A comparative study of the different parts of the brain during various conditions has also been made. We also try to answer the questions like, can one use this sensitive parameter to classify the different pathological conditions of the brain ? Can one use this as a diagnostic tool ?.

6.1 EEG MEASUREMENTS - DIFFERENT MODES OF ELECTRODE CONNECTIONS

As explained in the last two chapters EEG measurements are done based on 10-20-20-20-20-10 international scheme (Fig.4.10). Simultaneous measurement of EEG from different regions of the brain depends on the number of channels (8,16,32,64 etc.) available in the EEG equipment. In the most common type of EEG equipment 8 channels are available, so that simultaneous measurement of EEG from 8 positions of the brain is possible. But, again the choice of electrode positions depends on the type of disease and affected regions of the brain.

Various types of electrode configurations commonly used with an 8 channel EEG equipment are explained in this section. For convenience, the following notations are used.

A1	—	left ear lobe
A2	—	right ear lobe
F	—	frontal
C	—	central
T	—	temporal
P	—	parietal
O	—	occipital

1. EC1

This is one of the common types of EEG recording and is bipolar in nature. This electrode configuration has been used for recording EEG of a "clinically" normal person during rest and mental activity and in certain pathological conditions like, Grand mal epilepsy, Migraine and epilepsy with demylinated disease. In this configuration (Fig 6.1a) simultaneous measurement of EEG from eight regions of the brain is possible - i.e, four regions from the right half and four regions from the left half of the brain. The positions are represented as follows

Right frontal (channel 1) — F_{p_2} → F_8

Right temporal (channel 2) — F_8 → T_4

Right parietal (channel 3) — T_4 → T_6

Right occipital (channel 4) — T_6 → O_2

Left frontal (channel 5) — F_{p_1} → F_7

Left temporal (channel 6) — F_7 → T_3

Left parietal (channel 7) — T_3 → T_5

Left occipital (channel 8) — T_5 → O_1

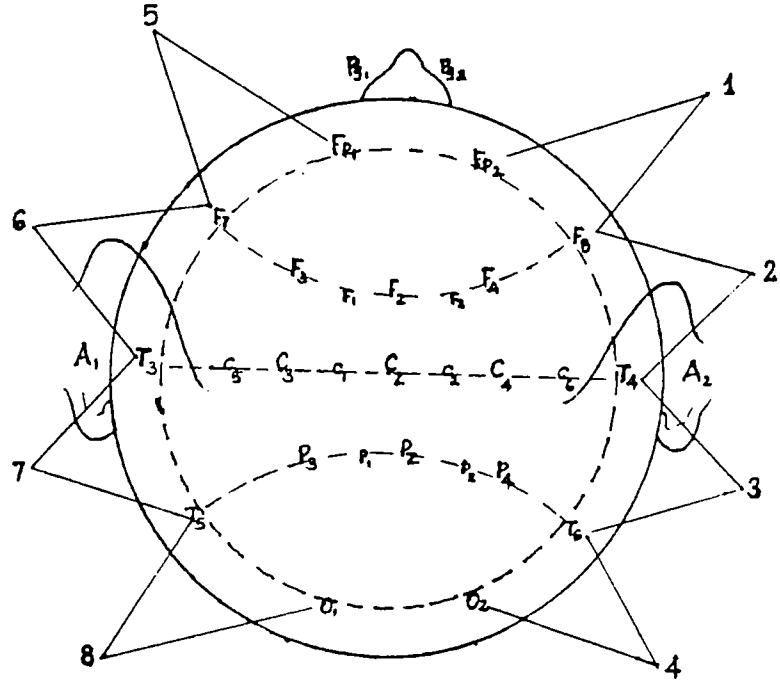

FIG 6.1a EC1

2. EC2

EC2 looks similar to EC1 (Fig 6.1b). In EC2, the central and parietal regions are also included and connection is mainly between second layer like F_4 - C_4, C_4 - P_4 etc. The positioning of electrodes are

Channel 1 — F_{P_2} → F_4

Channel 2 — F_4 → C_4

Channel 3 — C_4 → P_4

Channel 4 — P_4 → O_2

Channel 5 — F_{P_1} → F_3

Channel 6 — F_3 → C_3

Channel 7 — C_3 → P_3

Channel 8 — P_3 → O_1

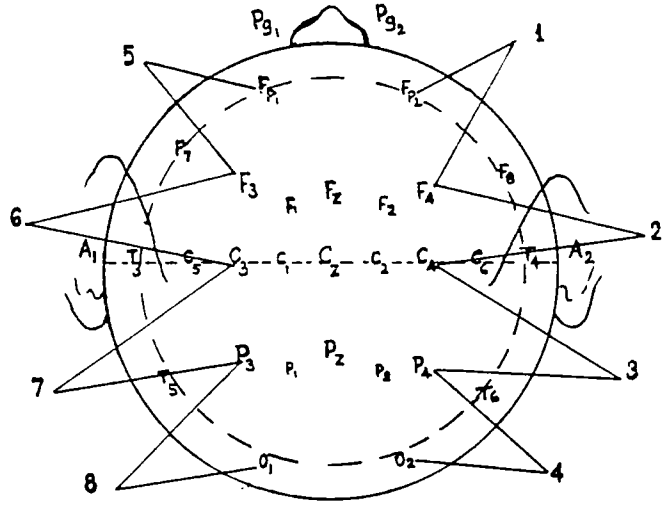

Fig 6.1b EC2

3. EC3

EC3 is bipolar in nature but it is entirely different from EC1 and EC2. Only upper and lower regions are located (Fig.6.1c). Channels 1,2,3 and 4 are frontal regions and Channels 5,6,7 and 8 are parietal regions. Central and occipital regions are excluded

Channel 1 — F_8 → F_4

Channel 2 — F_4 → F_z

Channel 3 — F_z → F_3

Channel 4 — F_3 → F_7

Channel 5 — T_6 → P_4

Channel 6 — P_4 → P_z

Channel 7 — P_z → P_3

Channel 8 — P_3 → T_5

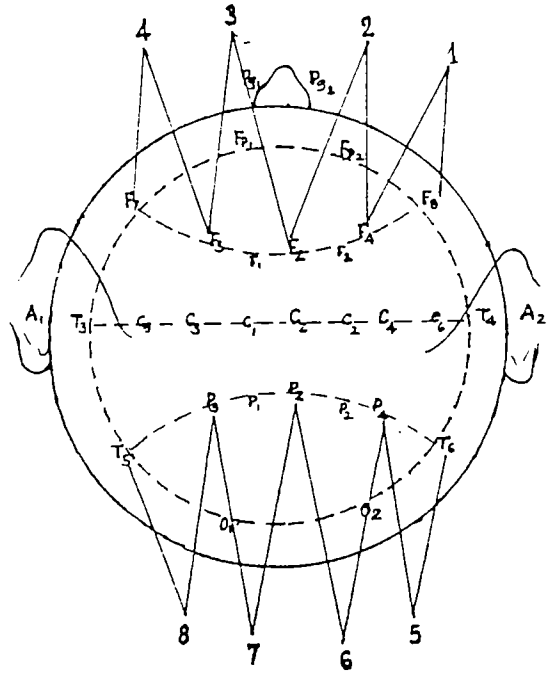

Fig 6.1c EC3

4. EC4

EC4 is similar to EC3, but instead of frontal regions, central regions are monitored (the channels 1,2,3 and 4 Fig.6.1d). EC4 is represented as

Channel 1 — T_4 → C_4

Channel 2 — C_4 → C_z

Channel 3 — C_z → C_3

Channel 4 — C_3 → T_3

Channel 5 — T_6 → P_4

Channel 6 — P_4 → P_z

Channel 7 — P_z → P_3

Channel 8 — P_3 → T_5

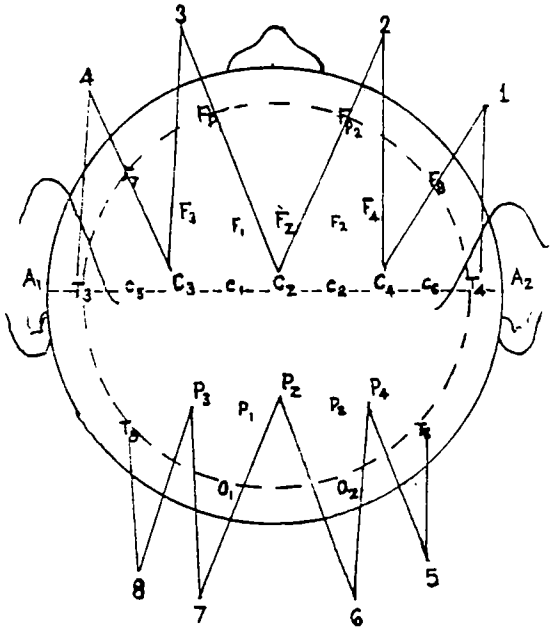

Fig 6.1d EC4

5. EC5

EC5 is also similar to EC3, except in the 5^{th}, 6^{th}, 7^{th} and 8^{th} channels. Instead of parietal region, these channels occupy the central region. Channels are (Fig.6.1e)

Channel 1 — F_8 → F_4

Channel 2 — F_4 → F_z

Channel 3 — F_z → F_3

Channel 4 — F_3 → F_7

Channel 5 — T_4 → C_4

Channel 6 — C_4 → C_z

Channel 7 — C_z → C_3

Channel 8 — C_3 → T_3

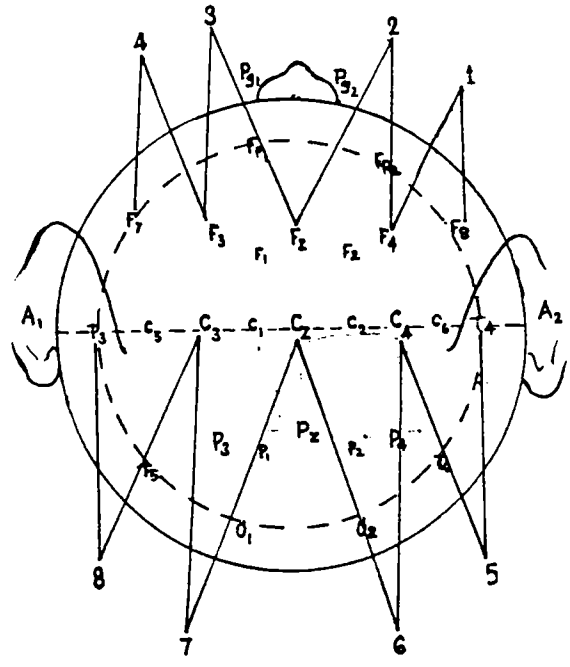

Fig 6.1e EC5

6. EC6

Monopolar technique is used in EC6. Only one electrode is active, and other one is connected to the ear lobe. It is represented as (Fig. 6.1f)

Channel 1 — F_4 → A2

Channel 2 — T_4 → A2

Channel 3 — C_4 → A2

Channel 4 — P_4 → A2

Channel 5 — F_3 → A1

Channel 6 — T_3 → A1

Channel 7 — C_3 → A1

Channel 8 — P_3 → A1

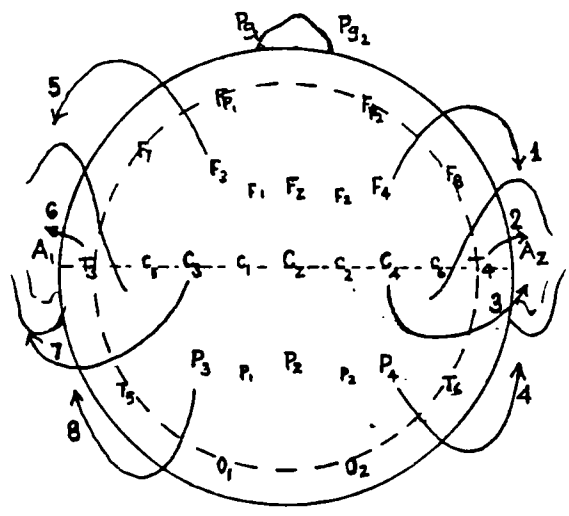

Fig 6.1f EC6

Occipital region is not included in this configuration.

7. EC7

EC7 is also monopolar and is similar to EC6, but central region is not included, instead of that, frontal region is more concentrated (Fig.6.1g).

Channel 1 — F_{P_2} → A2

Channel 2 — F_8 → A2

Channel 3 — T_6 → A2

Channel 4 — O_2 → A2

Channel 5 — F_{P_1} → A1

Channel 6 — F_7 → A1

Channel 7 — T_5 → A1

Channel 8 — O_1 → A1

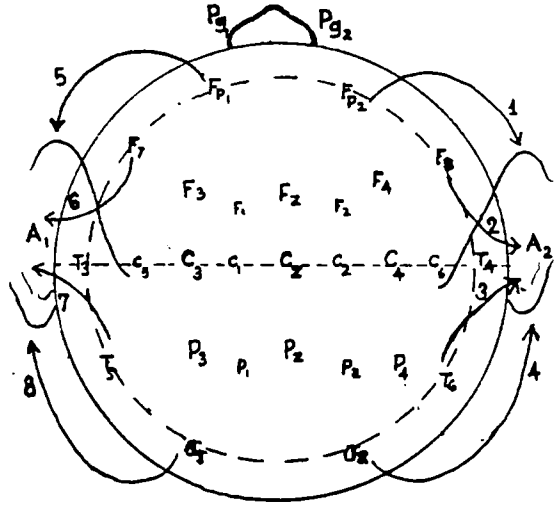

Fig 6.1g EC7

8. EC8

EC8 is bipolar but, it is different from all other configurations. Here, the electrodes are concentrated in the lower part of the brain, i.e, in the parietooccipital region. Only seven regions are located (Fig.6.1h). Electrode positions are

Channel 1 — P_z → P_4

Channel 2 — P_4 → T_6

Channel 3 — T_6 → O_2

Channel 4 — O_2 → O_1

Channel 5 — O_1 → T_5

Channel 6 — T_5 → P_3

Channel 7 — P_3 → P_z

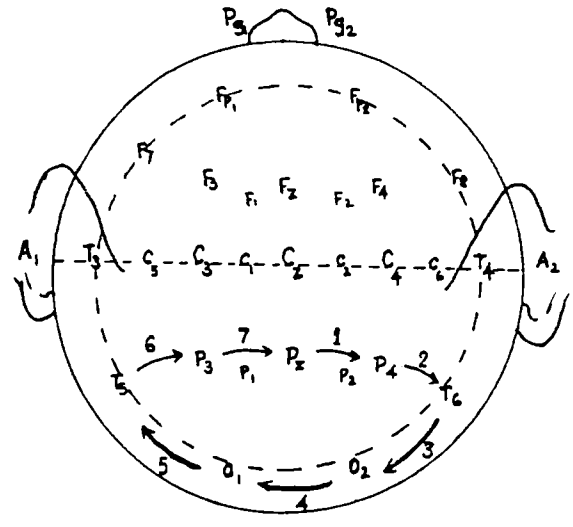

Fig 6.1h EC8

The different pathological conditions which we analysed are as follows.

6.2 EPILEPSY

Epilepsy is defined as a particular state of the brain as explained in section 4.10. Behavioural treatment of epileptic patients or simulation at the appropriate moment employed as a warning system to the patient or his surroundings, might have a greater advantage than the ordinary methods of treatment in epilepsy (Rogowski et al 1981). Rogowski explained the primary cause of generation of seizures as due to the changes in the "parameters" of the neural system, causing disproportion between excitative and inhibitive mechanism, and bringing the system into the verge of instability.

According to Kaczmarek et al [1977], the visual inspection of micro electrode recordings of cortical neurons, made under normal conditions in the absence of external stimuli, usually shows no correlation either between any one unit and the local gross EEG activity. Under certain conditions, this situation may

change dramatically. Most of the neuronal cells, picked up by a micro electrode start to oscillate and fire in phase. This is the phenomenon of the epileptic seizure. It is accompanied by a large increase in the amplitude of the EEG which manifest as extremely regular sharp waves. The firing pattern of the individual unit generally progresses from the tonic pattern in which neurons fire continually and at very high frequencies over a slower, small oscillation in membrane potential, to the clonic pattern in which each neuron repetitively gives a high frequency burst of action potentials followed by a period of strong depolarization during which the cell - firing mechanism is inactivated.

In the absence of seizure activity, the firing patterns of neurons frequently resemble with the chaotic behaviour of the sparsely connected networks. A cell may alternate between high frequency bursts of action potentials and periods of spike-inactivation without clear cut rhythmic oscillations in membrane potential that are characteristic of large stages of seizure. The seizure itself may start with a few irregular spikes after which the wave actively becomes very regular.

The frequency of the spikes and its amplitude increase as the seizure progresses. It can be clearly attributed to the recruitment of greater number of neurons into a homogeneous oscillation. It is tempting to suggest therefore that the connectivity of the cortex may be transformed during the course of a seizure from a sparsely connected network, with rather chaotic behaviour and complex spatio-temporal patterns into a densely connected network capable of truly homogeneous activity (Kaczmarek et al, 1977).

There are two types of epilepsy. One is petit mal (Fig.4.12c) in which EEG patterns show identical spikes, and its amplitude is very small. Babloyantz et al [1986] analysed petit mal case and obtained a dimension of 2.05±0.09. They have found that autocorrelation function dies down as time increases and FFT

is broad banded, and thus established the existence of chaos in the neural system during petit mal. However they have not calculated the value of K_2 and have gone only up to d=7. Dvorak and Siska [1986] obtained the dimension to fluctuate between 3.8 and 5.4, at the occipital region. EEG record of Grand mal epilepsy shows vigorous patterns (Fig.4.12b) with amplitudes going occasionally high.

In the present studies EEG signal of grand mal case were analysed for all eight channels. In order to study the time evolution of the dynamics , analysis was carried out on EEG taken for three different time intervals - during, before and after seizure.

The mode of configuration is EC1 (Fig.6.1a) and the EEG is measured from eight points of the brain. One can represent

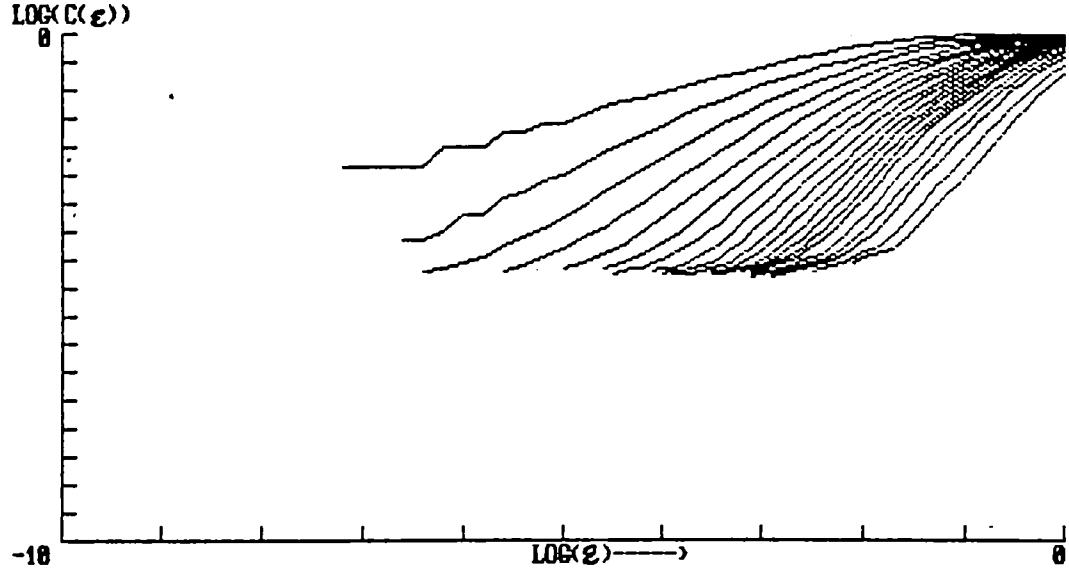

Fig 6.2 A plot of log $C_d(\varepsilon)$ for the 6th channel (epilepsy).

corresponding sets as frontal (1,5), temporal (2,6), parietal (3,7) and occipital regions (4,8) which are systematically located on the lobes on either side of the brain. The EEG is

digitized at an interval of 20 msec, and the digitized data is analysed using the method (Atmanspacher 1986, Abraham et al 1986) described in chapter 2. A typical plot of log $C_d(\varepsilon)$ vs log(ε) for various dimensions d, for the 6th channel of the first 10 sec data is given in Figure (6.2). The slope ν of the linear part of the curves of Figure (6.2) against dimension is plotted in Figure (6.3).

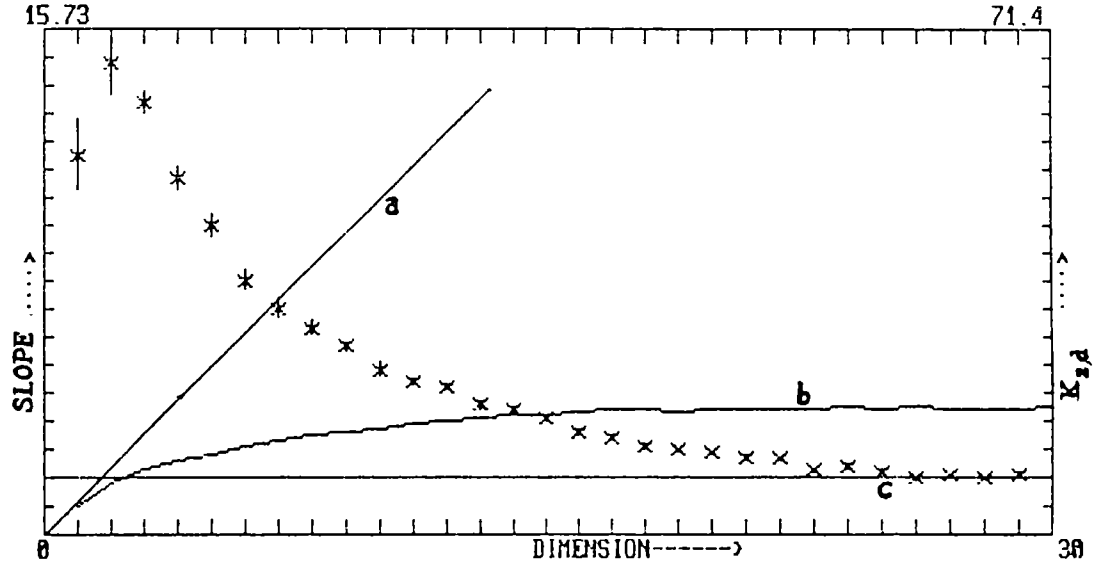

Fig 6.3 The plot gives three curves: slope vs dimension d a) for a completely stochastic case b) for the curves in Fig.6.2. c) $K_{2,d}$ as a function of d (epilepsy).

For a completely random behaviour, this plot will be a straight line with slope unity (curve a). Curve b gives the dimensions of the attractor, and curve c gives the Kolmogorov entropy. The saturated nature of slopes and Kolmogorov entropy shows that the system is nonlinear and dissipative and also exhibits the existence of a deterministic component. Values of D_2 and K_2 evaluated for all eight channels of the EEG are given in the table (6.1). The distribution of D_2 and K_2 are also represented in box diagram (Fig.6.4 & 6.5). The three groups belong to 3 time segments of EEG during epileptic seizure and time goes from left to right. Each group characterizes 10 sec of data.

Table 6.1 D_2 and K_2 obtained for Epilepsy before, during and after attack.

Table for D_2				Table for K_2			
Sheet → Channel	1	2	3	Sheet → Channel	1	2	3
1	2.26	6.43	5.71	1	4.88	11.42	11.69
5	2.09	5.29	5.22	5	4.51	7.32	10.52
2	3.46	5.48	5.12	2	7.91	11.30	9.76
6	3.27	6.23	4.98	6	6.38	12.51	10.18
3	5.36	5.53	4.45	3	10.02	10.59	8.84
7	4.94	5.90	5.68	7	9.70	9.10	9.05
4	4.98	5.93	5.21	4	10.67	12.11	10.98
8	5.02	7.53	9.29	8	9.76	14.53	17.35

In the case of D_2 plot (Fig.6.4), the set (1,5) seems to be small in the first 10 seconds while the magnitude increases in

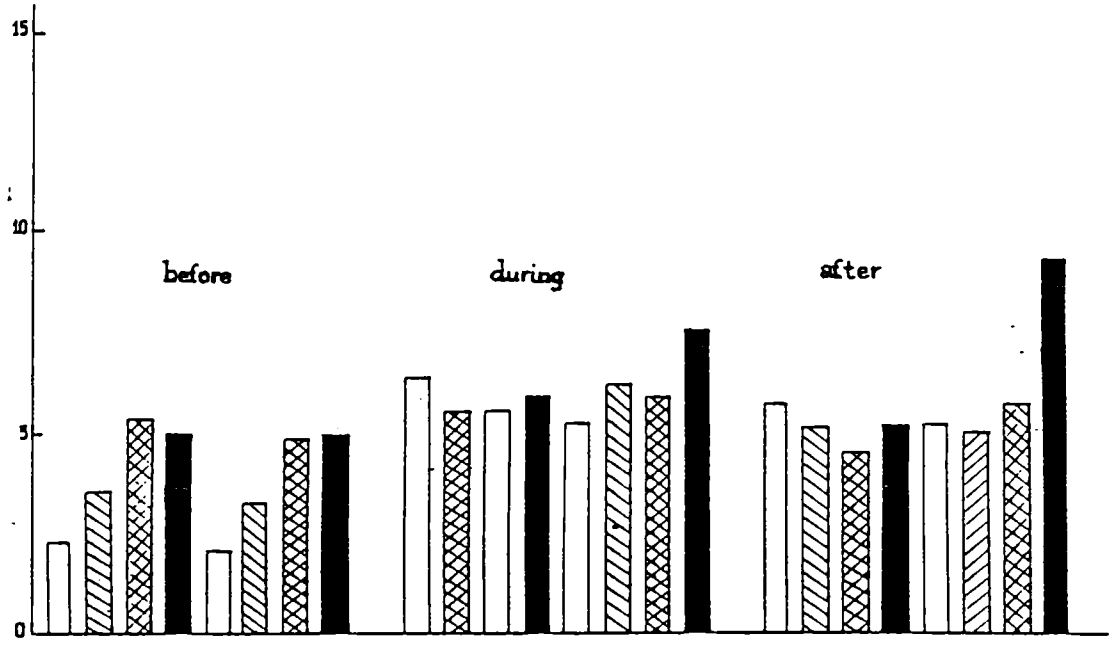

Fig 6.4 Distribution of D_2 values as evaluated from 8 channel EEG (epilepsy - before, during and after attack) recorded at three different times.

the 2nd 10 seconds and again shows a reducing tendency in the 3rd 10 seconds. All D_2's are fractal and this information can be attributed to the time evolution of strange attractor behaviour of corresponding points in the neural system. It is also realized that values corresponding to the set (4,8) seem to be higher than the others. This pair goes on increasing as we go from the first set to 3rd set and in this, the eighth point goes on increasing in time. This implies, that the eighth point or the left parietooccipital region is more active than the other points. The same trend is also seen in K_2 . One can easily see that the fractal dimensions are asymmetric from the left and right halves of the brain, as well as in time. It may be realized that this gives the time evolution of the dimension of the attractor and also the information capacity. Thus the eighth channel (dark shaded) goes as 5.02 ,7.23 and 9.29, in D_2 and 9.76, 14.53 and 17.53 in K_2 while the first channel goes from 2.26, 6.43 and 5.71 in D_2 and 4.88, 11.42 and 11.69 in K_2 (Fig.6.5).

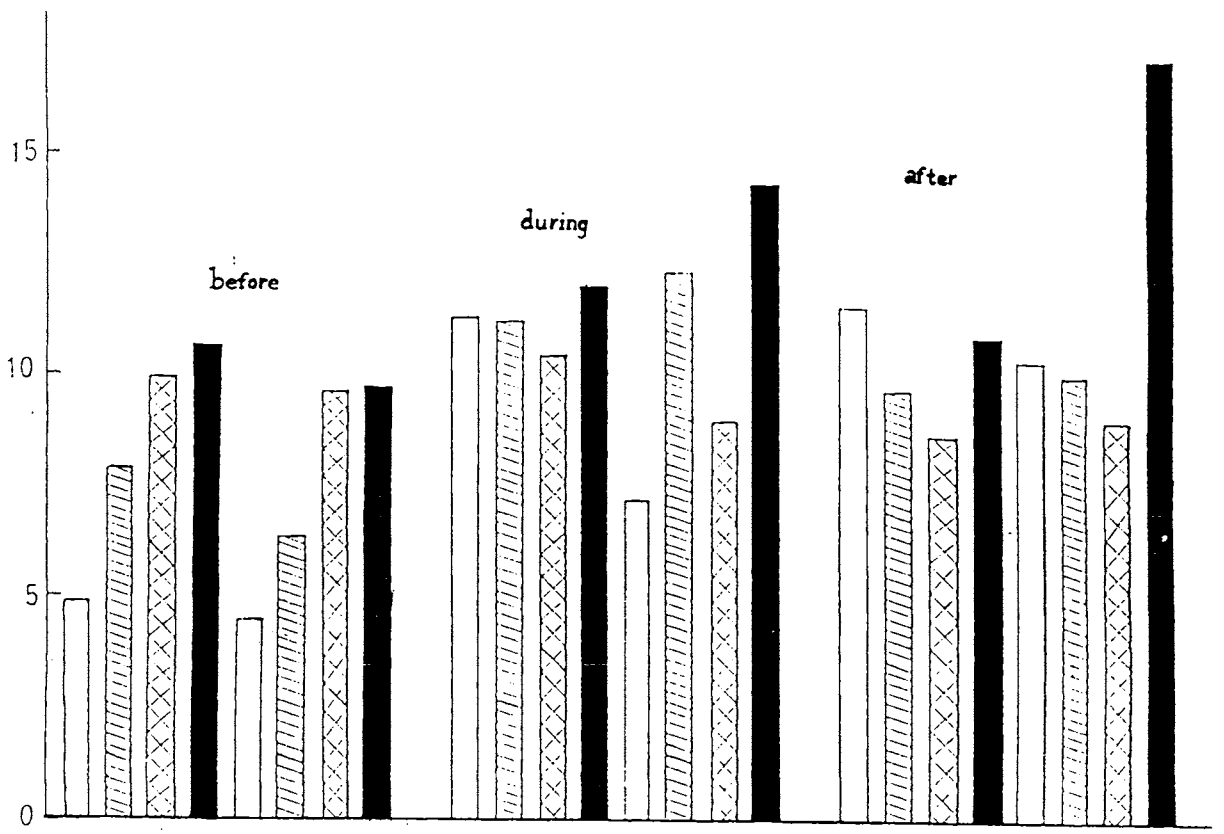

Fig 6.5 Distribution of K_2 values as evaluated from 8 channel EEG (epilepsy - before, during and after attack) recorded at three different times.

Thus the attractor evolves in time in a very complicated manner. The behaviour of all channels excepting the eighth show an increase and then a decrease. These results very well agree with the result of Kaczmarek et al [1977]. It is suggested that inhomogeneous pattern may occur in the early stages of the seizure only, and after that the system tries to attain the homogeneous activity. That is, a transfer from high degree chaotic behaviour to low degree of chaotic activity.

In the parietooccipital region, the right side shows a slow decrease in K_2 as time advances while the left side registers a regular increase in K_2. More pronounced and clear changes are seen in K_2 than in D_2 as seen in the 8th channel. Hence the eighth channel is different from others, and eighth point is more significant in the case of epilepsy.

The same type of behaviour is observed in the case of epileptic person with demylinated disease. The demylination is a disease, caused due to the pealing of the myelin sheath of the nerve cell. The main symptom is the paralysis and loss of sight. We analysed the EEG of such a person, who has the demylinated disease as well as a history of epilepsy, but the EEG appeared normal. Two sheets of EEG is digitized at a sampling interval of 20 msec, each for a period of 10 secs is analysed.

D_2 is noninteger and K_2 is greater than zero for all eight channels. The variation of K_2 and D_2 is much pronounced in the eighth channel (Parietooccipital region) (Fig.6.6a &b). This again inferred that the parietooccipital region is the seat of epilepsy.

It should be noted that EEG recording in this case was taken not during the seizure and EEG appeared to be normal. However, the present analysis show the abnormalities clearly, which implies the superiority of the method over the conventional

technique.

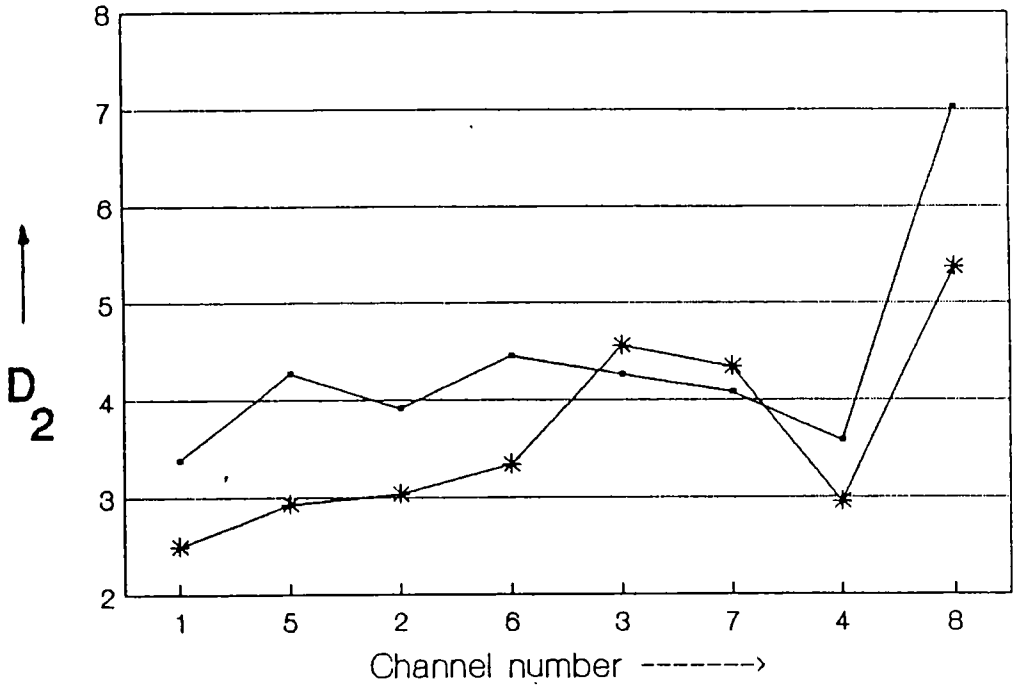

Fig 6.6a) D_2 evaluated at at two different time (Epilepsy with demylination). -•- first 10 secs -*- second 10 secs.

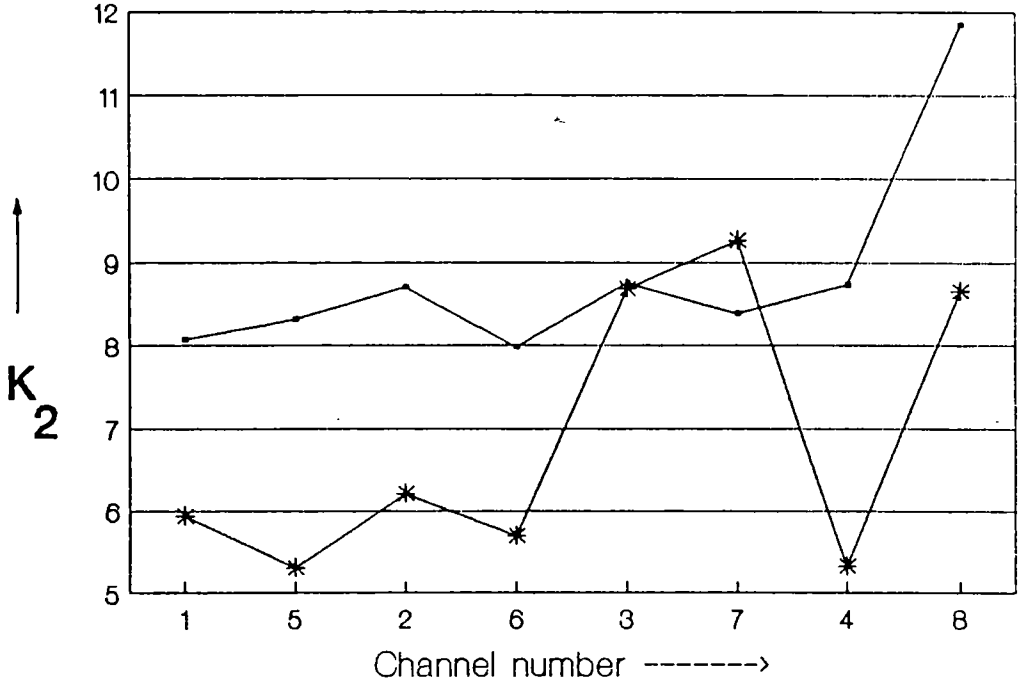

Fig 6.6b) K_2 values evaluated at two different time (Epilepsy with demylination). -•- first 10 secs -*- second 10 secs.

6.3 MIGRAINE

Migraine is a mild type of neurological disorder as explained in section (4.10).

EEG recording of a person suffering from migraine was analysed. The EEG records, which are used for analysis contains only small regular sharp spikes with no sign of vigorous signals and almost normal in appearance. D_2 and K_2 were evaluated using the recording of all the eight channels. Fig.(6.7a) and (6.7b) show the variation of K_2 and D_2 with respect to channel number (mode of connection is EC1). As obvious from the figure, K_2 is more sensitive than D_2 with respect to the state of the system.

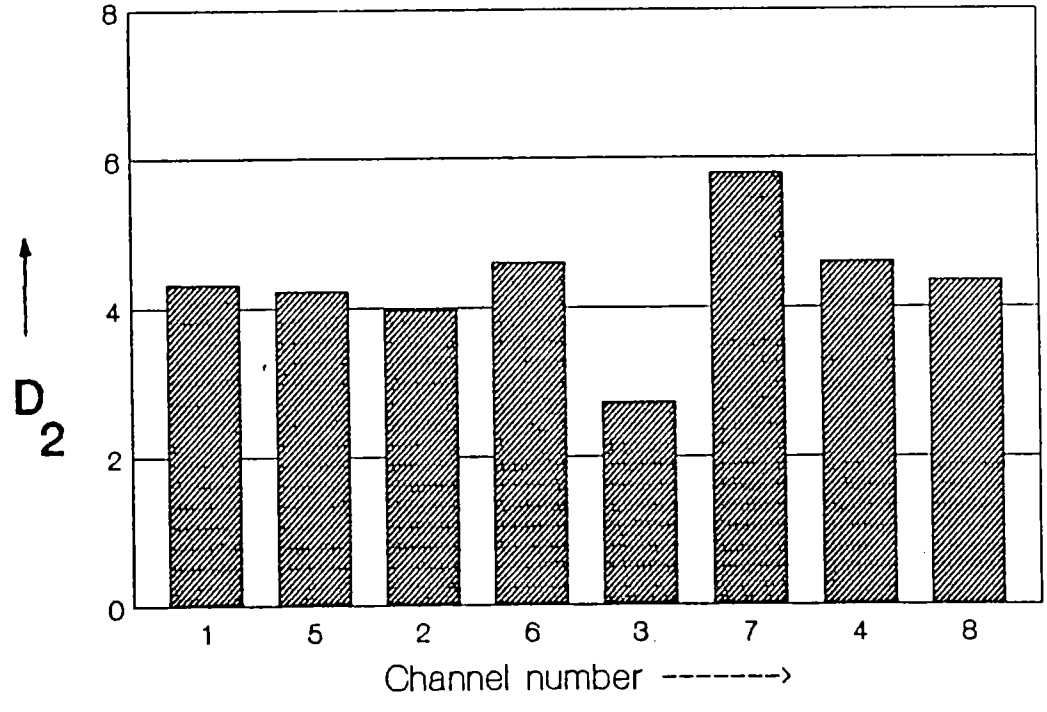

Fig 6.7a) D_2 as a function of channel number for Migraine.

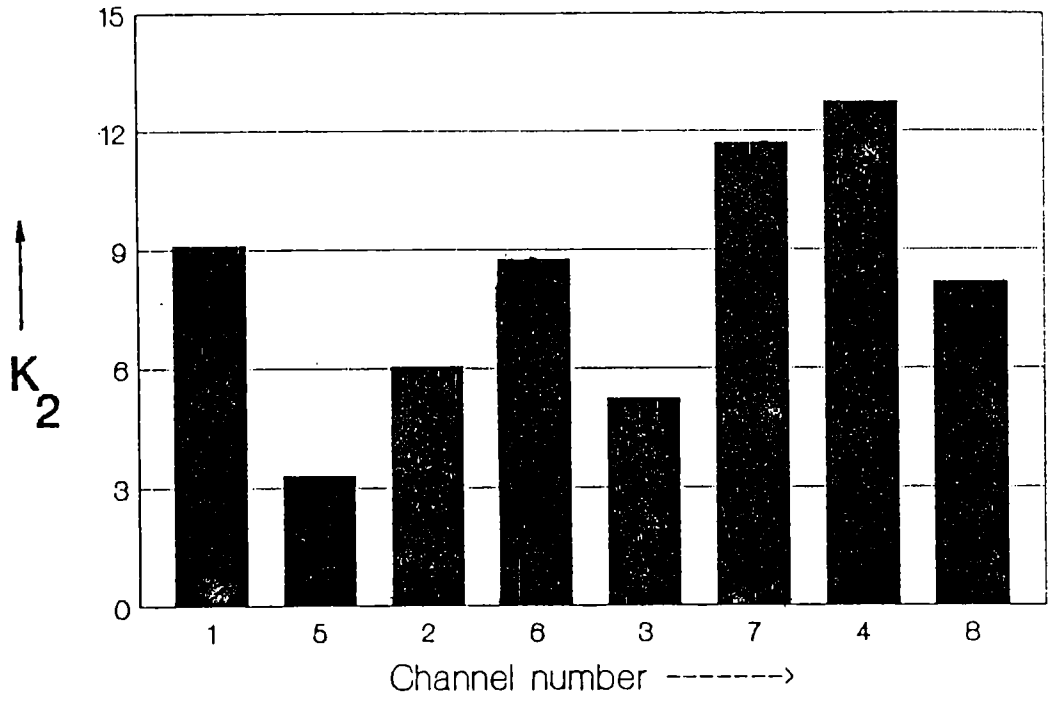

Fig 6.7b) K_2 as a function of channel number for Migraine.

Analyses were carried out using two continuous sheets of EEG recordings, each of 10 seconds duration. Results show that frontal part of the brain are very much sensitive as compared to parietal and occipital region. The time evolution of K_2 and D_2 are given in Fig.(6.8a&b).

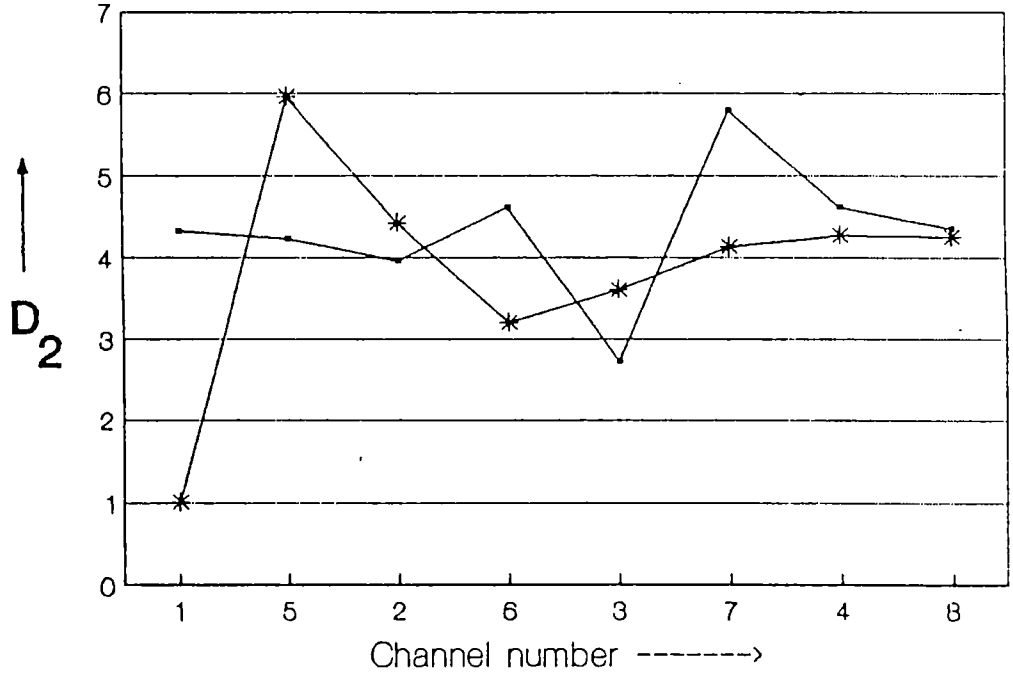

Fig 6.8a) D_2 evaluated at at two different time (Migraine). —•— first 10 secs —*— second 10 secs.

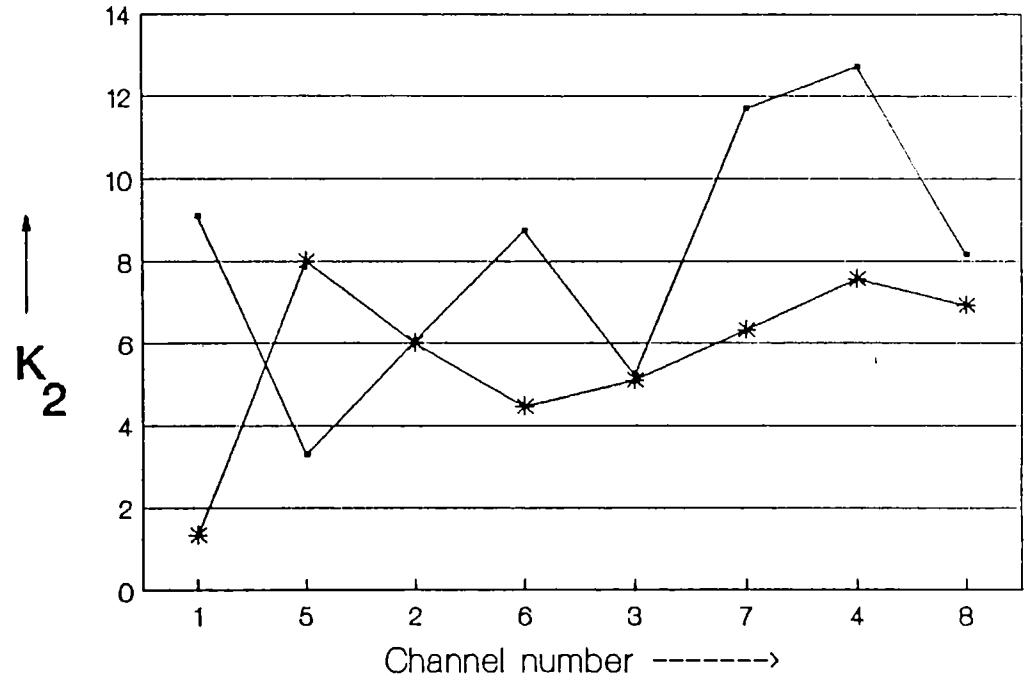

Fig 6.8b) K_2 evaluated at at two different time (Migraine). —•— first 10 secs —✱— second 10 secs.

6.4 HEADACHE

EEG used for this analysis was of a person suffering from headache and the pattern according to medical doctors, was found to be normal. EEG patterns were digitized at sampling intervals of 20 msec for a total span of 10 seconds(mode of configuration is EC1). In order, to study the time evolution, analyses were carried out for EEG taken at different intervals. The K_2 and D_2 were calculated for all eight channels and for 4 sheets (each sheet is of 10 sec duration) of EEG, and are given in the table (6.2) and in Fig.(6.9a & b). The variation of K_2 and D_2 is much pronounced in the 5th channel, i.e, in the left frontal region. K_2 is found to be more sensitive as compared to D_2. In order to get a clear idea, about the variation of K_2, we compared it with that of a normal person. It is to be noted that the distribution of K_2 is similar to that of normal in the right part of the brain (channel 1 to 4). The left part, especially channel 5 shows considerable variation in K_2 value implying that

the possible seat of abnormality is the frontal area of the brain. Channel 8 also has similar behaviour as in channel 5 but with smaller amplitude.

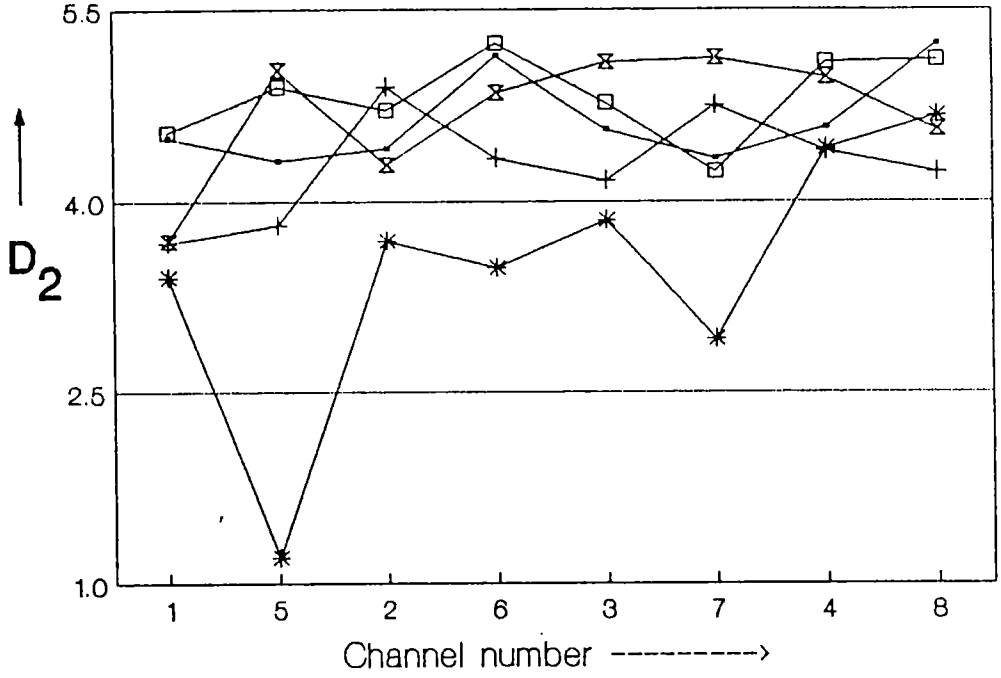

Fig 6.9a) D_2 evaluated at four different time for headache case and compared with D_2 of a 'clinically' normal brain. —•— first 10 secs —✱— after 110 secs -□- after 240 secs -+- after 290 secs ··×- normal.

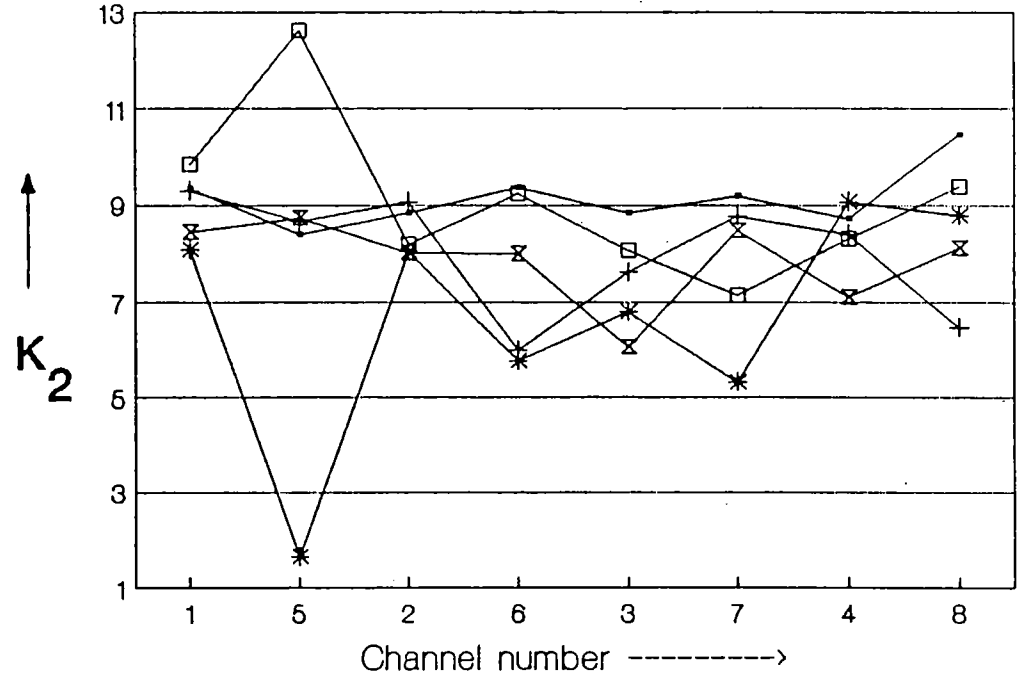

Fig 6.9b) K_2 evaluated at four different time for headache case and compared with K_2 of a 'clinically' normal brain. —•— first 10 secs —✱— after 110 secs -□- after 240 secs -+- after 290 secs -×-normal.

Table 6.2 D_2 and K_2(compared with normal) for Headache

Table for D_2

Channel/ sheet	1	5	2	6	3	7	4	8
1	4.49	4.31	4.41	5.13	4.56	4.33	4.58	5.22
2	3.40	1.21	3.68	3.47	3.85	2.92	4.41	4.67
3	4.54	4.89	4.71	5.23	4.77	4.23	5.08	5.10
4	3.67	3.81	4.89	4.33	4.16	4.75	4.39	4.22

Table for K_2

Channel/ sheet	1	5	2	6	3	7	4	8
1	9.33	8.40	8.83	9.36	8.84	9.18	8.71	10.45
2	8.09	1.65	8.05	5.76	6.79	5.32	9.06	8.79
3	9.84	12.61	8.18	9.23	8.07	7.13	8.31	9.37
4	9.29	8.67	9.06	5.99	7.62	8.77	8.40	8.46
Normal	8.44	8.73	8.01	7.99	6.06	8.48	7.11	8.12

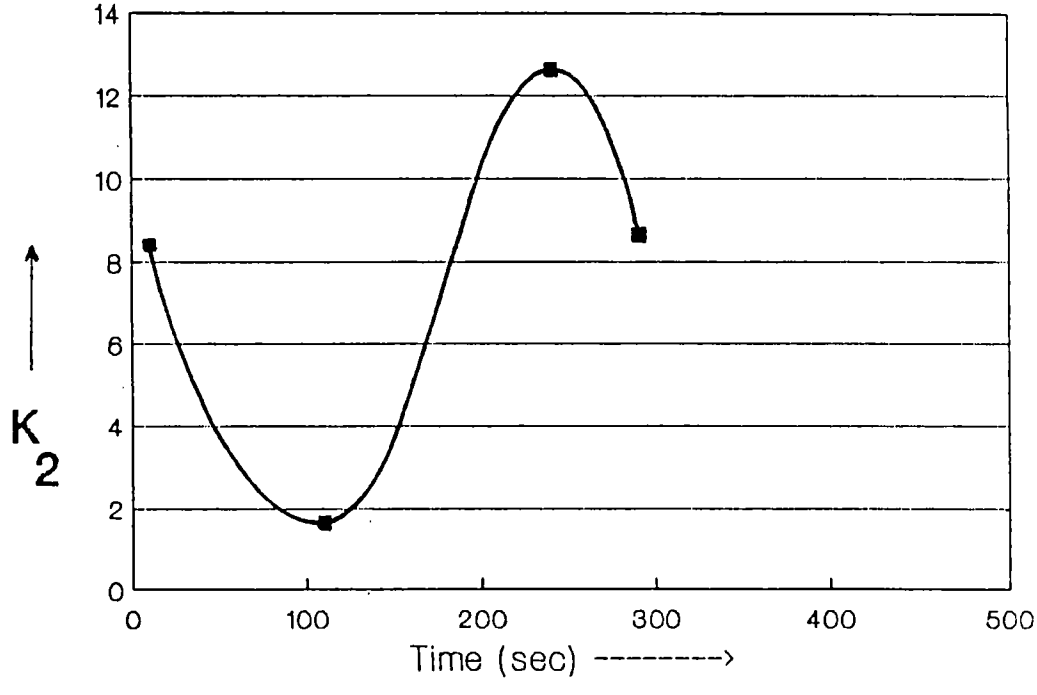

Fig..6.10 Variation of of K_2 in the left frontal region with time (Headache).

Fig.(6.10) shows the time dependence of K_2 for the 5th channel

which is almost periodic. The value of K_2 quantifies the degree of chaos in the dynamical system. Higher the K_2 value higher is the degree of complexity in the underlying dynamics. The periodic variation of K_2 in the frontal region shows the presence of repairing mechanism of the brain.

6.5 ANALYSIS AT HIGHER SPATIAL RESOLUTION

In all the previous cases, EEG has been recorded in only one mode *viz.*, EC1 (Fig 6.1a). This is the most commonly used configuration for EEG recording. The limitations of the available EEG equipment was that, only 8 simultaneous recording is possible. This 8 recording is not sufficient to study the entropy flow in the system at sufficient spatial resolution.

In order to study the K_2 variation with high spatial resolution (HSR), EEG recording was done using various types of electrode configurations (Fig. 6.1a - 6.1h). Due to the constrains in the instrumentation, it was not possible to record signals from all points simultaneously. Hence, it may not possible to compare all the results due to possible time evolution in the system. Such comparison is possible only if we exclude the time variation. We analysed three pathological cases in this high spatial resolution, epilepsy, tumour and psychotic.

EPILEPSY

In the EC2 configuration (Fig.6.1b) we analysed two sheets of EEG separately. In both cases channel 2 show peak in K_2 and D_2 values. In the channel 8 (Parietooccipital region), K_2 is very high, which is a common behaviour observed in epilepsy. Enhancement of K_2 values in time was observed in channels 3,6 and 7 (Fig 6.11).

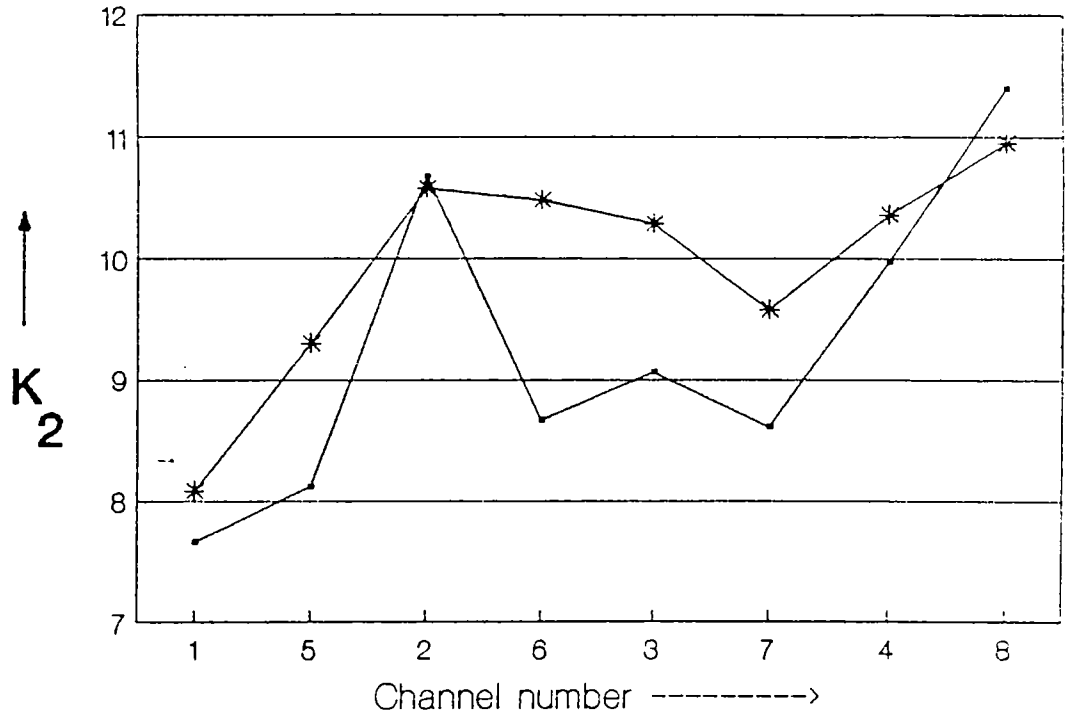

Fig 6.11 K_2 evaluated at two different time in EC2 mode (Epilepsy). —·— first 10 secs —*— second 10 secs.

Analysis of EEG were carried out using the electrode configuration EC4 (Fig.6.1d). K_2 and D_2 were evaluated for two separate times (10 secs separated). Initially channel 1 has K_2 value of 11.8 which has been decreased to 10.6 in the second case. The upper part i.e, channel 1 to 4 shows pronounced variation in K_2, as time evolves, as compared to the lower part i.e, channel 5 to 7. The variation of K_2 at the eighth channel (left parietotemporal region) is high (Fig 6.12).

We have also done the analysis in EC8 mode (Fig.6.1h). In this configuration back portion of the brain was scanned at seven places. This is a localized analysis. The channel 4 (Occipital region) shows large fluctuation in K_2 value as compared to other channels. In channel 6 and 7 also, the variation of K_2 is very much pronounced (Fig.6.13).

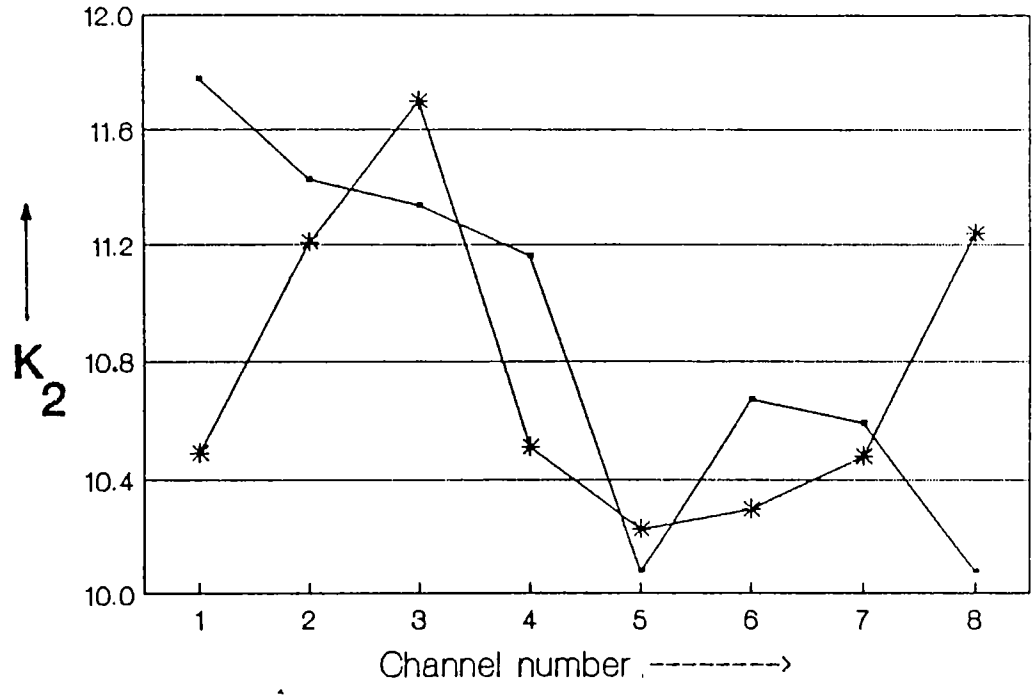

Fig 6.12 K_2 evaluated at two different time in EC4 mode (Epilepsy). —•— first 10 secs —✱— second 10 secs.

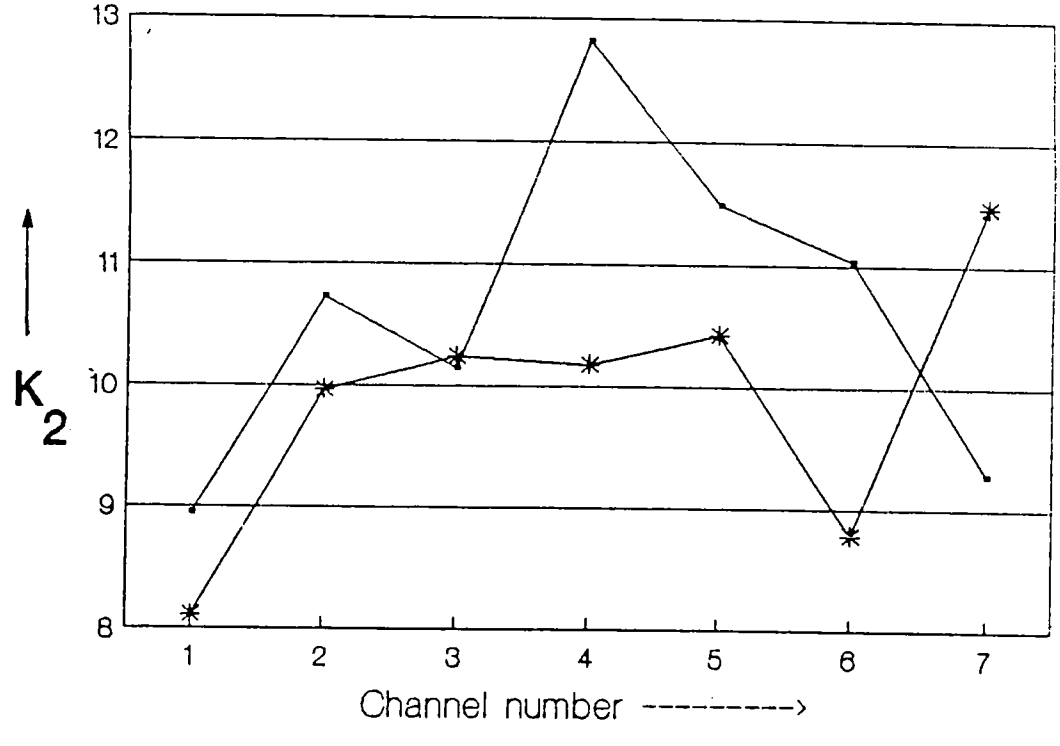

Fig 6.13 K_2 evaluated at two different time in EC8 mode (Epilepsy). —•— first 10 secs —✱— second 10 secs.

We compare all the K_2 values, evaluated in the epileptic case, using various electrode configuration. Comparatively large K_2 value can be observed in the central region (T_3-C_3-C_z-C_4-T_4) (Fig 6.14). This creates in the central region some type of K_2 barrier between the frontal and occipital regions. Low K_2 activity is seen in the right occipital as compared to the left occipital.

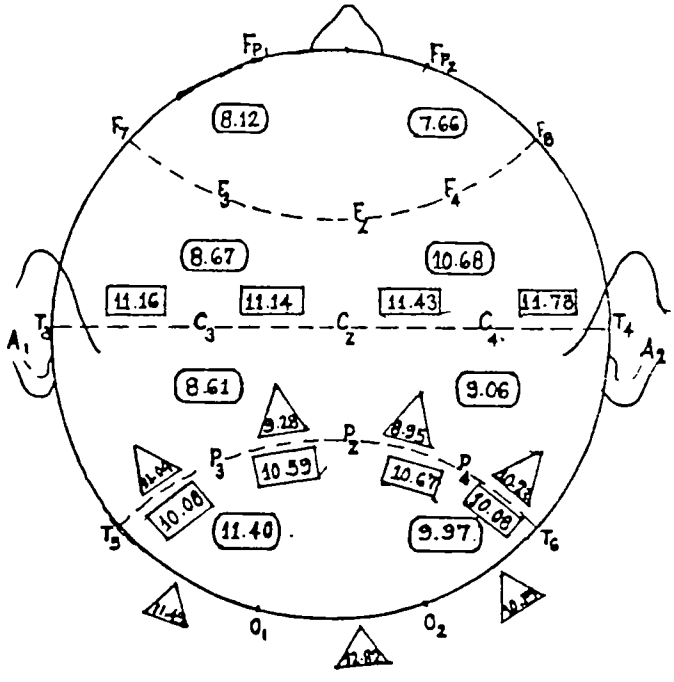

Fig 6.14 Spatial variation of K_2 in brain (Epilepsy). ▭ EC2, ▭ EC4 △ EC8.

TUMOR

In the case of Tumor, EEG analyses for four electrode configurations were carried out. *viz.*, EC2, EC5, EC6 and EC7. Both monopolar and bipolar techniques are used for this analysis.

Doctors have located the tumor in the right parietooccipital region. The analysis shows that there is a dip in K_2 in the right parietooccipital region as compared to that of left. Variation of K_2 with respect to channel number is represented in box diagram (6.15). There is a depression of K_2 in the frontal region also.

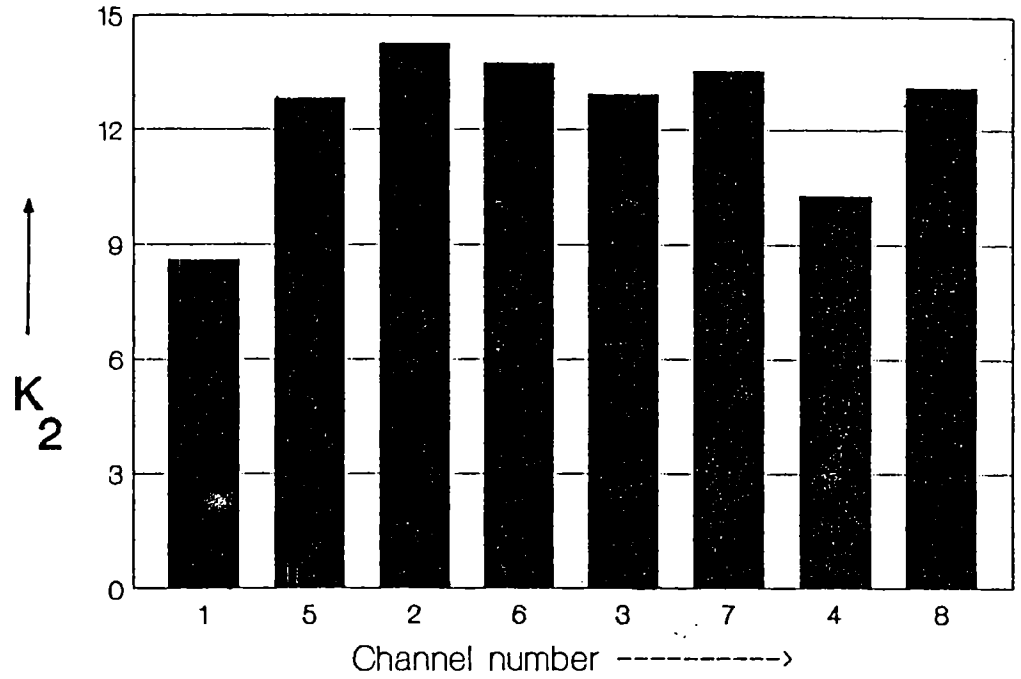

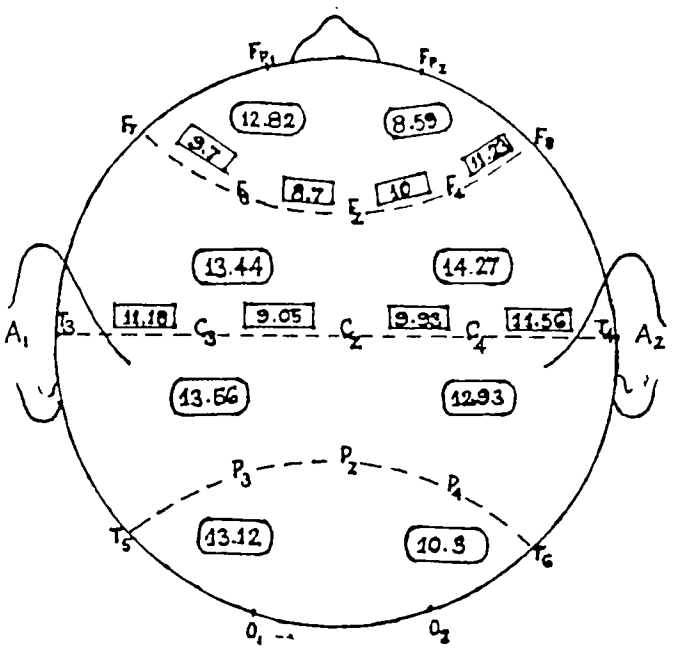

Fig 6.16 Spatial variation of K_2 in brain (Tumor), biploar technique. EC2, EC5.

The comparison of K_2 at different time interval using bipolar technique is studied in Fig.(6.16). It should also be noticed that a "crack" exists in the central 'K_2 barrier'.

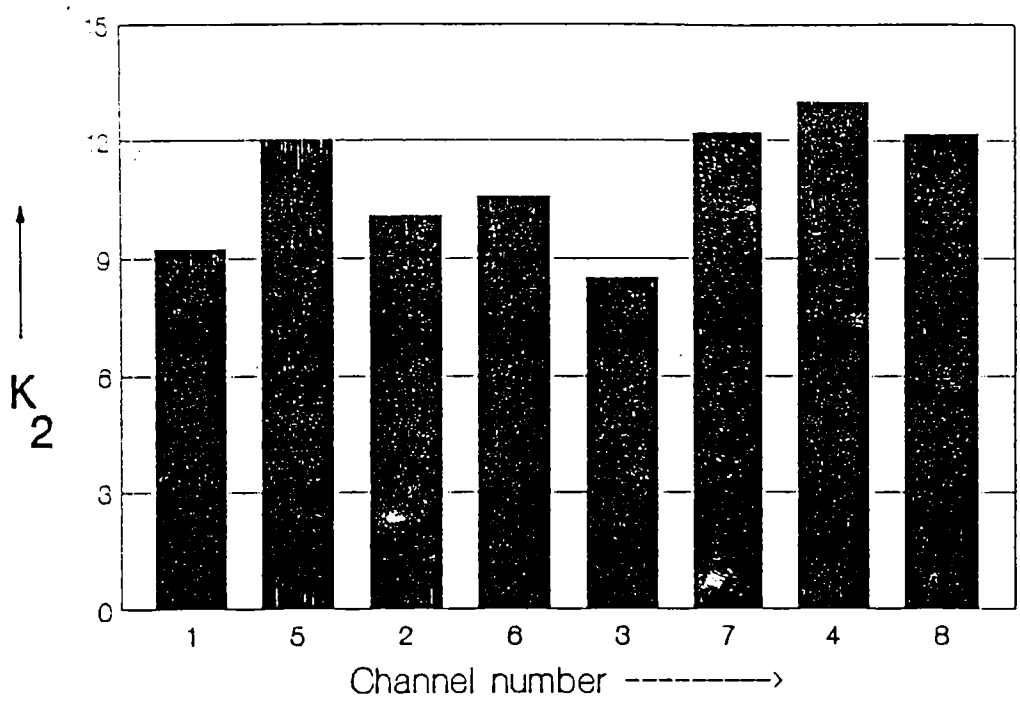

Fig 6.17 K_2 as a function of channel number, for Tumour in EC7 mode, monopolar technique.

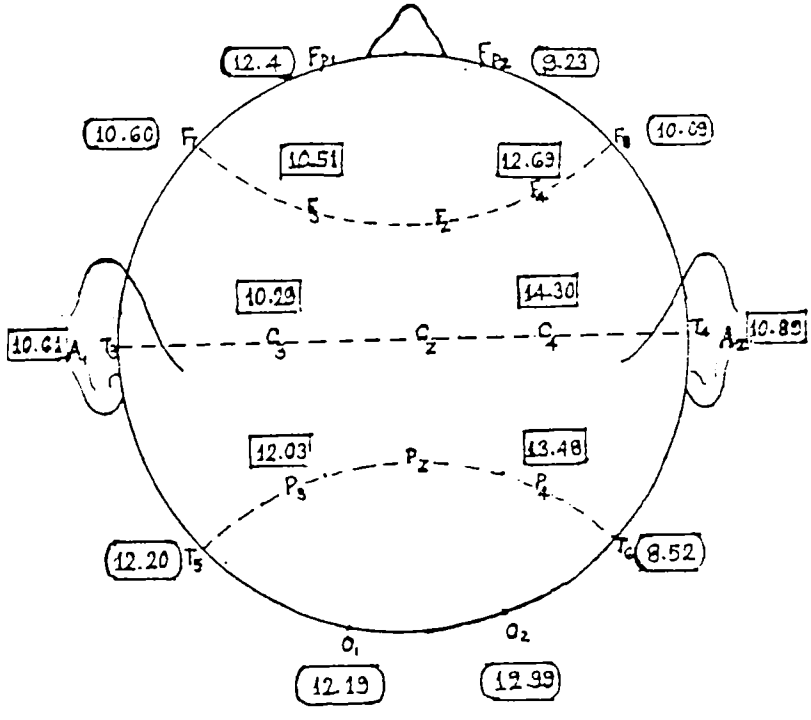

Fig 6.18 Spatial variation of K_2 in brain (Tumor), monopolar technique. ▭ EC6, ▭ EC7.

We studied the K_2 values obtained from monopolar technique as well. It also shows a dip in K_2 near parietooccipital region, (Fig.6.17) i.e, 8.52 in the T_6 region (channel 3). There is a depression of K_2 in the frontal region also i.e, 9.23 in the F_{P_2} region. In all other regions K_2 is very high. The spatial distribution of K_2 is shown schematically in Fig.(6.18)

PSYCHOTIC

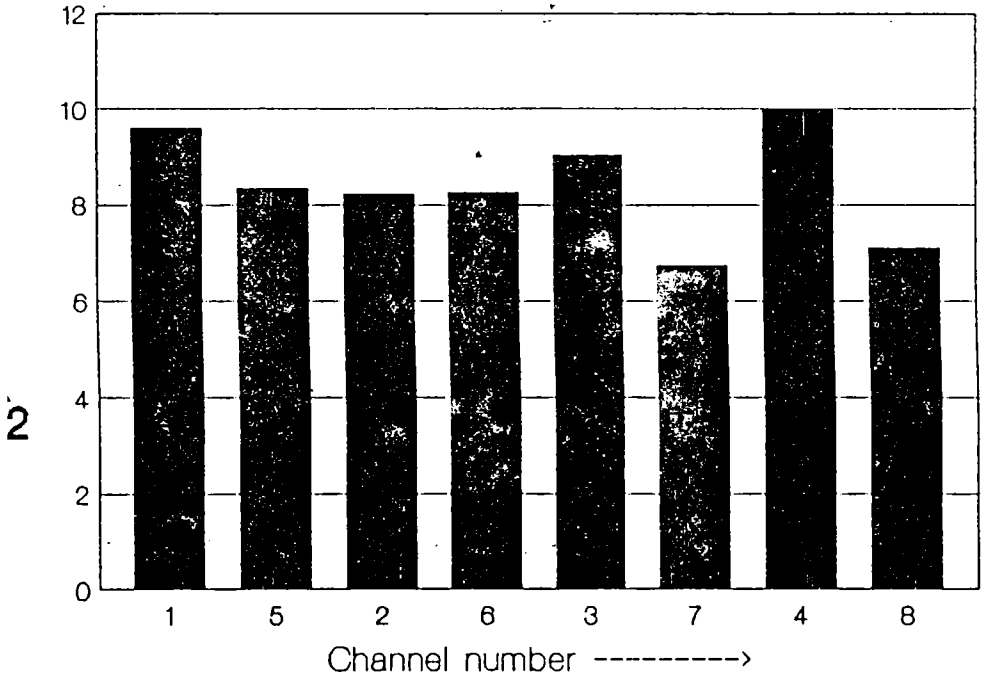

Fig 6.19 K_2 as a function of channel number, for psychotic in EC2 mode.

In this case we analysed the EEG of a psychotic patient of age 17, in two electrode configurations. *viz.*, EC2 and EC3.

The K_2 distribution is represented in Fig.(6.19). Left occipital region has low K_2 entropy as compared to right occipital region in contrast to tumour and epilepsy. Comparat-

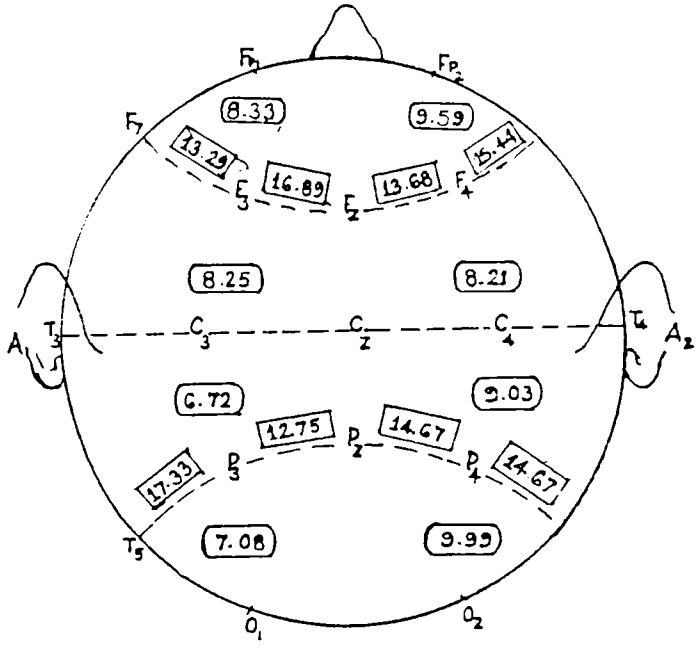

Fig 6.20 Spatial variation of K_2 in brain (Psychotic case). EC2 EC3

ively low K_2 values are registered in the central region. In the vicinities of F_7-F_3- F_Z-F_4-F_8 and T_5-P_3-P_z-P_4-T_6 regions, large K_2 values are observed, thus creating a kind of partitions in K_2 distribution (Fig.6.20).

In all these analyses, D_2 behaviour has been found to be similar to K_2, except that K_2 is more sensitive than D_2 to the state of the brain. Hence K_2 may be identified as a parameter which describes the state of brain under different pathological conditions and possibly may be taken as a diagnostic tool. However, more detailed analyses and standardization are necessary to put this in practical use.

CHAPTER 7

NONLINEAR DYNAMICS IN CERTAIN ASTROPHYSICAL SYSTEMS

The studies on certain astronomical systems viz., Asteroidal belt and Saturn ring structure using the technique of nonlinear dynamics are done in this chapter. Detailed analysis based on D_2 and K_2 values is included. To make the thesis self contained some of the features of Asteroidal belt and Saturn ring are also described.

NONLINEAR DYNAMICS IN CERTAIN ASTROPHYSICAL SYSTEMS

Time series analysis of the neural system has revealed the fact that a single measurable quantity can characterize complex nonlinear systems. It was found that under various pathological conditions, the parameters like D_2 and K_2 can adequately represent the deterministic component present in the dynamics of the neural system. Since these are invariants of the system they can be used to characterize the system. This method, being very general, can be applied to any dynamical system.

In this chapter, we propose to apply this method to certain astronomical systems, like the Asteroidal belt and Saturn rings and determine whether such systems are chaotic or not. But, before going into details of these, we shall describe the physical nature of the Asteroidal belt and the Saturn ring system in sections 7.2 and 7.6 respectively.

7.1 GENERAL INTRODUCTION

Matter - ring formation in solar system in general (such as Asteroidal belt) and in planetary environment (Galilian planets) etc., are still not completely understood. Various theories, based on Newtonian mechanics of three body dynamics, have been put forward to explain the formation of gaps by

gravitational collisional self focussing (Trulson 1971) and scavenging of matter by satellites involving resonance theory (Berry 1978), but only with limited success. However, there seem to be only few attempts to analyse the data obtained by the various space missions, towards an understanding of the dynamics of these systems. Recently developed theory of deterministic chaos (Schuster 1984, Hao Bai-Lin 1985, Berge et al 1984) is found to be suitable to explain many natural phenomena like atmospheric studies using climatic data (Nicolis and Nicolis 1984 & 1986, Krishna Mohan et al 1987), Lorenz model for fluid flow (Lorenz 1963), EEG analysis for human brain (Babloyantz et al 1985 & 1986), membrane potential analysis of Paramecium (Nagai et al 1988) and ECG analysis of cardiac oscillator (Glass et al 1983 and Babloyantz et al 1988). Time series analysis of observed solar radio pulsations suggests that there must be a low dimensional attractor (Kurths et al 1987) present in the system. We propose to apply this theory to the data acquired by the Voyager missions (Photopolarimeter recordings; Esposito et al 1983). It may be mentioned that a similar study is relevant in the case of Asteroidal belt and Saturn rings, in view of the results of Wisdom [1983] wherein he has shown that in asteroidal belt, 3:1 Kirkwood gap coincides with the outer boundary of a chaotic zone. The significance of 3:1 resonance out of all resonances was pointed out for the first time by Pratap [1977], where a spectral analysis study of matter distribution in the asteroidal belt has been done. He has fourier analysed this distribution, obtained the autocorrelation and power spectrum and has identified the ratios from the resonance theory. He has shown that Kirkwood gaps are essentially the interference pattern due to two spatial density waves and not merely due to the three body resonance phenomena between Jupiter, the sun and the asteroid. This also shows that this phenomenon is due to collective effects between the particles of the system together with gravitational field provided by the sun, all the planets and probably by the stars as well.

7.2 ASTEROIDAL BELT

The asteroids are a cluster of solid bodies with sizes greater than that of an ordinary comet and orbiting around the Sun in a flat cloud mainly concentrated in the main belt between the orbits of Mars and Jupiter (Fig 7.1). Physical and dynamical investigations of the asteroids suggest that the asteroids form a population of minor solid bodies which suffered collisions. Asteroids move mostly on low eccentric and low inclined orbits. Other important dynamical features of the asteroidal belt, like

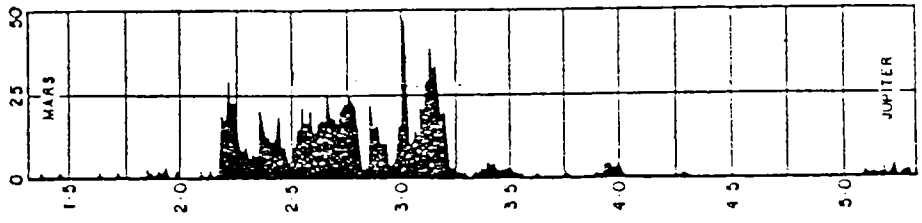

Fig 7.1 A plot of number density of asteroids >1.6km in diameter against the radial distance from the sun in AU.

1) Orbital and secular resonances due to gravitational forces mainly exerted by Jupiter.

2) Under populated regions in the asteroidal belt.

3) Planet-crossing orbits (will help us to understand the existence of ordered and chaotic regions in asteroidal belt).

The under populated regions and narrow empty zones in the asteroidal belt represent possible chaotic regions where asteroids have been removed. The populated regions on the other hand are eventually ordered regions or can even be chaotic regions but with time scales much larger than the age of the Solar System for removing asteroids. One of the other characteristics of the asteroids is that they move mostly on low eccentric and low inclined orbits interior to Jupiter's orbit avoiding a close approach to Jupiter.

At present we know accurate orbital elements of about 3000 elements in the belt. The main belt can be clearly seen between 2 AU and about 3.3 AU as shown in Fig (7.1). Both edges of the main belt coincide with the location of resonances. The inner edge of the main belt coincides clearly with the position of the ν_6 secular resonances (Williams et al 1981). At the ν_6 secular resonance, the frequency for an asteroidal orbital precession rate matches a main frequency for planetary eccentricities.

The outer edge of the main belt coincides with one of the Kirkwood gaps, namely with 2/1 resonance. An m/n resonance means that an asteroid completes m revolutions around the Sun during n revolutions of Jupiter. The 2/1 resonance is therefore a resonance in mean motion with Jupiter while the ν_6 secular resonance is a resonance with respect to a change of planetary eccentricities.

Resonances do seem to determine also the orbital energy distribution within the main belt and in the outer region between the 2/1 resonance and the orbit of Jupiter. Within the main belt three narrow gaps (the Kirkwood gaps) appear at the following orbital resonances: the 3/1 resonance located at 2.5 AU, the 5/2 resonance located at 2.82 AU and the 7/3 resonance located at 2.95 AU.

Two different types of resonances are known to determine the dynamical structure of the asteroidal belt, namely secular resonances and orbital resonances. The dynamical system established by the planets can be considered as an oscillating system. The perturbations exerted by the planets on asteroidal orbits are determined by the frequencies of this system. An asteroidal orbit can be interpreted as an oscillator. If a very long-periodic frequency, a so-called secular frequency, of the asteroidal oscillator is equal to one of the secular main frequencies of the planetary system, a secular resonance occurs. At a secular resonance, an asteroidal orbit, for instance, precesses with about the same velocity as Jupiter's orbit. As a result, very strong variations in orbital eccentricity and

inclination can occur. In particular, secular resonant orbits may become Mars - and Earth - crossing orbits.

An orbital resonance occurs when the ratio between an asteroidal and the Jovian mean motion is equal to (p+q)/p, where p and q are small integers. For a ratio of 5/2, for instance, p=2 and q=3. In this case, an asteroid completes 5 revolutions while Jupiter completes two revolutions around the Sun. As a consequence, conjuctions between the asteroid and Jupiter repeat at almost the same locations of the asteroidal orbit which may cause particularly strong perturbations in the asteroidal orbit. In a resonant case, perturbations exerted by Jupiter add up for a comparatively long period in the same way. This means that in resonance an asteroid is either accelerated or decelerated over much longer time scales than in a non-resonant case. Since in the main belt, orbital resonances coincide with the Kirkwood gaps, it is natural to conjecture that the formation of the Kirkwood gaps is due to orbital resonances.

Giffen [1973] started to investigate asteroidal motion under a different aspect. He tried to determine chaotic and ordered regions at the 2/1 and 3/2 resonances applying the surface of section method. Giffen found a small chaotic region at the 2/1 resonance, which he did not find at 3/2 resonance. In an ordered region, the phase space which can be filled by an asteroidal orbit, is confined to a surface due to the existence of an additional quasi-integral of motion which cannot be obtained analytically but numerically. In chaotic region no such quasi-integral confines the motion to a surface. Froeschle and Scholl searched more systematically in the 2/1, 3/1 , 5/2 and 7/2 resonances for ordered and chaotic regions by applying the same surface section method like Giffen. Froeschle and Scholl concluded that chaotic regions are rare. In addition, they showed (Froeschle and Scholl 1976), that the chaotic regions seem to be closed by forbidden regions and a quasi-integral of motion. This means that an asteroid located in a chaotic region is trapped and cannot leave the gap. Since these results were obtained in a restricted model it cannot be excluded that in a

more realistic model, asteroids might leave the gap by a diffusion process on a very long time scale. All these results were obtained by a numerical integration of the equation of motion. Wisdom [1982] succeeded to find a new and more rapid method to calculate orbital revolution at the 3/1 resonance which allows to cover time span of the order of 10^7 years on modern computers within reasonable computing time. Using Chirikov's function method (Chirikov 1979), Wisdom derived a mapping for calculating orbital evolution.

Wisdom [1983] determined ordered and chaotic regions at the 3/1 resonance by calculating Lyapunov characteristic numbers, which was applied by Froeschle and Scholl [1981] for two cases at 2/1 resonance. Wisdom concluded that the size of the chaotic region at the 3/1 resonance is about equal to the observed size of the gap. According to Wisdom an asteroid situated in the chaotic region of the 3/1 gap increases its eccentricity so strongly that it becomes a Mars-crosser. Hence, the asteroid is removed from the 3/1 resonance after a collision with Mars. Milani and Nobili [1983] tried to determine chaotic regions in the outer belt. Scholl's aim [1985] was that an asteroid located in the chaotic regions will suffer a collision with Jupiter. A collision of an asteroid with a planet implies a sufficiently close approach to the planet which ejects the asteroid out of the corresponding region.

7.3 SPECTRAL ANALYSIS

Recent advances in the studies of dynamical systems (Grassberger and Procaccia 1984, Broomhead and King 1986) have given deep insight on nonlinear collective modes, as well as, forces which drive a state from order to turbulence and going back to order from chaotic oscillations. This theory has recently been applied to Asteroidal belt (Wisdom 1983, Scholl 1985) at 3:1 resonance. This particular resonance is very significant, since it is at this, that the particle changes from positive to negative correlations (Pratap 1977). Furthermore, it

is again at this point that maximum power is concentrated in a power spectrum analysis. It has been further established that this resonance is the only significant one and the rest of the resonances given in literature are not real as revealed in the power spectrum analysis. Besides these, the following results are also established (Pratap 1977).

a) The different vectors plotted in Fourier space clustered in two distinct domains defined by the phase angle $50^\circ < \phi_n < 200^\circ$ and $286^\circ < \phi_n < 355^\circ$, In Fig (7.2), the vectors represent amplitude and the corresponding phase of the Fourier components. The number against each vector represents the number n of the fourier component

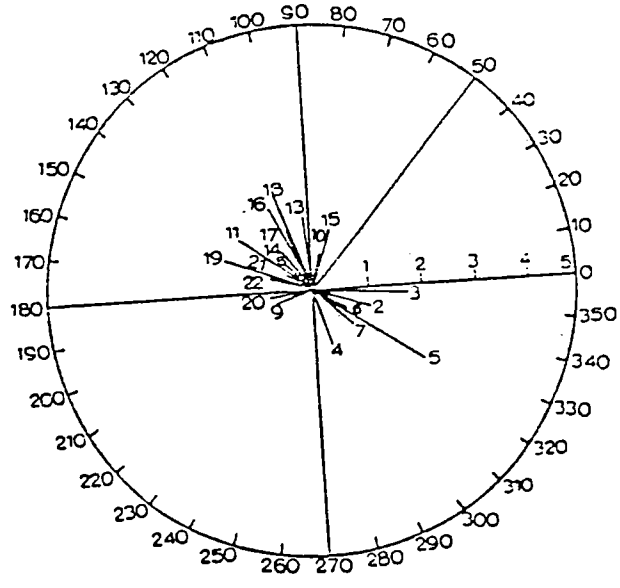

Fig 7.2 Fourier space representation of the distribution in Fig.7.1.

b) Power spectrum analysis showed that there were five dominant frequencies involved in the dynamics (Fig.7.3). One cannot assert whether these frequencies are commensurate or incommensurate. The crosses on the abscissa in Fig 7.3 depict the frequency at which maximum power resides and vertical arrows are the frequencies given by the resonance theory.

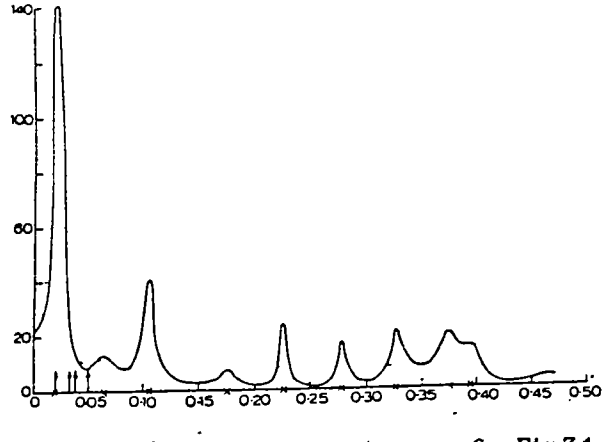

Fig 7.3 Power spectrum of Fig.7.1. The position of maximum power (f=0.02) corresponds to the ratio of 3:1.

c) Particles could be divided into essentially two groups mutually correlated amongst themselves but uncorrelated groupwise, the change of correlation taking place at a lag point corresponding to 3:1 resonance (Fig.7.4)

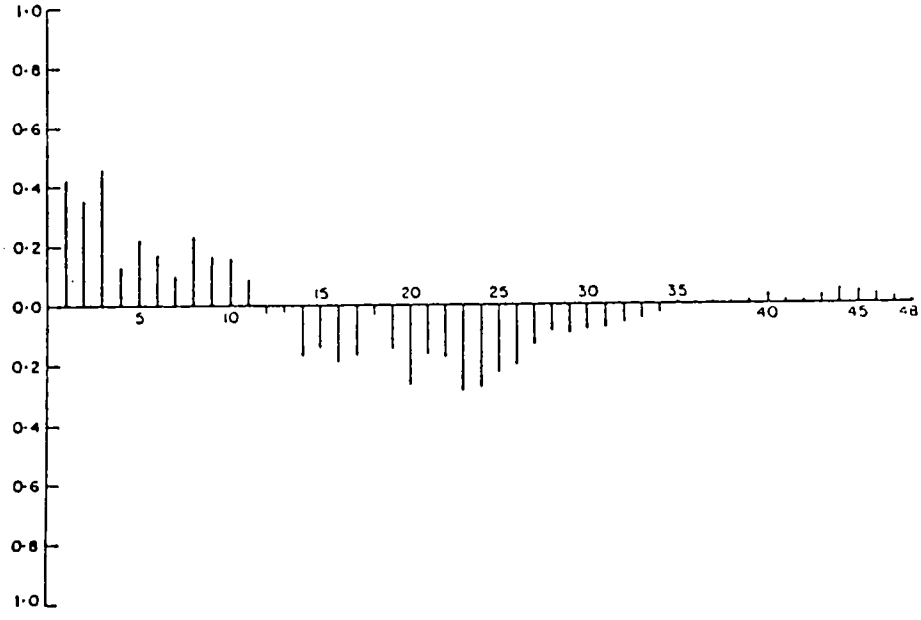

Fig 7.4 Autocorrelation function of distribution in Fig.7.1. The change of correlation takes place at the position of 3:1 ratio.

The above five frequencies, as obtained from the power spectrum analysis, however, are not explained by the resonance theory excepting that of 3:1. The method of analysis adopted by Wisdom was to evaluate the LEs for trajectories near 3:1 resonance. Even though LEs can characterize the nature of dynamics, evaluation of these values are difficult in most of the cases. But the approach described by Atmanspacher and Scheingraber [1986] is useful for the evaluation of other quantities which characterize the dynamics of asteroidal belt. The present analysis is based on the method developed by Abraham et al [1986] for small data sets which is especially useful in astronomical systems, for which sometimes the duration of the phenomena are very small. This method is also found to be successful in solar time series analysis (Kurths et al 1987), where the data of radio waves in the Sun's atmosphere is

analysed. Usually the duration of solar radio pulsation event in the frequency range of 480-800 mHz is not longer than a minute. The duration of the considered pulsations is only 40 sec at a sampling rate of $\Delta t=0.0645$. A comparison with Lorenz model for same number of data points revealed that correlation function agrees the power law.

The data obtained for our analysis is the density distribution of asteroids as given by Pratap [1977]. We do not presuppose a Hamiltonian structure for the system or any other interactions. Hence the problem as to whether a planetoid is subjected to force due to the Sun and Jupiter as taken at present, or whether other planets also play a role in the dynamics, does not arise. This problem is significant since from a nonequilibrium point, it has been shown by Prigogine and Serverne [1966] that if the system has only attracting gravitational force then there does not exist screening as in the case of electrically charged system and hence the system cannot have thermodynamic equilibrium. Now, can there be equilibrium in the information sense ? This is ascertained by evaluating the K_2 entropy for the system. Furthermore we get a physical explanation for the five significant frequencies obtained in the power spectrum analysis.

7.4 ATTRACTOR DIMENSION AND KOLMOGOROV ENTROPY IN ASTEROIDAL SYSTEM

Analysis

The radial plot of asteroid density distribution as given in Pratap [1977] was digitized and written as a sequence

$$X(t) = X(t_o),\ X(t_o+\Delta t) \quad \ldots\ldots\ldots\ldots \quad X(t_o+N\Delta t) \qquad (7.1)$$

Time series in general is a series of values sampled at

regular interval as a function of space or time (Packard et al 1980). Hence the above sequence can be considered as a "time series" and can be rearranged in the form of "delayed matrix" as explained in chapter 2.

$$
\begin{matrix}
X(t_o) & X(t_o+\Delta t) & X(t_o+2\Delta t) & \ldots\ldots X(t_o+m\Delta t) \\
X(t_o+\Delta t) & X(t_o+2\Delta t) & X(t_o+3\Delta t) & \ldots\ldots X(t_o+(m+1)\Delta t) \\
\\
X(t_o+d\Delta t) & X(t_o+(d+1)\Delta t) & \ldots\ldots & X(t_o+(d+m)\Delta t)
\end{matrix}
\qquad (7.2)
$$

The matrix (7.2) can be considered as an array of m column vectors defined in a d-dimensional space and this can be written as in the case of neural system as

$$
X(t_i) = \left\{ X(t_i),\ X(t_i+\Delta t) \ldots\ldots\ldots X(t_i+d\Delta t) \right\} \qquad (7.3)
$$

where $t_i = t_o+i\Delta t$ with i being an integer running from 0 to m. We shall now define the correlation function $C_d(\varepsilon)$ as (see Chapter 2)

$$
C_d(\varepsilon) = \lim_{N\to\infty} \sum_{i,j=1}^{N} N^{-2} \ \Theta\ (\varepsilon - |\vec{X}_i - \vec{X}_j|) \qquad (7.4)
$$

The plot of log $C_d(\varepsilon)$ vs log ε for asteroidal belt is shown in Fig (7.5).

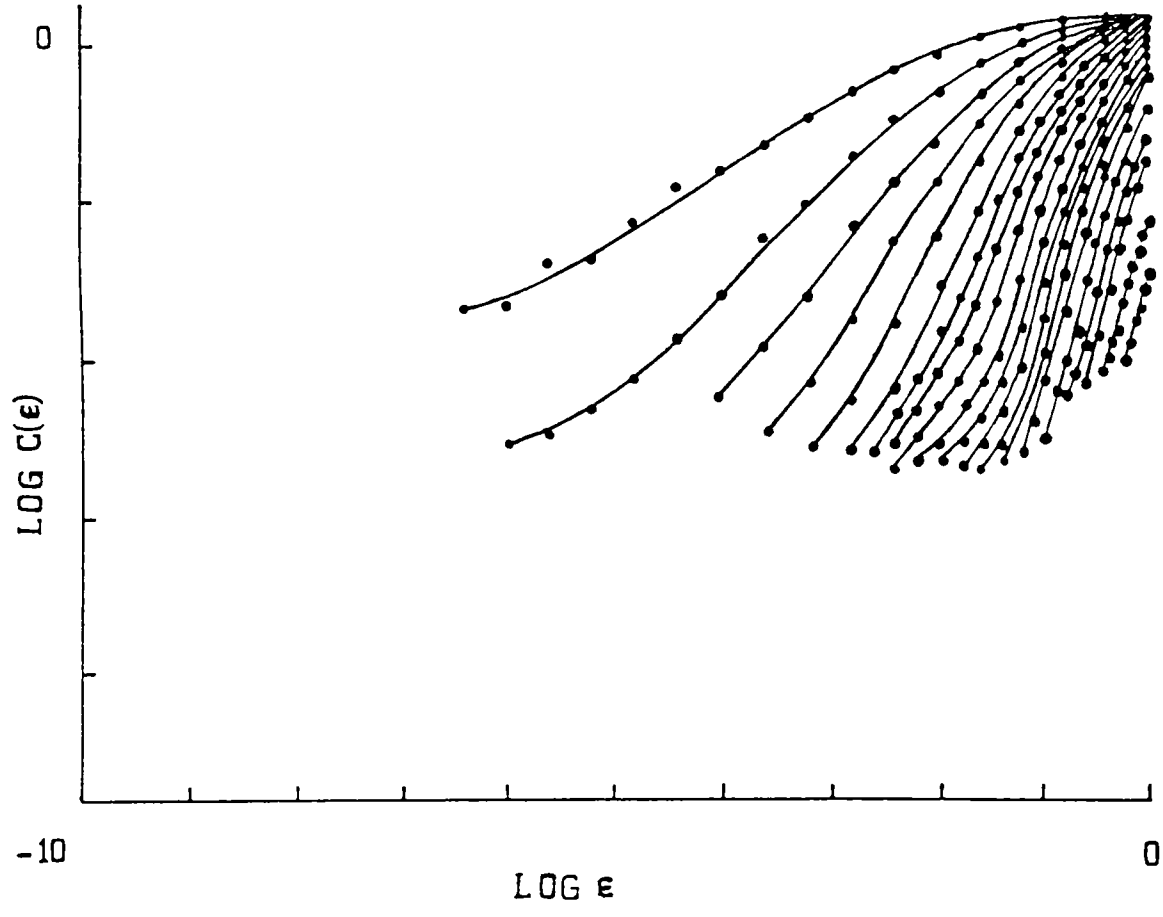

Fig 7.5 Log-log plot of Aseroidal belt

It has been shown in chapter 2, that if we consider the trajectory of a particle crossing a given plane repeatedly then if the points at which the trajectory crosses the plane are all confined in a neighbourhood, then this is called basin of the attractor. ε in equation (7.4) gives a measure of the basin of the attractor. One can use the probability $p_i (=N_i/N)$ where N_i are the number of points at which a trajectory visits a given neighbourhood in order to define quantities D_q, which are called the qth order Hausdorff dimension of the attractor (Grassberger et al 1983 a,b,c). The most significant of D_q's, however, is D_2 (Caputo and Atten 1987) which can be defined in terms of correlation function. It can be calculated using the power law.

$$C_d(\varepsilon) \sim \varepsilon^{\nu} \qquad (7.5)$$

From the plot of log $C_d(\varepsilon)$ vs log(ε) (Fig 7.5), we can calculate ν as the slope of the linear part of each curve for d varying from 1 to 30. It can be shown that if the data set is generated from a completely stochastic Guassian white noise, then ν=d or a plot of slope against dimension would be a straight line making an angle 45° with dimension axis (Babloyantz and Destexhe 1986). Usually we try to explain different phenomena of astronomical systems by considering it to be stochastic. But the present analysis indicates the existence of a deterministic component in the system, indicated by the deviation of ν-d curve from the 45° line (Fig. 7.6).

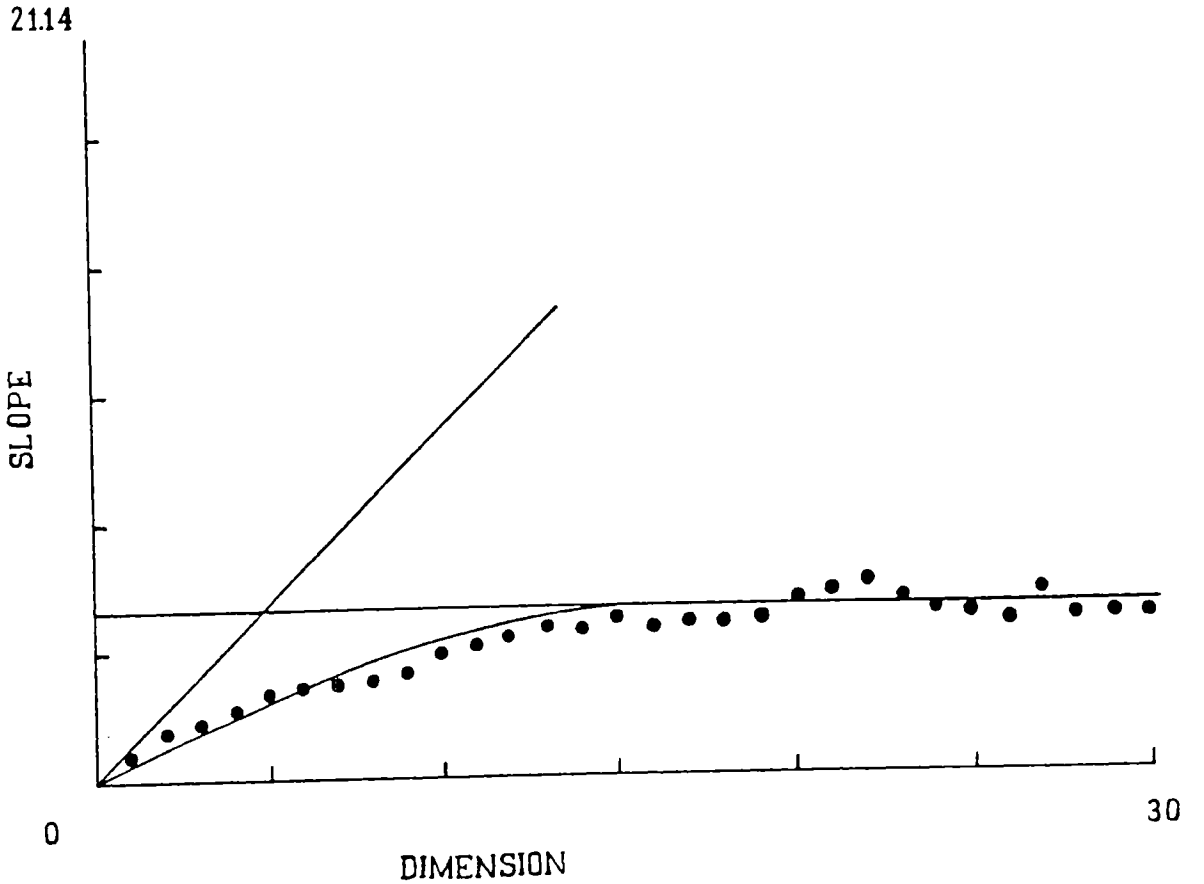

Fig 7.6 The slope of the curves in fig.7.5 as a function of d. The asymptotic value, D_2 is 5.

This means that as dimension increases, the effect of noise is reduced and the deterministic part becomes dominant. As one can

see in the Fig (7.6), the slope ν attains an asymptotic value (as $d \to \infty$). Hence d should be chosen so as to obtain this asymptote. The asymptotic value is defined as D_2. This is an invariant of the system and is a static parameter, as it is independent of length scales. D_2 is the minimum number of initial conditions which are necessary to characterize the system, in the asymptotic limit, or this gives the dimension of the subspace to which the system gets embedded in the phase space. The remarkable feature in this is that the curve saturates to a slope 5, showing that the characteristic attractor dimension is integer, indicating that the attractor is a regular one. This also means that the Asteroid-dynamics is described by five independent initial conditions.

A second point to be observed is the dimension d at which the curve meets the asymptotic line. The part of the curve defined for lower dimension goes almost with the stochasticity line (i.e., the ν=d line), while that at the asymptotic region represents order. Hence the dimension at which the curve meets the asymptote could denote the boundary between chaos and order. This is what has been observed by Wisdom [1983] in Asteroidal belt and it has been verified by us using a time series analysis. In this case, saturation takes place at about d=15 and this implies that the system is an attractor of characteristic dimension 5 which is embedded in a subspace of dimension 15, as it evolves asymptotically, thereby giving the 3:1 Kirkwood gap. This probably could be a significant point which has not been realized earlier, as no importance is attached to the dimension at which the asymptote meets the curve. Since saturation starts at d=15, we are not going to get any additional information by increasing the dimension beyond 30. In terms of time scales, using Kepler's law a^3/T^2 = constant , the system can be completely characterized by five incommensurate frequencies and it is these five frequencies that has appeared in the power spectrum analysis of Pratap [1977]. This would further imply that the Fourier space is basically divided into five sections instead of two as has been visually realized by Pratap [1977].

The second invariant quantity of interest is the second order Kolmogorov entropy K_2,

$$K_{2,d}(\varepsilon) = \frac{1}{\tau} \ln \left\{ \frac{C_d(\varepsilon)}{C_{d+1}(\varepsilon)} \right\} \qquad (7.6)$$

$$K_2 \sim \lim_{\substack{d \to \infty \\ \varepsilon \to 0}} K_{2,d}(\varepsilon) \qquad (7.7)$$

where τ =0.02 AU, which is the sampling interval. The Kolmogorov entropy is the most dominant term in the general set of information entropies. It is a dynamic parameter and very sensitive to the length scales of the system.

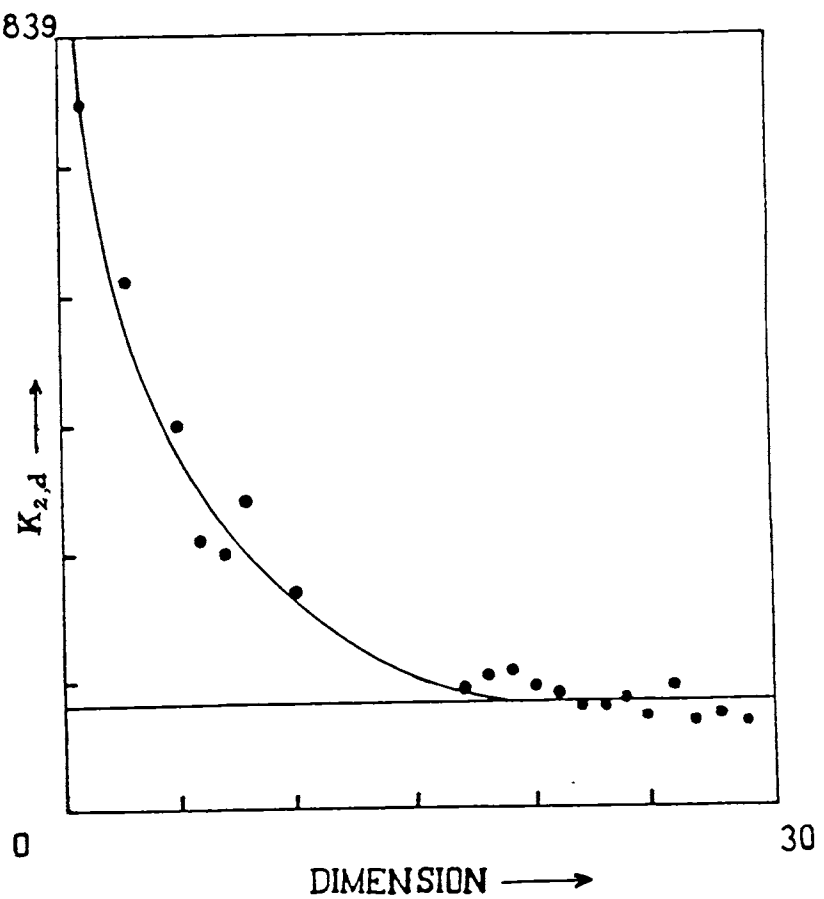

Fig 7.7 $K_{2,d}$ against dimension d. The asymptotic value K_2 is 0.074

The curve $\log\left[C_d(\varepsilon)/C_{d+1}(\varepsilon)\right]$ for asteroidal belt is plotted against dimension in Fig (7.7) and two significant features are to be noted. The function saturates asymptotically with d, and in the present case again at about d=15. This also shows that the attractor has a saturation in a subspace of

dimension 15. The phase space however in the present case is the correlation space and K_2 is information entropy as against the usual Boltzman entropy which is defined in canonical space and which indicates thermodynamic equilibrium.

Secondly, the saturation value of K_2 is about 0.04 which is indeed a very small quantity and indicates that the system is more or less completely ordered in the information sense and has very low stochasticity. Nevertheless it does indicate the existence of a deterministic chaos component.

7.5 DISCUSSION

The method of analysis adopted here discriminate three cases - regular, chaotic and completely stochastic. An integral value of the dimension of an attractor implies that the deterministic component of the system is regular. In the present case of the asteroidal belt, the dynamics is that of a regular attractor, as the dimension is 5. This would further imply that the Fourier space would actually be divided into five domains, each having a distinct fundamental frequency. Thus the curve can be represented by a summation of five distinct fourier series each having a fundamental frequency, and that these are incommensurate. This kind of resolution however is not possible in the usual fourier expansion. These five frequencies, when expressed in the phase space variables, would be interpreted as the five Poincare's Summational invariants. In the gravitational case, the five known summational invariants are

the semi major axis $a + r/[\,2 - rv^2]$,

angular momentum, $\vec{L} = \vec{r} \times \vec{v}$

Perihelion vector $\vec{P} = (\vec{r} \times \vec{v}) \times \vec{v} - \frac{\hat{r}}{r}$

These constitute seven variables, but as can be seen, they are not completely independent. Two constraints can be obtained *viz.*,

$$\vec{P}.\vec{L} = 0$$
$$L^2 = a\ [\ 1-p^2\ ] \qquad (7.8)$$

With these conditions, we are left with only five independent variables which could be identified as the invariants corresponding to five frequencies. The saturation of $K_{z,d}$ beginning at d=15 can therefore be identified as an attractor of dimension 5 embedded in a subspace of dimension 15 in an infinite dimensional space and the ratio of which show up in more than one situation *viz.*, (a) as a resonance, (b) as a distance at which correlation changes its sign and (c) as the outer boundary of the chaotic zone which separates chaos from order. One could probably infer from the present analysis that the role of the Jovian resonance is to introduce the separation of order from chaos in the asteroidal belt.

7.6 RING STRUCTURE OF SATURN

Saturn is the second largest planet in the solar system and it is surrounded by a large flat ring. Saturn appears as an elliptical disk in telescopic observations (Fig 7.8) and has a diameter of about 121,505 Km. Main constituents of its atmosphere are hydrogen and helium and has the atmospheric temperature of about 120°K.

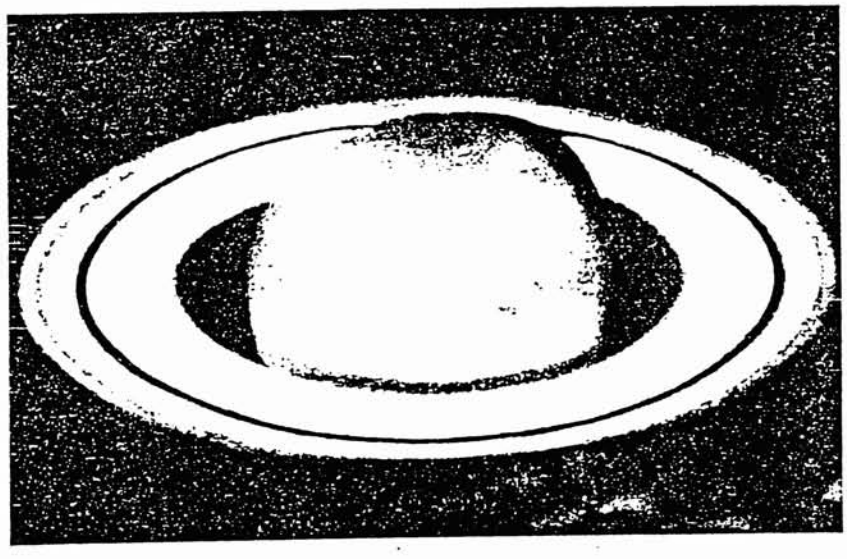

Fig 7.8 Saturn

The presence of rings is one of the most remarkable features of the Saturn's system. The ring system is divided into four main regions, *viz.*, A, B, C and D ring.

A is the outermost ring with moderate brightness, its outer diameter is 278,417 Km and inner diameter is 241,402 Km. A-ring and B ring are separated by the dark Cassini divisions, of 4023 Km wide. B ring is the brightest ring, with outer diameter of 233,355 Km and inner diameter of 180,247 Km. C is the innermost ring and is much fainter, and is separated from B ring by narrow dark division, known as French division, of 966 Km wide. C ring has an outer diameter of 178,637 Km and inner edge is at 11,265 Km above the planet surface. D ring is the fourth zone, and exists between the C ring and the globe. In the following sections, analyses of the Saturn ring structure carried out using nonlinear techniques are described in detail.

The data set obtained from Saturn rings consists of the extinction data as recorded by the photopolarimeter in the Voyager mission (Esposito et al 1983).

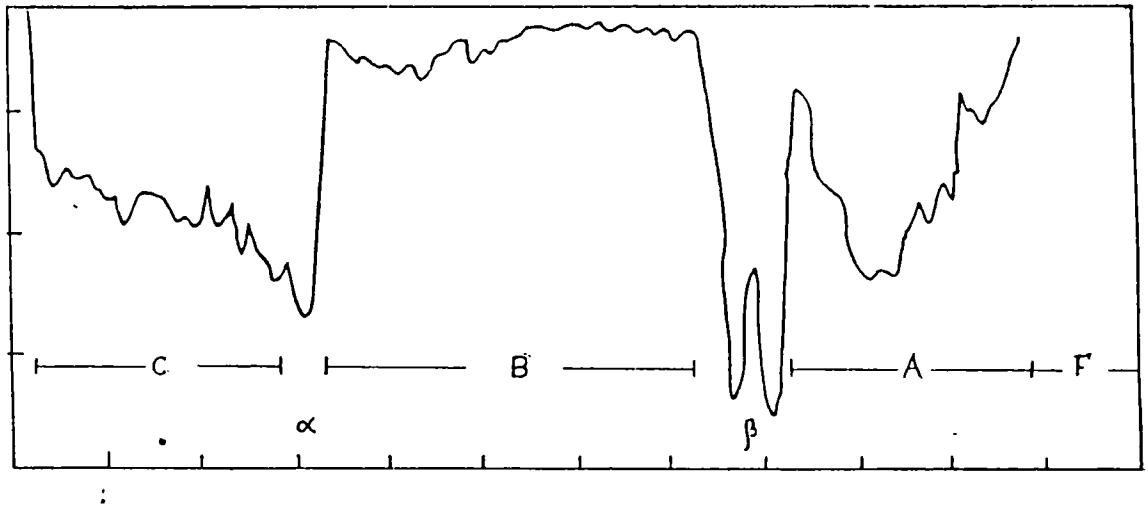

Fig 7.9 Matter distribution as a function of radial distance from the inner edge of the C ring to the outer edge including F ring.

The density distribution of matter in the Saturn rings as a function of distance is given in Fig 7.9. It is recorded at an

interval of 65 Km ($0.002R_s$) for a distance ranging from the inner edge of the innermost ring (C ring) to the outer edge of A ring. The F ring and the gap between A and F are not included in the present analysis, and also the D ring, which is supposed to exist between the planet and the C ring. The distance is about 1.03 R_s and the division of the domain is given in Table (7.1). These readings are given by the sequence

$$X(l) = X(l_o),\ X(l_o+\Delta l) \quad \ldots\ldots\ldots\ldots \quad X(l_o+N\Delta l)$$

where Δl is the distance (gap) between two consecutive readings. In the present case it is 65 Km, and l_o is the innermost edge of the C ring. The data so obtained is subjected to "time series" analysis as was done in the case of asteroidal belt. We have evaluated D_2 and K_2 for the various parts of ring and gap systems. The results are presented in two different sets - of the rings as well as gaps. In order to check whether the behaviour of the whole system is influenced by some particular regions like gaps or rings, analyses were carried out for whole data set also. But it shows that the behaviour is independent and the system consists of a spatial distribution of a large number of strange attractors which can be inferred from the existence of plateaus in the slope vs dimension curve. The evaluated values of D_2 and K_2 of each ring and gap is given in Table (7.1), along with the inner and outer edges in unit of R_s.

Table 7.1 Summary of Saturn ring system analysis

Ring/Gap	In units of R_s		Width	D_2	$K_2 \times 10^3$
	Inner edge	Outer edge			
C	1.24	1.45	0.21	1.65	1.00
Gap	1.45	1.53	0.08	2.81	0.83
B	1.53	1.95	0.42	4.26	2.58
Gap	1.95	2.03	0.08	2.55	3.20
A	2.03	2.27	0.24	1.71	1.23
Total System	1.24	2.27	1.03	1.78	0.87

7.7 BEHAVIOUR OF AUTOCORRELATION FUNCTION IN SATURN RING SYSTEM

In order to study the behaviour of particle distribution in Saturn ring, autocorrelation has been evaluated

using the method described in chapter 2. Analyses have been carried out taking the ring as a whole as well as treating the gaps and rings separately.

Analysis of the ring as a whole (R_s=1.24 to 2.03) reveals the switching of correlation from positive to negative beyond the lag point 192 (Fig. 7.10). The negative correlation dies out beyond the lag point 720. Beyond 720 lag points the distribution becomes completely uncorrelated.

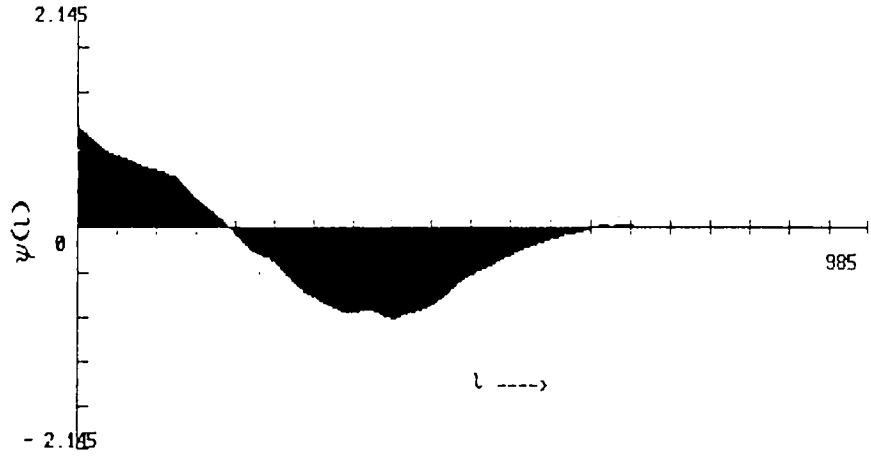

Fig 7.10 Autocorrelogram of Saturn (Total system, from C ring to A ring (1.03 R_s))

Autocorrelation studies of A ring has also revealed negative autocorrelation beyond a lag point of 80 (Fig. 7.11a). However the correlation does not go to zero within the range of observation.

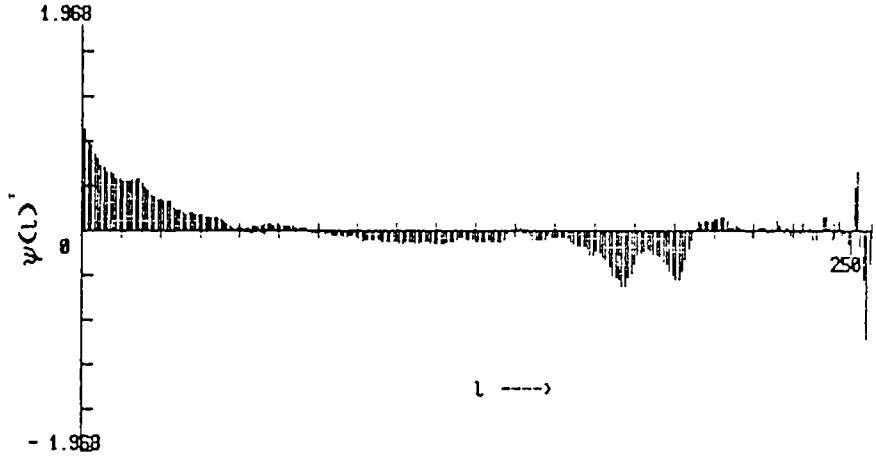

Fig 7.11a) Autocorrelogram of A ring

Autocorrelation patterns of B and C rings show different behaviour as compared to A ring. Results show (Fig.7.11b & c) an oscillatory behaviour in the autocorrelation which is well manifested in the case of C ring.

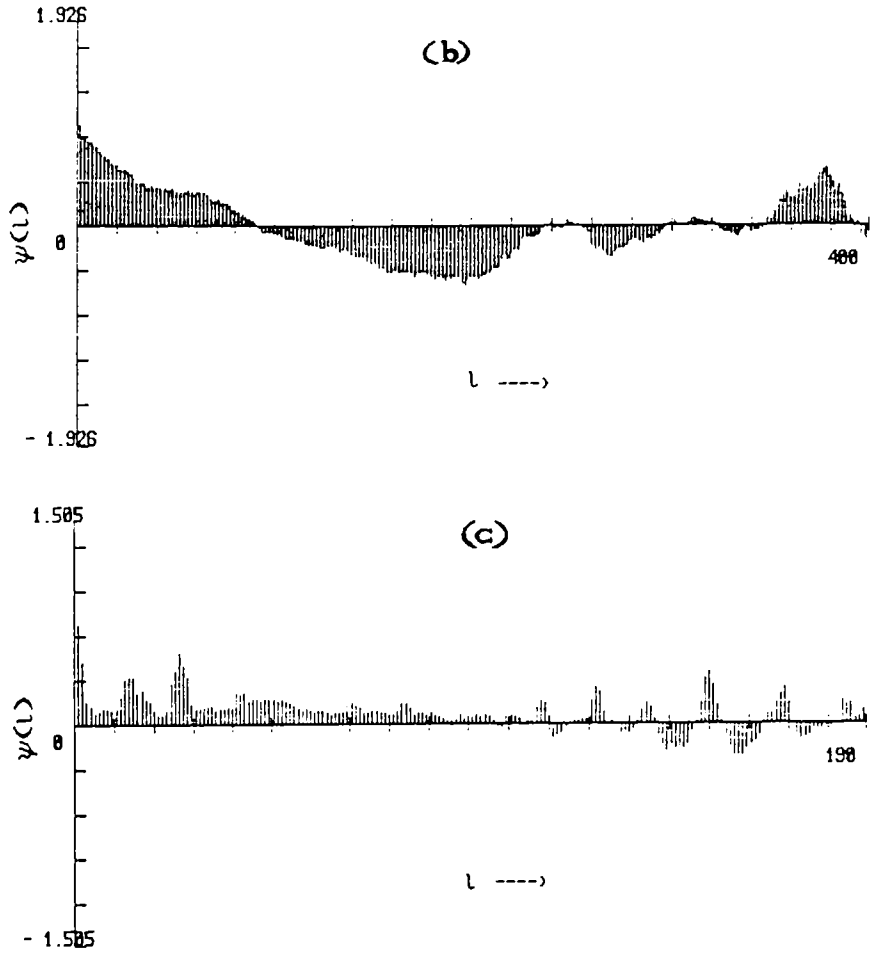

Fig 7.11 Autocorrelogram of (b) B ring (c) C ring

The distribution in B and C gaps show similar behaviour as in the case of B and C ring. The oscillatory behaviour in the gap structure has been observed more clearly (Fig. 7.12a & b).

When we take the ring as a whole, the oscillatory nature of autocorrelation function observed in the cases of B ring, C ring, B gap and C gap is overshadowed by resultant convergence of the function at high lag points.

Autocorrelation studies will give only a qualitative idea about the system. For deeper understanding we have to look of alternate treatments which takes into account of nonlinear interactions present in the system. Results obtained from such

analysis are described in the following section.

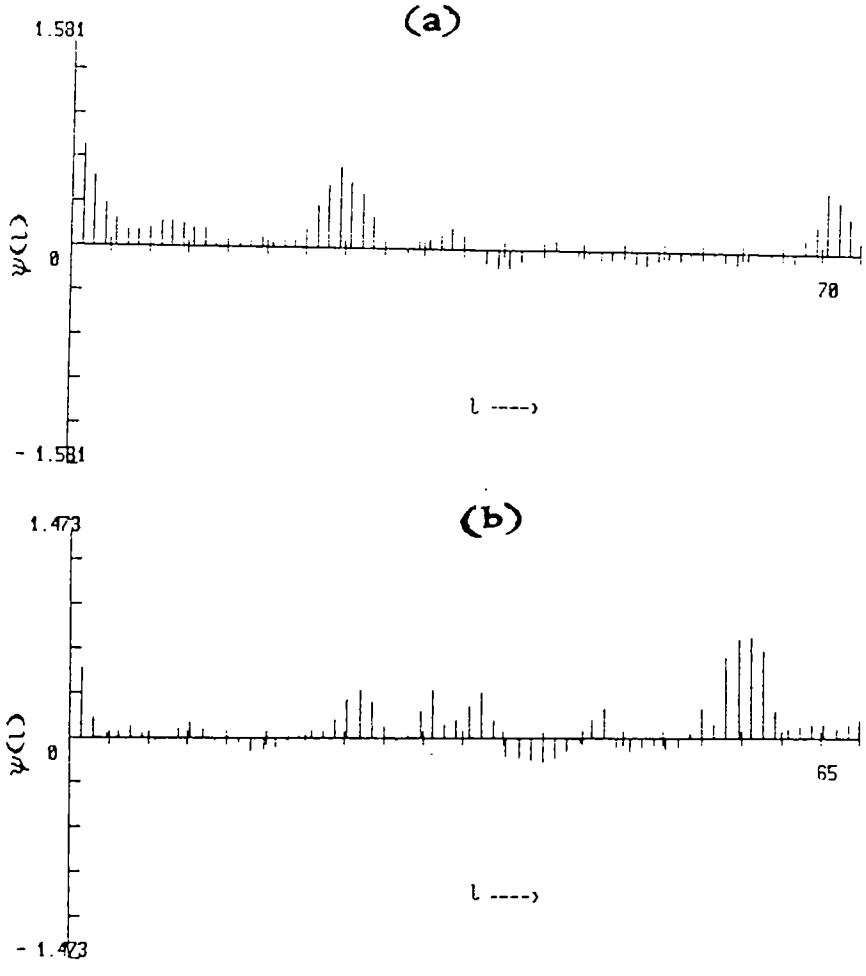

Fig 7.12 Autocorrelogram of (a) B gap or Cassini division (b) C gap or French division.

7.8 ATTRACTOR DIMENSION AND KOLMOGOROV ENTROPY IN SATURN RING SYSTEM

C Ring

This ring is the one closest to the planet that we are considering, and it experiences strong gravitational effect. The inner edge of the C ring is at a radial distance of 0.2 R_s from the planet's surface and has a width of 0.21 R_s (1.3×10^4 Km). Fig (7.13) gives the plot of log $C_d(\varepsilon)$ vs log(ε) for the

various dimensions d (the left hand side outermost is of dimension 1) and we evaluated up to 30 dimensions. In the Fig we have given only 20 curves to avoid overcrowding. The curve d=1 has some structure. But as d increases, these structures disappear even though some small wobbles do persist.

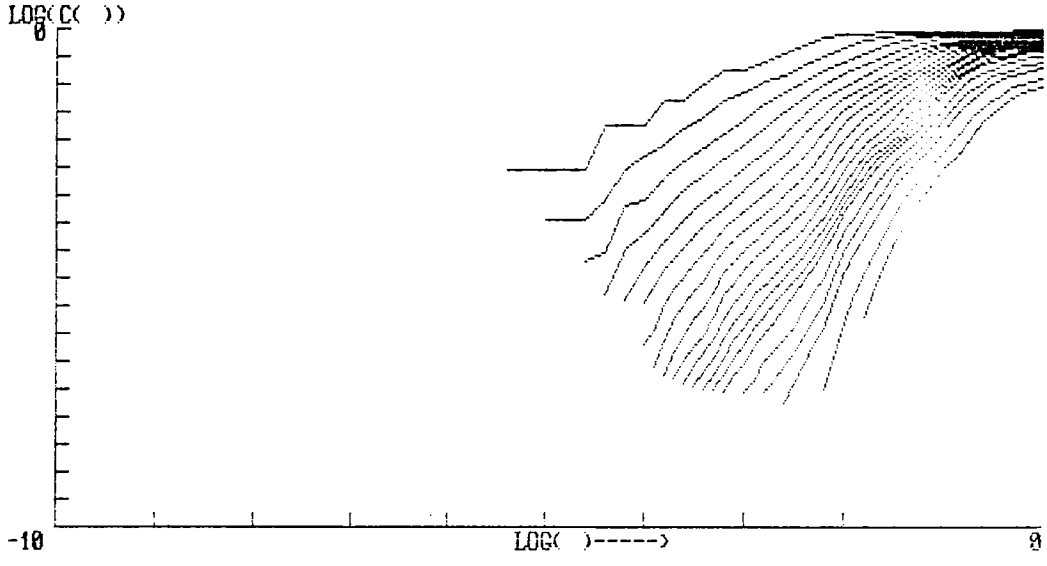

Fig 7.13 Plot of log $C_d(\varepsilon)$ against log ε for C ring.

Such wobbles do not appear in other dynamical systems such as neural networks and Asteroidal belt, and hence, does not seem to be an artifact due to smaller data set. Plot of slope against dimension is given in Fig 7.14, curve 'a'. The curve attains a saturation value of 1.65. In this figure we have drawn a line(b) at 45° to the x-axis along which all the points would lie if the process is totally stochastic. Hence the deviation from this line indicates the existence of a deterministic part. The initial points for small dimension indicate the noise component, while the asymptotic value gives the characteristic dimension of the attractor. The noninteger characteristic dimension indicates the existence of strange attractor. The points plotted in Fig (7.14) gives the Second Kolmogorov entropies - the most important component in the family of Kolmogorov entropies. The line 'c' drawn in Fig (7.14) is the asymptotic value K_2. It is mentioned that K_2 is a sensitive parameter and D_2 is a static parameter. Hence, the presence of multiple frequencies and length scales in

the system would get reflected in K_2 and D_2, as given in the table (7.1).

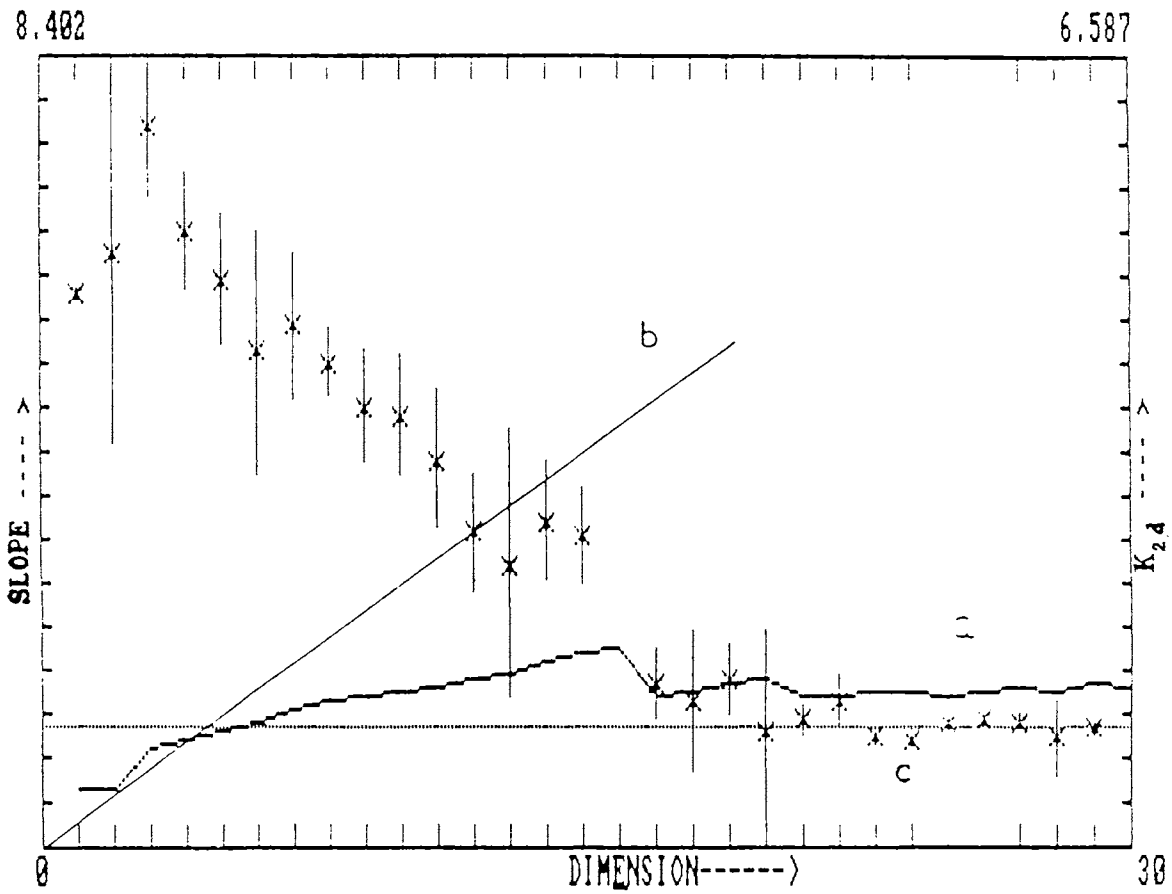

Fig 7.14 The plot gives three curves:(a) slope vs dimension d for the curves in Fig.7.13 (b) the same for completely stochastic case and (c) the plot of $K_{2,d}$ against dimension d. The asymptote give the value of K_2.

B Ring

It may be noted that the log $C_d(\varepsilon)$ vs log(ε) (Fig 7.15) do not show much of wobbles for the initial dimensions, but starts appearing in the higher dimensions. We have evaluated correlations only up to r=1, and hence the curves do not converge to log $C_d(\varepsilon)$=0. But the curve do converge to $C_d(\varepsilon)$=1 if we take

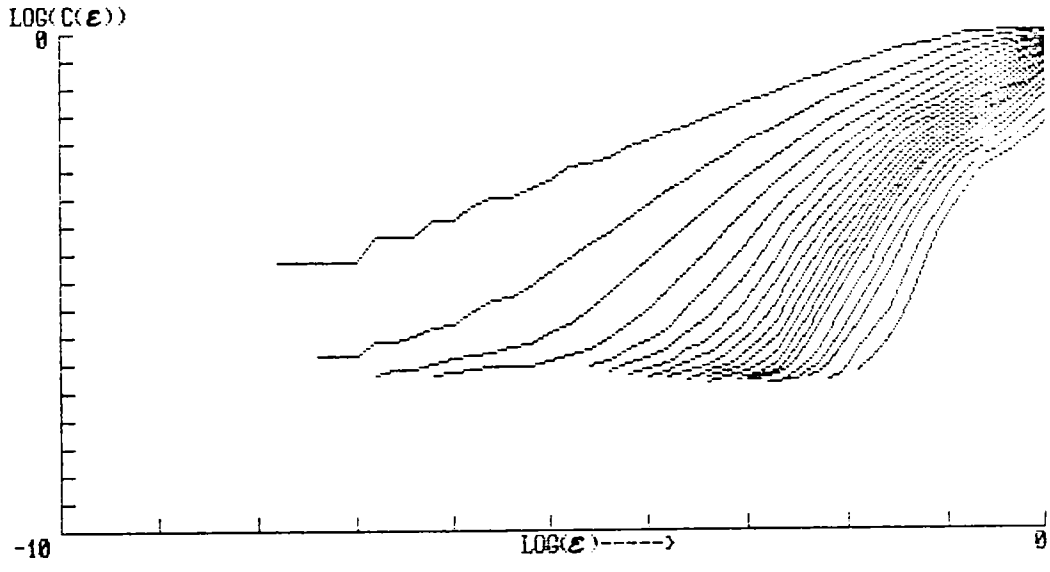

Fig 7.15 Curves giving log $C_d(\varepsilon)$ against log ε for B ring - the largest in the system.

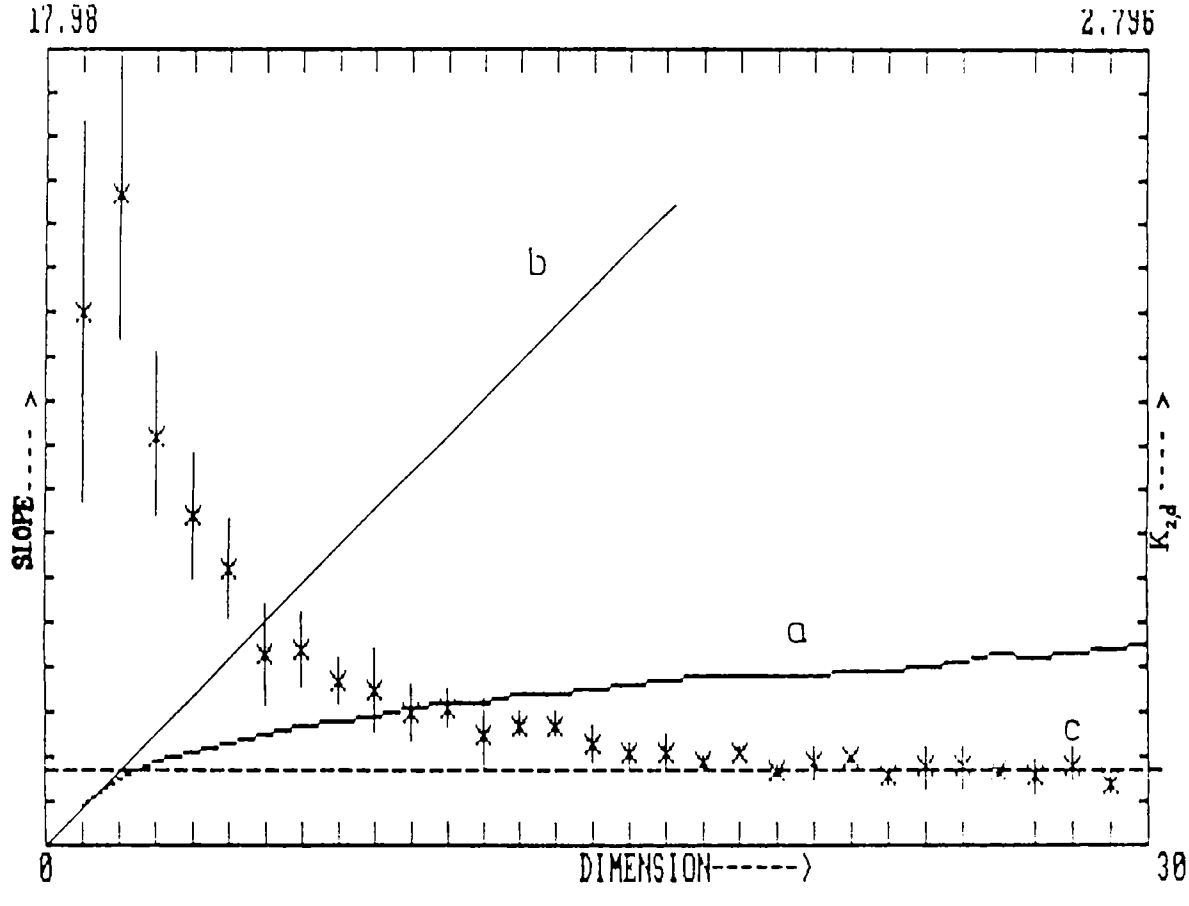

Fig 7.16 For the curves given in 7.15, (a) the slope vs d (c) the $K_{2,d}$ against d.

higher values of ε. However we did not go for the same, since we need only the slopes of the linear part of the curve and these do not change as ε is increased beyond 1. It may be mentioned that Fig 7.16, curve 'a', does show plateaus indicating the presence of more than one basin of attractors and if we take the mean value of this, we get the characteristic dimension as 4.26. The asymptotic value K_2 given by Fig 7.16, curve 'c', however is well defined and gives the value 2.58 Km^{-1}.

A Ring

A-ring is the outermost one and it experiences comparatively less gravitational force. The Voyager, however, observed knots and kinks in the ring system as well as concentric ring structures within the system. In the curves log $C_d(\varepsilon)$ vs log r, structures start appearing from the smaller dimensions onwards as is evident in Fig (7.17). These structures are indeed real and shows that there are more than one strange attractor in

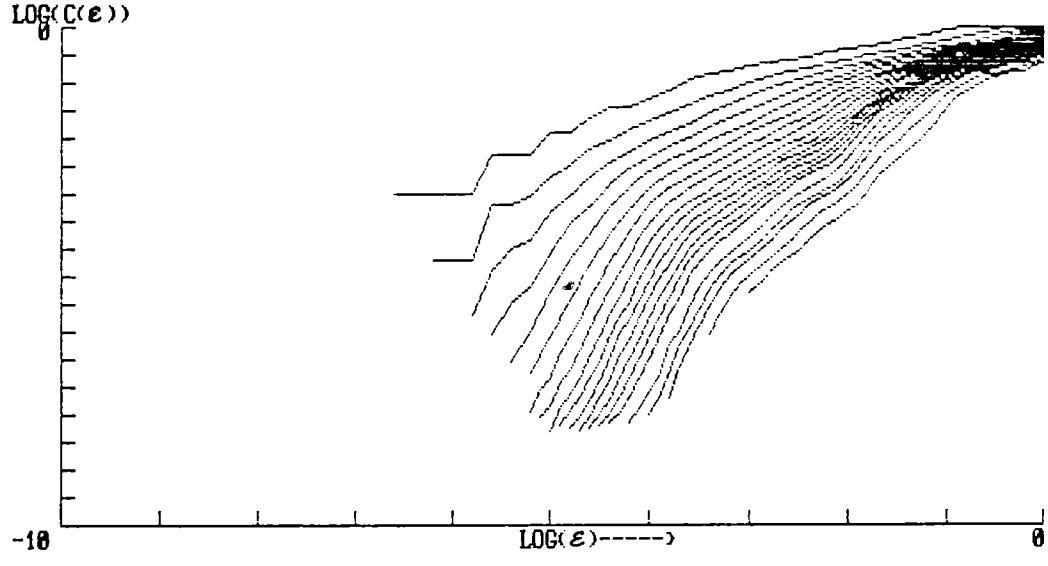

Fig 7.17 The graph depicting log $C_d(\varepsilon)$ vs log ε for A ring - the outermost one considered here.

the system. To separate the various components, however, would be difficult. This also became obvious in the slope vs dimension plot. As d increases, the attainment of the asymptotic value is

slow. This is given in Fig (7.18, curve 'a'), and which implies that the deviation from the stochastic line (b) is slow. This is also apparent in the K_2 entropy plot 'c' in Fig (7.18) wherein there exists oscillatory character, which dies down as d

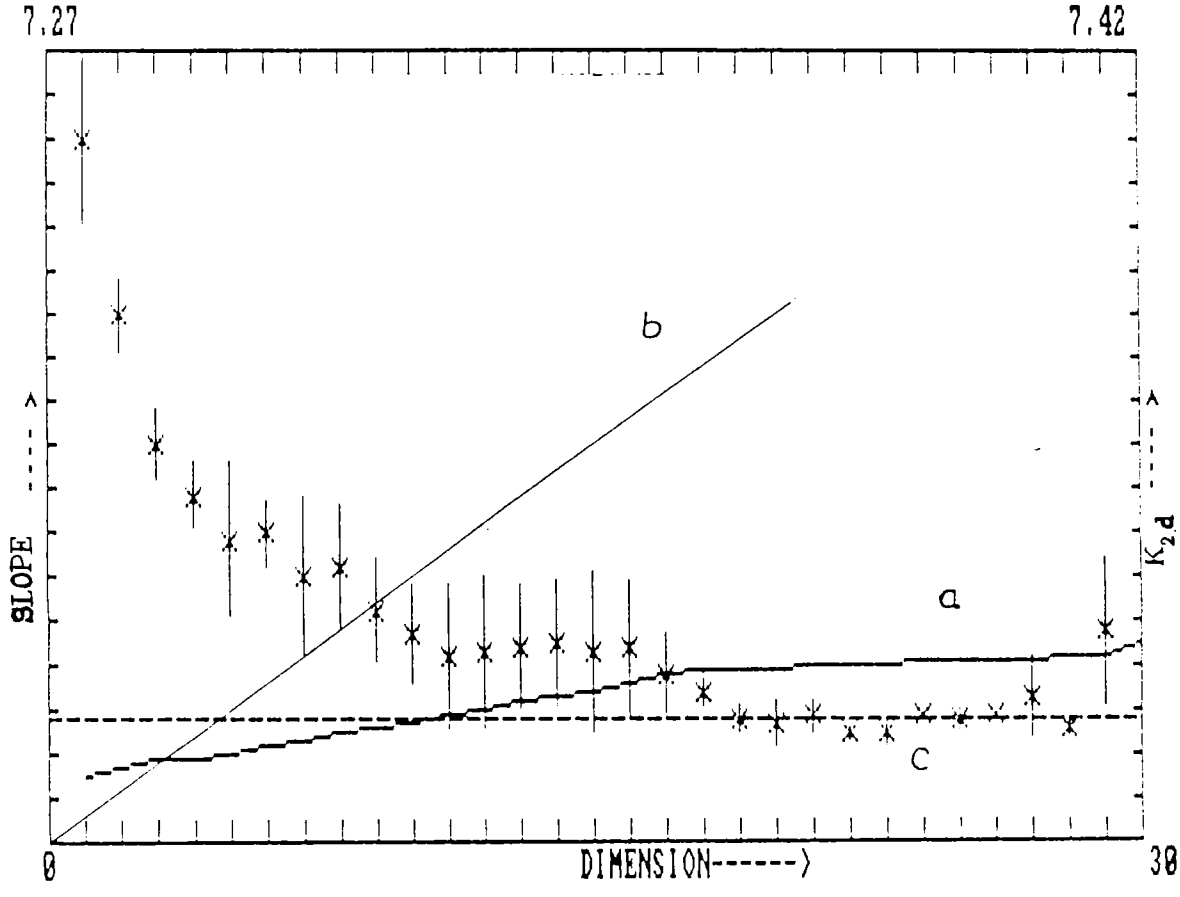

Fig 7.18 The plot of (a) the slope from 7.17 against d and (c) $K_{2,d}$ against d.

increases. Probably one can get an asymptotic value D_2 for larger dimensions. The existence of more than one attractor (regular or strange) in the system is quite apparent. It has a D_2 value of about 1.71 and $K_{2\sim}$ 1.23 Km^{-1}.

Gaps

We shall carry out a similar analysis for the two gaps *viz.* C gap - between C and B rings (French division) and B gap - between B and A rings (Cassini division).

C gap

The curve log $C_d(\varepsilon)$ vs log (ε) for this regions is given in Fig (7.19). A regular structure in the curve starts

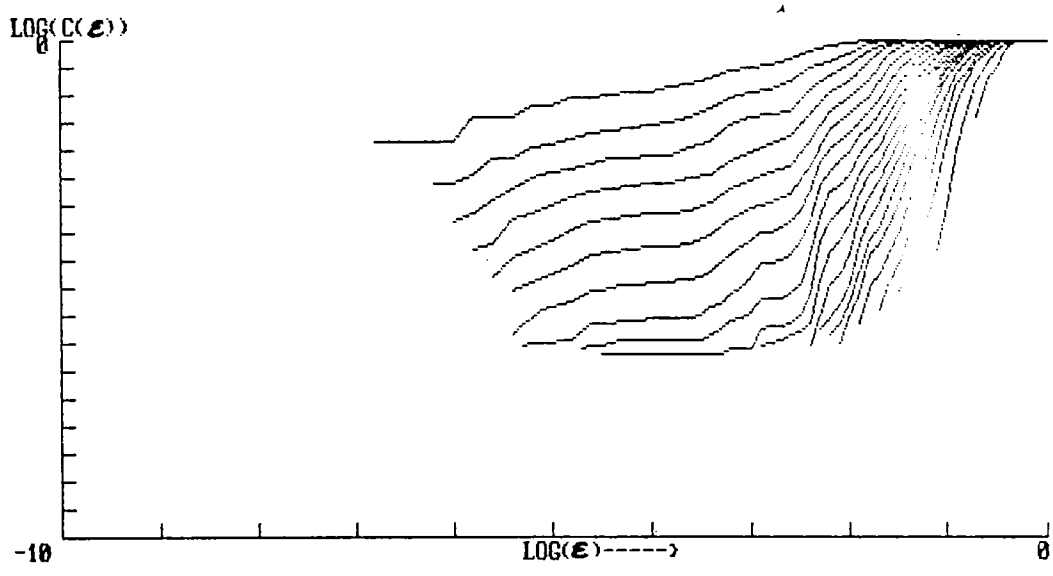

Fig 7.19 log $C_d(\varepsilon)$ vs log (ε) for the French Division or C gap.

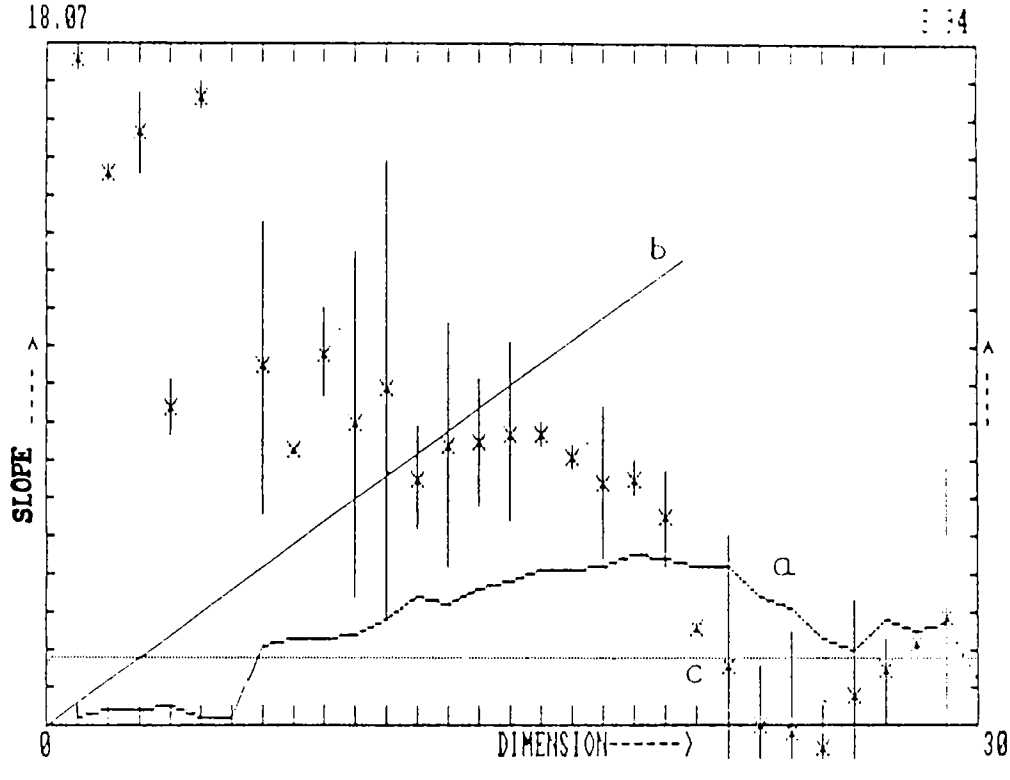

Fig 7.20 a) Slope derived from 7.19 against d and (c) $K_{2,d}$ against d.

appearing right from the 1st dimension onwards. and as d increases, the step like structure also become more and more dominant. This manifests itself in a peculiar manner in the curve of slope vs dimension (Fig 7.20, curve 'a'). There does not exist a clear-cut asymptote, nor are the points along the stochastic line (b). The curve could be considered as a combination of large number of step curves, which shows the presence of more than one attractor. This is also evident from the K_2 points distribution where these points exhibit a complicated oscillatory structure Fig (7.20, curve 'c').

B gap

Unlike the C gap, B gap or Cassini division is better structurewise. Structures start appearing as dimension increases and, here again, the curves converge to unit correlation for large r. This is given in Fig (7.21).

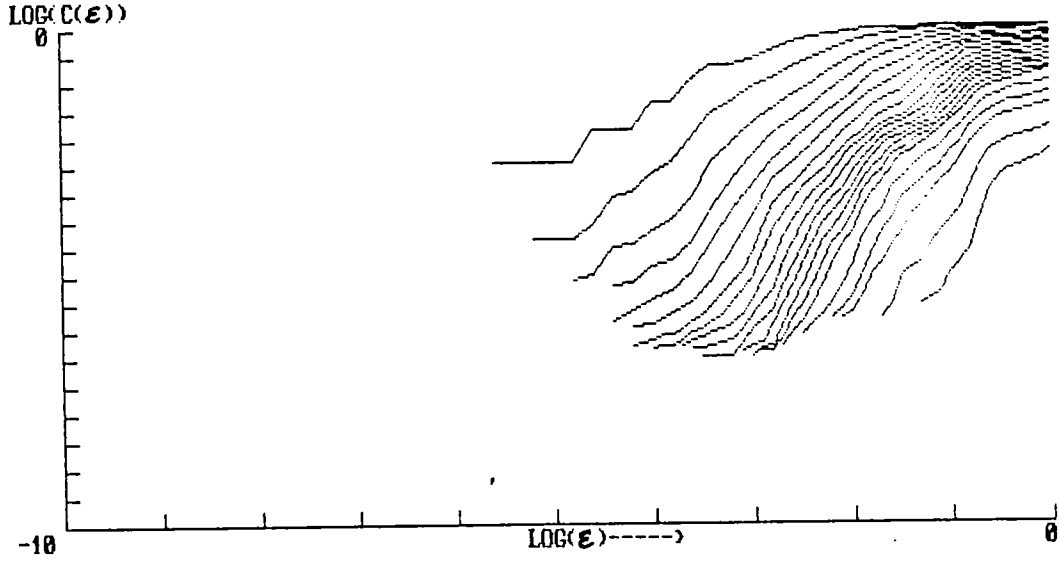

Fig 7.21 log $C_d(\varepsilon)$ is plotted against log(ε) for the Cassini Division or B gap.

The curve in Fig (7.22, curve 'a') however do not show any sign of convergence in the asymptotic limit for the number of dimensions we have taken here. One does require a large number of dimensions which implies a large number of closer data. The

curve shows horizontal portions for dimension around 10, but takes off as dimensions go beyond 20. The curve (7.22, curve 'c') depicting the Kolmogorov entropy also exhibit a peculiar behaviour. It does show a saturation beyond dimension 20.

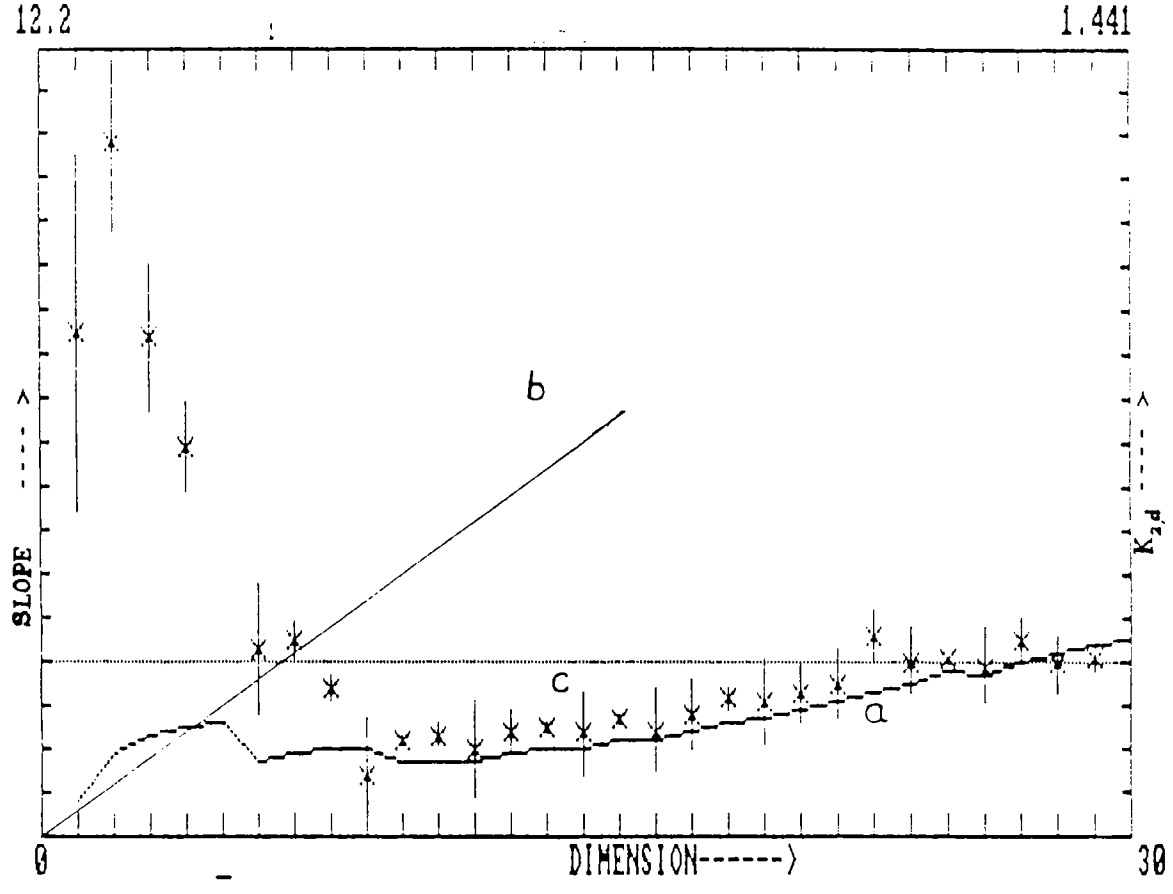

Fig 7.22 a) Slope derived from 7.21 against d and (c) $K_{2,d}$ against d. The stochastic line is given by the line **b**.

Ring system as a whole

Figure (7.23) gives the correlation curve for the entire ring system, for a range of 1.03 R_s or about 62,000 Km. As one can easily realise, the curve is not a sum of the previous ones, but has a different structure. There are pronounced wobbles in the diagram, implying distinct domains having different slopes. This manifests itself in the formation of plateaus in the various dimension ranges. Fig (7.24, curve

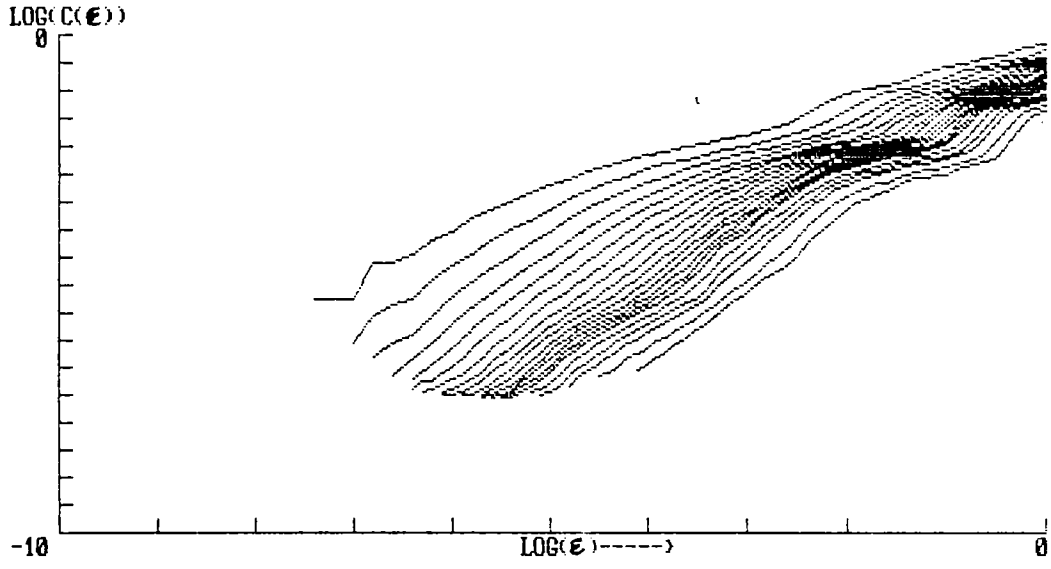

Fig 7.23 The entire ring system from the inner edge of C to the outer edge of A is taken as a single unit and the log $C_d(\varepsilon)$ vs log ε is plotted.

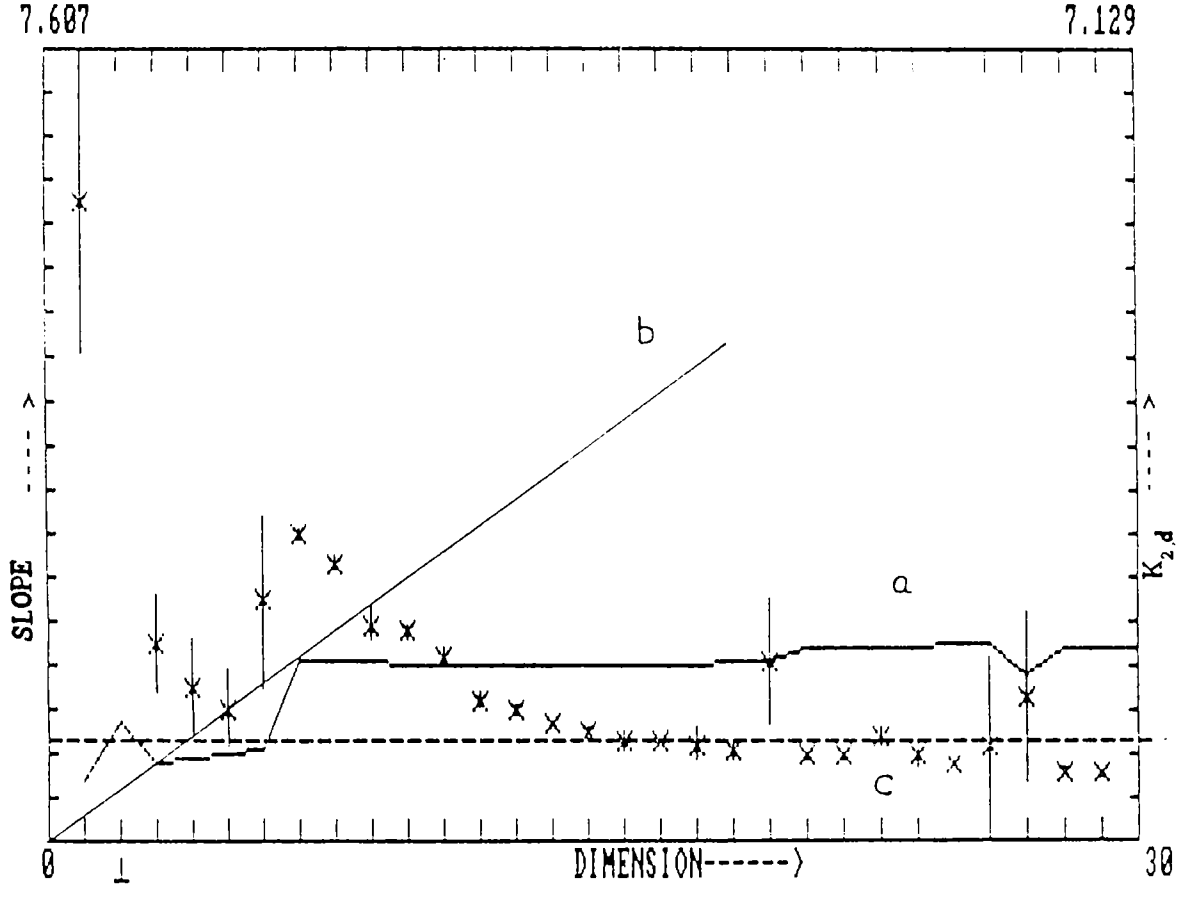

7.24 a) The slope of the curves of Fig.7.23 is plotted against dimension d (c) $K_{2,d}$ against dimension d.

'a') clearly implies the presence of various attractors having different characteristic dimensions. This is also quite evident from the fact that the deviation from the stochastic curve Fig (7.24, curve 'b') is also clearly pronounced. In the plot for K_2 Fig (7.24, curve 'c'), the ratio log $[\ C_d(r)/C_{d+1}(\varepsilon)]$ oscillates for lower dimensions but steadies itself as d increases. It is however evident that one would not be able to get details of the earlier curves from this one. It has a characteristic dimension of 1.78 and a low K_2 value of 0.87×10^{-3} Km^{-1}.

7.9 DISCUSSIONS

The results of the analysis is given in Table (7.1) and also in Fig (7.25). Some of the interesting features are that the characteristic dimension increases radially, and comes to a maximum around the B ring and then shows a steady decrease, while K_2 strikes a peak value around the Cassini gap and then decreases. This shows a phase lag between the dimension and the Kolmogorov entropy. An inspection of the dimensions reveal that all the attractors are strange and if we consider the total ring system, we get again a strange attractor. This is quite contrary to the results one obtained in the asteroidal belt wherein we get a regular attractor of dimension 5 for the system. We may conclude that the strange attractor for the total system is a consequence of a large number of interacting strange attractors, while if we extend this to the asteroidal system we may have a similar conclusion *viz.*, a system of strange attractors resulting in the formation of a regular attractor. This implies that the Saturn ring system is chaotic piecewise as well as in total, while in the asteroidal belt, the total system is a regular attractor, and is an example of chaos - inducing order. Saturn ring system form an open, dissipative, and non Markovian system consisting of more than one characteristic scale, manifesting itself as a collection of spatially distributed strange attractors (Schuster [1984]).

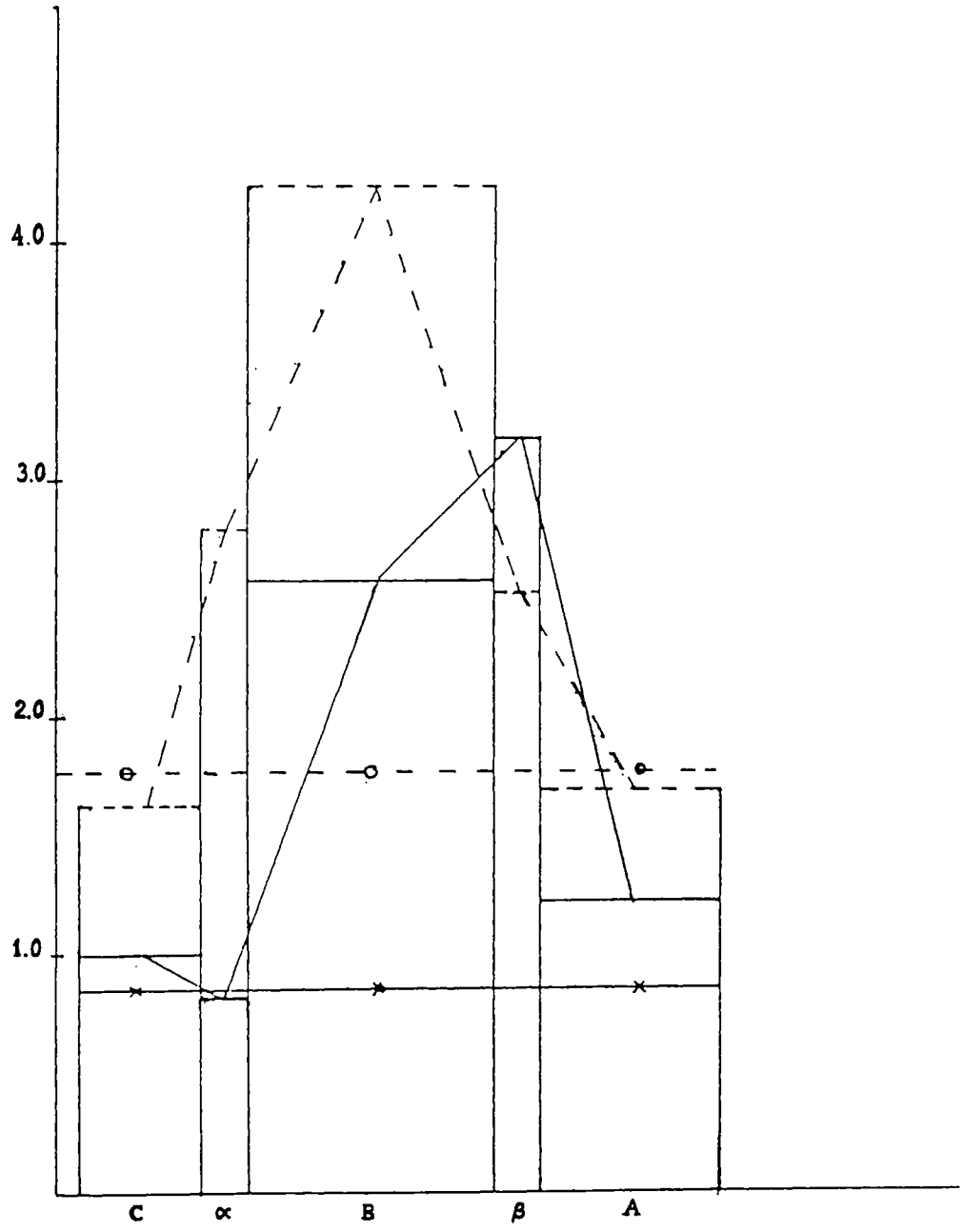

Fig 7.25 The results given in the table is plotted against distance from the surface of the planet. This reveals the relation (if any) between D_2 and 10^3 K_2. Here solid line is for K_2 and dashed line is for D_2.

Hence in developing a Statistical Mechanics of the system, it could be more realistic to consider a collection of strange attractors mutually interacting, giving rise to a resultant strange attractor or a regular one.

CHAPTER 8

RESULTS AND DISCUSSIONS

The general conclusions derived from the present studies. Future scope of the work is highlighted.

RESULTS AND DISCUSSIONS

Time series analysis, as described in previous chapters, can be used to study nonlinear systems and is an effective method from experimental point of view. We described certain applications of the technique to different systems like human brain, Asteroidal distribution and Saturn rings.

The analysis does not demand any equation of the state of the system and hence is an efficient tool to study complex nonlinear systems. As described at length, a pseudo phase space is constructed from the discrete time series using the method of delayed matrix. The matrix consists of m vectors in a d-dimensional phase space with $m \geq d$. From the set of m vectors, a q^{th} order correlation integral in d-dimensional phase space, $C_d^q(r)$ can be constructed. By varying q from $-\infty$ to ∞, $C_d(r)$ has been calculated from which generalized attractor dimension D_q and generalized Kolmogorov entropy K_q are evaluated. D_o, D_1 and D_2 are fractal dimension, information dimension and correlation or second order dimension respectively of the attractor which characterizes the nonlinear dynamics. K_2 is known as second order Kolmogorov entropy.

For a homogeneous system, $D_o = D_1 = D_2$ and for a nonhomogeneous system, $D_o > D_1 > D_2$ (Schuster 1984). D_2 is the lower bound of the Hausdorff dimension. Of all the generalized quantities D_q and K_q, D_2 and K_2 are the most important parameters (Caputo and Atten 1987) which depend sensitively on the state of the nonlinear system. Moreover, these quantities can be derived easily from a time series and it is independent of the number of

data. Integer D_2 value corresponds to K_2=0 and will represent regular dynamics, while a noninteger value of D_2 corresponds to $K_2 > 0$ will quantify the degree of chaos. For a completely stochastic system $K_2 = \infty$ and D_2 is not defined. In this case the plot slope - dimension will have slope unity.

The programme we used to evaluate D_2 and K_2 is given in the appendix and was tested using a sinusoidal signal as the data. Result yielded the values $D_2 = 1$ and $K_2 = 0$.

It has been found that the present algorithm is more efficient than other methods like the box counting algorithm. The technique has inbuilt mechanism to remove noise, and it also differentiates between deterministic and nondeterministic components of the signal.

If the SNR is very low, we should search for alternate methods to remove noise from time series signals before applying the algorithm. In chapter 3 we described such a method to filter out noise from experimental data. This is an extension of the method described by Broomhead and King [1986]. The method has been demonstrated by filtering a noise - embedded sinusoidal signal. It has been found that the EEG is more or less free of noise and hence filtering technique is not necessary for time series analysis of EEG data.

In the thesis, various types of rhythms present in the electrical activity have been described along with the dynamical aspects of the neural system. A brief description of various types of time scales present in the neural system is also presented.

Our analyses show that D_2 and K_2 are sensitive to the state of the neural system, of which K_2 is more sensitive as compared to D_2. In comparison with other systems like certain astronomical systems, Raman attractor etc., the neural dynamics has attractor with high D_2 & K_2 values. This explains the complexity of the system.

All previous works (Babloyantz et al 1985, 1986) deal with the analysis of only one of the channels of EEG and described the dynamics only in terms of D_2. We have analysed all the eight channels of EEG of a "clinically" normal brain during rest and mental activity. It was found that in all eight channels, D_2 is fractal and K_2 is positive. Analyses suggest the existence of a collection of strange attractors in the system and K_2 is very high compared to other systems. Left and right lobes are not symmetric with respect to the neural activity. In other words, brain has asymmetric activities in left and right lobes.

The study of information flow in the system in terms of K_2 variation shows that, the information flow is unidirectional when the person is immersed in some mental exercise. That is, the random firings are suppressed when the person is undergoing a mental exercise. Whereas, during the rest time, the random firings become prominent, and unidirectional nature of information flow disappears. The generalized dimension was also calculated for both mental activity and rest condition. From this the $f(\alpha)$ spectrum was deduced. The $f(\alpha)$ spectrum shows a well defined double peak during both at rest and mental activity, which suggests the existence of two attractors.

The present method of analysis gives the quantitative measures D_2 and K_2, which can be used to quantify chaos. Hence, D_2 and K_2 can be used as diagnostic tools since the degree of chaos depends on the state of the neural system under various pathological conditions like, epilepsy, migraine, tumour and psychotic.

We analysed the EEG of an epileptic (grand mal) patient during, before and after attack. The eighth channel (left parietooccipital region) shows a steady variation in K_2. It can be suggested that seizure is a defensive mechanism of the brain against any alteration of the neural dynamics.

The other epileptic case, which we have analysed is that

of a patient having both demylinated disease and epilepsy. In this case also we found that left parietooccipital region is more sensitive. The EEG in this case has been recorded while the patient had no seizure and the record indicated normal brain activity. However, our analysis shows the abnormality in the neural activity. This suggests the superiority of the present technique over the conventional method of EEG analysis.

The analysis of EEG of a patient having headache (EEG looks normal) revealed the fact that the left frontal region is the seat of abnormality. The K_2 shows periodic activity in the left frontal region as time evolves. In the case of Migraine also, frontal region is found to be sensitive, and K_2 shows large variation in this region as time evolves.

The analysis of epilepsy, tumour and psychotic cases at higher spatial resolution have also been carried out, by taking EEG at different electrode configurations. The pattern of K_2 distribution varies for different pathological conditions.

The K_2 value has been found to be low in the right parietooccipital region, where the tumour is growing, which is in the primary stage. Studies using both bipolar and monopolar techniques show the same behaviour.

The K_2 distribution in the psychotic case, shows a low K_2 value in the central region and high K_2 in the frontal and parietal regions, and thus creating certain segments in brain activity. The K_2 value is low in the left occipital region.

We have applied our analysis to two astronomical systems *viz.*, asteroidal belt and saturn rings.

The studies by Wisdom [1983] showed that there exists an ordered and chaotic regions in the asteroidal belt and 3:1 resonance is the boundary between these two. Power spectrum analysis by Pratap [1977] showed that there are five dominant frequencies present in the system, and there is a change of

correlation from positive to negative at 3:1 resonance. This result agrees with our studies in Asteroidal belt.

We have analysed the density distribution of asteroids, and found that D_2 is 5 and embedding dimension is 15. The K_2 value is close to zero. This shows that the system is more or less completely ordered in the information sense and has very low stochasticity.

In the case of Saturn ring system, we have analysed the density distribution of matter (as a function of the distance from the planet saturn), for a total span of 1.03 R_s, i.e., from C ring (innermost ring) to the outer edge of A ring. We have calculated D_2 and K_2 for various ring and gap systems, as well as for the entire ring system.

For all rings and gaps D_2 is noninteger, and K_2 is positive but very low. For the Saturn ring system as a whole also, the D_2 is noninteger and K_2 is positive. That is, the system is chaotic both piecewise as well as, as a whole. The chaotic behaviour of the total system as a whole is a consequence of large number of interacting strange attractors, i.e., chaos - inducing chaos, whereas in Asteroidal belt it may be the case of chaos - inducing order.

FUTURE SCOPE OF THE WORK

The second order Kolmogorov entropy is identified as a sensitive parameter to characterize the neural system. By analysing the EEG of large number of patients with same type of abnormality or disease, we can standardize K_2, for each particular disease and can be used as a diagnostic tool. With this analysis, we can identify different stages of a disease. Also, we can develop the information flow pattern for "clinically" normal brain as well as for affected brain. The

change in the normal flow pattern can be used as a symbol of abnormality. The flow pattern also enables us to identify the mechanism of thought-processes in brain. If EEG is obtained with higher spatial resolution such as 32 channel or 64 channel, we can identify the localized effect of the brain, or detect which part of the brain is more involved in a particular activity. This will amount to certain type of imaging of the brain.

Simulation of complete signal from a part of the data is an interesting part of this analysis. By taking a part of the signal one can develop the whole signal by following the method by Parikh and Pratap [1990].

The neural system does not have an ideal equation. D_2 gives the number of independent parameters required to describe the state of the system. Thus by knowing K_2 and D_2, we can construct certain model equations of the system by the method suggested by Broomhead and King [1986].

We are now applying this analysis in Interplanetary scintillations (IPS), and also in Raman system. The spatial behaviour of stimulated Raman scattering in a medium can be studied by analysing the spatial variation of amplitude of stokes, antistokes and pump mode.

Developing the statistical mechanics of Neural system is a very exciting work, which will be carried out in the near future. Work in this direction has already been initiated by Parikh and Pratap [1984] and Pratap [1988]. This can also be carried out in the frame work of nonequilibrium statistical mechanics, as employed by Pratap and Sreekumar [1989] in the study of a many electron system.

REFERENCE

Abarbanel, H.D.I., R.Brown and J.B.Kadtke Phys. Lett. **138A** No.8 (1989) 401.

Abraham, N.B., A.M.Albano, B.Das, G.De Guzman, S.Yong, R.S.Gioggia, G.P.Puccioni and J.R.Tredicce Phys. Lett **114A** No.5 (1986) 217.

Albano, A.M., J.Abounadi, T.H.Chyba, C.E.Searle and S.Yong, R.S.Gioggia and N.B.Abraham J. Opt. Soc. Am. **2B** No.1 (1985) 47.

Anninos, P.A., and R.Cyrulnik J. Theor. Biol. **66** (1977) 695.

Atmanspacher, H. and H.Scheingraber Phys. Rev. **34A** No.1 (1986) 253.

Babcock, K.L. and R.M.Westervelt Physica **28D** (1987) 305.

Babloyantz, A., J.M.Salazar and C.Nicolis Phys. Lett. **111A** No.3 (1985) 152.

Babloyantz, A., and A.Destexhe Proc. Natl. Acad. Sci. (USA), **83** (1986) 3513.

Babloyantz, A. and A.Destexhe Biol. Cybern. **58** No.3 (1988) 203.

Babsky, E.B., B.I.Khodorov, G.I.Kositsky and A.A.Zubkov *'Human physiology'* Vol.2 Mir Publishers (Moscow 1989).

Benettin, G., L.Gangani and J.M.Strelcyn Phys. Rev. **14A** No.6 (1976) 2338.

Berge, P., Y.Pomeau and C.Vidal *'Order within Chaos'* John Wiley & Sons (New York 1984).

Berry, M.V., **AIP Conference Proc.** No.46 (1978) 16.

Brandstater, A., J.Swift, H.L.Swinney, A.Wolf, J.D.Framer, E.Jen and P.J.Crutchfield Phys. Rev. Lett **51** No.16 (1983) 1442.

Broggi, G., B.Derighetti and M.Ravani Phys. Rev. **39A** No.1 (1989) 434.

Broomhead, D.S. and G.P.King Physica **20D** (1986) 217.

Cameron, J.R., and J.G.Skofronick *'Medical Physics'* John Wiley & Sons (New York 1978).

Caputo, J.G., and P.Atten Phys. Rev. **35A** No.3 (1987) 1311.

Chay, T.R., Biol. Cybern. **50** (1984) 301.

Chirikov, B.V. Phys. Rep. **52** (1979) 263.

Choi, M.Y. and B.A.Huberman Phys. Rev. **28A** (1983) 1204.

Clark, J.W., J.Rafelski and J.V.Winston Phys. Rep. **123** No.4 (1985) 215. See also Clark, J.W., J.V.Winston and J.Rafelski Phys. Lett. **102A** (1984) 207.

Cohen, A. and I.Procaccia Phys. Rev. **31A** No.3 (1985) 1872.

Cooper, L.N., Proc. of the Nobel Symposium on Collective properties of physical systems ed. Lindquist, B. and S.Lindquist Academic press (New York 1973).

Curry, J. Commun. Math. Phys. **60** (1978) 193.

Cvitanovic, P. *'Universality in chaos'* Adam Hilger Ltd (Bristol 1984)

Das, A.K., Physics Education (April-June 1987) 19.

Destexhe, A., J.A.Sepulchre and A.Babyloyantz Phys. Lett. **132A** No.2,3 (1988) 101.

Domany, E. J. Stat. Phy. **51** No.5,6 (1988) 743.

Dumermuth, G. and L.Molinari Neuropsychobiology **17** (1987) 85.

Dvorak, I. and J.Siska Phys. Lett. **118A** No.2 (1986) 63.

Eckmann, J.P. Rev. Mod. Phys. 53 (1981) 643.

Eckmann, J.P. and D.Ruelle Rev. Mod. Phys. 57 No.3 (1985) 617.

Eckmann, J.P., S.O.Kamphorst, D.Ruelle and S.Ciliberto Phys. Rev. **34A** (1986) 4971.

Esposito, L.W., O' Callaghan M, K.E.Simmons, C.W.Hord, R.A.West, Lane A.L, Pomphrey R.B, Coffeen D.L and M.Sato J. Geoph. Res. **88** (1983) 8643.

Farmer, J.D. Physica **4D** (1982) 366.

Farmer, J.D., E.Ott and J.A.Yorke Physica **7D** (1983) 153.

Froehling, H., J.P.Crutchfield, D.Farmer, N.H.Packard and R.Shaw Physica **3D** (1981) 605.

Froeschle, C. and H.Scholl Astron. Astrophys. **48** (1976) 389.

Froeschle, C. and H.Scholl Astron. Astrophys. **93** (1981) 62.

Giffen, R. Astron. Astrophys. **23** (1973) 387.

Glass, L., M.R.Guevara, A.Shrier and R.Perez Physica **7D** (1983) 89.

Gollub, J.P. and H.L.Swinney Phys. Rev. Lett. **35** (1975) 927.

Grassberger, P. and I.Procaccia Phys. Rev. Lett **50** No.5 (1983a) 346.

Grassberger, P. and I.Procaccia Physica **9D** (1983b) 189.

Grassberger, P., and I.Procaccia Phys. Rev. **28A** No.4 (1983c) 2591. A method of obtaining Kolmogorov entropy from a time series is also described in Termonia, Y. Phys. Rev. **29A** No.3 (1984) 1612.

Grassberger, P. and I.Procaccia Physica **13D** (1984) 34.

Grebogi, C., E.Ott and J.A.Yorke Phys. Rev. **37A** No.5 (1988) 1711.

Greenside, H.S., A.Wolf, J.Swift and T.Pignataro Phys. Rev. **25A** No.6 (1982) 3453.

Halsey, T.C., M.H.Jensen, L.P.Kadanoff, I.Procaccia and B.I.Shraiman Phys. Rev. **33A** No.2 (1986a) 1141.

Halsey, T.C., P.Meakin and I.Procaccia Phys. Rev. Lett. **56** (1986b) 854.

Halsey, T.C. and M.H.Jensen Phsica **23D** (1986c) 112.

Hao Bai-Lin *'Chaos'* World Scientific (Singapore 1985).

Hentschel, H.G.E. and I.Procaccia Phsica **8D** (1983) 435.

Hinrichs, H. Neuropsychobiology **17** (1987) 77.

Hodgkin, A.L. *'The conduction of the nerve impulse'* University Press (Liverpool 1964).

Holden, A.V., W.Winlow and P.G.Haydon Biol. Cybern. **43** (1982) 169.

Holden, A.V. *'Chaos'* Princeton University Press (Princeton 1986).

Hopfield, J.J. Proc. Natl. Acad. Sci. (U.S.A) **79** (1982) 2554.

Hopfield, J.J. Proc. Natl. Acad. Sci. (U.S.A) **81** (1984) 3088.

Kaczmarek, L.K. and A.Babloyantz Biol. Cybern. **26** (1977) 199.

Kooi, K.A., R.P.Tucker and R.E.Marshall *'Fundamentals of Electroencephalography'* Harper & Row Publishers Inc. (Maryland, II Edition 1978).

Krishna Mohan, T.R., J.Subba Rao and R.Ramaswamy (1987) Submitted to J. Atmos. Sci.

Kürten, K.E. and J.W.Clark Phys. Lett. **114A** No.7 (1986) 413.

Kurths, J. and H.Herzel Phsica **25D** (1987) 165.

Laidlaw, J.P. and J.B.Stanton *'The EEG in clinical Practice'* Churchil Livingston (London 1966).

Law and Constantin-Paton M. J. Neuro Sci. **1** (1981) 741.

Lichtenberg, A.J. and M.A.Lieberman *'Regular and Stochastic motion'* Springer (New York 1983).

Lorenz, E.N. J. Atmos. Sci. **20** (1963) 130.

Lorenz, E.N. Physica **13D** (1984) 90.

Milani, A. and A.M.Nobili *'Asteroids, Comets, Meteors'*, ed. Lagerkvist, C.I. and H.Rickman Uppsala Universitet (1983) 127.

Minorsky, N. *'Nonlinear Oscillations'* D. Van Nostrand (New York 1969) East-West Press.

Mizrachi, A.B., I.Procaccia and P.Grassberger Phys. Rev. **29A** No.2 (1984) 975.

Nagai, Y., R.Hara, T.Tsuchiya and N.Saito J. Phys. Soc. Jpn. 57 No.10 (1988) 3305.

Nicolis, C., and G.Nicolis Nature **311** (1984) 529.

Nicolis, C. and G.Nicolis Proc. Natl. Acad. Sci. (U.S.A) **83** (1986) 536.

Ott, E. Rev. Mod. Phys. **53** (1981) 655.

Packard, N.H., J.P.Crutchfield, J.D.Farmer and R.S.Shaw Phys. Rev. Lett. **45** (1980) 712.

Parikh, J.C. and R.Pratap J. Theor. Biol. **108** (1984) 31.

Parikh, J.C., V.Satyan and R.Pratap Intl. J. Neuro Sci. **44** (1989) 327.

Parikh, J.C. and R.Pratap J. Theor. Biol. (1990) preprint.

Parker, T.S. and L.O.Chua Proc. IEEE 75 No.8 (1987) 982.

Passamante, A., T.Hediger and M.Gollub Phys. Rev. **39A** No.7 (1989) 3640.

Pawelzik, K. and H.G.Schuster Phys. Rev. **35A** No.1 (1987) 481.

Pratap, R. Pramana **8** No.5 (1977) 438.

Pratap, R., V.P.N. Nampoori and Lalaja V. Intl. J. Neuro Sci. **39** (1988) 245.

Pratap, R. *'Statistical Mechanics of Neural System'* (1988) unpublished.

Pratap, R. and J.Sreekumar Pramana - J.Phys. **33** No.3 (1989) 421.

Prigogine, I. and G.Severne Physica **32D** (1966) 1376.

Rapp, P.E., I.D.Zimmerman, A.M.Albano, G.C.De Guzman and N.N.Greenbaun Phys. Lett. **110A** No.6 (1985) 335.

Rapp, P.E., I.D.Zimmerman, A.M.Albano, G.C.De Guzman, N.N.Greenbaun and T.R.Bashore *'Nonlinear Oscillations in Chemistry and Biology'* ed. Othmer, H.G. Springer-Verlag (New York 1987) 175.

Reghunath, A.T. and V.P.N.Nampoori Pramana **29** (1987) 461.

Rogowski, Z., I.Gath and E.Bental Biol. Cybern. **42** (1981) 9.

Rosseler, O.E. Phys. Lett. **57A** No.5 (1976) 397.

Roux, J.C., R.H.Simoyi and H.L.Swinney Physica **8D** (1983) 257.

Ruelle, D. The Mathematical Intelligencer **2** (1980) 126.

Ruelle, D. and F.Takens Comm. Math. Phys. **20** (1971) 167.

Ruelle, D. and F.Takens Comm. Math. Phys. **50** (1976) 69.

Sato, S., M.Sano and Y.Sawada Prog. Th. Phys. **77** No.1 (1987) 1.

Schmidt, R.P. and J.B.Wilder *'Epilepsy'* Cotemporary Neurology Series F.A.Davis Co. (Philadalphia 1965).

Scholl, H. Adv. Space Res. 5 No.2 (1985) 123.

Schuster, H.G. *'Deterministic Chaos'* Physik Verlag (F.R.G 1984).

Shaw, R. Naturforsch **36A** (1981) 80.

Stephenson, W.K. *'Concepts in Neurophysiology'* John Wiley & Sons (New York 1980).

Stoop, R. and P.F.Meier J. Opt. Soc. Am. **B5** No.5 (1988) 1037.

Swinney, H.L. Physica **7D** (1983) 3.
Takens, F. Proceedings of the Warwick Symposium ed. Rand, D. and L.S.Young Springer (New York 1981)

Trulsen, J. *'Physical studies of Minor planets'*, ed. Gehrels, T. NASA SP-267 (1971).

Volkenshtein, M.V. *'Biophysics'* Mir Publishers (Moscow 1983).

Whitney, H. *'Differentiable Manifolds'* Ann. Math. **37** (1936) 645.

Williams, J.G. and J.Faulkner ICARUS **46** (1981) 390.

Wisdom, J. Astron. J. **67** (1982) 577.

Wisdom, J. ICARUS **56** (1983) 51.

Wolf, A., J.B.Swift, H.L.Swinney and J.A.Vastano Physica **16D** (1985) 285.

Young, L.S. IEEE Transactions on Circuits and Systems **30** No.8 (1983) 599.

Zardecki, A. Phys. Lett. **90A** (1982) 274.